



HAL
open science

Port-Hamiltonian modeling of fluid-structure interactions in a longitudinal domain

Luis Mora Araque

► **To cite this version:**

Luis Mora Araque. Port-Hamiltonian modeling of fluid-structure interactions in a longitudinal domain. Fluids mechanics [physics.class-ph]. Université Bourgogne Franche-Comté; Universidad técnica Federico Santa María (Valparaiso, Chili), 2020. English. NNT : 2020UBFCD058 . tel-03224301

HAL Id: tel-03224301

<https://theses.hal.science/tel-03224301>

Submitted on 11 May 2021

HAL is a multi-disciplinary open access archive for the deposit and dissemination of scientific research documents, whether they are published or not. The documents may come from teaching and research institutions in France or abroad, or from public or private research centers.

L'archive ouverte pluridisciplinaire **HAL**, est destinée au dépôt et à la diffusion de documents scientifiques de niveau recherche, publiés ou non, émanant des établissements d'enseignement et de recherche français ou étrangers, des laboratoires publics ou privés.

SPIM

Thèse de Doctorat



Modélisation port-Hamiltonienne des Interactions
Fluide-Structure dans un Domaine Longitudinal

Port-Hamiltonian Modeling of Fluid-Structure
Interactions in a Longitudinal Domain

■ Luis Alejandro MORA ARAQUE



THÈSE DE DOCTORAT DE L'UNIVERSITÉ
BOURGOGNE FRANCHE-COMTÉ EN ACCORD DE
DOUBLE DIPLÔME AVEC L'UNIVERSIDAD TÉCNICA
FEDERICO SANTA MARÍA PRÉPARÉ À
L'UNIVERSITÉ DE FRANCHE-COMTÉ

ÉCOLE DOCTORALE N° 37
SCIENCES POUR L'INGÉNIEUR ET MICROTECHNIQUES

Doctorat de Automatique (UBFC)
Doctorado en Ingeniería Electrónica (UTFSM)

PAR

Luis Alejandro MORA ARAQUE

**Modélisation port-Hamiltonienne des
Interactions Fluide-Structure dans un
Domaine Longitudinal**

Thèse présentée et soutenue à Besançon, le 17 décembre 2020

Composition du Jury :

Denis MATIGNON	Professeur, ISAE-SUPAERO, Toulouse, France	Président
Bernhard MASCHKE	Professeur, Claude Bernard University Lyon 1, Lyon, France	Rapporteur
Thomas HÉLIE	Directeur de Recherches, IRCAM-CNRS-UPMC, Paris, France	Rapporteur
Daniel SBÁRBARO	Professeur, Universidad de Concepción, Concepción, Chile	Examinateur
Yann LE GORREC	Professeur, UBFC/ENSMM/FEMTO-ST, Besançon, France	Director de thèse
Juan YUZ	Professeur Associé, UTFSM, Valparaiso, Chile	Co-Director de thèse
Héctor RAMÍREZ	Professeur Assistant, UTFSM, Valparaiso, Chile	Co-Director de thèse



DOCTORAL THESIS FROM UNIVERSITÉ
BOURGOGNE FRANCHE-COMTÉ IN DOUBLE
DEGREE AGREEMENT WITH UNIVERSIDAD
TÉCNICA FEDERICO SANTA MARÍA PREPARED AT
THE UNIVERSITÉ DE FRANCHE-COMTÉ

DOCTORAL SCHOOL N° 37
SCIENCES POUR L'INGÉNIEUR ET MICROTECHNIQUES

Doctorat de Automatique (UBFC)
Doctorado en Ingeniería Electrónica (UTFSM)

By

Luis Alejandro MORA ARAQUE

**Port-Hamiltonian Modeling of
Fluid-Structure Interactions in a
Longitudinal Domain**

Thesis presented and defended at Besançon, December 17, 2020

Composition of the Jury :

Denis MATIGNON	Professor, ISAE-SUPAERO, Toulouse, France	President
Bernhard MASCHKE	Professor, Claude Bernard University Lyon 1, Lyon, France	Examiner
Thomas HÉLIE	Directeur de Recherches, IRCAM-CNRS-UPMC, Paris, France	Examiner
Daniel SBÁRBARO	Professor, Universidad de Concepción, Concepción, Chile	Member
Yann LE GORREC	Professor, UBFC/ENSMM/FEMTO-ST, Besançon, France	Supervisor
Juan YUZ	Associate Professor, UTFSM, Valparaiso, Chile	Co-Supervisor
Héctor RAMÍREZ	Assistant Professor, UTFSM, Valparaiso, Chile	Co-Supervisor

To my beloved wife and children.

My inspiration and motivation to improve every day.

To my parents.

Thanks for the support received since my childhood.

Acknowledgement

Firstly, I want to express my gratitude to my guide team: Doctors Juan Yuz, Yann Le Gorrec and Héctor Ramírez. To Dr. Juan yuz, who initially accepted me under his tutelage, allowing me to enter the Doctorate program in Electronic Engineering at the Universidad Técnica Federico Santa María (UTFSM), in Chile. Thank you for all your support and guide, both academic and personal, since my arrival to Chile from Venezuela. To Dr. Héctor Ramírez, thank you very much for taking me into account to continue my doctoral studies in a double degree agreement with the Université Bourgogne Franche-Comté (UBFC). To Dr. Yann Le Gorrec, my professor guide in the UBFC/ENSMM, thank you for your advice and patient, I have learned a lot from you.

I am thankful to the jury members, Professors Bernhard Maschke, Thomas Hélie, Denis Matignon and Daniel Sbárbaro for their careful revision of the thesis manuscript. Their comments during the thesis dissertation contributed to improving the final version of this manuscript and gave me new viewpoints about my work.

I acknowledge the Agencia Nacional de Investigación y Desarrollo (ANID), previously called CONICYT, of the Chilean Government for financial support of my doctoral studies through the fellowship Beca Doctorado Nacional 2017-21170472.

I am very grateful to all the staff of the Universidad Técnica Federico Santa María, especially with the personnel of the Electronic Department, the Advanced Center of Electrical and Electronic Engineering, the DGIIIP and the Office of International Affairs (OAI), for your support and help during my stay in Chile. Similarly, I also want to thank the staff of Doctoral School SPIM and AS2M department, for your help during my stay in the UBFC and the Institute FEMTO-ST. In especial, the Dr. Yongxin Wu, whom my family and I hold in high esteem for his help since our arrival in Besançon. Thank you so much.

I will never forget the professors, Ph.D. and Master students with whom I shared moments in Valparaiso and Besançon. It is impossible to mention all of them. In particular, I want to thank the Lab Fourier people: José Rojas, Claudia Sanchez, Rafael Orellana, María Coronel and Angel Cedeño, and PHS team: Ning Liu, Jesús Toledo and Andrea Mattioni, for the great moments we share together. I acknowledge each of them.

Finally, I wish to thank the people most important to me. My beloved wife Ilianny, without your support I could never achieve this goal. My children, Valeria and David, who are my inspiration to improve every day. My parents, Luis Alipio (R.I.P) and Astrid whose support and guidance since my childhood, sowed my interest in science and research.

Notation

Spatial Variables

- t time
- ζ Longitudinal axis
- ξ Transverse axis
- \mathfrak{z} Sagittal axis
- Ω Spatial Domain

Port-Hamiltonian Systems

- \mathcal{H} Total energy or Hamiltonian
- \mathbf{u} Input vector
- \mathbf{y} Output vector
- \mathbf{x} State vector
- \mathcal{X} State space
- \mathbf{e} Efforts variables
- \mathbf{f} Flow variables
- \mathbf{e}_∂ Boundary effort port variables
- \mathbf{f}_∂ Boundary flow port variables

Mathematical Operations

- \top Transpose of a vector or matrix
- Tr Trace of a matrix
- $\mathbf{u}_1 \cdot \mathbf{u}_2$ dot product, $\mathbf{u}_1^\top \mathbf{u}_2$
- $\mathbf{u}_1 \mathbf{u}_2$ Diadic product, also called external product, $\mathbf{u}_1 \mathbf{u}_2 = \mathbf{u}_1 \mathbf{u}_2^\top = \mathbf{u}_1 \otimes \mathbf{u}_2$
- $\mathbf{u}_1 \times \mathbf{u}_2$ cross product
- $\sigma_1 : \sigma_2$ scalar product between 2 tensors, $Tr(\sigma_1^\top \sigma_2)$
- $\mathbf{u} \cdot \sigma$ dotted product of a tensor with a tensor. The i -th component of $\mathbf{u} \cdot \sigma$ is $\sum_j u_j \sigma_{ji}$ and the i -th component of $\sigma \cdot \mathbf{u}$ is $\sum_j \sigma_{ij} u_j$
- $|v|$ Absolute value
- $\|\mathbf{u}\|$ l^2 -norm: $\sqrt{\mathbf{u} \cdot \mathbf{u}}$
- $\|\mathbf{u}\|_X$ Weighted l^2 -norm: $\sqrt{\mathbf{u} \cdot [X\mathbf{u}]}$ with $X > 0$

Differential Operators^{1,2}

- $\dot{\mathbf{x}}$ Total time derivative, $\frac{d\mathbf{x}}{dt}$
- ∂_x Partial derivative, $\frac{\partial}{\partial x}$, $x \in \{t, \zeta, \xi, \mathfrak{z}, \mathbf{x}\}$
- δ_x Variational derivative, $\frac{\delta}{\delta \mathbf{x}}$
- div** Divergence of a vector, $\text{div } \mathbf{u} := \nabla \cdot \mathbf{u}$, return a scalar
- div** Divergence of a tensor, $\text{div } \sigma := \nabla \cdot \sigma$, return a vector
- grad** Gradient of a scalar, $\text{grad } f := \nabla f$, return a vector
- Grad** Gradient of a vector, $\text{Grad } \mathbf{u} := \nabla \mathbf{u}$, return a tensor
- curl** Curl or rotational, $\text{curl } \mathbf{u} := \nabla \times \mathbf{u}$, return a vector

¹ Nabla operator: $\nabla = [\partial_\zeta \quad \partial_\xi \quad \partial_\mathfrak{z}]^\top$.

² Operators single notation returns a scalar, as for example **div** ; operators with bold notation returns a column vector, as for example **div** , **grad** and **curl** ; and operators with bold notation and capital first letter return a tensor, as for example **Grad** .

Structure

μ, λ	Lamé coefficients of the structure material
ρ_s	Density of the structure material
r, h, L	Internal radius, thickness and length of a flexible tube
ℓ_s	Length of structure sections
n_s	Number of structure sections
m_j	j -th mass of the MSD approximation
π_{sj}	Momentum of the j -th mass
v_{sj}	Velocity of mass j
q_{sj}	Position of mass j
q_{sj}^0	Position of mass j at instant $t = 0$
q_j	Displacement of mass j , $q_j = q_{sj} - q_{sj}^0$
k_j, k_{cj}, k_j^{col}	Coefficients of j -th lateral, coupling and collision springs
η_j, η_j^{col}	Non-linear parameter of j -th lateral and collision springs
d_j	Coefficient of the j -th damper
ζ_j	Dimensionless dissipation factor of j -th damper
$\boldsymbol{\pi}_s, \boldsymbol{q}_s$	Sets of structure momenta and displacements
\mathcal{K}_{sj}	Kinetic energy associated with mass j
\mathcal{P}_{sj}	Potential energy associated with spring j

Fluid

ρ	Density
\mathbf{v}	Velocity field
v, v	Velocities on ζ and ξ axis
$\boldsymbol{\tau}$	Newtonian viscosity tensor
μ, κ	Kinematic and dilatational viscosities
p	Static pressure
p_d	Dynamic pressure
P	Total pressure, $P = p + p_d$
P_i, P_o	Total pressures on inlet and outlet boundaries
Q, Q^m	Volumetric and mass flow
β_S, m	Bulk modulus and mass of nodes
A_j, A_{cj}	Cross-sectional area and fluid-structure contact area of j -th fluid section
$\pi_{\zeta j}$	Longitudinal momentum of the j -th fluid section
$\mathcal{K}_f, \mathcal{P}_f$	Kinetic and internal energies of the fluid
u, s, h	Specific (per unit mass) internal energy, entropy and enthalpy
T	Temperature
f_T, f_s	Heat and entropy fluxes
ρ_0	Reference density
p_0, h_0	pressure and enthalpy at ρ_0
\hat{p}, \hat{h}	Relative pressure and specific enthalpy, $\hat{p} = p - p_0$, $\hat{h} = h - h_0$
\bar{u}	Available specific internal energy

Abbreviations

PHS	port-Hamiltonian system
FSI	Fluid-structure interactions
BC	Boundary conditions

Contents

Acknowledgement	i
Notation	iii
Contents	v
1 Introduction	1
1.1 Motivation	1
1.2 Background on port-Hamiltonian systems (PHS)	5
1.2.1 Finite-dimensional port-Hamiltonian systems	5
1.2.2 Infinite-dimensional port-Hamiltonian systems	9
1.2.3 Irreversible port-Hamiltonian systems	13
1.3 Thesis organization and contributions	15
1.4 Associated publications	16
2 Mechanical description of the structure	17
2.1 Flexible tube model	18
2.1.1 Mass-spring-damper model	19
2.1.2 Port-Hamiltonian Formulation	21
2.2 Vocal folds model	22
2.2.1 Body-cover model	23
2.2.2 Port-Hamiltonian formulation	25
2.3 Conclusion	28
3 Finite-dimensional port-Hamiltonian FSI model with in- compressible fluids	29
3.1 Fluid description	30
3.1.1 Finite-dimensional modeling of the fluid	30
3.1.2 Macroscopic power dissipation in the flow	31
3.1.3 Fluid dynamics of the incompressible sections and nodes	32

3.2	Port-Hamiltonian formulation of the FSI model	36
3.2.1	Power-preserving interconnection of incompressible fluid sections and nodes	39
3.3	Fluid-structure power-preserving interconnection	42
3.4	Example: Pressure wave propagation in a flexible tube	44
3.5	Conclusion	47
4	Finite-dimensional port-Hamiltonian FSI model for com- pressible fluids	49
4.1	Fluid description	49
4.1.1	Finite-dimensional modeling	50
4.1.2	Dynamics of fluid sections	51
4.2	Port-Hamiltonian formulation	53
4.2.1	Total energy of the fluid	53
4.2.2	Scalable finite-dimensional model	55
4.3	Fluid-Structure power-preserving interconnection	58
4.4	Example: Airflow in the glottis	60
4.5	Conclusion	65
5	Infinite-dimensional port-Hamiltonian Formulation of com- pressible Fluids	67
5.1	Non-isentropic fluids	68
5.1.1	Governing equations	68
5.1.2	Pseudo port-Hamiltonian formulation	69
5.2	Isentropic fluids	75
5.2.1	Governing equations	75
5.2.2	Dissipative port-Hamiltonian formulation	77
5.3	Considerations for 2D and 1D flows	80
5.4	On thermodynamics and available internal energy of compress- ible fluids	81
5.4.1	Non-isentropic fluid	82
5.4.2	Isentropic fluid	83
5.4.3	Considerations for small temperature variations	83
5.4.4	Available specific internal energy	85
5.5	Irreversible port-Hamiltonian formulation of 1D compressible fluids	87

5.5.1	Governing equations of non-reactive thermodynamic compressible fluid.....	87
5.5.2	Irreversible port-Hamiltonian formulation.....	88
5.6	Conclusion.....	93
6	Conclusion.....	95
A	Useful Identities and Theorems	99
	Bibliography	103
	List of Figures	115
	List of Tables.....	117

Chapter 1

Introduction

1.1 MOTIVATION

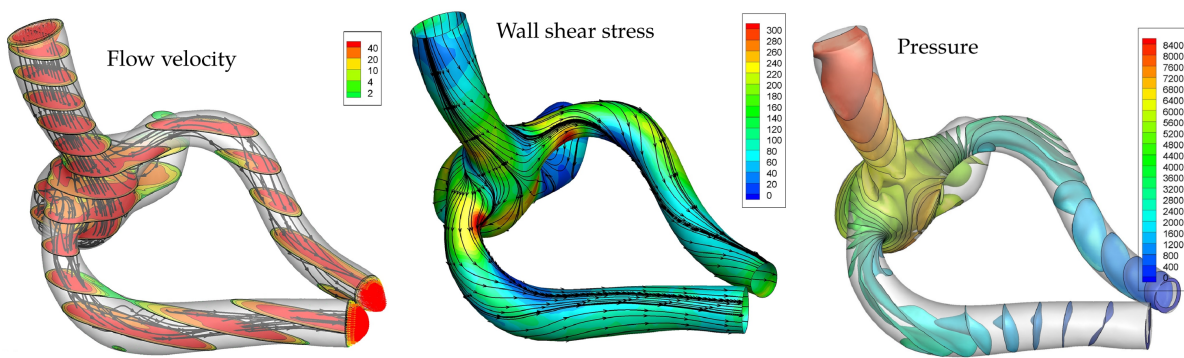
Fluid-structure interaction (FSI) is a sub-discipline in science and engineering, focused on the description of the interactions between fluids and mechanical structures [1]. FSI raises challenges associated with the fluid and structural mechanics subproblems, as well as with their coupling. FSI can be characterized as a class of problems for which exists a mutual dependence between the fluid and the structural mechanical domains. The flow behavior is driven by the shape of the structure and its motion, and the motion and deformation of the structure is driven by the fluid forces acting on the contact surface, also called coupling surface [1, 2].

FSI can be found in problems in engineering, science and medicine, such as performance analysis of power generation with wind turbines [3, 4] and aerodynamics of aircrafts [5], modeling of insect flight [6, 7], interactions between water waves and floating objects [8], in the analysis of blood flow [9, 10, 11, 12] with several applications, ranging from analyzing the blood flow in an cerebral aneurysm, to study the pressure wave propagation in an artery, as shown in Figures 1.1a and 1.1b, respectively ; human voice production [13, 14, 15, 16] as the analysis of the intraglottal airflow during the vocal folds vibration cycle, as shown in Figure 1.1c, and in sound generation of musical instruments [17].

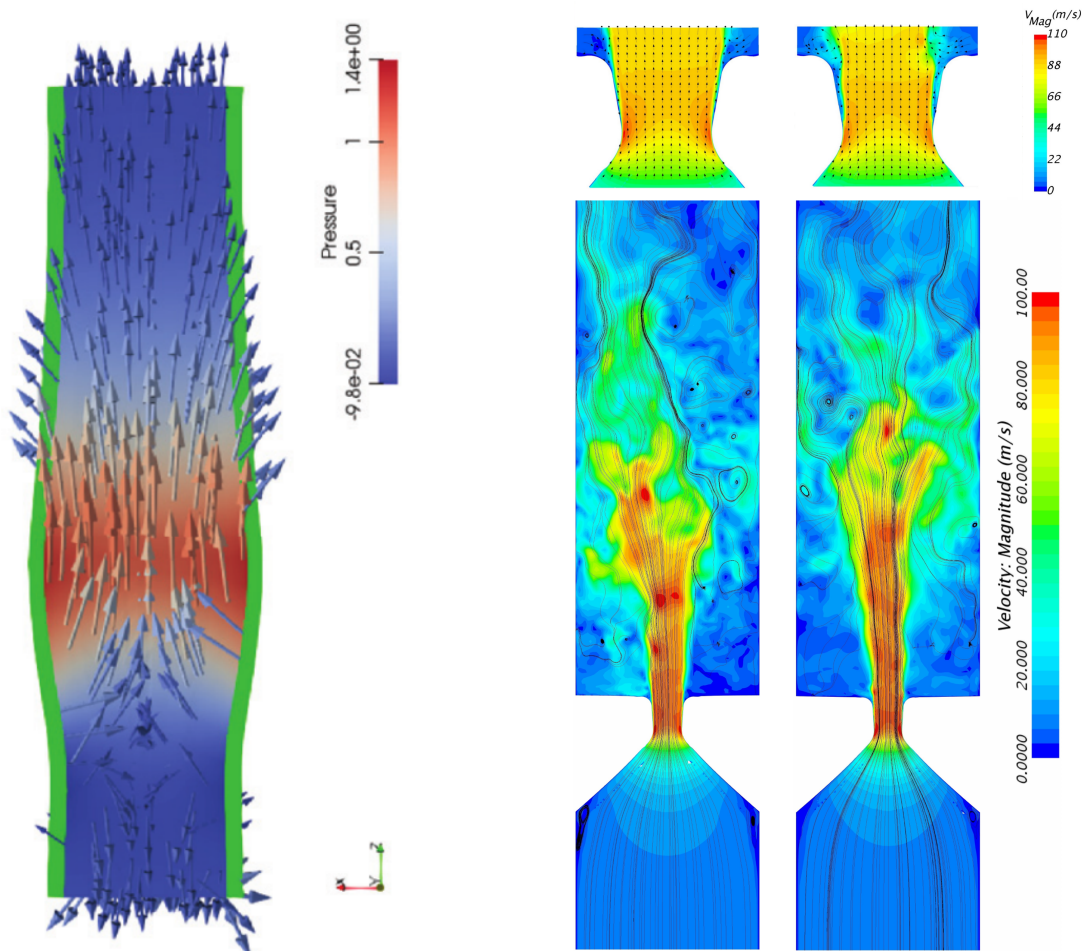
FSI can be described by a set of differential equations and boundary conditions which belong to the fluid and structure domains. The structure domain is governed by motion equations, obtained by an Euler-Lagrange formulation. The fluid domain is usually described using the Navier-Stokes equations. When modeling the coupling between the fluid and structure domains the following three conditions have to be satisfied [19]:

- A *geometric condition*, i.e., the domains can not overlap.
- A *kinematic condition*, i.e., the velocities of the fluid and the structure at the coupling surface are the same, and finally,
- A *dynamic condition* that prescribes a balance of normal stresses at the boundary in terms of *actio et reactio*.

From a numerical point of view, FSI problems are very challenging to handle, as they are described by nonlinear partial differential equations (PDEs) defined on moving boundaries. They require an appropriate grid for the mechanical and fluid domains, a clear delineation of fluid-



(a) Blood flow in a cerebral aneurysm [18]. Left: flow velocity contours and stream lines. Middle: Shear stress in the arterial wall. Right: flow pressure contours.



(b) FSI in blood flow. Arterial pressure wave propagation [12].

(c) Comparison of the intraglottal airflow in the vocal folds using different meshes [14].

Figure 1.1 – Examples of FSI systems in engineering, biology and biomedical sciences.

structure interface, an appropriate estimation of the nonlinear dynamics, and the numerical stability of the discretization methods. In the literature, different approaches have been proposed to tackle these problems. For example, to guarantee the numerical stability of the fluid-structure time discretization, algorithms as the nonlinear generalized- α time integration scheme [20], Leap Frog-Implicit Euler time discretization scheme and First order Backward Difference-Implicit Euler scheme [21] are used. In [22] an axisymmetric Navier-Stokes Prandtl (RNS-P) system is used to simplify the analysis of the fluid-structure dynamics applying finite volume “multiring” space-time discretization algorithm. Other well-known algorithms that prevent numerical instabilities in the computation of the fluid-structure dynamics are the streamline-upwind/Petrov–Galerkin (SUPG) [23, 19] and the pressure-stabilizing/Petrov–Galerkin (PSPG) methods [1, 19].

On the other hand, regarding the problem of moving boundaries in the fluid domain, there are approaches such as space-time methods [24, 1] and the well-known arbitrary Lagrangian-Eulerian (ALE) schemes [25, 26, 19]. In these methods, also called interface-tracking techniques, adaptive mesh (or moving-mesh) and remeshing algorithms are used. In these algorithms, the mesh moves to accommodate to the shape changes in the spatial domain occupied by the fluid, and as the mesh moves, sometimes it is necessary to remesh, i.e., to generate a partial or complete new set of elements or new set of nodes and elements, as shown in Figure 1.2, to improve the accuracy of the computational solution [27].

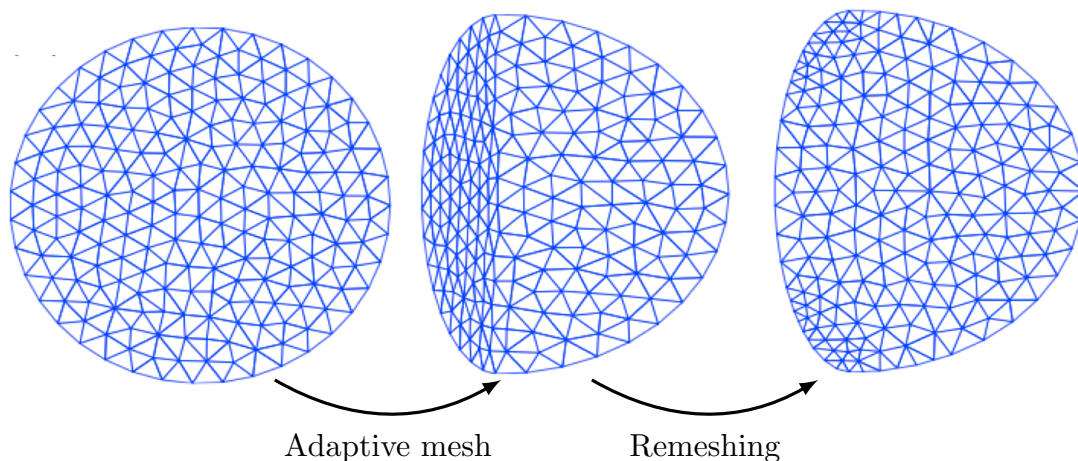


Figure 1.2 – Adaptive mesh and remeshing of the fluid domain in interface-tracking techniques [28].

In problems where contact between structural surfaces is involved and bringing the flow through the gap to zero is relevant, as for example in the description of the airflow in the glottis, the adaptive mesh methods would be more difficult to use [27]. As commented in [14], during phases with narrow gap or contact between structural surfaces, extremely distorted cells with a zero or even negative volume impair the numerical simulation and lead to a break-off in the worst case. In this sense, several approaches have been proposed in the literature. In [14] an overset mesh around the structure is used. Wherever the overset and background meshes overlap, the occluded cells of the background mesh become disabled and the overset cells become enabled and to avoid elements with zero or negative volume, at least four cells remain between the structural surfaces during the closure, allowing a minimum gap with a

small and negligible flow leakage. In [29], when the distance between the structural surfaces is less than a threshold value, the mesh at the corresponding zone is not further modified and the flow velocity is set to zero, and in [30, 31] a remesh strategy is used at each time instant.

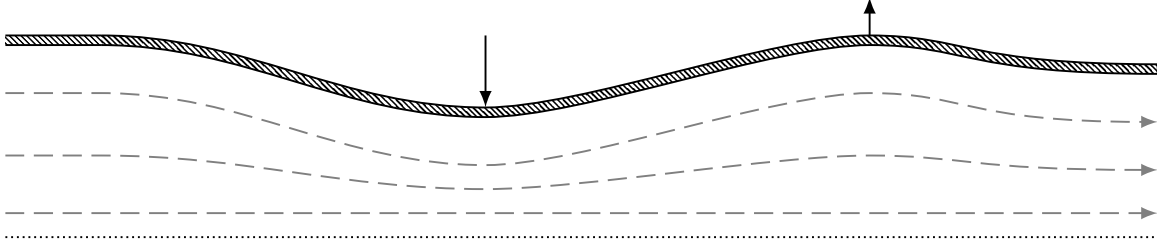


Figure 1.3 – Longitudinal fluid flow interacting with a mechanical structure with transverse motion.

In this thesis we consider the FSI between a longitudinal fluid flow and a mechanical structure with transverse motion, as shown in Figure 1.3. Even if this problem is simplified regarding the 3D fluid-structure interactions, it has interesting applications in different research areas, as for example the study of hemo-dynamic in veins and arteries [32, 11] and the human phono-respiratory system [14, 16], among others. In the classical analysis of this problem, discretizing the PDE's that describe the fluid and structure behavior, the application of several computational algorithms is necessary to guarantee the appropriate coupling of physical domains, the stability and the accuracy of the numerical results, as discussed above. As a first approximation, we consider some symmetrical assumptions, as shown in Chapters 2, 3 and 4, in the behavior of the fluid and structure, to obtain finite-dimensional models of both subsystems with an appropriate description of the fluid-structure dynamics. This allows us to avoid the use of mesh algorithms as in classical discretization of infinite-dimensional formulations. The use of finite-dimensional models in FSI problems is common in applications such as the vocal-folds vibrating cycle, where the layered tissue-epithelium, lamina propria and vocalis muscle exhibit two dominant eigenfrequencies whose behavior can be described through simplified mass-spring-damper models [33]. Moreover, we use the port-Hamiltonian framework in the modeling and coupling of both finite-dimensional subsystem. The advantage of this framework is that it focuses on the energy flux description between the system elements, proving stability and passivity properties to the model, allowing to define fluid-structure power transfer through a power-preserving interconnection. The aim of this approach is to obtain an appropriate description of the FSI problem described in Figure 1.3, reducing the model complexity of the classical numerical models. Finally, to advance in the numerical formulation of the FSI problem, we present general infinite-dimensional port-Hamiltonian models for Newtonian compressible fluids under isentropic and non-isentropic assumptions.

In the next section, we present the basic concepts of port-Hamiltonian systems, considering the finite-dimensional and the infinite-dimensional formulations, and also the irreversible port-Hamiltonian systems used in non-isentropic thermodynamics problems. In this sense, a bold notation is used to define vectors, $\partial_{\mathbf{x}} = \frac{\partial}{\partial \mathbf{x}}$ and $\delta_{\mathbf{x}} = \frac{\delta}{\delta \mathbf{x}}$ are used to denote partial and variational derivatives, respectively, and $\dot{\mathbf{x}} = \frac{d\mathbf{x}}{dt}$ denotes the time derivative of \mathbf{x} .

1.2 BACKGROUND ON PORT-HAMILTONIAN SYSTEMS (PHS)

As mentioned above, port-Hamiltonian formulations define a modeling framework that focuses on the energy flux. This framework has been initially introduced in [34, 35, 36] for finite-dimensional systems and in [37, 38, 39, 40] for infinite-dimensional systems. In this framework, the system dynamics is described in terms of driving forces expressed through derivatives (partial and variational derivatives for finite-dimensional and infinite-dimensional systems, respectively) of the total energy stored by the system, i.e., a non-negative function \mathcal{H} with respect to energy variables, i.e., the state vector \mathbf{x} . Similarly, the input \mathbf{u} and output \mathbf{y} are power-conjugated, describing the power supplied through the system ports. A feature of the finite-dimensional PHS is given by the inequality $\dot{\mathcal{H}} \leq \mathbf{u}^\top \mathbf{y}$, i.e., the rate of change of the system stored energy is bounded by the instantaneous power supplied through the ports. This feature combined with non-negativity characteristic of \mathcal{H} , guarantees passivity and stability properties which are useful for control purposes [41]. As shown in [42, 43], these properties can be extended to infinite-dimensional PHS. Additionally, energy-based control methods, such as energy-shaping, damping injection and IDA-PBC, are based on PHS models [42, 41]. Other advantage is that PHS are associated with a Dirac structure (see [44] for details), allowing the use of differential geometry tools to work without considering coordinates, which is suitable for the discretization of infinite-dimensional formulations. In order to exploit these advantages, the port-Hamiltonian framework has been used to describe dynamic systems in several application areas, such as the sound generation in musical instruments [45, 46, 47], the human voice production [48, 49], plasma dynamics [50] and mechanical systems [51, 52, 53], among others.

From the FSI point of view, the principal advantage of using PHS is the use of the energy as *lingua franca* between different physical domains, allowing the coupling of two systems through a power-preserving interconnection. This implies that fluid and structure models are described using the same tool and can be coupled by the power transfer between the sub-systems, as shown in [54, 55, 56].

1.2.1 Finite-dimensional port-Hamiltonian systems

Finite-dimensional PHS are described using a set of ODEs. According to [44, 42], the general finite-dimensional PHS formulation, called input-state-output port-Hamiltonian system with feed-through term, is defined as follows.

Definition 1.1. [44, 42] Consider the state space \mathcal{X} of a dynamic system, and the non-negative function $\mathcal{H} : \mathcal{X} \rightarrow \mathbb{R}$ defining the stored energy. An input-state-output port-Hamiltonian system with feed-through term is described by the following dynamic equations:

$$\dot{\mathbf{x}} = [J(\mathbf{x}) - R(\mathbf{x})] \partial_{\mathbf{x}} \mathcal{H} + [G(\mathbf{x}) - P(\mathbf{x})] \mathbf{u} \quad (1.1a)$$

$$\mathbf{y} = [G(\mathbf{x}) + P(\mathbf{x})]^\top \partial_{\mathbf{x}} \mathcal{H} + [M(\mathbf{x}) + S(\mathbf{x})] \mathbf{u} \quad (1.1b)$$

where $\mathbf{x} \in \mathcal{X}$ is the state vector, \mathbf{u} and \mathbf{y} are the input and output vectors, respectively, $J(\mathbf{x}) = -J^\top(\mathbf{x})$, $M(\mathbf{x}) = -M^\top(\mathbf{x})$, and matrices $R(\mathbf{x})$, $P(\mathbf{x})$ and $S(\mathbf{x})$ satisfy

$$\begin{bmatrix} R(\mathbf{x}) & P(\mathbf{x}) \\ P^\top(\mathbf{x}) & S(\mathbf{x}) \end{bmatrix} \geq 0 \quad (1.2)$$

such that, the power balance satisfies the following relationship:

$$\dot{\mathcal{H}} = \mathbf{u}^\top \mathbf{y} - \begin{bmatrix} \partial_{\mathbf{x}} \mathcal{H} \\ \mathbf{u} \end{bmatrix}^\top \begin{bmatrix} R(\mathbf{x}) & P(\mathbf{x}) \\ P^\top(\mathbf{x}) & S(\mathbf{x}) \end{bmatrix} \begin{bmatrix} \partial_{\mathbf{x}} \mathcal{H} \\ \mathbf{u} \end{bmatrix} \leq \mathbf{u}^\top \mathbf{y} \quad (1.3)$$

where $\mathbf{u}^\top \mathbf{y}$ denotes the power supplied to the system.

Remark 1.1. Notice that in (1.1) the matrices are function of the state. This implies that (1.1) describes a non-linear system (see [41] for details). In the case of linear systems all matrices in (1.1) are constant, i.e., the PHS framework encompasses both, linear and non-linear systems.

Given the non-negative condition (1.2), $S(\mathbf{x}) = 0$ implies that $P(\mathbf{x}) = 0$. Then, in this case the input-state-output port-Hamiltonian system with feed-through term (1.1) can be expressed as:

$$\dot{\mathbf{x}} = [J(\mathbf{x}) - R(\mathbf{x})] \partial_{\mathbf{x}} \mathcal{H} + G(\mathbf{x}) \mathbf{u} \quad (1.4a)$$

$$\mathbf{y} = G^\top(\mathbf{x}) \partial_{\mathbf{x}} \mathcal{H} + M(\mathbf{x}) \mathbf{u} \quad (1.4b)$$

satisfying

$$\dot{\mathcal{H}} = \mathbf{u}^\top \mathbf{y} - [\partial_{\mathbf{x}} \mathcal{H}]^\top R(\mathbf{x}) \partial_{\mathbf{x}} \mathcal{H} \leq \mathbf{u}^\top \mathbf{y} \quad (1.5)$$

Similarly, if $M(\mathbf{x}) = 0$ the ODEs (1.4) are simply called input-state-output port-Hamiltonian system. Moreover, PHS are associated to a geometric structure named Dirac structure. In this respect, according to [44, p. 48] the skew-symmetric matrix $J(\mathbf{x}) = -J^\top(\mathbf{x})$ must satisfy an integrability condition associated with the Jacobi identity, i.e., for every $\mathcal{E}, \mathcal{F}, \mathcal{G} : \mathcal{X} \rightarrow \mathbb{R}$, then

$$\{\mathcal{E}, \{\mathcal{F}, \mathcal{G}\}\} + \{\mathcal{F}, \{\mathcal{G}, \mathcal{E}\}\} + \{\mathcal{G}, \{\mathcal{E}, \mathcal{F}\}\} = 0 \quad (1.6)$$

where $\{\mathcal{F}, \mathcal{G}\} = [\partial_{\mathbf{x}} \mathcal{F}]^\top J(\mathbf{x}) \partial_{\mathbf{x}} \mathcal{G}$ is the Poisson bracket on \mathcal{X} . If the integrability condition (1.6) is not satisfied, then, the structure generated by (1.1)-(1.3) is called pseudo-Dirac structure, and the system described in Definition 1.1 is considered as a pseudo port-Hamiltonian system (see [44, 42] for details). Notice that, in the linear case the skew-symmetric matrix $J = -J^\top$ is constant and satisfies directly the Jacobi identity, i.e., all linear PHS generate a Dirac structure.

1.2.1.a Interconnection of port-Hamiltonian systems

An advantage of PHS is the use of the energy as *lingua franca*. This allows the coupling of two subsystems defined on different physical domains through a power-preserving interconnection. In this sense, according to [44] two types of power-preserving interconnections are commonly used in the PHS framework: the interconnection by ports and the interconnection by energy.

To explain these interconnection methods, consider two PHS in the form:

$$\dot{\mathbf{x}}_j = [J_j - R_j] \partial_{\mathbf{x}_j} \mathcal{H}_j + G_j \mathbf{u}_j \quad (1.7a)$$

$$\mathbf{y}_j = G_j^\top \partial_{\mathbf{x}_j} \mathcal{H}_j \quad (1.7b)$$

with $j \in \{1, 2\}$.

The *interconnection by ports* is used when the ports of the two systems are compatible, i.e., the power transfer between the systems is given by $\bar{\mathbf{u}}_1^\top \bar{\mathbf{y}}_1 = -\bar{\mathbf{u}}_2^\top \bar{\mathbf{y}}_2$, where $\bar{\mathbf{u}}_j \subseteq \mathbf{u}_j$ and $\bar{\mathbf{y}}_j \subseteq \mathbf{y}_j$, such that $\{\bar{\mathbf{u}}_j, \bar{\mathbf{y}}_j\}$ define the connection ports of the system j . Then, the two systems can be coupled using the following interconnection rule:

$$\begin{bmatrix} \bar{\mathbf{u}}_1 \\ \bar{\mathbf{u}}_2 \end{bmatrix} = C \begin{bmatrix} \bar{\mathbf{y}}_1 \\ \bar{\mathbf{y}}_2 \end{bmatrix} \quad (1.8)$$

where $C = -C^\top$ is the coupling matrix. To illustrate this method, let us consider a mass-spring system, as shown in Figure 1.4a. The potential energy stored by the spring is given

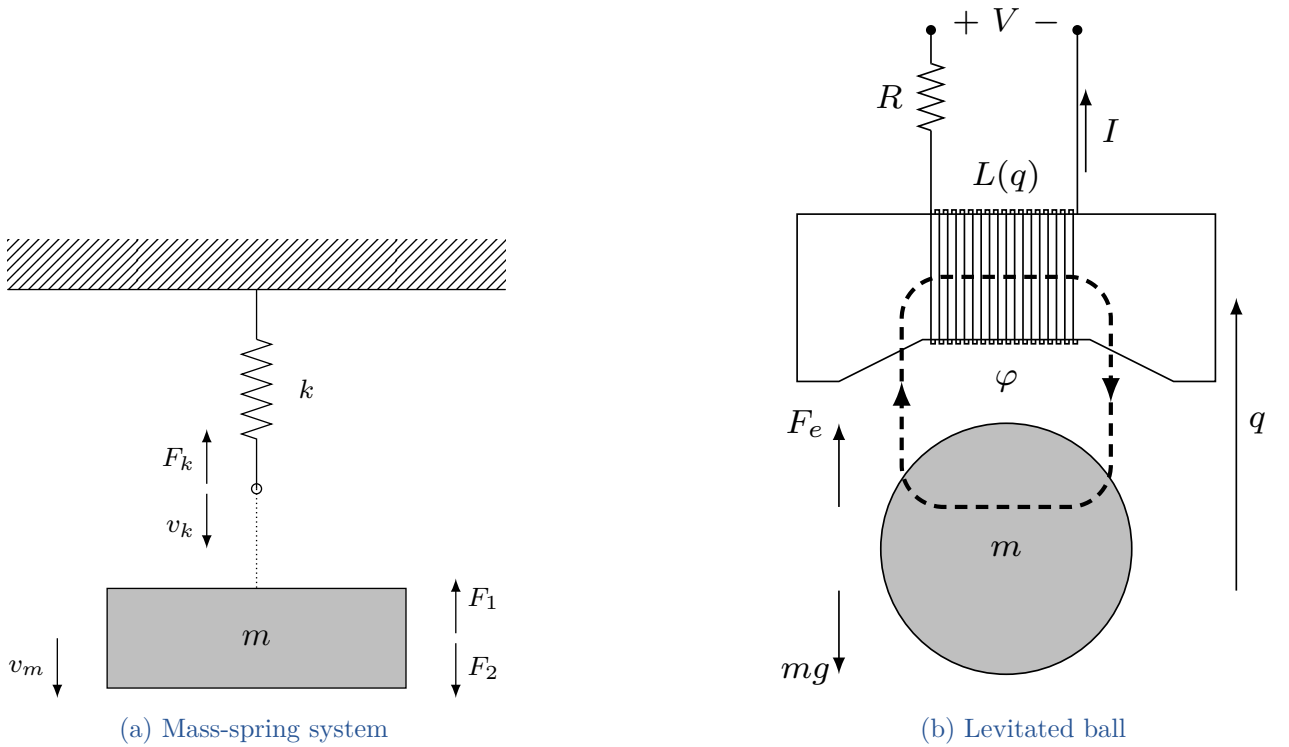


Figure 1.4 – Illustrative examples of power-preserving interconnections. a) Mass-spring system uses interconnection by ports b) levitated ball uses interconnection by energy.

by $\mathcal{H}_k = \frac{1}{2}kq^2$ where k and q are the spring coefficient and elongation, respectively, and $F_k = \partial_q \mathcal{H}_k = kq$ is the restoring force associated with q . Then, the PHS model for this spring is given by:

$$\begin{aligned} \underbrace{\dot{q}}_{\mathbf{x}_1} &= 0 \partial_q \mathcal{H}_k + \underbrace{v_k}_{\mathbf{u}_1} \\ \underbrace{F_k}_{\mathbf{y}_1} &= \partial_q \mathcal{H}_k \end{aligned}$$

Similarly, the kinetic energy stored by the mass is given by $\mathcal{H}_m = \frac{1}{2}p^2/m$ where $p = mv_m$ and $v_m = \partial_p \mathcal{H}_k = p/m$ denote the mass momentum and velocity, respectively. Then, the PHS formulation of the mass dynamics is expressed as:

$$\underbrace{\dot{p}}_{\mathbf{x}_2} = 0 \partial_p \mathcal{H}_m + \begin{bmatrix} -1 & 1 \end{bmatrix} \underbrace{\begin{bmatrix} F_1 \\ F_2 \end{bmatrix}}_{\mathbf{u}_2}$$

$$\underbrace{\begin{bmatrix} -v_m \\ v_m \end{bmatrix}}_{\mathbf{y}_2} = \begin{bmatrix} -1 \\ 1 \end{bmatrix} \partial_p \mathcal{H}_m$$

Notice that the power transfer between the mass and the spring is given by $v_k F_k = v_m F_1$. Then, defining the connection ports $\{\bar{\mathbf{u}}_1, \bar{\mathbf{y}}_1\} = \{v_k, F_k\}$ and $\{\bar{\mathbf{u}}_2, \bar{\mathbf{y}}_2\} = \{F_1, -v_m\}$, mass and spring can be coupled using the interconnection:

$$\begin{bmatrix} \bar{\mathbf{u}}_1 \\ \bar{\mathbf{u}}_2 \end{bmatrix} = C \begin{bmatrix} \bar{\mathbf{y}}_1 \\ \bar{\mathbf{y}}_2 \end{bmatrix} \implies \begin{bmatrix} v_k \\ F_1 \end{bmatrix} = \begin{bmatrix} 0 & -1 \\ 1 & 0 \end{bmatrix} \begin{bmatrix} F_k \\ -v_m \end{bmatrix}$$

leading to the following mass-spring PHS model:

$$\begin{bmatrix} \dot{q} \\ \dot{p} \end{bmatrix} = \begin{bmatrix} 0 & 1 \\ -1 & 0 \end{bmatrix} \begin{bmatrix} \partial_q \mathcal{H} \\ \partial_p \mathcal{H} \end{bmatrix} + \begin{bmatrix} 0 \\ 1 \end{bmatrix} F_2$$

$$v_m = \begin{bmatrix} 0 & 1 \end{bmatrix} \begin{bmatrix} \partial_q \mathcal{H} \\ \partial_p \mathcal{H} \end{bmatrix}$$

where $\mathcal{H} = \mathcal{H}_k + \mathcal{H}_m$.

Regarding the *interconnection by energy*, it is used when the ports are not compatible and the energy of one or both systems are linked such that the coupling is only possible considering a combination of the two energies. Consider for example a magnetically levitated iron ball system, as shown in Figure 1.4b. In this case, the potential and kinetic energy stored by the ball is given by $\mathcal{H}_b = mgq + \frac{1}{2}p^2/m$ where m , q and p are the mass, position and momentum of the ball, respectively, and g is the gravity acceleration, such that $F_g = \partial_q \mathcal{H}_b = mg$ is the gravitational force acting on the ball and $v_b = \partial_p \mathcal{H}_b = p/m$ is the corresponding displacement velocity. Then, considering that the momentum balance is given by $\dot{p} = -F_g + F_e$, where F_e is the force induced by the electromagnetic field, and $\dot{q} = v_b$, the PHS model of the ball is given by:

$$\underbrace{\begin{bmatrix} \dot{q} \\ \dot{p} \end{bmatrix}}_{\mathbf{x}_1} = \begin{bmatrix} 0 & 1 \\ -1 & 0 \end{bmatrix} \begin{bmatrix} \partial_q \mathcal{H}_b \\ \partial_p \mathcal{H}_b \end{bmatrix} + \begin{bmatrix} 0 \\ 1 \end{bmatrix} \underbrace{F_e}_{\mathbf{u}_1}$$

$$\underbrace{v_b}_{\mathbf{y}_1} = \begin{bmatrix} 0 & 1 \end{bmatrix} \begin{bmatrix} \partial_q \mathcal{H}_b \\ \partial_p \mathcal{H}_b \end{bmatrix}$$

On the other hand, the energy stored by the electric circuit is given by $\mathcal{H}_e = \frac{1}{2}\varphi^2/L(q)$ where φ is the magnetic flux-linkage of the inductor, $L(q)$ is the corresponding inductance, and $I = \partial_\varphi \mathcal{H}_e$ denotes the circuit current. Then, the corresponding PHS model is expressed as:

$$\begin{aligned} \underbrace{\dot{\varphi}}_{\mathbf{x}_2} &= -R\partial_\varphi \mathcal{H}_e + \underbrace{V}_{\mathbf{u}_2} \\ \underbrace{I}_{\mathbf{y}_2} &= \partial_\varphi \mathcal{H}_e \end{aligned}$$

where R is the resistance and V denotes the source voltage. In this case, the ports $\{\mathbf{u}_1, \mathbf{y}_1\}$ and $\{\mathbf{u}_2, \mathbf{y}_2\}$ are not compatible, hence an interconnection by ports is not possible. However, given the dependence of the inductance L on the ball position q , the force induced by the electromagnetic field on the ball can be expressed as $F_e = -\partial_q \mathcal{H}_e = \left(\frac{\varphi}{L(q)}\right)^2 \partial_q L(q)$, i.e., the coupling of the electric and the mechanical systems is obtained by combining the energy of the two systems, $\mathcal{H} = \mathcal{H}_b + \mathcal{H}_e$, such that $F_g - F_e = \partial_q \mathcal{H}$. Thus, the coupled system is described as:

$$\begin{aligned} \begin{bmatrix} \dot{q} \\ \dot{p} \\ \dot{\varphi} \end{bmatrix} &= \begin{bmatrix} 0 & 1 & 0 \\ -1 & 0 & 0 \\ 0 & 0 & -R \end{bmatrix} \begin{bmatrix} \partial_q \mathcal{H} \\ \partial_p \mathcal{H} \\ \partial_\varphi \mathcal{H} \end{bmatrix} + \begin{bmatrix} 0 \\ 0 \\ 1 \end{bmatrix} V \\ I &= \begin{bmatrix} 0 & 0 & 1 \end{bmatrix} \begin{bmatrix} \partial_q \mathcal{H} \\ \partial_p \mathcal{H} \\ \partial_\varphi \mathcal{H} \end{bmatrix} \end{aligned}$$

This example illustrates how two systems can be interconnected by energy. In the case of FSI problem, the mechanical and the fluid subsystems are described using finite-dimensional PHS models that have ports associated with the velocities and the forces on the contact surface between the two subsystem. This implies a compatibility to make an interconnection by ports. However, notice that the fluid domain varies according to the structure motion. This implies that the fluid energy is linked to the state variables of the structure model, and, as a consequence, additional driving forces appear when both system are coupled. To solve this problem, in [57], for example, an additional state variable is included in the fluid model to describe the changes in the fluid domain. In this thesis, we propose a power-preserving interconnection that combine the properties of the interconnection by ports and by energy, as shown in Chapters 3 and 4, guarantying that the kinematic and dynamic conditions, described in Section 1.1, are satisfied.

1.2.2 Infinite-dimensional port-Hamiltonian systems

When the PHS are defined on infinite dimensional domains Ω with boundary $\partial\Omega$, the state variables depends on time t and on the spatial variable ζ , i.e., $\mathbf{x} = \mathbf{x}(\zeta, t) \in L^2(\Omega, \mathbb{R}^n)$. Similarly, the total energy is defined as a functional in Ω , i.e., $\mathcal{H} = \mathcal{H}(\mathbf{x}) \in \mathcal{F}$, where \mathcal{F} denotes the space of smooth functionals of the form:

$$\mathcal{F}(\mathbf{x}) = \int_{\Omega} f(\mathbf{x}) d\Omega \quad (1.9)$$

with $f(\mathbf{x})$ as a smooth function that defines the density of \mathcal{F} in Ω , and satisfies $\delta_{\mathbf{x}}\mathcal{F} = \partial_{\mathbf{x}}f(\mathbf{x})$, where $\delta_{\mathbf{x}}\mathcal{F} = \frac{\delta\mathcal{F}}{\delta\mathbf{x}}$ denotes the variational derivative of the functional \mathcal{F} , that is defined as the unique function that satisfy:

$$\mathcal{F}(\mathbf{x} + \varepsilon\delta\mathbf{x}) = \mathcal{F}(\mathbf{x}) + \varepsilon \int_{\Omega} \delta_{\mathbf{x}}\mathcal{F}\delta\mathbf{x}d\Omega + O(\varepsilon^2) \quad (1.10)$$

for every $\varepsilon \in \mathbb{R}$ and smooth real function $\delta\mathbf{x}(\zeta), \zeta \in \Omega$, such that their derivatives satisfy $\delta^{(j)}\mathbf{x}(\zeta)|_{\partial\Omega} = 0, j = 0, \dots, n$ [58, 42].

In infinite-dimensional PHS the driving forces are given by the variational derivative of the total energy functional, $\delta_{\mathbf{x}}\mathcal{H}$, and the dynamics are described using a Hamiltonian differential operator acting on $\delta_{\mathbf{x}}\mathcal{H}$. A Hamiltonian operator is defined as follows.

Definition 1.2. [58] *A linear operator \mathcal{J} is called Hamiltonian if it satisfies the following conditions for every $(\mathcal{F}, \mathcal{G}, \mathcal{E}) \in \mathcal{F}$:*

a.- *Skew-symmetry:*

$$\{\mathcal{F}, \mathcal{G}\}_{\mathcal{J}} = -\{\mathcal{G}, \mathcal{F}\}_{\mathcal{J}} \quad (1.11)$$

b.- *Jacobi identity:*

$$\{\mathcal{F}, \{\mathcal{G}, \mathcal{E}\}_{\mathcal{J}}\}_{\mathcal{J}} + \{\mathcal{G}, \{\mathcal{E}, \mathcal{F}\}_{\mathcal{J}}\}_{\mathcal{J}} + \{\mathcal{E}, \{\mathcal{F}, \mathcal{G}\}_{\mathcal{J}}\}_{\mathcal{J}} = 0 \quad (1.12)$$

where $\{\mathcal{F}, \mathcal{G}\}_{\mathcal{J}} = \int_{\Omega} (\delta_{\mathbf{x}}\mathcal{F})^{\top} \mathcal{J} \delta_{\mathbf{x}}\mathcal{G}d\Omega$, with boundary conditions equal to 0, denotes a Poisson bracket on infinite-dimensional domains.

In [39] a parametrization of the boundary flow and effort variables is given in order to define a Dirac structure for 1D linear systems and then to define a PHS described by PDEs in the form $\partial_t\mathbf{x} = \mathcal{J}\delta_{\mathbf{x}}\mathcal{H}$, where $\delta_{\mathbf{x}}\mathcal{H} = \mathcal{L}\mathbf{x}$, with $\mathcal{L} = \mathcal{L}^{\top} \geq 0 \in \mathbb{R}^{n \times n}$, and \mathcal{J} is a Hamiltonian operator of order n , in a domain $\Omega := \{\zeta \in [a, b] \subset \mathbb{R}\}$, defined as:

$$\mathcal{J}\mathbf{e} = \sum_{j=0}^n P_j \partial_{\zeta}^j \mathbf{e}, \quad \zeta \in [a, b] \quad (1.13)$$

with $P_j = (-1)^{j+1} P_j^{\top}$. The parameterization of the boundary flow and effort port variables, \mathbf{f}_{∂} and \mathbf{e}_{∂} respectively, is given in terms of matrices P_1, P_2, \dots, P_n and the system efforts $\delta_{\mathbf{x}}\mathcal{H}$ at the boundary. These boundary port variables are used to define the system inputs and outputs, $\mathbf{u}(t)$ and $\mathbf{y}(t)$ respectively, using full rank matrices W_b and W_c such that $\begin{bmatrix} W_b \\ W_c \end{bmatrix}$ is invertible and

$$W_b \Sigma W_b^{\top} \geq 0 \quad (1.14)$$

where $\Sigma = \begin{bmatrix} \mathbf{0} & \mathbf{I} \\ \mathbf{I} & \mathbf{0} \end{bmatrix}$. This parametrization of the boundary flow and effort port variables and the system inputs and outputs, guarantee the existence of solutions and the exponential stability of linear systems, i.e., the PHS is well-posed [39, 43].

In this Thesis only differential operators of order 1 are used, i.e., in the case of 1D linear systems the Hamiltonian operators is defined as:

$$\mathcal{J}\mathbf{e} = P_1\partial_\zeta\mathbf{e} + P_0\mathbf{e}, \quad \zeta \in [a, b] \quad (1.15)$$

where $P_1 = P_1^\top$ and $P_0 = -P_0^\top$.

Definition 1.3. [39] *Let $\mathcal{H} \in \mathcal{F}$ be the total energy of a linear 1D dynamical system with state variables $\mathbf{x} = [x_1 \cdots x_n]^\top$. Then, the impedance passive port-Hamiltonian formulation is given by:*

$$\partial_t\mathbf{x} = \mathcal{J}\delta_x\mathcal{H} \quad (1.16a)$$

$$\mathbf{u}(t) = W_b \begin{bmatrix} \mathbf{f}_\partial \\ \mathbf{e}_\partial \end{bmatrix} \quad (1.16b)$$

$$\mathbf{y}(t) = W_c \begin{bmatrix} \mathbf{f}_\partial \\ \mathbf{e}_\partial \end{bmatrix} \quad (1.16c)$$

where $\begin{bmatrix} W_b \\ W_c \end{bmatrix}$ invertible, such that

$$W_c\Sigma W_c^\top = W_b\Sigma W_b^\top = \mathbf{0} \text{ and } W_b\Sigma W_c^\top = \mathbf{I} \quad (1.17)$$

satisfying the balance equation

$$\dot{\mathcal{H}} = \mathbf{f}_\partial^\top \mathbf{e}_\partial = \mathbf{y}^\top \mathbf{u} \quad (1.18)$$

with the boundary port variables $(\mathbf{f}_\partial, \mathbf{e}_\partial)$ defined as

$$\begin{bmatrix} \mathbf{f}_\partial \\ \mathbf{e}_\partial \end{bmatrix} = R_{ext} \begin{bmatrix} \delta_x\mathcal{H}|_b \\ \delta_x\mathcal{H}|_a \end{bmatrix} \quad (1.19)$$

where $R_{ext} = \frac{1}{\sqrt{2}} \begin{bmatrix} P_1 & -P_1 \\ \mathbf{I} & \mathbf{I} \end{bmatrix}$ is invertible and satisfies $R_{ext}^\top \Sigma R_{ext} = \begin{bmatrix} P_1 & 0 \\ 0 & -P_1 \end{bmatrix}$.

Notice that the previous definition provides a basic PHS formulation for non-dissipative system with differential operators of order 1. For a general formulation with 1D operators of order n see [39]. The case of dissipative systems is considered in [40], extending the port-Hamiltonian approach for PDEs of the form:

$$\partial_t\mathbf{x} = \mathcal{J}\delta_x\mathcal{H} - \mathcal{G}^*S\mathcal{G}\delta_x\mathcal{H} \quad (1.20)$$

where the term $\mathcal{G}^*S\mathcal{G}\delta_x\mathcal{H}$ describes the dissipative elements of the system, with $\mathcal{G}^* = -G_1^\top\partial_\zeta + G_0^\top$ as the formal adjoint of the 1D operator $\mathcal{G} = G_1\partial_\zeta + G_0$ and S is a coercive operator on $L^2(\Omega, \mathbb{R}^n)$, i.e., there exist a $c > 0$ such that $\langle S\mathbf{x}, \mathbf{x} \rangle_{L^2} \geq c \langle \mathbf{x}, \mathbf{x} \rangle_{L^2}$.

Definition 1.4. [40] Let $\mathcal{H} \in \mathcal{F}$ be the total energy of a dynamic system with state variables $\mathbf{x} = [x_1, \dots, x_n]^\top$. Denoting by $\mathbf{f}_R = \mathcal{G}\delta_x\mathcal{H}$ and $\mathbf{e}_R = S\mathbf{f}_R$ the flows and efforts associated with the system power dissipation. Then, the associated dissipative port-Hamiltonian system is given by:

$$\begin{bmatrix} \partial_t \mathbf{x} \\ \mathbf{f}_R \end{bmatrix} = \begin{bmatrix} \mathcal{J} & -\mathcal{G}^* \\ \mathcal{G} & 0 \end{bmatrix} \begin{bmatrix} \delta_x \mathcal{H} \\ \mathbf{e}_R \end{bmatrix} \quad (1.21a)$$

$$\mathbf{u}(t) = W_c \begin{bmatrix} \mathbf{f}_\partial \\ \mathbf{e}_\partial \end{bmatrix} \quad (1.21b)$$

$$\mathbf{y}(t) = W_b \begin{bmatrix} \mathbf{f}_\partial \\ \mathbf{e}_\partial \end{bmatrix} \quad (1.21c)$$

where $\begin{bmatrix} W_c \\ W_b \end{bmatrix}$ invertible, such that

$$W_c \Sigma W_c^\top = W_b \Sigma W_b^\top = \mathbf{0} \text{ and } W_b \Sigma W_c^\top = \mathbf{I} \quad (1.22)$$

satisfying the balance equation

$$\dot{\mathcal{H}} \leq \mathbf{y}^\top \mathbf{u} \quad (1.23)$$

with the boundary port variables $(\mathbf{f}_\partial, \mathbf{e}_\partial)$ defined as

$$\begin{bmatrix} \mathbf{f}_\partial \\ \mathbf{e}_\partial \end{bmatrix} = R_{ext} \begin{bmatrix} \delta_x \mathcal{H}|_b \\ \mathbf{e}_R|_b \\ \delta_x \mathcal{H}|_a \\ \mathbf{e}_R|_a \end{bmatrix} \quad (1.24)$$

where $R_{ext} = \frac{1}{\sqrt{2}} \begin{bmatrix} \tilde{P}_1 & -\tilde{P}_1 \\ \mathbf{I} & \mathbf{I} \end{bmatrix}$ is invertible and satisfies $R_{ext}^\top \Sigma R_{ext} = \begin{bmatrix} \tilde{P}_1 & \mathbf{0} \\ \mathbf{0} & -\tilde{P}_1 \end{bmatrix}$ with $\tilde{P}_1 = \begin{bmatrix} P_1 & G_1^\top \\ G_1 & \mathbf{0} \end{bmatrix}$.

The port-Hamiltonian formulations (1.3) and (1.21) can also be extended to multi-dimensional systems, as shown [59, 60, 61] for 2D models of the wave equation and thin plates, and [62] for 3D isentropic compressible fluids with irrotational flows, among others.

It is important to notice that in the above port-Hamiltonian formulations the Hamiltonian operators are independent of the state variables and generate a Dirac structure, see [39, 40] for details. However, in the general nonlinear case, according to [58] a Hamiltonian operator can depend on the state. In this sense, [57, 63] prove that a particular skew-symmetric operator $\mathcal{J}(\mathbf{x})$ of the form $\mathcal{J}\mathbf{e} = \frac{1}{2} [P(\mathbf{x})^\top \partial_\zeta \mathbf{e} + \partial_\zeta (P(\mathbf{x})\mathbf{e})]$ can also generate a Dirac structure.

On the other hand, it is necessary to highlight that the dissipative port-Hamiltonian formulations described in subsections 1.2.1 and 1.2.2 are useful to describe irreversible physical systems where the thermal domain is irrelevant and can be neglected. In problems where the thermodynamic of the system is relevant, as for example exothermic and endothermic chemical reactions, heat exchangers and transport of superheated steam, among others, other

approaches as GENERIC [64] and pseudo port-Hamiltonian formulations are used [65, 66]. In the next section we introduce the irreversible port-Hamiltonian formulation, that is, a pseudo port-Hamiltonian approach focused on the appropriate description of the entropy \mathcal{S} (second law of thermodynamic) to model the thermal domain.

1.2.3 Irreversible port-Hamiltonian systems

An irreversible port-Hamiltonian system is an energy-based formulation focused in the description of irreversible process, proposed initially in [67, 68]. Unlike the dissipative port-Hamiltonian system, where the irreversible phenomena is described through energy dissipative elements, neglecting the thermal effects, in the irreversible port-Hamiltonian approach the thermal domain is described using the entropy as a state variable, including in the port-Hamiltonian structure an element defined by the Poisson brackets that is useful to describe the second law of Thermodynamics in the dynamic equations (see [67, 68] for details).

To describe the thermodynamics we consider first the Gibbs equation:

$$d\mathcal{U} = -pdV + Td\mathcal{S} + \sum_i \nu_i dN_i \quad (1.25)$$

that describes the local variations of the internal energy \mathcal{U} as a function of the intensive variables p , T and ν_i , respectively pressure, absolute temperature and chemical potential of i -th chemical specie; and the variations of the extensive variables V , \mathcal{S} and N_i , respectively the volume, entropy and number of moles of the i -th chemical specie. Equation (1.25) defines the thermodynamic equilibrium of a system where $-pdV + \sum_i \nu_i dN_i$ and $Td\mathcal{S}$ describe the energy contributions by "work" and "heat", respectively, i.e., the Gibbs equation represents a geometric structure in the space of thermodynamic variables, building the thermodynamic framework [69] and it naturally leads to Legendre transformations between thermodynamic potentials, depending on which variables are chosen as the independent ones, (see [69, Appendix A.4] for details).

The finite-dimensional irreversible PHS are defined as follows.

Definition 1.5. [67] *Let $\mathbf{x} \in \mathbb{R}^n$ be the state vector of an irreversible system with total internal energy $\mathcal{U} = \mathcal{U}(\mathbf{x})$ and entropy \mathcal{S} . An irreversible port-Hamiltonian system is defined as*

$$\dot{\mathbf{x}} = R(\mathbf{x}, \partial_{\mathbf{x}}\mathcal{U})J\partial_{\mathbf{x}}\mathcal{U} + W(\mathbf{x}, \partial_{\mathbf{x}}\mathcal{U}) + g(\mathbf{x}, \partial_{\mathbf{x}}\mathcal{U})\mathbf{u} \quad (1.26)$$

where $\mathbf{u} \in \mathbb{R}^m$ is the input vector, $J \in \mathbb{R}^{n \times n}$ is a constant skew-symmetric matrix, the input matrix $g(\mathbf{x}, \partial_{\mathbf{x}}\mathcal{U})$ and vector field $W(\mathbf{x}, \partial_{\mathbf{x}}\mathcal{U})$ are smooth functions that define the input map associated with the ports of the system, and $R(\mathbf{x}, \mathcal{U})$ is the product between the positive function $\gamma = \gamma(\mathbf{x}, \partial_{\mathbf{x}}\mathcal{U}) > 0$ and the Poisson bracket $\{\mathcal{S}, \mathcal{U}\} = [\partial_{\mathbf{x}}\mathcal{S}]^\top J\partial_{\mathbf{x}}\mathcal{U}$, i.e., $R(\mathbf{x}, \partial_{\mathbf{x}}\mathcal{U}) = \gamma\{\mathcal{S}, \mathcal{U}\}$.

Given that $R(\mathbf{x}, \partial_{\mathbf{x}}\mathcal{U})$ depends on $\partial_{\mathbf{x}}\mathcal{U}$, the linearity of any Poisson structure associated with the matrix $R(\mathbf{x}, \partial_{\mathbf{x}}\mathcal{U})J$ is broken. Furthermore, the terms $W(\mathbf{x}, \partial_{\mathbf{x}}\mathcal{U})$ and $g(\mathbf{x}, \partial_{\mathbf{x}}\mathcal{U})$ may also depends on the states variables and $\partial_{\mathbf{x}}\mathcal{U}$.

To analyze the thermodynamic properties of Definition 1.5 consider that the rate of change of the internal energy is given by $\dot{\mathcal{U}} = [\partial_{\mathbf{x}}\mathcal{U}]^\top \dot{\mathbf{x}}$. Then, substituting the irreversible PHS formulation (1.26) we obtain

$$\begin{aligned}\dot{\mathcal{U}} &= R(\mathbf{x}, \partial_{\mathbf{x}}\mathcal{U}) [\partial_{\mathbf{x}}\mathcal{U}]^\top J \partial_{\mathbf{x}}\mathcal{U} + [\partial_{\mathbf{x}}\mathcal{U}]^\top [W(\mathbf{x}, \partial_{\mathbf{x}}\mathcal{U}) + g(\mathbf{x}, \partial_{\mathbf{x}}\mathcal{U})\mathbf{u}] \\ &= [\partial_{\mathbf{x}}\mathcal{U}]^\top [W(\mathbf{x}, \partial_{\mathbf{x}}\mathcal{U}) + g(\mathbf{x}, \partial_{\mathbf{x}}\mathcal{U})\mathbf{u}]\end{aligned}\quad (1.27)$$

Similarly, the rate of change of the entropy is given by

$$\begin{aligned}\dot{\mathcal{S}} &= R(\mathbf{x}, \partial_{\mathbf{x}}\mathcal{U}) [\partial_{\mathbf{x}}\mathcal{S}]^\top J \partial_{\mathbf{x}}\mathcal{U} + [\partial_{\mathbf{x}}\mathcal{S}]^\top [W(\mathbf{x}, \partial_{\mathbf{x}}\mathcal{U}) + g(\mathbf{x}, \partial_{\mathbf{x}}\mathcal{U})\mathbf{u}] \\ &= \gamma\{\mathcal{S}, \mathcal{U}\}^2 + [\partial_{\mathbf{x}}\mathcal{S}]^\top [W(\mathbf{x}, \partial_{\mathbf{x}}\mathcal{U}) + g(\mathbf{x}, \partial_{\mathbf{x}}\mathcal{U})\mathbf{u}]\end{aligned}\quad (1.28)$$

i.e., if there is not exchange with the environment (the system is isolated), $W(\mathbf{x}, \partial_{\mathbf{x}}\mathcal{U}) + g(\mathbf{x}, \partial_{\mathbf{x}}\mathcal{U})\mathbf{u} = 0$, the internal energy is a conserved quantity, $\dot{\mathcal{U}} = 0$, satisfying the first law of thermodynamics, and the entropy balance (1.28) is non-negative and equal to the internal entropy production, $\sigma_{int} = \gamma\{\mathcal{S}, \mathcal{U}\}^2 \geq 0$, satisfying the second law of Thermodynamics. This implies that the irreversible PHS formulation described in Definition 1.5 provides a proper framework to describe finite-dimensional irreversible systems with a thermal domain (see [67, 68] for details).

The extension of this framework to 1D infinite-dimensional systems has been proposed initially in [70] for diffusion processes and extended in [71] for a general formulation of 1D irreversible PHS on infinite-dimensional domains. In this sense, the internal energy and entropy are considered as functionals on the space $\Omega := \{\zeta \in [a, b] \subset \mathbb{R}\}$, i.e.,

$$\mathcal{U} = \int_{\Omega} u(\mathbf{x})d\Omega \quad \text{and} \quad \mathcal{S} = \int_{\Omega} s d\Omega \quad (1.29)$$

where $u(\mathbf{x})$ and s denote the internal energy and entropy per unit length, respectively, and the state is given by $\mathbf{x} = [x_1 \cdots x_{n-1} s]^\top$. Furthermore, considering an incompressible medium with constant volume, the Gibbs equation can be expressed as $du = Tds + \sum_i \nu_i dc_i$ where c_i is the number of moles per unit length of the i -th specie, satisfying that

$$\delta_{\mathbf{x}}\mathcal{S} = \partial_{\mathbf{x}}s = \begin{bmatrix} 0 \\ \vdots \\ 0 \\ 1 \end{bmatrix}, \quad \text{and} \quad \delta_s\mathcal{U} = \partial_s u = T, \quad \zeta \in [a, b] \quad (1.30)$$

Similarly, the following operator is defined as

$$\{\mathcal{F}, \mathcal{E}\}_{\mathcal{J}}^* = [\delta_{\mathbf{x}}\mathcal{F}]^\top \mathcal{J} \delta_{\mathbf{x}}\mathcal{E} \quad (1.31)$$

for every $(\mathcal{F}, \mathcal{E}) \in \mathcal{F}$, where \mathcal{J} is a skew-symmetric operator. The irreversible port-Hamiltonian system can be defined as follows on a 1D infinite dimensional space.

Definition 1.6. [71] Consider the real functions $R_{ij} = \gamma_{ij} \{ \mathcal{S}, \mathcal{U} \}_{\mathcal{J}_{ij}}^*$ where $\gamma_{ij} = \gamma_{ij}(\mathbf{x}, \delta_{\mathbf{x}} \mathcal{U}) \geq 0$ is a nonlinear positive scalar function and $\mathcal{J}_{ij} = P_{ij} \partial_{\zeta}^i$, with $P_{ij} = (-1)^{i+1} P_{ij}^{\top}$, is a Hamiltonian operator. An infinite dimensional irreversible port-Hamiltonian system is defined by the PDE

$$\partial_t \mathbf{x} = \sum_{j=1}^n R_{1j} \mathcal{J}_{1j} \delta_{\mathbf{x}} \mathcal{U} + \sum_{j=1}^n R_{0j} \mathcal{J}_{0j} \delta_{\mathbf{x}} \mathcal{U} + \partial_{\zeta} [\mathbf{R}_1 \delta_{\mathbf{x}} \mathcal{U}], \quad \zeta \in [a, b], \quad (1.32)$$

with boundary inputs and outputs given by

$$\mathbf{u}(t) = \begin{bmatrix} [\mathbf{R}_1 \delta_{\mathbf{x}} \mathcal{U}]|_b \\ [\mathbf{R}_1 \delta_{\mathbf{x}} \mathcal{U}]|_a \end{bmatrix} \quad \text{and} \quad \mathbf{y}(t) = \begin{bmatrix} \delta_{\mathbf{x}} \mathcal{U}|_b \\ -\delta_{\mathbf{x}} \mathcal{U}|_a \end{bmatrix}, \quad (1.33)$$

respectively, where $\mathbf{R}_1 = [R_{11} \ \cdots \ R_{1n}]^{\top}$ satisfies

$$\sum_{j=1}^n R_{1j} \mathcal{J}_{1j} \delta_{\mathbf{x}} \mathcal{U} = \begin{bmatrix} 0 \\ \vdots \\ 0 \\ \mathbf{R}_1^{\top} \partial_{\zeta} [\delta_{\mathbf{x}} \mathcal{U}] \end{bmatrix} \quad (1.34)$$

such that

$$\dot{\mathcal{U}} = \mathbf{u}^{\top} \mathbf{y} \quad \text{and} \quad \dot{\mathcal{S}} = \int_a^b \sigma_{int} d\zeta + (R_{1n} \delta_{\mathbf{x}} \mathcal{U})|_a^b \quad (1.35)$$

where σ_{int} is a non-negative function that describes the internal entropy production.

Notice that according to (1.35) the rate of change of the total internal energy stored by the system (1.32) is given by the power supplied through the boundary ports. Similarly, if (1.32) is a closed system, i.e., $\mathbf{u} = 0, \forall t$, then $\dot{\mathcal{U}} = 0$ and $\dot{\mathcal{S}} \geq 0$, satisfying the first and second law of thermodynamics, respectively.

1.3 THESIS ORGANIZATION AND CONTRIBUTIONS

To describe the FSI in a longitudinal domain, in Chapters 2-4 we propose a finite-dimensional model of the structure and the fluid subsystems based on the port-Hamiltonian framework. This allows us to avoid the use of moving-mesh and remeshing algorithms and stabilization methods, like SUPG or PSPG, and provides an appropriate power-transfer fluid-structure coupling, simplifying the FSI model. In Chapter 5, we propose an energy-based infinite-dimensional modeling for isentropic and non-isentropic Newtonian fluids.

In Chapter 2 two examples, a flexible tube and the vocal folds, are used to illustrate the structure mass-spring-damper formulation. The flexible tube example describes the methodology to obtain a scalable PHS-based mass-spring-damper model, assuming an axi-symmetric behavior of the tube motion. In the case of the vocal folds, a PHS formulation of the well-known body-cover model [72] is proposed, without the use of auxiliary variables to describe the tissue deformation during the vocal fold collisions, reducing the number of state variables, in comparison with others PHS-based models [73, 74].

In Chapter 3, a scalable PHS model of incompressible isentropic fluids is developed, introducing the use of an instrumental element, called node, that allows, from a port-Hamiltonian point of view, an appropriate coupling of the incompressible fluid sections. Additionally, a power-preserving interconnection that combines the properties of the interconnection by ports and by energy, is proposed for fluid-structure coupling.

Chapter 4 shows the development of a scalable PHS model of compressible isentropic fluids. Considering an irrotational flow and other constraints that allows to reduce the fluid analysis to a 1D model. Similarly, a switched power-preserving fluid-structure interconnection is proposed, focused in allowing a structure elastic collision, useful to describe systems as the vocal folds.

Finally, in Chapter 5 several energy-based infinite dimensional formulations are proposed for non-reactive compressible fluids. General pseudo and dissipative port-Hamiltonian models are developed for the non-isentropic and isentropic Newtonian compressible fluids, respectively, including the operator considerations to preserve the model structure in 1D and 2D fluids cases. Additionally, the thermodynamic properties of the internal energy per unit mass and the use of an availability function in the total energy description in previous models is also discussed. Similarly, an irreversible PHS formulation is proposed for 1D non-reactive fluids.

1.4 ASSOCIATED PUBLICATIONS

As a result of the work presented in this thesis, the following papers have been published:

- Mora, L. A., Yuz, J. I., Ramírez, H., & Le Gorrec, Y. (2018). *A port-Hamiltonian Fluid-Structure Interaction Model for the Vocal folds*. IFAC-PapersOnLine, 51(3), 62-67. 6th IFAC Workshop on Lagrangian and Hamiltonian Methods for Nonlinear Control LHMNC 2018.
<https://doi.org/10.1016/j.ifacol.2018.06.016>
- Mora, L. A., Ramírez, H., Yuz, J. I., & Le Gorrec, Y. (2019). *A Scalable port-Hamiltonian Model for Incompressible Fluids in Irregular Geometries*. IFAC-PaperOnline, 52 (2) 102-107. 3rd IFAC Workshop on Control of Systems Governed by Partial Differential Equations CPDE 2019, page 102-107.
<https://doi.org/10.1016/j.ifacol.2019.08.018>
- Mora, L. A., Le Gorrec, Y., Matignon D., Ramírez, H. & Yuz, J (2020). *About dissipative and pseudo Port-Hamiltonian Formulations of irreversible Newtonian Compressible Flows*. 21st IFAC World Congress in Berlin, Germany.
- Mora, L.A., Le Gorrec, Y., Ramírez, H., & Yuz, J. (2020) *Fluid-Structure Port-Hamiltonian Model for Incompressible Flows in Tubes with Time Varying Geometries*. Mathematical and Computer Modelling of Dynamical Systems, 26, 409–433.
- Mora, L.A., Ramírez, H., Yuz, J.I., Le Gorrec, Y., & Zañartu, M. (2020) *Energy-based fluid-structure model of the vocal folds*. IMA Journal of Mathematical Control and Information, DOI: 10.1093/imamci/dnaa031.

Mechanical description of the structure

In this thesis we consider FSI systems where the mechanical structure motion is transverse with respect to the fluid flow, as shown in Figure 2.1a. From a material point of view, this flexible structure, according to its material nature, is commonly described by hyper-elastic or elastic models.

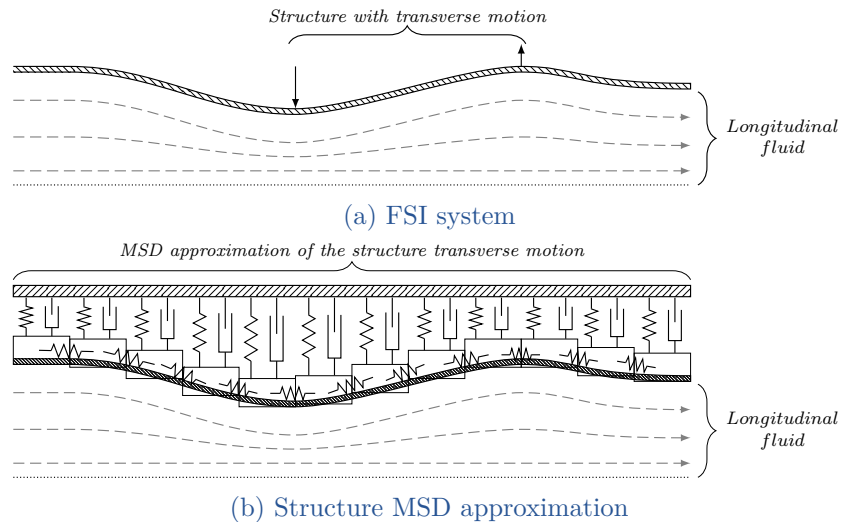


Figure 2.1 – Mechanical description of the structure motion

In the literature, different formulations to model elastic and hyper-elastic material can be found, such as the Mooney-Rivlin, Neo-Hookean and polynomial models [75], and the well known Saint Venant-Kirchhoff model (SVK) and its linearized form [76]. Similarly, to describe the dissipation associated with the conversion of kinetic energy into heat by the material motion, different approaches have been proposed, as for example the standard linear solid, Maxwell and Burgers formulations [77] and the Kelvin-Voigt approach [78]. These models require of numerical schemes for their simulation and to obtain a detailed description of the material motion, such as spatial discretization schemes, like finite-elements or finite-volumes methods, coupling algorithms for the interaction with fluids [76], and appropriate time discretization to guarantee the numerical stability of the simulation [79, 10, 12].

In this chapter we focus on two case studies for structures that have transverse motion to a fluid flow: flexible tubes and vocal folds.

Contribution

To reduce the complexity in modeling of elastic or hyper-elastic materials, we propose the use of interconnected mass-spring-damper (MSD) systems to describe the transverse motion of the structure, as shown in Figure 2.1b. These models are described using the port-Hamiltonian framework. For the flexible tube case we propose a scalable MSD model and for the vocal folds case we propose an alternative port-Hamiltonian formulation of the body-cover model [72], that reduces the number of state variables, in comparison with other energy-based models in the literature [73].

2.1 FLEXIBLE TUBE MODEL

In this section we consider a cylindrical and flexible tube with inner radius r , length L and thickness h , as shown in Figure 2.2. According to [10], flexible tubes have special relevance in biological applications, such as the interaction between the elastic arteries and the blood flow [22] or the phono-respiratory system [80], among others. This class of structures has been studied using multi-layer [10] and single-layer [12] materials approaches. The interaction between this class of flexible tubes and some internal fluid flows has been a relevant benchmark to test the accuracy of numerical methods suitable for the simulation of FSI problems, such as partitioned [10, 9, 81, 82, 83] and monolithic [12, 18, 84] finite-element schemes, and mesh-free finite pointset methods [85]. To simplify the analysis and to obtain a MSD formulation, we consider the following assumptions:

Assumption 2.1. *To describe the flexible vessel as a mass-spring damper system we make the following assumptions:*

- *The material is isotropic.*
- *The motion of tube walls is only radial.*
- *The motion is axisymmetric.*

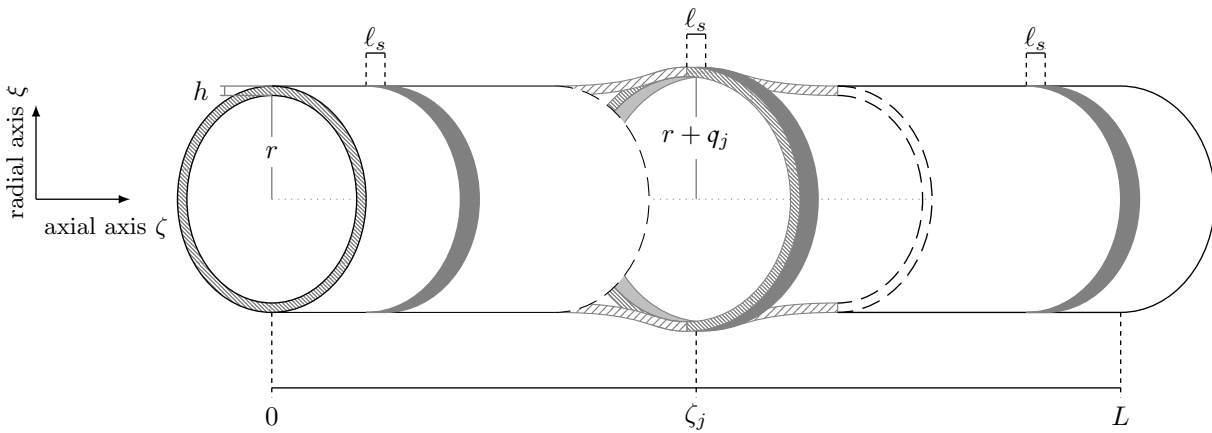


Figure 2.2 – Cylindrical flexible tube description.

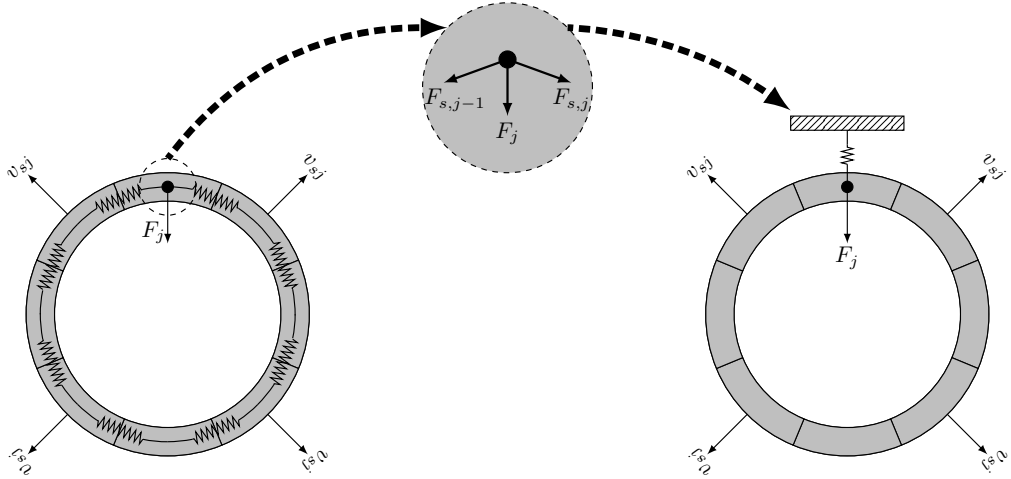


Figure 2.3 – Cross-sectional view of the flexible tube and the forces acting at a point by an axisymmetric circumferential strain. The expansion velocity v is axisymmetric.

2.1.1 Mass-spring-damper model

In order to derive a MSD formulation of the system shown in Figure 2.1b, we divide the flexible tube in n_s sections of length $\ell_s = L/n_s$, as shown in Figure 2.2, i.e., we divide the axial axis in n_s parts and we analyze the radial motion of the structure at $x \in \{\zeta_1, \dots, \zeta_{n_s}\}$ where $\zeta_j = (j - 1/2)\ell_s$ is the axial coordinate of the j -th tube section. The mass of each section is given by:

$$m_j = 2\pi\rho_s r h \ell_s \quad (2.1)$$

where ρ_s is the material density. Denoting by q_j the average radial displacement of j -th section and by $\pi_{sj} = m_j v_{sj}$ the corresponding momentum, the motion of the j -th section is given by:

$$\dot{q}_j = v_{sj} \quad (2.2a)$$

$$\dot{\pi}_{sj} = \sum F \quad (2.2b)$$

where v_{sj} is the average expansion velocity and $\sum F$ denotes the sum of forces acting on section j . The equivalent springs and dampers in each section are deduced from the restoring forces exercised by the material. In the case of springs, these forces are given by the circumferential and shear strains of the tube.

Figure 2.3 shows a cross-sectional view of the j -th tube section at $\zeta = \zeta_j$. From Assumption 2.1, the velocity of the structure circumference is uniform, then, the tube expansion is axisymmetric and the forces associated with circumferential strains acting on an arbitrary point of section j induce an inward radial force when the tube expands. This inward force can be characterized by a radial spring, as shown on the right hand side of Figure 2.3. Assuming a linear behavior of this radial spring, the inward force F_j is given by:

$$F_j = -k_j q_j \quad (2.3)$$

where k_j is the corresponding spring coefficient.

Similarly, the force associated with the shear strain between two adjacent section is modeled through a coupling spring.

$$F_{cj} = -k_{cj} (q_j - q_{j+1}) \quad (2.4)$$

where k_{cj} is the coefficient of the coupling spring.

Coefficients k_j and k_{cj} are obtained from the material properties and are given by [86]:

$$k_j = \beta_1 \lambda \frac{\ell_s h}{\pi r} \quad (2.5)$$

$$k_{cj} = \beta_2 \mu \frac{\pi r h}{\ell_s} \quad (2.6)$$

where λ and μ are the Lamé coefficients, and β_1 and β_2 are dimensionless factors.

On the other hand, the dissipation induced by the motion of the section is described by a damper, whose force is given by:

$$F_{dj} = -d_j v_{sj} \quad (2.7)$$

where $d_j \geq 0$ is the damper coefficient. In this work we consider a Kelvin-Voigt model [77], i.e., the force F_{dj} corresponds to one damper in parallel with the j -th radial spring, as shown in Figure 2.1b. From a material point view, the parameters associated with the dissipative terms of the stress tensor can be parametrized as the product between the Lamé's parameters (responsible of the elasticity) and time terms responsible of the viscosity [87, eq. (8)]. In this sense, we define the damper coefficients as $d_j = k_j \eta_j$ where η_j is a time parameter associated with the viscosity. For simplicity, it is convenient to express η_j as a function of the mass and the spring coefficient of the j -th section, and a dimensionless damping factor λ_s , i.e., $\eta_j = \lambda_s \sqrt{\frac{m_j}{k_j}}$, obtaining the simple formula [72, 88],

$$d_j = \lambda_s \sqrt{m_j k_j} \quad (2.8)$$

Considering the restoring forces associated with the strain and dissipation in each tube section, (2.3), (2.4) and (2.7), the sum of forces acting on the j -th section is given by $\sum F = F_j + F_{cj} - F_{cj-1} + F_{dj} + F_{ej}$, where F_{ej} denotes the external forces. Then, the governing equations of the j -th tube section can be expressed as:

$$\dot{q}_j = v_{sj} \quad (2.9a)$$

$$\dot{\pi}_{sj} = F_j + F_{cj} - F_{cj-1} + F_{dj} + F_{ej} \quad (2.9b)$$

Notice that in the tube sections 1 and n_s a coupling springs with an exterior point is not defined, as shown in Figure 2.1b. This implies that the restoring forces F_{c0} and F_{cn_s} are neglected in the corresponding momentum balance of the first and last sections of the tube.

2.1.2 Port-Hamiltonian Formulation

To obtain a port-Hamiltonian model of the system, we first describe the total energy stored in the flexible tube. In this respect, the total kinetic energy is derived from the sum of the kinetic energy in each section, i.e.,

$$\mathcal{K}_s = \sum_{j=1}^{n_s} \frac{1}{2} \frac{\pi_{sj}^2}{m_j} \quad (2.10)$$

Similarly, the total potential energy is obtained by the sum of the radial and coupling springs potential energies. The potential energy of the flexible tube is then given by:

$$\mathcal{P}_s = \underbrace{\sum_{j=1}^{n_s} \frac{1}{2} k_j q_j^2}_{\text{Radial Springs}} + \underbrace{\sum_{j=1}^{n_s-1} \frac{1}{2} k_{cj} (q_j - q_{j+1})^2}_{\text{Coupling Springs}} \quad (2.11)$$

The total energy, of the mechanical system that describes the flexible tube motion is given by:

$$\mathcal{H}_s(\boldsymbol{\pi}_s, \mathbf{q}_s) = \mathcal{K}_s + \mathcal{P}_s \quad (2.12)$$

where $\mathbf{q}_s = [q_1 \cdots q_{n_s}]^\top$ and $\boldsymbol{\pi}_s = [\pi_{s1} \cdots \pi_{sn_s}]^\top$ denote the sets of displacements and momenta of the n_s tube sections, respectively.

The efforts variables associated to each tube section are given by the partial derivative of \mathcal{H}_s with respect to the corresponding state variables, i.e., for the j -th tube section we obtain:

$$\partial_{q_j} \mathcal{H}_s = k_j q_j + k_{cj} (q_j - q_{j+1}) - k_{c_{j-1}} (q_{j-1} - q_j) = -F_j - F_{c_j} + F_{c_{j-1}} \quad (2.13)$$

$$\partial_{\pi_{sj}} \mathcal{H}_s = \frac{\pi_{sj}}{m_j} = v_{sj} \quad (2.14)$$

Then, the governing equations in an arbitrary section j are given by:

$$\dot{q}_j = \partial_{\pi_{sj}} \mathcal{H}_s \quad (2.15a)$$

$$\dot{\pi}_{sj} = -\partial_{q_j} \mathcal{H}_s - d_j \partial_{\pi_{sj}} \mathcal{H}_s + F_{ej} \quad (2.15b)$$

Proposition 2.1. Consider $\mathbf{q}_s = [q_1 \cdots q_{n_s}]^\top$ and $\boldsymbol{\pi}_s = [\pi_{s1} \cdots \pi_{sn_s}]^\top$ the sets of displacements and momenta of the n_s tube sections, respectively. Then, the dynamics of the flexible tube can be expressed as the following port-Hamiltonian system:

$$\dot{\mathbf{x}}_s = [J_s - R_s] \partial_{\mathbf{x}_s} \mathcal{H}_s + G_s \mathbf{u}_s \quad (2.16a)$$

$$\mathbf{y}_s = G_s^\top \partial_{\mathbf{x}_s} \mathcal{H}_s \quad (2.16b)$$

where $\mathbf{x}_s = [\mathbf{q}_s^\top \boldsymbol{\pi}_s^\top]^\top$ is the state vector, $\mathbf{u}_s = [F_{e1} \cdots F_{en_s}]^\top$ and $\mathbf{y}_s = [v_{s1} \cdots v_{sn_s}]^\top$ are the sets of external forces and velocities of the flexible tube sections, respectively, and

$$\partial_{\mathbf{x}_s} \mathcal{H}_s = \begin{bmatrix} \partial_{\mathbf{q}_s} \mathcal{H}_s \\ \partial_{\boldsymbol{\pi}_s} \mathcal{H}_s \end{bmatrix}, \quad J_s = \begin{bmatrix} \mathbf{0} & \mathbf{I} \\ -\mathbf{I} & \mathbf{0} \end{bmatrix}, \quad R_s = \begin{bmatrix} \mathbf{0} & \mathbf{0} \\ \mathbf{0} & R_1 \end{bmatrix}, \quad \text{and } G_s = \begin{bmatrix} \mathbf{0} \\ \mathbf{I} \end{bmatrix} \quad (2.17)$$

with

$$R_1 = \begin{bmatrix} d_1 & 0 & \cdots & 0 \\ 0 & \ddots & \ddots & \vdots \\ \vdots & \ddots & \ddots & 0 \\ 0 & \cdots & 0 & d_{n_s} \end{bmatrix} \geq 0 \quad (2.18)$$

satisfying the balance

$$\dot{\mathcal{H}} = -[\partial_{\pi_s} \mathcal{H}_s]^\top R_1 \partial_{\pi_s} \mathcal{H}_s + \mathbf{u}_s^\top \mathbf{y}_s \leq \mathbf{u}_s^\top \mathbf{y}_s \quad (2.19)$$

Proof. Considering n_s sections, from (2.15) the displacements and momenta dynamics can be expressed as:

$$\begin{aligned} \dot{\mathbf{q}}_s &= \partial_{\pi_s} \mathcal{H}_s \\ \dot{\pi}_s &= \partial_{\mathbf{q}_s} \mathcal{H}_s - R_1 \mathcal{H}_s + \mathbf{u}_s \end{aligned}$$

where $\mathbf{u}_s = [F_{e1} \cdots F_{ens}]^\top$ and R_1 is given by (2.18). Defining the skew-symmetric matrix $J_s = \begin{bmatrix} \mathbf{0} & \mathbf{I} \\ -\mathbf{I} & \mathbf{0} \end{bmatrix}$, the matrix $R_s = \begin{bmatrix} \mathbf{0} & \mathbf{0} \\ \mathbf{0} & R_1 \end{bmatrix} \geq 0$ and the input matrix as $G_s = \begin{bmatrix} \mathbf{0} \\ \mathbf{I} \end{bmatrix}$, then, the dynamics of the n_s sections of a flexible tube can be expressed as the port-Hamiltonian system (2.16). Finally, the relationship (2.19) can be easily derived substituting (2.16) in the energy balance $\dot{\mathcal{H}}_s = [\partial_{\mathbf{x}_s} \mathcal{H}_s]^\top \dot{\mathbf{x}}_s$. \square

2.2 VOCAL FOLDS MODEL

Another example of FSI system is the vocal folds model. The vocal folds structure is composed by several layers of tissue, as shown on the left hand side of Figure 2.4. The most superficial is the epithelium layer that protects the delicate tissue of the vocal folds. The next layer is the lamina propria. It is composed by elastic and collagen fibers that make up the vocal ligament. The deep layer of vocal folds is a muscular layer composed by the vocalis and muscularis parts of the Thyoarytenoid muscle, that makes up the bulk of the vocal fold [89]. The interactions of the vocal folds with the intragottal airflow induce a vibrating cycle that

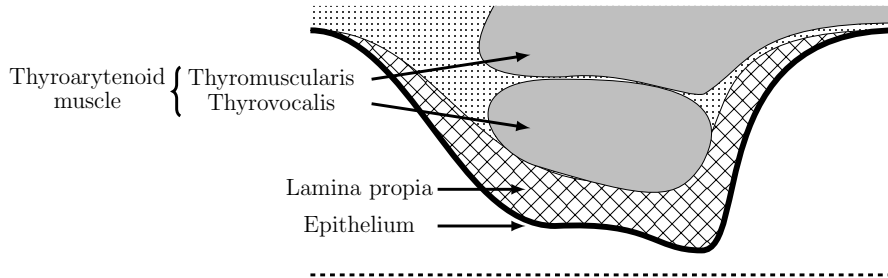


Figure 2.4 – Tissue layers of the structure of vocal folds. Dotted line: Midasagittal plane of the glottis.

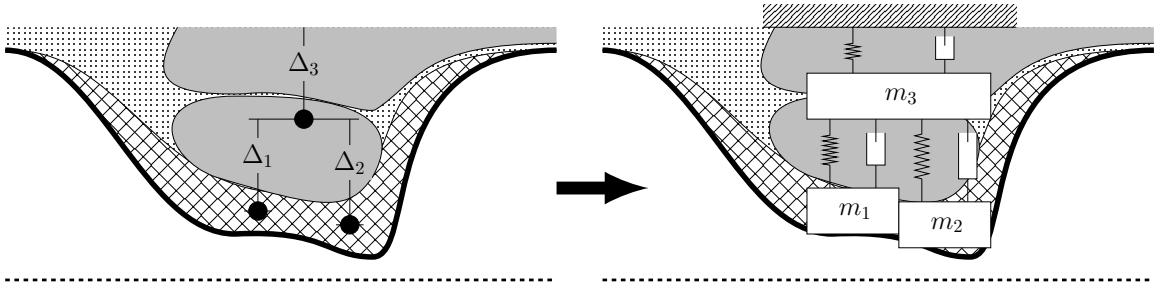


Figure 2.5 – Simplification of the vocal folds mechanics using the body-cover model. Δ_j 's represents the tissue deformations during the vocal folds vibration cycle.

includes: the vocal folds collision, with the associated fluid domain closure and the restoring forces associated with tissue deformations during the collisions. This kind of phenomena do not appear in the tube example considered in the previous section.

In the literature, continuum mechanics models have been used to describe the physical behavior of the vocal folds sections, i.e., the epithelium lamina, the lamina propria and the vocalis muscle [90]. In [91, 31] a linear stress-strain (elastic material) model is considered to describe the tissue of each vocal folds section. A non-linear approach for the stress-strain (hyper-elastic material) has been proposed in [92, 93, 13]. Viscoelastic models are also used in [29, 94]. However, the vibrations of the vocal folds commonly exhibit two dominant eigenfrequencies whose behavior can be described through simplified MSD models [33]. Similarly, given that the velocity of the vocal folds motion is much less than the intraglottal airflow velocity, it is common to reduce the analysis of the airflow to a 1D fluid [72, 95, 96]. This allows us to study the vocal folds vibration cycle as a FSI problem between a longitudinal fluid and a structure with transverse motion. As a consequence, in this thesis we consider a symmetrical behavior of the vocal folds using the well-know body-cover model (BCM) proposed in [72] to describe its mechanical motion.

2.2.1 Body-cover model

From a mechanical point of view, the BCM is a simplified description of the vocal folds behavior, as shown in Figure 2.5. Cover masses, m_1 and m_2 , describe the motion of the epithelial layer and lamina propria layer of the vocal folds and the body mass m_3 describes the motion of the thyrovocalis muscle that is effective in the vibration (see [72] for details). In the formulation of the BCM the deformation of the tissue subject to the transverse stress-strain is modeled as a hyper-elastic material. This implies that the transverse stress-strain is described through non-linear springs between the cover masses and the body mass and between the body mass and the glottal wall. The elongations of these non-linear springs are denoted by Δ_1 , Δ_2 and Δ_3 , as shown in Figure 2.5, whose associated restoring forces are given by [72]:

$$F_j = - \left(k_j \Delta_j + k_j \eta_j \Delta_j^3 \right), j \in \{1, 2, 3\} \quad (2.20)$$

where k_j and η_j are the linear and nonlinear coefficients of the corresponding springs. The shear stress-strain in the epithelial layer is described through a linear coupling spring, with coefficient k_{c1} . The force associated with this spring is given by:

$$F_{cj} = -k_{c1} \Delta_{12} \quad (2.21)$$

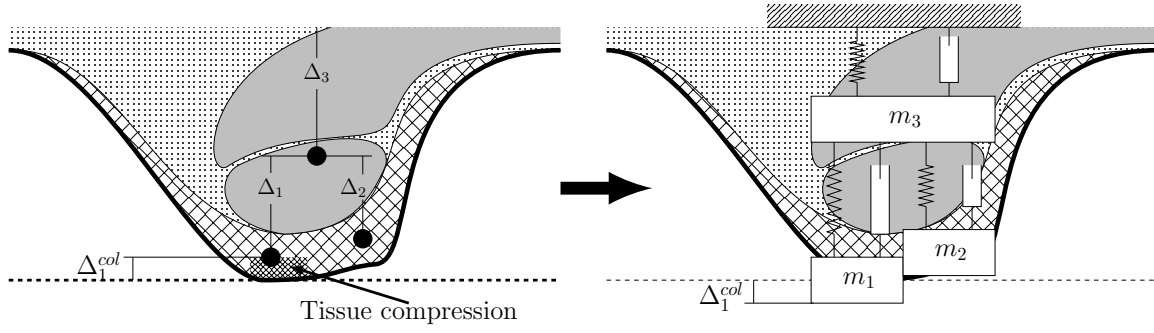


Figure 2.6 – Vocal folds collision description using the body-cover model. Left: tissue compression during the collision. Right: overlap of the cover mass to describe the collision.

where Δ_{12} describes the elongation of the coupling spring.

On the other hand, the energy dissipation due to the tissue viscosity is described through linear dampers between the cover and body masses and between the body mass and the glottal wall. The coefficients of these dampers are defined as $d_j = \lambda_{sj} \sqrt{m_j k_j}$ where λ_{sj} is a dimensionless loss factor. Then, the forces associated with these dampers are given by:

$$F_{d_j} = -d_j \dot{\Delta}_j, j \in \{1, 2, 3\} \quad (2.22)$$

where $\dot{\Delta}_j$ denotes the time derivative of Δ_j .

When the vocal folds collide, an additional mechanical stress-strain appears as a consequence of the tissue motion inertia. This strain is due to the tissue compression around the collision area, as shown in Figure 2.6 (left), making an additional restoring force on the vocal folds to appear. Typically, in lumped-parameter models of the vocal-folds the masses are assumed to be perfectly rigid. Then, to describe the collision, an overlap of the cover masses, Δ_j^{col} $j \in \{1, 2\}$, is allowed [97], as shown in Figure 2.6 (right). During the overlap, additional restoring forces are added to the dynamics of the cover masses. These restoring forces are modeled through non-linear collision springs that are activate only when the vocal folds collide. The restoring force associated with this collision springs is given by:

$$F_j^{col} = - \left(k_j^{col} \Delta_j^{col} + k_j^{col} \eta_j^{col} (\Delta_j^{col})^3 \right), j \in \{1, 2\} \quad (2.23)$$

where k_j^{col} and η_j^{col} are the linear and nonlinear coefficients, and Δ_j^{col} denotes the overlap of the j -th cover mass. Then, denoting by π_{sj} the momentum of mass m_j , the dynamics of the BCM can be expressed as:

$$\dot{\pi}_{s1} = F_1 + F_{c1} + F_{d1} + F_1^{col} + F_{e1} \quad (2.24)$$

$$\dot{\pi}_{s2} = F_2 - F_{c1} + F_{d2} + F_2^{col} + F_{e2} \quad (2.25)$$

$$\dot{\pi}_{s3} = F_3 + F_{d3} - (F_1 + F_2 + F_{d1} + F_{d2}) \quad (2.26)$$

where F_{ej} denotes the external force applied in the j -th cover mass.

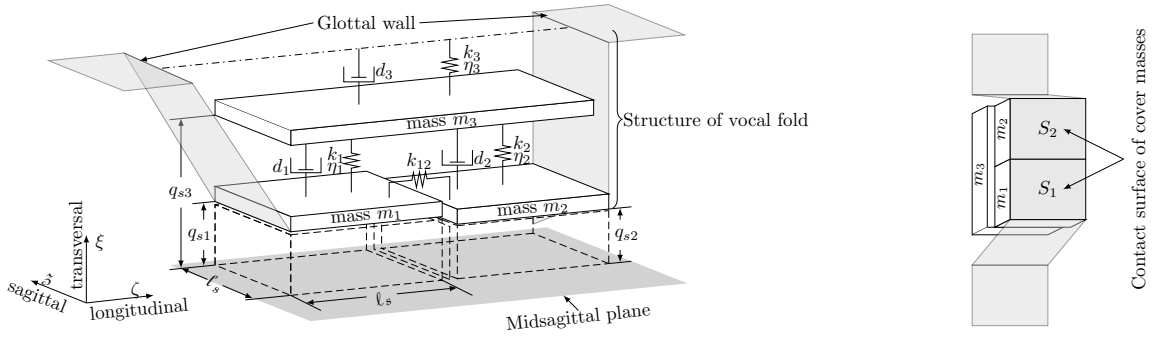


Figure 2.7 – Body-cover model of vocal folds showing a Hemi-larynx representation for symmetrical vocal folds oscillations. Left: 3-dimensional view, displaying the mass positions. Right: bottom view, displaying the contact surfaces.

2.2.2 Port-Hamiltonian formulation

Port-Hamiltonian formulations of the BCM have been proposed in [73, 74]. These formulations use auxiliary variables to describe the overlap of cover masses during the collision. The dynamics of these auxiliary variables and the associated spring forces are enabled by switches that are activated when the corresponding cover mass collides and disabled otherwise. However, these formulations present some significant drawbacks. For example, some of the states and auxiliary variables need to be appropriately initialized to 0 after each collision to avoid numerical errors. In this thesis we propose an alternative formulation without the use of auxiliary variables. Considering a symmetric behavior of the vocal folds, only the mechanical part of a hemi-larynx is modeled, as shown in Figure 2.7, where S_1 and S_2 denote the contact surfaces of cover masses with the intra-glottal airflow. The surfaces have length ℓ_s and depth ℓ_s . We denote by q_{sj} the position of the mass m_j from midsagittal plane and $q_j = q_{sj} - q_{sj}^0$ the corresponding displacement, where q_{sj}^0 is the equilibrium point at the reference pressure p_0 in the glottis. The spring elongations are $\Delta_1 = q_1 - q_3$, $\Delta_2 = q_2 - q_3$, $\Delta_3 = q_3$ and $\Delta_{c1} = q_1 - q_2$. To describe the collision of the vocal folds, we define the elongation of the collision springs as $\Delta_j^{col} = s_j q_{sj} = s_j (q_j + q_{sj}^0)$, $j \in \{1, 2\}$, where s_j is a switch variable defined as:

$$s_j = \begin{cases} 1, & q_{sj} \leq 0 \\ 0, & q_{sj} > 0 \end{cases}, j \in \{1, 2\} \quad (2.27)$$

Additionally, when a collision occurs, the loss factor of the dampers interconnected between the cover masses and the body mass increase. We define these loss factors as $\lambda_{sj} = \lambda_{sj}^0 + s_j \lambda_{sj}^{col}$, $j \in \{1, 2\}$.

To obtain the port-Hamiltonian formulation of the overall system we first describe the total energy stored in the BCM. The kinetic energy stored by the mass m_j is given by:

$$\mathcal{K}_{sj} = \frac{1}{2} \frac{\pi_{sj}^2}{m_j} \quad (2.28)$$

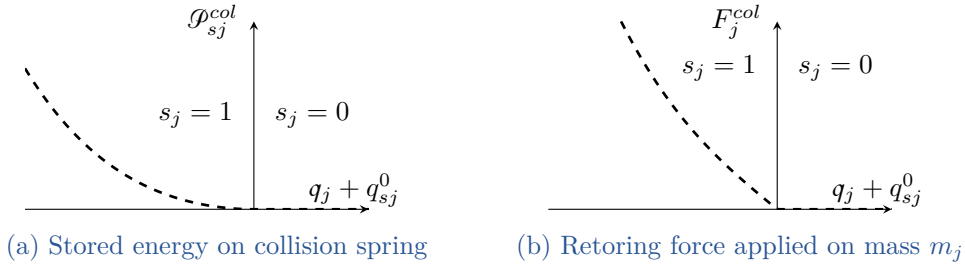


Figure 2.8 – Stored potential energy of collision spring (left) and the corresponding applied force over mass m_j . Normalized behavior, $k_{cj} = 1$ and $\eta_{cj} = 1$, for $j \in \{1, 2\}$.

and $\partial_{\pi_{sj}} \mathcal{K}_{sj} = \frac{\pi_{sj}}{m_j} = \dot{q}_j$ gives the mass velocity. Additionally, from the expression of the restoring forces of the springs connecting the cover masses with the body mass, we obtain that the stored potential energy is given by:

$$\mathcal{P}_{sj} = \frac{1}{2} k_j (q_j - q_3)^2 + \frac{1}{4} k_j \eta_j (q_j - q_3)^4, \quad j \in \{1, 2\} \quad (2.29)$$

where $\partial_{q_j} \mathcal{P}_{sj} = -F_j$ and $\partial_{q_3} \mathcal{P}_{sj} = F_j$. Similarly, the stored potential energies of the spring connecting the body mass with the glottal wall and the cover masses coupling spring are expressed as:

$$\mathcal{P}_{s3} = \frac{1}{2} k_3 q_3^2 + \frac{1}{4} k_3 \eta_3 q_3^4 \quad (2.30)$$

$$\mathcal{P}_{s4} = \frac{1}{2} k_{c1} (q_1 - q_2)^2 \quad (2.31)$$

respectively, where $\partial_{q_3} \mathcal{P}_{s3} = -F_3$, $\partial_{q_1} \mathcal{P}_{s4} = -F_{c1}$ and $\partial_{q_2} \mathcal{P}_{s4} = F_{c1}$.

In the case of collision, the stored energy in the additional springs is given by:

$$\mathcal{P}_{sj}^{col} = \frac{1}{2} k_j^{col} s_j (q_j + q_{sj}^0)^2 + \frac{1}{4} k_j^{col} \eta_j^{col} s_j (q_j + q_{sj}^0)^4, \quad j \in \{1, 2\} \quad (2.32)$$

where $\partial_{q_j} \mathcal{P}_{sj}^{col} = -F_j^{col}$. Note that the stored potential energy contained in the collision springs depends on the discontinuous variables, s_j . However, \mathcal{P}_{sj}^{col} is smooth and the restoring force F_j^{col} is continuous, as shown in Figure 2.8.

The total energy of the BCM is given by:

$$\mathcal{H}_s = \underbrace{\sum_j \mathcal{K}_{sj}}_{\text{Kin. ener. in masses}} + \underbrace{\sum_j \mathcal{P}_{sj}}_{\text{Pot. ener. in springs}} + \underbrace{\sum_j \mathcal{P}_{sj}^{col}}_{\text{Pot. ener. in col. springs}} \quad (2.33)$$

Proposition 2.2. *Consider the total energy defined in (2.33). The port-Hamiltonian model of the BCM is of the form:*

$$\dot{\mathbf{x}}_s = [J_s - R_s] \partial_{\mathbf{x}_s} \mathcal{H}_s + G_s \mathbf{u}_s \quad (2.34a)$$

$$\mathbf{y}_s = G_s^\top \partial_{\mathbf{x}_s} \mathcal{H}_s \quad (2.34b)$$

where $\mathbf{x}_s = [q_1 \ q_2 \ q_3 \ \pi_{s1} \ \pi_{s2} \ \pi_{s3}]^\top$ is the state vector, $\mathbf{u}_s = [F_{e1} \ F_{e2}]^\top$ is the input vector given by the external forces applied on the cover masses, $\mathbf{y}_s = [\dot{q}_1 \ \dot{q}_2]^\top$ is the output vector given by the cover mass velocities, $J_s = \begin{bmatrix} \mathbf{0} & \mathbf{I} \\ -\mathbf{I} & \mathbf{0} \end{bmatrix}$ where \mathbf{I} and $\mathbf{0}$ are 3×3 identity and zero matrices, respectively, $R_s = \begin{bmatrix} \mathbf{0} & \mathbf{0} \\ \mathbf{0} & R_2 \end{bmatrix}$ and $G_s = \begin{bmatrix} \mathbf{0}_{3 \times 2} \\ G_1 \end{bmatrix}$ with

$$R_2 = \begin{bmatrix} d_1 & 0 & -d_1 \\ 0 & d_2 & -d_2 \\ -d_1 & -d_2 & d_1 + d_2 + d_3 \end{bmatrix} \quad \text{and} \quad G_1 = \begin{bmatrix} 1 & 0 \\ 0 & 1 \\ 0 & 0 \end{bmatrix} \quad (2.35)$$

Proof. Consider the total energy of the BCM in (2.33). Defining the state vector as $\mathbf{x}_s = [q_1 \ q_2 \ q_3 \ \pi_{s1} \ \pi_{s2} \ \pi_{s3}]^\top$, then, the BCM efforts are given by:

$$\begin{aligned} \partial_{q_1} \mathcal{H}_s &= -F_1 - F_{12} - F_{c1} & \partial_{\pi_{s1}} \mathcal{H}_s &= \dot{q}_1 \\ \partial_{q_2} \mathcal{H}_s &= -F_2 + F_{12} - F_{c2} & \partial_{\pi_{s2}} \mathcal{H}_s &= \dot{q}_2 \\ \partial_{q_3} \mathcal{H}_s &= F_1 + F_2 - F_3 & \partial_{\pi_{s3}} \mathcal{H}_s &= \dot{q}_3 \end{aligned}$$

On the other hand, note that $\dot{\Delta}_1 = \dot{q}_1 - \dot{q}_3$, $\dot{\Delta}_2 = \dot{q}_2 - \dot{q}_3$ and $\dot{\Delta}_3 = \dot{q}_3$. The forces associated with the dampers can be expressed as $F_{d1} = -d_1 (\partial_{\pi_{s1}} \mathcal{H}_s - \partial_{\pi_{s3}} \mathcal{H}_s)$, $F_{d2} = -d_2 (\partial_{\pi_{s2}} \mathcal{H}_s - \partial_{\pi_{s3}} \mathcal{H}_s)$ and $F_{d3} = -d_3 \partial_{\pi_{s3}} \mathcal{H}_s$, and the dynamics on the momentum can be rewritten as:

$$\begin{aligned} \dot{\pi}_{s1} &= -\partial_{q_1} \mathcal{H}_s - d_1 (\partial_{\pi_{s1}} \mathcal{H}_s - \partial_{\pi_{s3}} \mathcal{H}_s) + F_{e1} \\ \dot{\pi}_{s2} &= -\partial_{q_2} \mathcal{H}_s - d_2 (\partial_{\pi_{s2}} \mathcal{H}_s - \partial_{\pi_{s3}} \mathcal{H}_s) + F_{e2} \\ \dot{\pi}_{s3} &= -\partial_{q_3} \mathcal{H}_s + d_1 (\partial_{\pi_{s1}} \mathcal{H}_s - \partial_{\pi_{s3}} \mathcal{H}_s) + d_2 (\partial_{\pi_{s2}} \mathcal{H}_s - \partial_{\pi_{s3}} \mathcal{H}_s) - d_3 \partial_{\pi_{s3}} \mathcal{H}_s \end{aligned}$$

Then, considering the matrix R_2 defined in (2.35) and $G_1 = \begin{bmatrix} 1 & 0 & 0 \\ 0 & 1 & 0 \end{bmatrix}^\top$, we can describe the BCM as the port-Hamiltonian system (2.34) where $J_s = \begin{bmatrix} \mathbf{0} & \mathbf{I} \\ -\mathbf{I} & \mathbf{0} \end{bmatrix}$, $R_s = \begin{bmatrix} \mathbf{0} & \mathbf{0} \\ \mathbf{0} & R_2 \end{bmatrix}$ and $G_s = \begin{bmatrix} \mathbf{0} \\ G_1 \end{bmatrix}$. \square

Remark 2.1. Note that the port-Hamiltonian formulation of the BCM in Proposition 2.2 does not use auxiliary variables, reducing the number of states in comparison with the formulation in [73, 74]. Instead, the proposed model use switch variables, s_j , in the definition of the stored potential energy associated with the collision springs. Even though the stored potential energies are a function of discontinuous variables, they are smooth, as shown in Figure 2.8a, i.e., the total energy of the BCM is a smooth function of the states variables. The restoring forces of the collision springs are a continuous function of the mass positions that vanishes when the cover masses are not colliding, as shown in Figure 2.8b. This implies that the continuity of the dynamic equations is preserved. Similar switching principles have been regularly used, outside the port-Hamiltonian framework, in lumped-parameter model of the vocal folds, see e.g. [95, 98].

2.3 CONCLUSION

In this chapter mass-spring-damper systems have been considered to describe the transverse motion of longitudinal structures using a PHS formulation. In this respect, two examples have been used: a single layer flexible tube and the vocal folds. In the first case, considering an axisymmetric behavior, the flexible tube is divided into n_s sections of length ℓ_s , as shown in Figure 2.2. Section 2.1.1 describes the procedure to obtain the MSD coefficients from the physical parameters of the tube, such as the Lamé coefficients, material density and thickness. This MSD model is used to obtain a scalable PHS formulation considering a linear behavior of the springs, as shown in Section 2.1.2. The scalability of the finite-dimensional model proposed, allows us to adjust the space resolution in the longitudinal domain, increasing or decreasing the number of sections n_s , for the description of the structure transverse motion. This is equivalent to vary the number of elements of the mesh in discretized infinite-dimensional formulations. However, the proposed model does not require the meshing and stabilization algorithms used in infinite-dimensional approaches.

In the vocal folds example, the well-known BCM proposed in [72] is used to describe the vocal folds motion. Considering symmetrical behavior, a PHS formulation of a Hemi-larynx vocal folds model is proposed in Section 2.2.2. In [73, 74] the PHS formulation of the BCM uses auxiliary state variables to describe the tissue compression during the collisions. The model described in Section 2.2.2 provides an alternative PHS formulation that allows to reduce the dimension of the state vector. In this respect, we include in this representation two switching functions in the definition of the energy (2.33) to describe the energy stored by the collision springs used in the BCM. This allows us to include the extra forces applied to the cover masses during the collision without the use of auxiliary variables as proposed in [73, 74]. Additionally, it is important to notice that even if (2.33) depends on discontinuous variables (collision switches), the total energy and the forces acting on masses are continuous, as shown in Figure 2.8.

The port-Hamiltonian models proposed in this Chapter will be used to obtain a finite-dimensional FSI system, according to the fluid models developed in next Chapters.

Chapter 3

Finite-dimensional port-Hamiltonian FSI model with incompressible fluids

In the previous Chapter, a finite-dimensional PHS model based on a MSD formulation is proposed to describe the transverse motion of a longitudinal structure. For a FSI description an appropriated model of the fluids that interacts with the structure is necessary. In this Chapter we focus on the description of a longitudinal incompressible fluid based on a finite-dimensional PHS formulation that allows us an appropriated coupling with the structure.

From a practical point view, a fluid is considered incompressible when the density variations can be neglected. According to [99] a criteria to analyze when the density variations are small enough to be neglected is using the Mach number M (ratio between the fluid velocity and the speed of sound in the media). In this sense, an incompressibility assumption for the fluid is adequate if the Mach number satisfies $M \leq 0.3$ [99].

In the literature, the interaction between an incompressible fluid and a structure is a problem widely studied. Several computational approaches have been proposed to obtain an appropriated fluid description and its coupling with the structure using different spatial and time discretization methods, see for example [10, 12, 19, 21] and [22] among others. A special problem related with the numerical description of incompressible fluids is the definition of the pressure in the fluid domain. A possible way to construct an equation for the pressure is using the Poisson equation, where the Laplacian of the pressure is described through the velocity field of the fluid. However, in computational methods, as the finite-elements techniques, it is necessary the use of algorithms, such as the pressure-pressure coupling algorithms, to guarantee the numerical stability of the simulations. Examples of these pressure-pressure coupling algorithms are backward approximation pressure correction schemes [100] and pseudo-compressible algorithms, such as the PSPG method [23]. However, from a port-Hamiltonian point of view, these methods are not useful to obtain a power-preserving interconnection between the discretized momentum sections.

Contribution

In this chapter, we present a scalable port-Hamiltonian model for longitudinal incompressible fluids and the interconnection with a structure with transverse motion. We introduce the use of instrumental elements, called nodes, that allow us to obtain a power-preserving pressure-pressure coupling for the ODE's obtained from the spatial discretization of the momentum equation.

3.1 FLUID DESCRIPTION

In this thesis the fluid dynamics is described by the well-know continuity and motion equations [101], in their incompressible form and neglecting the gravitational effects, leading to:

$$\operatorname{div} \mathbf{v} = 0 \quad (3.1)$$

$$\rho \partial_t \mathbf{v} + \rho \mathbf{v} \cdot \mathbf{Grad} \mathbf{v} + \mathbf{grad} p = \mu \operatorname{div} (\mathbf{Grad} \mathbf{v}) \quad (3.2)$$

where ρ , \mathbf{v} , p and μ are the density, velocity field, pressure and viscosity of the fluid flow, respectively, and the operators div , \mathbf{grad} , div , \mathbf{Grad} and ∂_t are detailed in the Notation Section at the beginning of this thesis.

Notice that (3.1) is, from a mathematical point of view, the approximation of the more general mass balance $\partial_t \rho + \operatorname{div} \rho \mathbf{v} = 0$, where we assume negligible variations of the density, i.e., $\Delta \rho \ll \rho$. We use the Mach number M , the ratio between the fluid velocity and the speed of sound c in the media ($M = \|\mathbf{v}\|/c$), to consider when this incompressibility assumption is adequate. In this Chapter we study flows with $M \leq 0.3$ [99].

In different studies on incompressible flows it is common to relax the condition in (3.1) to use pseudo-compressible algorithms to define appropriate pressure-pressure couplings in the space discretization of (3.2), such as the Pressure Stabilization Petrov-Galerkin method, where $-\operatorname{div} \mathbf{v} + \varepsilon \Delta p = 0$, the penalty method, where $-\operatorname{div} \mathbf{v} - \varepsilon p = 0$, and the artificial compressibility method, where $-\operatorname{div} \mathbf{v} - \varepsilon \partial_t p = 0$, and where ε is some parameter which has to be chosen appropriately [23]. Similarly, in this chapter we relax the incompressible hypothesis to describe the pressure in different zones of the fluid domain, allowing us to define an appropriate coupling, from a port-Hamiltonian point of view, between the incompressible fluid sections.

3.1.1 Finite-dimensional modeling of the fluid

In what follows we consider n_f sections of the fluid with uniform cross-sectional area where the flow is incompressible, as shown in Figure 3.1.a, and infinitesimal compressible sections, that will be referred to as nodes, to describe the pressure in the coupling zone between two adjacent incompressible sections, as shown in Figure 3.1.b. The use of nodes to couple incompressible sections has been applied in [102] for tubes with fixed irregular geometries.

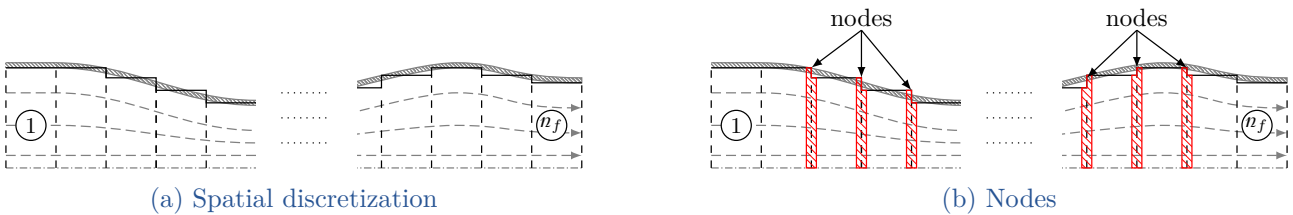


Figure 3.1 – Spatial discretization of the fluid domain. a) Division of the fluid domain in n_f sections with uniform cross-sectional area. b) Definition of nodes between adjacent incompressible fluid sections.

From an energy point of view, incompressible sections are kinetic energy storage elements, describing the fluid motion through the momentum balance:

$$\rho_0 \partial_t \mathbf{v} = -\rho_0 \mathbf{v} \cdot \mathbf{Grad} \mathbf{v} - \mathbf{grad} p + \mu \operatorname{div} [\mathbf{Grad} \mathbf{v}] \quad (3.3)$$

subject to $\text{div } \mathbf{v} = 0$, where ρ_0 is the reference density of the fluid and $\mathbf{v} = [v \ \mathbf{v}]^\top$ with v and \mathbf{v} as the longitudinal and transverse velocities of the fluid, respectively.

We define the fluid behavior in nodes using the following assumption.

Assumption 3.1. *The volume of a node is small enough, such that the density distribution is uniform, and the changes in density are only caused by changes in the volume [103, Sec. 5.1, p.78]. This implies that the mass in each node is constant, i.e., the following relationship is satisfied*

$$\rho_j \bar{V}_j = m \quad (3.4)$$

where ρ_j and \bar{V}_j are the density and volume of the j -th node, and m is the total mass in the node.

Then, the nodes store potential energy and are used to describe the pressure distribution in the fluid. Their dynamics are governed by the changes of the fluid density. Then, the governing equation in a node is given by:

$$\partial_t \rho + \text{div } \rho \mathbf{v} = 0 \quad (3.5)$$

The loss of kinetic energy of a fluid is given by different phenomena [101], such as viscosity friction with the walls, turbulences and irregularities in the geometry. Thus, we first discuss the energy dissipation in the fluid, in order to describe a scalable model from the models of n_f incompressible sections and nodes.

3.1.2 Macroscopic power dissipation in the flow

As shown in [101], the dissipation in a Newtonian fluid is associated with the divergence of the viscosity tensor $\boldsymbol{\tau} = -\mu (\mathbf{Grad } \mathbf{v} + [\mathbf{Grad } \mathbf{v}]^\top) + \left(\frac{2}{3}\mu - \kappa\right) (\text{div } \mathbf{v}) \mathbf{I}$. Note that the term $\mu \mathbf{div } [\mathbf{Grad } \mathbf{v}]$ in (3.3) is the incompressible simplification of $-\mathbf{div } \boldsymbol{\tau}$. Then, from a macroscopic point of view, the power dissipated in a volume V_j is given by:

$$\mathcal{E}_{\lambda_j} = - \int_{V_j} (\mathbf{v} \cdot \mathbf{div } \boldsymbol{\tau}) dV_j \geq 0 \quad (3.6)$$

According to [101], the dissipated power \mathcal{E}_{λ_j} in volume V_j must have the general form:

$$\mathcal{E}_{\lambda_j} = \frac{1}{2} \lambda_j \underline{\rho}_j \underline{v}_j^3 \underline{A}_j \geq 0 \quad (3.7)$$

where $\underline{\rho}_j$, \underline{v}_j and \underline{A}_j are the characteristic density, velocity and area of the fluid domain in volume V_j . The dimensionless term λ_j can be expressed as $\lambda_j = \lambda_j^f + \lambda_j^g$, where λ_j^f , the friction loss factor, is a function of the Reynolds number, viscous losses, and λ_j^g is a loss factor associated with additional resistances determined by the geometry of the fluid domain, such as sudden changes in the cross-sectional area (see [101, Section 7.5] for details). Then, (3.7) can be rewritten as

$$\mathcal{E}_{\lambda_j} = \underline{\rho}_j \underline{v}_j \left(\frac{1}{2} \lambda_j \underline{A}_j |\underline{v}_j| \underline{v}_j \right) \geq 0 \quad (3.8)$$

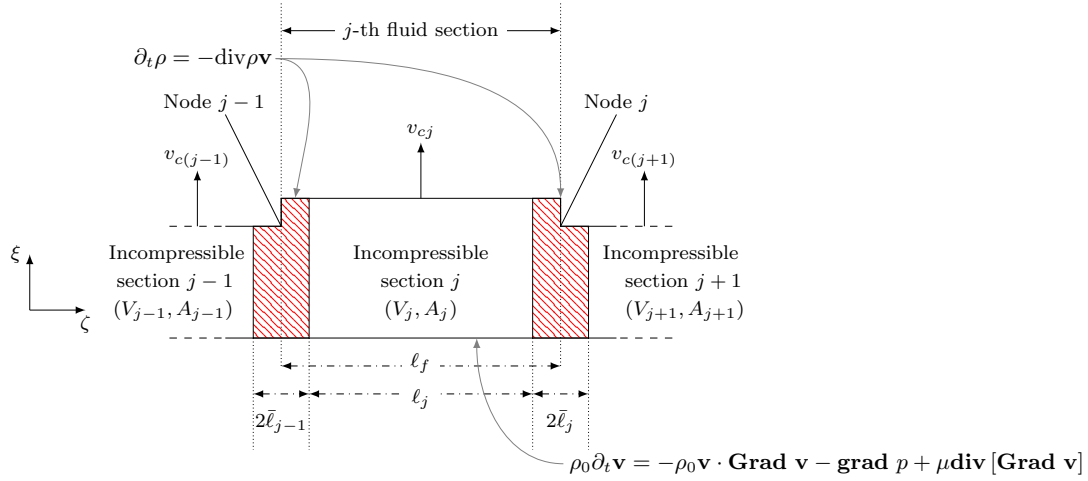


Figure 3.2 – Coupling incompressible fluid sections using nodes with compressible behavior.

where $|\underline{v}_j|$ denotes the absolute value of \underline{v}_j , and the term $\frac{1}{2}\lambda_j A_j |\underline{v}_j| \underline{v}_j$ describes the rate of velocity drop in volume V_j due to energy losses. This term is equivalent to dissipative terms used in others works. For example, in [104] the dissipation term, in an infinite-dimensional form, of 1D flow in a rough pipeline is described by $\frac{1}{2}\lambda^f |v|v/D$ where D is the pipe diameter and λ^f is obtained from the Haaland equation [101]. Integrating this term in a pipe section with volume V_j , we obtain $\int_{V_j} \frac{1}{2D} \lambda^f |v|v dV = \frac{1}{2}\lambda_j^f A_j |\underline{v}_j| \underline{v}_j$. This result is equivalent to the rate of velocity drop derived from (3.8), neglecting the geometrical losses.

The λ_j^f formula depends on the assumptions considered for the fluid. For example, the Haaland equation used in [104] is valid only for rough pipelines. However, other equations, such as the Blasius and Prandtl formulas, can be used according to the fluid conditions (see [101, Chapter 6] for details). Regarding λ_j^g , given the spatial discretization described above, we focus on the losses associated with sudden expansions and contractions, i.e.,

$$\lambda_j^g = \begin{cases} 0.5 \left(1 - \frac{A_{j+1}}{A_j}\right), & \text{sudden contraction, } A_{j+1} \leq A_j \\ \left(1 - \frac{A_j}{A_{j+1}}\right)^2, & \text{sudden expansion, } A_{j+1} \geq A_j \end{cases} \quad (3.9)$$

where A_j is the cross-sectional area of the incompressible fluid section j .

3.1.3 Fluid dynamics of the incompressible sections and nodes

If we consider the j -th section of the fluid of length $\ell_j = L/n_f$, where L is the length of the fluid domain, and uniform cross-sectional area A_j , the upper boundary moves in the transverse direction with velocity v_{c_j} . Figure 3.2 shows that this section is divided in one incompressible section and the adjacent nodes. As consequence of Assumption 3.1, a change of density in a node implies a change of the corresponding volume, which generates a variation in the volume of adjacent incompressible sections.

The first effect of the moving longitudinal boundaries, is that the volume of the j -th incompressible section is a function of the density of adjacent nodes. Considering a node length of $2\bar{\ell}_j$, as shown in Figure 3.2, the node volume is given by $\bar{V}_j = \bar{\ell}_j (A_j + A_{j+1})$. Thus, the volume V_j of section j is described by a reference value $V_j^* = A_j \bar{\ell}_j$ minus the corresponding part of the adjacent nodes, see Figure 3.2, i.e.,

$$V_j = V_j^* - A_j(\bar{\ell}_j + \bar{\ell}_{j-1}) = V_j^* - \frac{m}{\rho_j} \alpha_j - \frac{m}{\rho_{j-1}} (1 - \alpha_{j-1}) \quad (3.10)$$

where $\alpha_j = A_j/(A_j + A_{j+1})$ is a dimensionless factor. As we will see in the next subsection, the description of V_j in (3.10) will help us to describe the dynamic pressure in each node.

The second effect of these moving boundaries is that part of the fluid moves in the transverse direction, induced by the boundary velocity v_{cj} . This implies that the longitudinal flow in the section is affected by the upper wall movement. As a consequence, from (3.1), we obtain the following relationship:

$$Q_{1j} - Q_{2j} - A_{cj} v_{cj} = 0 \quad (3.11)$$

where A_{cj} is the contact area of the fluid section with the moving boundary, Q_{1j} and Q_{2j} are the inlet and outlet flows in the j -th section, respectively. Thus, denoting by v_j the average longitudinal flow velocity in section j , to satisfy (3.11), we define the inlet and outlet flows as:

$$Q_{1j} = A_j v_j + \frac{1}{2} A_{cj} v_{cj} \quad (3.12)$$

$$Q_{2j} = A_j v_j - \frac{1}{2} A_{cj} v_{cj} \quad (3.13)$$

where $A_j v_j$ is the average longitudinal flow and $A_{cj} v_{cj}$ is the transverse flow in the contact surface of the moving boundary. Note that (3.12) and (3.13) are equal when the upper boundary does not move, $v_{cj} = 0$.

The third effect of the moving boundaries is that the geometry of the tube is time varying, inducing a rotation of the flow in each section. This rotation generates energy dissipation by viscous friction, that can be modeled (from a macroscopic point of view) in terms of the characteristic velocity of the fluid, as shown in Section 3.1.2. To simplify the model, we consider a two-dimensional flow and the following assumption

Assumption 3.2. *Denote by v the transverse component of the fluid velocity and by q_j the position of the moving wall in the j -th incompressible section. The gradient of v is uniform in each incompressible fluid section and is given by $\partial_\xi v = v_{cj}/q_j$ and $\partial_\zeta v = 0$ where ξ and ζ denote the variables of transversal and longitudinal axes, respectively.*

Note that, from Assumption 3.2, the transversal velocity in a section j is given by $v = v_{cj} \xi/q_j$. As a consequence, the corresponding mean transversal momentum satisfies the following algebraic relationship with the boundary velocity $\pi_{\xi i} = \int \rho_0 v dV_j = \rho_0 V_j v_{cj}/2$. This algebraic constraint implies that the dynamics of the transversal momentum in each incompressible section is given by a linear combination of the ODEs associated with the mechanical model, described in Chapter 2, and the ODEs that describes the density behavior in the nodes.

Thus, to obtain a minimal realization we consider the following proposition to describe the flow in one incompressible section.

Proposition 3.1. *In a fluid section of volume V_j and uniform gradient of transversal velocity, the flow is described by the longitudinal flow momentum dynamics:*

$$\dot{\pi}_{\zeta j} = -\phi_{\zeta j} - A_{cj}\rho_0 v_j v_{cj} + A_j(P_{1j} - P_{2j}) \quad (3.14)$$

where the term $A_{cj}\rho_0 v_j v_{cj}$ represents the effect of the moving boundary in the longitudinal flow, $\phi_{\zeta j}$ describes the dissipation associated with the viscous tensor, P_{1j} and P_{2j} are the total pressures at the inlet and outlet boundaries of the fluid section, respectively, and $\pi_{\zeta j} = \rho_0 V_j v_j$ denotes the longitudinal momentum in volume V_j with v_j as the corresponding average longitudinal velocity.

Proof. As mentioned above, the corresponding transversal momentum has an algebraic relationship with the boundary velocity, i.e., the boundary velocity defines the transversal behavior of the fluid. Thus, it is only necessary to know the longitudinal flow momentum to describe the fluid in one section. From (3.3) we obtain that:

$$\rho_0 \partial_t v + \rho_0 v \partial_\xi v + \partial_\zeta \left(\frac{1}{2} \rho_0 v^2 + p \right) = \mu \left(\partial_\zeta^2 v + \partial_\xi^2 v \right) \quad (3.15)$$

where v is the longitudinal velocity of the fluid and the term $\rho_0 v \partial_\xi v$ is associated with the conversion of longitudinal flow into transversal flow and vice versa, induced by the velocity of the boundary. Integrating in the section volume the first 2 terms of (3.15) and applying the Leibniz integral rule, we obtain

$$\int \rho_0 \partial_t v + \rho_0 v \partial_\xi v dV_j = \frac{d}{dt} \left(\int \rho_0 v dV_j \right) - \int \rho_0 v v_{cj} dS_{cj} + \int \rho_0 v \partial_\xi v dV_j$$

Defining the average longitudinal velocity as $v_j = \frac{1}{V_j} \int v dV_j$ and the corresponding momentum as $\pi_{\zeta j} = \rho_0 V_j v_j$, we have that $\dot{\pi}_{\zeta j} = \frac{d}{dt} \left(\int \rho_0 v dV_j \right)$. Then, considering the relationship $v \partial_\xi v = \partial_\xi (vv) - v \partial_\xi v$, the incompressibility constraint $\text{div } \mathbf{v} = 0$ and the Gauss divergence theorem, the previous equation can be rewritten as

$$\begin{aligned} \int \rho_0 \partial_t v + \rho_0 v \partial_\xi v dV_j &= \dot{\pi}_{\zeta j} - \int \rho_0 v v_{cj} dS_{cj} + \int \partial_\xi \rho_0 v v dV_j - \int \rho_0 v \partial_\xi v dV_j \\ &= \dot{\pi}_{\zeta j} - \int \rho_0 v v_{cj} dS_{cj} + \int \rho_0 v v_{cj} dS_{cj} + \int \rho_0 v \partial_\zeta v dV_j \\ &= \dot{\pi}_{\zeta j} + \frac{1}{2} \rho_0 \int \partial_\zeta v^2 dV_j = \dot{\pi}_{\zeta j} + A_j \frac{\rho_0}{2} \left(\left(\frac{Q_{2j}}{A_j} \right)^2 - \left(\frac{Q_{1j}}{A_j} \right)^2 \right) \end{aligned}$$

Substituting (3.12) and (3.13), we obtain the following relationship

$$\int \rho_0 \partial_t v + \rho_0 v \partial_\xi v dV_j = \dot{\pi}_{\zeta j} + A_{cj} \rho_0 v_j v_{cj} \quad (3.16)$$

where the term $A_{cj} \rho_0 v_j v_{cj}$ describes the effect of the upper moving wall on the longitudinal flow in the j -th incompressible section.

Integrating the remaining term of the left hand side of (3.15) and considering a uniform velocity in the inlet and outlet cross-sectional surfaces of V_j , we obtain:

$$\int \partial_\zeta \left(\frac{\rho_0}{2} v^2 + p \right) dV_j = -A_j (P_{1j} - P_{2j}) \quad (3.17)$$

where P_{1j} and P_{2j} are the inlet and outlet total pressures, respectively.

The integral of the viscous term $\mu (\partial_z^2 v + \partial_w^2 v)$ is given by:

$$\int \mu (\partial_\zeta^2 v + \partial_\xi^2 v) dV_j = -\phi_{\zeta j} \quad (3.18)$$

where $\phi_{\zeta j}$ represents the force associated with the viscous dissipation. Finally, combining (3.16), (3.17) and (3.18), and solving for $\dot{\pi}_{\zeta j}$ we obtain (3.14). \square

Defining $\boldsymbol{\pi}_\zeta = [\pi_{\zeta 1} \cdots \pi_{\zeta n_f}]^\top$ as the set of longitudinal momenta, the fluid dynamics in the n_f incompressible fluid sections can be expressed as:

$$\dot{\boldsymbol{\pi}}_\zeta = \vartheta_\pi \mathbf{P}_1 - \vartheta_\pi \mathbf{P}_2 - \varphi_\pi \mathbf{v}_c - \Phi \quad (3.19)$$

where $\mathbf{P}_1 = [P_{11} \cdots P_{1n_f}]^\top$ and $\mathbf{P}_2 = [P_{21} \cdots P_{2n_f}]^\top$ are the sets of inlet and outlet total pressures, respectively, of the incompressible sections; $\mathbf{v}_c = [v_{c1} \cdots v_{cn_f}]^\top$ is the set of boundary velocities associated with the structure motion, and

$$\vartheta_\pi = \begin{bmatrix} A_1 & 0 & \cdots & 0 \\ 0 & \ddots & \ddots & \vdots \\ \vdots & \ddots & \ddots & 0 \\ 0 & \cdots & 0 & A_{n_f} \end{bmatrix} \quad \varphi_\pi = \rho_0 \begin{bmatrix} A_{c1} v_1 & 0 & \cdots & 0 \\ 0 & \ddots & \ddots & \vdots \\ \vdots & \ddots & \ddots & 0 \\ 0 & \cdots & 0 & A_{cn_f} v_{n_f} \end{bmatrix} \quad \Phi = \begin{bmatrix} \phi_{\zeta 1} \\ \vdots \\ \phi_{\zeta n_f} \end{bmatrix}$$

We now focus on the fluid dynamics in each node. As explained in Assumption 3.1, the density in each node is assumed to be uniform. Then, from (3.5) the density dynamics of the j -th node is derived in Proposition 3.2.

Proposition 3.2. *Let ρ_j be the density of the node j . The rate of change of ρ_j is given by:*

$$\dot{\rho}_j = \frac{\rho_j^2}{m} (Q_{1j}^\rho - Q_{2j}^\rho) - A_{nj} \frac{\rho_j^2}{m} (v_{cj} + v_{c(j+1)}) \quad (3.20)$$

where Q_{1j}^ρ and Q_{2j}^ρ are the inlet and outlet flows of the node, respectively, v_{cj} and $v_{c(j+1)}$ are the velocities of adjacent moving boundaries associated with the motion of the structure, A_{nj} is the corresponding contact area, and m is the fluid mass of the node.

Proof. Let \bar{V}_j be the volume of the j -th node enclosed by a surface \bar{S}_j , and let the velocity of any surface element be $\mathbf{v}_{\bar{S}}$. Consider that the part of \bar{S}_j in contact with the structure has an area of $2A_{nj}$, with $A_{nj} = \ell_j \ell$, where ℓ denotes the depth of the node. Then, integrating (3.5) in volume \bar{V}_j , applying the Leibniz integral rule we obtain:

$$\begin{aligned} 0 &= \int \partial_t \rho d\bar{V}_j + \int \operatorname{div} (\rho \mathbf{v}) d\bar{V}_j \\ &= \frac{d}{dt} \left(\int \rho_j d\bar{V}_j \right) - \int \rho_j (\mathbf{v}_{\bar{S}} \cdot \mathbf{n}) d\bar{S}_j + \int \rho_j (\partial_\zeta v + \partial_\xi v) d\bar{V}_j \end{aligned}$$

where \mathbf{n} is the outward unitary vector to \bar{S}_j . Given that ρ_j is uniform in \bar{V}_j we obtain that $\int \rho_j d\bar{V}_j = \rho_j \int d\bar{V}_j = \rho_j \bar{V}_j$. Similarly, notice that the rate of change of the node volume is given by $\dot{\bar{V}}_j = \int (\mathbf{v}_{\bar{S}} \cdot \mathbf{n}) d\bar{S}_j$, and that $\int \partial_\zeta v d\bar{V}_j = Q_{2j}^\rho - Q_{1j}^\rho$, where Q_{1j}^ρ and Q_{2j}^ρ are the inlet

and outlet flows of the node, and $\int \partial_\xi v d\bar{V}_j = A_{nj} (v_{cj} + v_{c(j+1)})$, where v_{cj} and $v_{c(j+1)}$ are the structure velocities in the contact surface and A_{nj} is the contact area with each moving boundary associated with the structure motion. Then, the previous equation can be rewritten as

$$\begin{aligned} 0 &= \frac{d}{dt} (\rho_j \bar{V}_j) - \rho_j \dot{\bar{V}}_j + \rho_j (Q_{2j}^\rho - Q_{1j}^\rho) + A_{nj} \rho_j (v_{cj} + v_{c(j+1)}) \\ &= \bar{V}_j \dot{\rho}_j + \rho_j (Q_{2j}^\rho - Q_{1j}^\rho) + A_{nj} \rho_j (v_{cj} + v_{c(j+1)}) \end{aligned} \quad (3.21)$$

Rewriting (3.21) we obtain that the rate of change of the node density ρ_j is given by:

$$\dot{\rho}_j = \frac{\rho_j}{\bar{V}_j} (Q_{1j}^\rho - Q_{2j}^\rho) - A_{nj} \frac{\rho_j}{\bar{V}_j} (v_{cj} + v_{c(j+1)}) \quad (3.22)$$

Finally, using the relationship (3.4) we obtain (3.20). \square

Defining $\boldsymbol{\rho} = [\rho_1 \ \cdots \ \rho_{n_f-1}]^\top$ as the set of node densities, the fluid dynamics in the $n_f - 1$ nodes can be expressed as:

$$\dot{\boldsymbol{\rho}} = \vartheta_\rho \mathbf{Q}_1^\rho - \vartheta_\rho \mathbf{Q}_2^\rho - \varphi_\rho \mathbf{v}_c \quad (3.23)$$

where $\mathbf{Q}_1^\rho = [Q_{11} \ \cdots \ Q_{1(n_f-1)}]^\top$ and $\mathbf{Q}_2^\rho = [Q_{21} \ \cdots \ Q_{2(n_f-1)}]^\top$ are the sets of inlet and outlet volumetric flows of the nodes, respectively, and matrices ϑ_ρ and φ_ρ are given by

$$\vartheta_\rho = \frac{1}{m} \begin{bmatrix} \rho_1^2 & 0 & \cdots & 0 \\ 0 & \ddots & \ddots & \vdots \\ \vdots & \ddots & \ddots & 0 \\ 0 & \cdots & 0 & \rho_{n_f-1}^2 \end{bmatrix} \quad \text{and} \quad \varphi_\rho = \frac{1}{m} \begin{bmatrix} A_{n1} \rho_1^2 & A_{n1} \rho_1^2 & 0 & \cdots & 0 \\ 0 & \ddots & \ddots & \ddots & \vdots \\ \vdots & \ddots & \ddots & \ddots & 0 \\ 0 & \cdots & 0 & A_{n(n_f-1)} \rho_{n_f-1}^2 & A_{n(n_f-1)} \rho_{n_f-1}^2 \end{bmatrix}$$

respectively. This density variation implies a change in the pressure in the nodes, which, in turn, has an associated energy. In this sense, we denote by $p_j^\rho = p_j - p_0$ the variation of the static pressure in the j -th node, where p_0 is the pressure at reference density ρ_0 and p_j is the absolute static pressure in the node. Thus, from the definition of the bulk modulus, β_S , [105] we obtain:

$$p_j^\rho = \beta_S \ln \left(\frac{\rho_j}{\rho_0} \right) \quad (3.24)$$

This implies that the density variation allows us to describe the static pressure between 2 adjacent incompressible sections, that can be coupled using a power-preserving interconnection, as shown in the next section.

3.2 PORT-HAMILTONIAN FORMULATION OF THE FSI MODEL

To obtain a port-Hamiltonian formulation of the overall system we first define the stored energy in the fluid. For the incompressible fluid sections, the stored energy is the kinetic energy given by $\frac{1}{2} \rho_0 V_j v_j^2$ for the j -th fluid section. Considering the momentum of fluid sections,

$\pi_{\zeta j} = \rho_0 V_j v_j$, the total kinetic energy of the fluid can be expressed as:

$$\mathcal{K}_f = \sum_{j=1}^{n_f} \frac{1}{2} \rho_0 V_j v_j^2 = \sum_{j=1}^{n_f} \frac{1}{2} \frac{\pi_{\zeta j}^2}{\rho_0 V_j} \quad (3.25)$$

where $\partial_{\pi_{\zeta j}} \mathcal{K}_f = \frac{\pi_{\zeta j}}{\rho_0 V_j} = v_j$. To describe the energy associated with the nodes we consider the fluid as an isentropic process. Then, from the Gibbs equation the variation of the internal energy of the fluid in the node, \mathcal{U}_j , is given by its work, $d\mathcal{U}_j = -p_j^\rho d\bar{V}_j$. Using (3.4), the differential of the internal energy can be rewritten as

$$d\mathcal{U}_j = p_j^\rho \frac{m}{\rho_j^2} d\rho_j \quad (3.26)$$

Substituting (3.24) in (3.26) and solving for \mathcal{U}_j , the internal energy in node j is then given by the following non-negative function $\mathcal{U}_j = m\beta_S \frac{\rho_j - \rho_0 (1 + \ln(\rho_j/\rho_0))}{\rho_j \rho_0}$. Thus, for the $n_f - 1$ nodes, the total energy is

$$\mathcal{U}_f = \sum_{j=1}^{n_f-1} m\beta_S \frac{\rho_j - \rho_0 (1 + \ln(\rho_j/\rho_0))}{\rho_j \rho_0} \quad (3.27)$$

and $\partial_{\rho_j} \mathcal{U}_f = \frac{m}{\rho_j^2} p_j^\rho$.

As mentioned in Section 3.1.2, the changes in the geometry of the fluid domain induce a rotation of the flow that generates energy dissipation by viscous friction. From a port-Hamiltonian point of view, the power dissipated in the j -th incompressible fluid section is given by $\partial_{\pi_{\zeta j}} \mathcal{K}_f \phi_{\zeta j}$. Comparing this result with (3.8) and defining the characteristic density, velocity and area as ρ_0 , v_j and A_j , respectively, the force associated with the dissipations in the j -th incompressible fluid section can be expressed as

$$\phi_{\zeta j} = \frac{1}{2} \lambda_j \rho_0 A_j |v_j| v_j = \frac{1}{2} \frac{\lambda_j}{\ell_j} |\pi_{\zeta j}| \partial_{\pi_{\zeta j}} \mathcal{K}_f \quad (3.28)$$

Similarly, note that the inlet and outlet flows can be rewritten as:

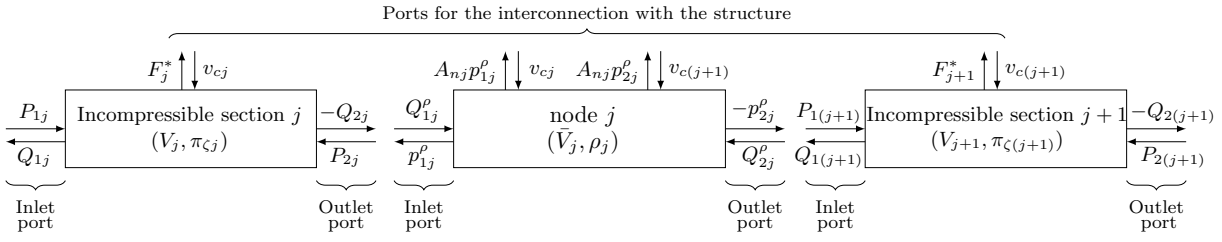
$$Q_{1j} = A_j \partial_{\pi_{\zeta j}} \mathcal{K}_f + \frac{A_{cj}}{2} v_{cj} \quad (3.29)$$

$$Q_{2j} = A_j \partial_{\pi_{\zeta j}} \mathcal{K}_f - \frac{A_{cj}}{2} v_{cj} \quad (3.30)$$

Then, the dynamics of the fluid in the j -th incompressible fluid section can be expressed as the following port-Hamiltonian formulation:

$$\dot{\pi}_{\zeta j} = -\frac{1}{2} \frac{\lambda_j}{\ell_j} |\pi_{\zeta j}| \partial_{\pi_{\zeta j}} \mathcal{K}_f + [A_j \quad -A_j \quad -\frac{A_{cj}}{V_j} \pi_{\zeta j}] \begin{bmatrix} P_{1j} \\ P_{2j} \\ v_{cj} \end{bmatrix} \quad (3.31a)$$

$$\begin{bmatrix} Q_{1j} \\ -Q_{2j} \\ -F_j^* \end{bmatrix} = \begin{bmatrix} A_j \\ -A_j \\ -\frac{A_{cj}}{V_j} \pi_{\zeta j} \end{bmatrix} \partial_{\pi_{\zeta j}} \mathcal{K}_f + \begin{bmatrix} 0 & 0 & \frac{A_{cj}}{2} \\ 0 & 0 & \frac{A_{cj}}{2} \\ -\frac{A_{cj}}{2} & -\frac{A_{cj}}{2} & 0 \end{bmatrix} \begin{bmatrix} P_{1j} \\ P_{2j} \\ v_{cj} \end{bmatrix} \quad (3.31b)$$


 Figure 3.3 – Inputs/outputs diagram of the node j and the adjacent incompressible sections.

Similarly, the dynamics of the fluid in j -th node are modeled by the following port-Hamiltonian formulation:

$$\dot{\rho}_j = 0\partial_{\rho_j}\mathcal{U}_f + \begin{bmatrix} \frac{\rho^2}{m} & -\frac{\rho^2}{m} & -A_{nj}\frac{\rho^2}{m} & -A_{nj}\frac{\rho^2}{m} \end{bmatrix} \begin{bmatrix} Q_{1j}^\rho \\ Q_{2j}^\rho \\ v_{cj} \\ v_{c(j+1)} \end{bmatrix} \quad (3.32a)$$

$$\begin{bmatrix} p_{1j} \\ -p_{2j} \\ -A_{nj}p_{1j} \\ -A_{nj}p_{2j} \end{bmatrix} = \begin{bmatrix} \frac{\rho^2}{m} \\ -\frac{\rho^2}{m} \\ -A_{nj}\frac{\rho^2}{m} \\ -A_{nj}\frac{\rho^2}{m} \end{bmatrix} \partial_{\rho_j}\mathcal{U}_f \quad (3.32b)$$

Figure 3.3 shows a diagram with the ports of the PHS model of node j and the adjacent incompressible sections. Notice that inputs of the inlet and outlet ports of node j , namely Q_{1j}^ρ and Q_{2j}^ρ , respectively, are compatible with the output of the outlet port in the incompressible section j and the output of the inlet port in the incompressible section $j+1$, Q_{2j} and $Q_{1(j+1)}$ respectively. The static pressures in the outputs of the inlet and outlet ports in the node, namely p_{1j}^ρ and p_{2j}^ρ respectively, are only one part of the total pressures in the inputs of the adjacent incompressible section, namely P_{2j} and $P_{1(j+1)}$. This implies that an interconnection by ports, as described in Section 1.2.1.a, can not be done. However, given the relationship between the volume of the incompressible sections and the density of the nodes described in (3.10), we can made a power-preserving interconnection between the fluid sections, as will be shown in Section 3.2.1. Additionally, notice that the PHS formulation of the nodes and the incompressible sections provides a set of inputs and outputs that are useful for the fluid-structure interconnection, as will be shown in Section 3.3.

In the case of n_f sections, the term Φ in (3.19), can be rewritten as $\Phi = R_3\partial_{\pi_\zeta}\mathcal{K}_f$. Then, the governing equations can be expressed as:

$$\dot{\pi}_\zeta = -R_3\partial_{\pi_\zeta}\mathcal{K}_f + [\vartheta_\pi \quad -\vartheta_\pi \quad -\varphi_\pi] \begin{bmatrix} \mathbf{P}_1 \\ \mathbf{P}_2 \\ \mathbf{v}_c \end{bmatrix} \quad (3.33a)$$

$$\begin{bmatrix} \mathbf{Q}_1 \\ -\mathbf{Q}_2 \\ -\mathbf{F}^* \end{bmatrix} = \begin{bmatrix} \vartheta_\pi^\top \\ -\vartheta_\pi^\top \\ -\varphi_\pi^\top \end{bmatrix} \partial_{\pi_\zeta}\mathcal{K}_f + \begin{bmatrix} \mathbf{0} & \mathbf{0} & M_\pi \\ \mathbf{0} & \mathbf{0} & M_\pi \\ -M_\pi^\top & -M_\pi^\top & \mathbf{0} \end{bmatrix} \begin{bmatrix} \mathbf{P}_1 \\ \mathbf{P}_2 \\ \mathbf{v}_c \end{bmatrix} \quad (3.33b)$$

where $\mathbf{Q}_1 = [Q_{11} \cdots Q_{1n_f}]^\top$ and $\mathbf{Q}_2 = [Q_{21} \cdots Q_{2n_f}]^\top$ are the sets of inlet and outlet flows in the incompressible sections, respectively, $\mathbf{F}^* = [F_1^* \cdots F_{n_f}^*]^\top$ is a set of forces at the contact surfaces with the moving structure, and matrices $R_3 \geq 0$ and M_π are defined as

$$R_3 = \frac{1}{2} \begin{bmatrix} \lambda_1 |\pi_{\zeta_1}| / \ell_1 & 0 & \cdots & 0 \\ 0 & \ddots & \ddots & \vdots \\ \vdots & \ddots & \ddots & 0 \\ 0 & \cdots & 0 & \lambda_{n_f} |\pi_{\zeta_{n_f}}| / \ell_{n_f} \end{bmatrix} \quad M_\pi = \frac{1}{2} \begin{bmatrix} A_{c1} & 0 & \cdots & 0 \\ 0 & \ddots & \ddots & \vdots \\ \vdots & \ddots & \ddots & 0 \\ 0 & \cdots & 0 & A_{cn_f} \end{bmatrix} \quad (3.34)$$

The dynamics of the $n_f - 1$ nodes in (3.23) can be written as the following port-Hamiltonian system

$$\dot{\boldsymbol{\rho}} = \mathbf{0} \partial_\rho \mathcal{U}_f + \begin{bmatrix} \vartheta_\rho & -\vartheta_\rho & -\varphi_\rho \end{bmatrix} \begin{bmatrix} \mathbf{Q}_1^\rho \\ \mathbf{Q}_2^\rho \\ \mathbf{v}_c \end{bmatrix} \quad (3.35a)$$

$$\begin{bmatrix} \mathbf{p}_1^\rho \\ -\mathbf{p}_2^\rho \\ -\mathbf{F}^\rho \end{bmatrix} = \begin{bmatrix} \vartheta_\rho^\top \\ -\vartheta_\rho^\top \\ -\varphi_\rho^\top \end{bmatrix} \partial_\rho \mathcal{U}_f \quad (3.35b)$$

where $\mathbf{p}_1^\rho = [p_{11}^\rho \cdots p_{1(n_f-1)}^\rho]^\top$ and $\mathbf{p}_2^\rho = [p_{21}^\rho \cdots p_{2(n_f-1)}^\rho]^\top$ are the sets of pressures in the inlet and outlet node boundaries, respectively, and $\mathbf{F}^\rho = [F_1^\rho \cdots F_{n_f}^\rho]^\top$ denotes the forces at the contact surfaces between each section with uniform cross-sectional area and the corresponding node. Matrices ϑ_ρ and φ_ρ are defined in Section 3.1.3. Note that from the uniform density assumption in the nodes we have $p_{1j}^\rho = p_{2j}^\rho = p_j^\rho$. Additionally, the forces F_j^ρ are defined as $F_j^\rho = A_{n(j-1)} p_{j-1}^\rho + A_{nj} p_j^\rho, \forall j \in [2, n_f - 1]$, with $F_1^\rho = A_{n1} p_1^\rho$ and $F_{n_f}^\rho = A_{n(n_f-1)} p_{n_f-1}^\rho$.

3.2.1 Power-preserving interconnection of incompressible fluid sections and nodes

Note that the outputs $\{\mathbf{Q}_1, \mathbf{Q}_2\}$ of the incompressible section model are compatible with the inputs $\{\mathbf{Q}_1^\rho, \mathbf{Q}_2^\rho\}$ of the node model. Similarly, the inputs $\{\mathbf{P}_1, \mathbf{P}_2\}$ are compatible with outputs $\{\mathbf{p}_1^\rho, \mathbf{p}_2^\rho\}$. However, $\{\mathbf{p}_1^\rho, \mathbf{p}_2^\rho\}$ are static pressures and $\{\mathbf{P}_1, \mathbf{P}_2\}$ are total pressures. Thus, we describe the flow dynamics as shown in the following proposition.

Proposition 3.3. *Let $\mathbf{P}_1^\rho = \mathbf{p}_1^\rho + \mathbf{p}_d^\rho$ and $\mathbf{P}_2^\rho = \mathbf{p}_2^\rho + \mathbf{p}_d^\rho$ be the total pressure sets at the inlet and outlet boundaries of the nodes where \mathbf{p}_d^ρ is the set of dynamic pressures in the nodes, and $\{P_i, Q_i\}$ and $\{P_o, Q_o\}$ the pairs of total pressure and flow at the inlet and outlet boundaries of the fluid domain, respectively. There exist matrices C_1, C_2, C_{1*} and C_{2*} , defined as*

$$C_1 = \begin{bmatrix} 0_{(n_f-1) \times 1} & \mathbf{I} \end{bmatrix}, C_2 = \begin{bmatrix} \mathbf{I} & 0_{(n_f-1) \times 1} \end{bmatrix}, C_{1*} = \begin{bmatrix} 1 & 0_{1 \times (n_f-1)} \end{bmatrix} \quad \text{and} \\ C_{2*} = \begin{bmatrix} 0_{1 \times (n_f-1)} & 1 \end{bmatrix} \quad (3.36)$$

such that

$$\begin{aligned} \begin{bmatrix} C_1 \\ C_{1*} \end{bmatrix} \mathbf{Q}_1 &= \begin{bmatrix} \mathbf{Q}_2^\rho \\ Q_i \end{bmatrix}, \quad \begin{bmatrix} C_2 \\ C_{2*} \end{bmatrix} \mathbf{Q}_2 = \begin{bmatrix} \mathbf{Q}_1^\rho \\ Q_o \end{bmatrix}, \quad \begin{bmatrix} C_1 \\ C_{1*} \end{bmatrix}^\top \begin{bmatrix} \mathbf{p}_2^\rho + \mathbf{p}_d^\rho \\ P_i \end{bmatrix} = \mathbf{P}_1, \quad \text{and} \\ \begin{bmatrix} C_2 \\ C_{2*} \end{bmatrix}^\top \begin{bmatrix} \mathbf{p}_1^\rho + \mathbf{p}_d^\rho \\ P_o \end{bmatrix} &= \mathbf{P}_2. \end{aligned}$$

Then, the fluid sections can be interconnected using the following power-preserving rule:

$$\begin{bmatrix} \mathbf{Q}_1^\rho \\ \mathbf{Q}_2^\rho \\ \mathbf{P}_1 \\ \mathbf{P}_2 \\ -Q_i \\ Q_o \end{bmatrix} = \underbrace{\begin{bmatrix} \mathbf{0} & \mathbf{0} & \mathbf{0} & -C_2 & \mathbf{0} & \mathbf{0} \\ \mathbf{0} & \mathbf{0} & C_1 & \mathbf{0} & \mathbf{0} & \mathbf{0} \\ \mathbf{0} & -C_1^\top & \mathbf{0} & \mathbf{0} & C_{1*}^\top & \mathbf{0} \\ C_2^\top & \mathbf{0} & \mathbf{0} & \mathbf{0} & \mathbf{0} & C_{2*}^\top \\ \mathbf{0} & \mathbf{0} & -C_{1*} & \mathbf{0} & \mathbf{0} & \mathbf{0} \\ \mathbf{0} & \mathbf{0} & \mathbf{0} & -C_{2*} & \mathbf{0} & \mathbf{0} \end{bmatrix}}_{\mathcal{I}_f} \begin{bmatrix} \mathbf{p}_1^\rho + \mathbf{p}_d^\rho \\ -\mathbf{p}_2^\rho - \mathbf{p}_d^\rho \\ \mathbf{Q}_1 \\ -\mathbf{Q}_2 \\ P_i \\ P_o \end{bmatrix} \quad (3.37)$$

where \mathcal{I}_f is the skew-symmetric interconnection matrix of the fluid sections.

Proof. Note that $Q_i = Q_{11}$ and $Q_{2(j-1)}^\rho = Q_{1j}, \forall j \in \{2, \dots, n_f\}$. Similarly, $Q_o = Q_{2n_f}$ and $Q_{1j}^\rho = Q_{2j}, \forall j \in [1, n_f - 1]$. Then, defining the matrices C_1, C_2, C_{1*} and C_{2*} as (3.36) and denoting by $\mathbf{u}^\top = [\mathbf{Q}_1^{\rho\top} \ \mathbf{Q}_2^{\rho\top} \ \mathbf{P}_1^\top \ \mathbf{P}_2^\top \ -Q_j \ Q_o]$ the input of incompressible fluid section and nodes and by $\mathbf{y}^\top = [(\mathbf{p}_1^\rho + \mathbf{p}_d^\rho)^\top \ -(\mathbf{p}_2^\rho + \mathbf{p}_d^\rho)^\top \ \mathbf{Q}_1^\top \ -\mathbf{Q}_2^\top \ P_i \ P_o]$ the corresponding power conjugated outputs. Then, the total power exchange in the fluid is given by $\mathbf{u}^\top \mathbf{y}$. From the interconnection rule (3.37) we have $\mathbf{u} = \mathcal{I}_f \mathbf{y}$, and given the skew-symmetrical property of \mathcal{I}_f we obtain $\mathbf{u}^\top \mathbf{y} = 0$, i.e., (3.37) describes a power-preserving interconnection. \square

To apply the power-preserving interconnection described above, we need to define the dynamic pressure in the nodes. In this case we describe the dynamic pressure in node j as the weighted average of the dynamic pressure in adjacent incompressible fluid sections, i.e., $p_j^d = \frac{\rho_0}{2} v_j^2 \alpha_j + \frac{\rho_0}{2} v_{j+1}^2 (1 - \alpha_j)$, and $\mathbf{p}_d^\rho = [p_1^d \ \dots \ p_{n_f}^d]^\top$.

On the other hand, from (3.10), the kinetic energy of the fluid is a function of the node densities, such that,

$$\partial_{\rho_j} \mathcal{K}_f = \frac{\rho_0}{2} v_j^2 \partial_{\rho_j} V_j + \frac{\rho_0}{2} v_{j+1}^2 \partial_{\rho_j} V_{j+1} = \frac{m}{\rho_j^2} p_j^d \quad (3.38)$$

This implies that the dynamic pressure in each node can be expressed as:

$$\mathbf{p}_d^\rho = \vartheta_\rho^\top \partial_\rho \mathcal{K}_f \quad (3.39)$$

Then, defining the total energy of the fluid as:

$$\mathcal{H}_f = \mathcal{K}_f + \mathcal{U}_f \quad (3.40)$$

the fluid dynamics (3.33) and (3.35) can be formulated as in Proposition 3.4.

Proposition 3.4. *Let the state variables of the fluid be $\mathbf{x}_f^\top = [\boldsymbol{\pi}_\zeta^\top \boldsymbol{\rho}^\top]$. Using the interconnection rule (3.37), the fluid dynamics can be described as the following port-Hamiltonian system with feed-through term:*

$$\dot{\mathbf{x}}_f = (J_f - R_f) \partial_{\mathbf{x}_f} \mathcal{H}_f + G_f \mathbf{u}_f \quad (3.41a)$$

$$\mathbf{y}_f = G_f^\top \partial_{\mathbf{x}_f} \mathcal{H}_f + M_f \mathbf{u}_f \quad (3.41b)$$

where \mathcal{H}_f denotes the total energy, $\mathbf{u}_f = [P_i \ P_o \ \mathbf{v}_c^\top]^\top$ and $\mathbf{y}_f = [Q_i \ -Q_o \ \mathbf{F}_c^{*\top}]^\top$ describe the inputs and outputs in the fluid boundaries, respectively, with \mathbf{v}_c and \mathbf{F}_c^* the sets of velocities and forces at the contact surface with the mechanical structure. Matrices $J_f = -J_f^\top$, $R_f = R_f^\top \geq 0$, G_f and $M_f = -M_f^\top$ are given by:

$$J_f = \begin{bmatrix} \mathbf{0} & \psi \\ -\psi^\top & \mathbf{0} \end{bmatrix} \quad R_f = \begin{bmatrix} R_3 & \mathbf{0} \\ \mathbf{0} & \mathbf{0} \end{bmatrix} \quad G_f = \begin{bmatrix} \vartheta & -\varphi_\pi \\ \mathbf{0} & -\varphi \end{bmatrix} \quad M_f = \begin{bmatrix} \mathbf{0} & \psi_M \\ -\psi_M^\top & \mathbf{0} \end{bmatrix} \quad (3.42)$$

where $\vartheta = \vartheta_\pi [C_{1*}^\top \ -C_{2*}^\top]$ maps the boundary pressures in the corresponding fluid sections, $\varphi = \varphi_\rho + \vartheta_\rho (C_2 + C_1) M_\pi$ maps the upper boundary velocities in the nodes, $\psi = \vartheta_\pi (C_1^\top - C_2^\top) \vartheta_\rho^\top$ describes the energy flux between the state variables and $\psi_M = [C_{1*}^\top \ C_{2*}^\top]^\top M_\pi$ defines the feed-through terms.

Proof. Consider the interconnection rule (3.37) and the expression of the dynamic pressure (3.39). Systems (3.33) and (3.35) can be rewritten as:

$$\begin{aligned} \dot{\boldsymbol{\pi}}_\zeta &= -R_3 \partial_{\boldsymbol{\pi}_\zeta} \mathcal{K}_f + \vartheta_\pi (C_1^\top - C_2^\top) \vartheta_\rho^\top (\partial_\rho \mathcal{K}_f + \partial_\rho \mathcal{U}_f) + \vartheta_\pi C_{1*}^\top P_i - \vartheta_\pi C_{2*}^\top P_o - \varphi_\pi \mathbf{v}_c \\ \dot{\boldsymbol{\rho}} &= -\vartheta_\rho (C_1 - C_2) \vartheta_\pi^\top \partial_{\boldsymbol{\pi}_x} \mathcal{K}_f - (\varphi_\rho + \vartheta_\rho (C_1 + C_2) M_\pi) \mathbf{v}_c \end{aligned}$$

Using the total energy (3.40), we obtain the following port-Hamiltonian system:

$$\begin{aligned} \begin{bmatrix} \dot{\boldsymbol{\pi}}_\zeta \\ \dot{\boldsymbol{\rho}} \end{bmatrix} &= \begin{bmatrix} -R_3 & \psi \\ -\psi^\top & \mathbf{0} \end{bmatrix} \begin{bmatrix} \partial_{\boldsymbol{\pi}_\zeta} \mathcal{H}_f \\ \partial_\rho \mathcal{H}_f \end{bmatrix} + \begin{bmatrix} \vartheta & -\varphi_\pi \\ \mathbf{0} & -\varphi \end{bmatrix} \begin{bmatrix} \mathbf{u}_p \\ \mathbf{v}_c \end{bmatrix} \\ \begin{bmatrix} \mathbf{y}_Q \\ -\mathbf{F}_c^* \end{bmatrix} &= \begin{bmatrix} \vartheta^\top & \mathbf{0} \\ -\varphi_\pi^\top & -\varphi^\top \end{bmatrix} \begin{bmatrix} \partial_{\boldsymbol{\pi}_\zeta} \mathcal{H}_f \\ \partial_\rho \mathcal{H}_f \end{bmatrix} + \begin{bmatrix} \mathbf{0} & \psi_M \\ -\psi_M^\top & \mathbf{0} \end{bmatrix} \begin{bmatrix} \mathbf{u}_p \\ \mathbf{v}_c \end{bmatrix} \end{aligned}$$

where $\mathbf{u}_p = [P_i \ P_o]^\top$, $\mathbf{y}_Q = [Q_i \ -Q_o]^\top$ describe the power-conjugated input and output, respectively, at the inlet and outlet boundaries of the fluid domain, and \mathbf{F}_c^* contains the set of forces on the contact surface with the structure. The internal matrices are given by $\vartheta = \vartheta_\pi [C_{1*}^\top \ -C_{2*}^\top]$, $\varphi = \varphi_\rho + \vartheta_\rho (C_2 + C_1) M_\pi$, $\psi = \vartheta_\pi (C_1^\top - C_2^\top) \vartheta_\rho^\top$ and $\psi_M = [C_{1*}^\top \ C_{2*}^\top]^\top M_\pi$. Finally, defining the port-Hamiltonian matrices as in (3.42), we obtain the system (3.41). \square

We notice that $\mathbf{F}_c^* = \mathbf{F}_c + \hat{\mathbf{F}}$ where \mathbf{F}_c is the effective force applied on the contact surface between the fluid and the structure, and $\hat{\mathbf{F}}$ is a set of extra forces associated with the variation of volume of each fluid section induced by the motion of the structure. These extra forces are defined as $\hat{\mathbf{F}} = \partial_{\mathbf{q}_f} H_f$ where $\mathbf{q}_f = [q_{f1} \ \cdots \ q_{fn_f}]^\top$ is the set of heights of each fluid sections of uniform cross-sectional area.

In works such as [57], the extra force $\hat{\mathbf{F}}$ is compensated including a state variable to model the changes in the cross-sectional area, that is equivalent to include \mathbf{q}_f as a state variable. However, with this approach, the number of states increases and the resulting fluid-structure interaction system has a non-minimal realization. In the next section we propose an alternative way to compensate $\hat{\mathbf{F}}$.

3.3 FLUID-STRUCTURE POWER-PRESERVING INTERCONNECTION



Figure 3.4 – Finite-dimensional formulation of the fluid-structure system. MSD-based description of the structure motion. Fluid dynamics description based on nodes (red) and incompressible fluid sections.

In this section we describe the power-preserving interconnection between the fluid model (3.41) and the structure. We consider a MSD formulation of the structure motion, as shown in Figure 3.4, whose port-Hamiltonian model is given by:

$$\begin{bmatrix} \dot{\mathbf{q}}_s \\ \dot{\boldsymbol{\pi}}_s \end{bmatrix} = \begin{bmatrix} \mathbf{0} & \mathbf{I} \\ -\mathbf{I} & -R \end{bmatrix} \begin{bmatrix} \partial_{\mathbf{q}_s} \mathcal{H}_s \\ \partial_{\boldsymbol{\pi}_s} \mathcal{H}_s \end{bmatrix} + \begin{bmatrix} \mathbf{0} \\ \mathbf{I} \end{bmatrix} \mathbf{F}_s \quad (3.43a)$$

$$\mathbf{v}_s = \begin{bmatrix} \mathbf{0} & \mathbf{I} \end{bmatrix} \begin{bmatrix} \partial_{\mathbf{q}_s} \mathcal{H}_s \\ \partial_{\boldsymbol{\pi}_s} \mathcal{H}_s \end{bmatrix} \quad (3.43b)$$

where \mathbf{q}_s , \mathbf{v}_s and $\boldsymbol{\pi}_s$ denote the sets of displacement, velocity and momentum of the n_s masses describing the transversal structure motion, \mathbf{F}_s denotes the external forces acting on the masses and \mathcal{H}_s is the total stored energy. Considering that moving boundary of the fluid domain is given by the structure motion described in (3.43), there exists an $n_f \times n_s$ matrix C such that $C\mathbf{v}_s = \mathbf{v}_c$ and $C^\top \mathbf{F}_c = \mathbf{F}_s$. This matrix C is composed only with 0 and 1, and is defined according to the link between the masses and the corresponding fluid sections with uniform cross-sectional areas. For example, consider the fluid-structure system in Figure 3.4, where the length ℓ_f of the fluid section with uniform cross-sectional areas is equal to the length ℓ_s of the masses that describe the transversal structure motion. In this case the matrix C is equal to the identity matrix. Figure 3.5 shows another example where $\ell_s = 2\ell_f$ ($n_f \neq n_s$). In this case


 Figure 3.5 – Finite-dimensional formulation of the fluid-structure system with $n_f \neq n_s$.

the matrix C is defined as:

$$C = \begin{bmatrix} 1 & 0 & 0 & \cdots & 0 & 0 \\ 1 & 0 & 0 & \cdots & 0 & 0 \\ 0 & 1 & 0 & \ddots & \vdots & \vdots \\ 0 & 1 & 0 & \ddots & \vdots & \vdots \\ \vdots & \vdots & \vdots & \ddots & \vdots & \vdots \\ 0 & 0 & 0 & \cdots & 0 & 1 \\ 0 & 0 & 0 & \cdots & 0 & 1 \end{bmatrix}$$

Remark 3.1. In the previous examples, we considered that the length of the fluid domain and the length of the structure domain in motion are equal, as shown in Figures 3.4 and 3.5. However, in some problems the motion of the structure is constrained to one part of the structure domain. An example of this class of problems is the vocal folds, where finite-dimensional models, as the BCM, describe the motion only in the folds area that collides. In these cases, matrix C is defined according to the fluid sections under the moving structure area with motion, as will be shown in Section 4.4.

Defining $\mathbf{F}_s = C^\top \mathbf{F}_c + \mathbf{u}_e$ where \mathbf{u}_e denotes external forces, the fluid and structure models can be coupled using the following power-preserving interconnection rule

$$\begin{bmatrix} \mathbf{v}_c \\ \mathbf{F}_s \\ -\mathbf{y}_e \end{bmatrix} = \begin{bmatrix} \mathbf{0} & C & \mathbf{0} \\ -C^\top & \mathbf{0} & \mathbf{I} \\ \mathbf{0} & -\mathbf{I} & \mathbf{0} \end{bmatrix} \begin{bmatrix} -\mathbf{F}_c \\ \mathbf{v}_s \\ \mathbf{u}_e \end{bmatrix} \quad (3.44)$$

Considering the relationship $\mathbf{q}_f = \mathbf{q}_0 + C\mathbf{q}_s$, where $\mathbf{q}_0 = [q_{01} \cdots q_{0n_f}]^\top$ denotes the set of initial height of incompressible sections, we obtain the expression $C^\top \hat{\mathbf{F}} = C^\top \partial_{\mathbf{q}_f} \mathcal{H}_f = \partial_{\mathbf{q}_s} \mathcal{H}_f$. Then, the FSI system can be modeled as follows.

Proposition 3.5. Let the port-Hamiltonian models of the structure and the incompressible flow be described as in (3.43) and (3.41), respectively. Then, the PHS that describes the FSI between these two sub-systems is given by:

$$\dot{\mathbf{x}}_{fs} = (J_{fs} - R_{fs}) \partial_{\mathbf{x}_{fs}} \mathcal{H}_{fs} + G_{fs} \mathbf{u}_{fs} \quad (3.45)$$

$$\mathbf{y}_{fs} = G_{fs}^\top \partial_{\mathbf{x}_{fs}} \mathcal{H}_{fs} \quad (3.46)$$

where $\mathbf{x}_{fs}^\top = [\mathbf{q}_s^\top \ \boldsymbol{\pi}_s^\top \ \boldsymbol{\pi}_\zeta^\top \ \boldsymbol{\rho}^\top]$, $\mathbf{u}_{fs}^\top = [P_i \ P_o \ \mathbf{u}_e^\top]$, $\mathbf{y}_{fs}^\top = [Q_i \ -Q_o \ \mathbf{y}_e^\top]$ and $\mathcal{H}_{fs} = \mathcal{H}_f + \mathcal{H}_s$ denote the state vector, input, output and total stored energy of the FSI system, respectively, and matrices $J_{fs} = -J_{fs}^\top$, $R_{fs} = R_{fs}^\top \geq 0$ and G_{fs} are defined as:

$$J_{fs} = \begin{bmatrix} \mathbf{0} & \mathbf{I} & \mathbf{0} & \mathbf{0} \\ -\mathbf{I} & \mathbf{0} & [\varphi_\pi C]^\top & [\varphi C]^\top \\ \mathbf{0} & -\varphi_\pi C & \mathbf{0} & \psi \\ \mathbf{0} & -\varphi C & -\psi^\top & \mathbf{0} \end{bmatrix}, \quad R_{fs} = \begin{bmatrix} \mathbf{0} & \mathbf{0} & \mathbf{0} & \mathbf{0} \\ \mathbf{0} & R & \mathbf{0} & \mathbf{0} \\ \mathbf{0} & \mathbf{0} & R_3 & \mathbf{0} \\ \mathbf{0} & \mathbf{0} & \mathbf{0} & \mathbf{0} \end{bmatrix}, \quad G_{fs} = \begin{bmatrix} \mathbf{0} & \mathbf{0} \\ C^\top \psi_M^\top & \mathbf{I} \\ \vartheta & \mathbf{0} \\ \mathbf{0} & \mathbf{0} \end{bmatrix} \quad (3.47)$$

Proof. Consider the fluid and structure models (3.43) and (3.41), respectively. Using the interconnection rule (3.44) and expressing the effective force applied by the fluid on the structure as $\mathbf{F}_c = \mathbf{F}_c^* - \partial_{\mathbf{q}_f} H_f$, the dynamics of the structure and fluid can be rewritten as:

$$\begin{aligned} \dot{\mathbf{q}}_s &= \partial_{\boldsymbol{\pi}_s} \mathcal{H}_s \\ \dot{\boldsymbol{\pi}}_s &= -\partial_{\mathbf{q}_s} \mathcal{H}_s - R \partial_{\boldsymbol{\pi}_s} \mathcal{H}_s + C^\top (\mathbf{F}_c^* - \partial_{\mathbf{q}_f} \mathcal{H}_f) + \mathbf{u}_e \\ \dot{\boldsymbol{\pi}}_\zeta &= -R_3 \partial_{\boldsymbol{\pi}_\zeta} \mathcal{H}_f + \psi \partial_{\boldsymbol{\rho}} \mathcal{H}_f + \vartheta \mathbf{u}_p - \varphi_\pi C \mathbf{v}_s \\ \dot{\boldsymbol{\rho}} &= -\psi^\top \partial_{\boldsymbol{\pi}_\zeta} \mathcal{H}_f - \varphi C \mathbf{v}_s \end{aligned}$$

where $\mathbf{v}_s = \partial_{\boldsymbol{\pi}_s} \mathcal{H}_s$ and $\mathbf{F}_c^* = \varphi_\pi^\top \partial_{\boldsymbol{\pi}_\zeta} \mathcal{H}_f + \varphi^\top \partial_{\boldsymbol{\rho}} \mathcal{H}_f + \psi_M^\top \mathbf{u}_p$. Considering $C^\top \partial_{\mathbf{q}_f} H_f = \partial_{\mathbf{q}_s} H_f$ the fluid-structure system can be expressed as:

$$\begin{aligned} \begin{bmatrix} \dot{\mathbf{q}}_s \\ \dot{\boldsymbol{\pi}}_s \\ \dot{\boldsymbol{\pi}}_\zeta \\ \dot{\boldsymbol{\rho}} \end{bmatrix} &= \begin{bmatrix} \mathbf{0} & \mathbf{I} & \mathbf{0} & \mathbf{0} \\ -\mathbf{I} & -R & C^\top \varphi_\pi^\top & C^\top \varphi^\top \\ \mathbf{0} & -\varphi_\pi C & -R_3 & \psi \\ \mathbf{0} & -\varphi C & -\psi^\top & \mathbf{0} \end{bmatrix} \begin{bmatrix} \partial_{\mathbf{q}_s} \mathcal{H}_{fs} \\ \partial_{\boldsymbol{\pi}_s} \mathcal{H}_{fs} \\ \partial_{\boldsymbol{\pi}_\zeta} \mathcal{H}_{fs} \\ \partial_{\boldsymbol{\rho}} \mathcal{H}_{fs} \end{bmatrix} + \begin{bmatrix} \mathbf{0} & \mathbf{0} \\ C^\top \psi_M^\top & \mathbf{I} \\ \vartheta & \mathbf{0} \\ \mathbf{0} & \mathbf{0} \end{bmatrix} \begin{bmatrix} \mathbf{u}_p \\ \mathbf{u}_e \end{bmatrix} \\ \begin{bmatrix} \mathbf{y}_Q \\ \mathbf{y}_e \end{bmatrix} &= \begin{bmatrix} \mathbf{0} & \psi_M C & \vartheta^\top & \mathbf{0} \\ \mathbf{0} & \mathbf{I} & \mathbf{0} & \mathbf{0} \end{bmatrix} \begin{bmatrix} \partial_{\mathbf{q}_s} \mathcal{H}_{fs} \\ \partial_{\boldsymbol{\pi}_s} \mathcal{H}_{fs} \\ \partial_{\boldsymbol{\pi}_\zeta} \mathcal{H}_{fs} \\ \partial_{\boldsymbol{\rho}} \mathcal{H}_{fs} \end{bmatrix} \end{aligned}$$

Finally, defining the matrices J_{sf} , R_{fs} and G_{fs} as shown in (3.47) we obtain the fluid-structure interaction model described in (3.46). \square

3.4 EXAMPLE: PRESSURE WAVE PROPAGATION IN A FLEXIBLE TUBE

The pressure wave propagation in a flexible tube is a common benchmark for numerical algorithms applied to fluid-structure interaction analysis [10, 12, 9]. We consider a flexible tube with axisymmetric behavior and we approximate the tube structure and the fluid dynamics using the models described in Propositions 2.1 and 3.4, respectively. The structure parameters are approximated using formula (2.1), (2.5), (2.6) and (2.8). Defining $n_s = n_f = N$ we obtain

$$\ell_s = \ell_f = L/N \qquad q_{0i} = r, \forall j$$

Table 3.1 – Material parameters of the structure and the fluid.

Reference	Subsystem	Parameters
[10]	Structure	$\mu = 5.75 \times 10^4 \text{Pa}$, $\lambda = 17 \times 10^4 \text{Pa}$, $h = 0.001 \text{m}$, $r = 0.005 \text{m}$ $L = 0.06 \text{m}$, $\rho_s = 1.1 \times 10^3 \text{Kg/m}^3$
	Fluid	$\rho_0 = 1 \times 10^3 \text{Kg/m}^3$, $\beta_S = 2.15 \times 10^9 \text{Pa}$
[12]	Structure	$\mu = 11.538 \times 10^4 \text{Pa}$, $\lambda = 17.308 \times 10^4 \text{Pa}$, $h = 0.001 \text{m}$, $r = 0.005 \text{m}$ $L = 0.05 \text{m}$, $\rho_s = 1.2 \times 10^3 \text{Kg/m}^3$
	Fluid	$\rho_0 = 1 \times 10^3 \text{Kg/m}^3$, $\beta_S = 2.15 \times 10^9 \text{Pa}$

Table 3.2 – Parameters of the fluid-structure model [12].

Sections	Subsystem	Parameters
$N = 51$	Structure	$k_j = 73.9483 \text{N/m}$, $k_{cj} = 2.7 \times 10^{-2} \text{N/m}$, $d_j = 2.09 \times 10^{-2} \text{Ns/m}$ $m_j = 3.7 \times 10^{-5} \text{Kg}$, $\ell_s = 9.8 \times 10^{-4} \text{m}$
	Fluid	$\ell_f = 9.8 \times 10^{-4} \text{m}$, $m = 7.7 \times 10^{-8} \text{Kg}$
$N = 71$	Structure	$k_j = 51.9883 \text{N/m}$, $k_{cj} = 3.86 \times 10^{-2} \text{N/m}$, $d_j = 1.48 \times 10^{-2} \text{Ns/m}$ $m_j = 2.65 \times 10^{-5} \text{Kg}$, $\ell_s = 7.04 \times 10^{-4} \text{m}$
	Fluid	$\ell_f = 7.04 \times 10^{-4} \text{m}$, $m = 5.53 \times 10^{-8} \text{Kg}$

where L and r are the length and the internal radius of the tube, respectively. The fluid cross-sectional area is given by $A_j = \pi q_{fj}^2$. The areas of the contact surface in incompressible sections and nodes are defined as $A_{cj} = 2\pi q_{fj} \ell_j$ and $A_{nj} = 2\pi q_{fj} \bar{\ell}_j$, respectively. Similarly, the mass of nodes is given by $m = \rho_0 \pi r^2 \ell_f 10^{-3}$. As a consequence of $\ell_s = \ell_f$ the coupling matrix between the fluid and the structure is given by $C = \mathbf{I}$. Then, the matrices of the fluid-structure port-Hamiltonian model described in Proposition 3.5 are given by:

$$J_{fs} = \begin{bmatrix} \mathbf{0} & \mathbf{I} & \mathbf{0} & \mathbf{0} \\ -\mathbf{I} & \mathbf{0} & \varphi_\pi^\top & \varphi^\top \\ \mathbf{0} & -\varphi_\pi & \mathbf{0} & \psi \\ \mathbf{0} & -\varphi & -\psi^\top & \mathbf{0} \end{bmatrix}, \quad R_{fs} = \begin{bmatrix} \mathbf{0} & \mathbf{0} & \mathbf{0} & \mathbf{0} \\ \mathbf{0} & R_1 & \mathbf{0} & \mathbf{0} \\ \mathbf{0} & \mathbf{0} & R_3 & \mathbf{0} \\ \mathbf{0} & \mathbf{0} & \mathbf{0} & \mathbf{0} \end{bmatrix}, \quad G_{fs} = \begin{bmatrix} \mathbf{0} & \mathbf{0} \\ \psi_M^\top & \mathbf{I} \\ \vartheta & \mathbf{0} \\ \mathbf{0} & \mathbf{0} \end{bmatrix}$$

In this example, we neglect the viscous losses, considering only (3.9) to define the geometrical fluid loss factor λ_j . For the simulation we use the parameters proposed in [12, Section 5.1], summarized in Table 3.1. We divide the structure into two different numbers of sections, $N = 51$ and $N = 71$. We use $\beta_1 = 6.7$, $\beta_2 = 1.5 \times 10^{-5}$, and $\zeta = 0.4$. The parameter values are summarized in Table 3.2. Using the same input conditions as described in [12], i.e., $P_o = 0 \text{ Pa}$, and

$$P_i = \begin{cases} 1.333 \times 10^3 \text{ Pa}, & 0 \leq t \leq 3 \times 10^{-3} \text{ s} \\ 0 \text{ Pa}, & \text{otherwise} \end{cases}$$

with a sample time of $4 \times 10^{-5} \text{ s}$, we obtain the pressure wave propagation shown in Figure 3.6, where the structure displacements have been scaled 10 times for the sake of clarity. Note that the speed propagation and attenuation of pressure waves are in correspondence with the results in [12, Figure 2]. However, a difference from the results in [12] is the static pressure undershoot behind the pressure pulse propagation and a negative displacement of the tube walls (dashed boxes in Figure 3.6). Note that both, the distance between this undershoot and the pressure pulse, increase as the pulse propagates through the tube. This behavior is consistent with the results reported in [9, Figure 6], where a 3D model of the flexible tube is studied. Regarding

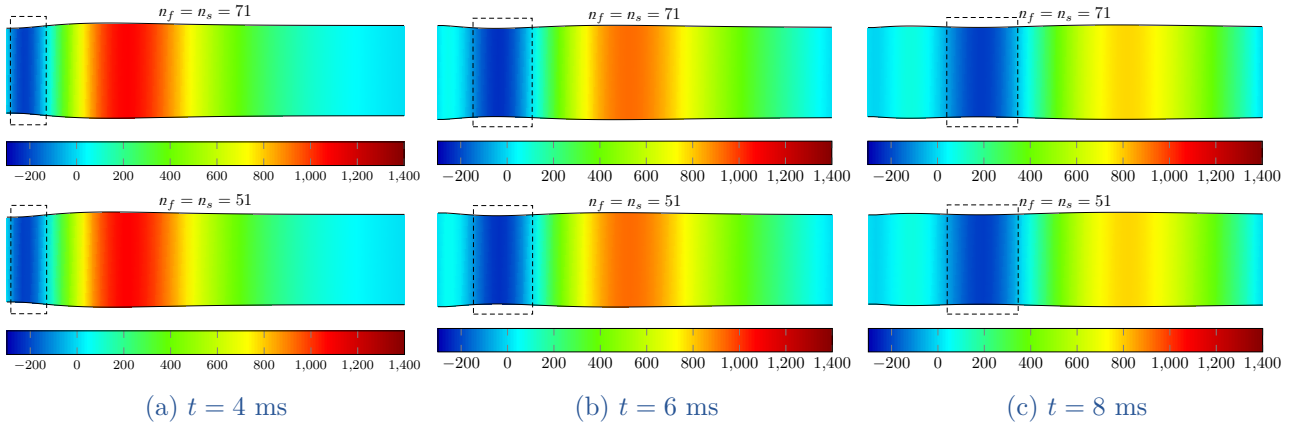


Figure 3.6 – Static pressure (Pa) distribution, \mathbf{p}_1^p , along the tube and scaled structure displacements for different time instants and two different numbers of sections. Dashed boxes: static pressure undershoot and negative displacement of the walls.

Table 3.3 – Parameters of the fluid-structure model using the material specifications of [10].

Sections	Subsystem	Parameters
$N = 71$	Structure	$k_j = 100.604\text{N/m}$, $k_{cj} = 90.85 \times 10^{-2}\text{N/m}$, $d_j = 4.34 \times 10^{-2}\text{Ns/m}$ $m_j = 2.92 \times 10^{-5}\text{Kg}$, $\ell_s = 8.45 \times 10^{-4}\text{m}$
	Fluid	$\ell_f = 8.45 \times 10^{-4}\text{m}$, $m = 6.63 \times 10^{-8}\text{Kg}$

the negative displacement, consider the displacement at the half length of the structure shown in Figure 3.7. This displacement shows the same pattern as the radial displacement reported

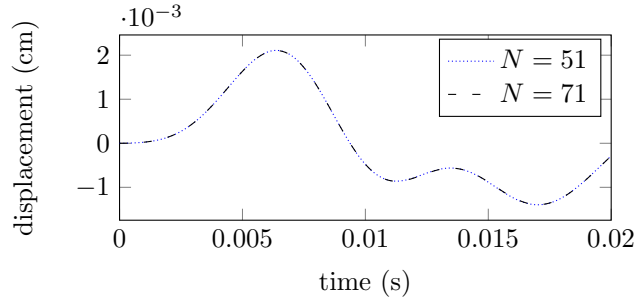


Figure 3.7 – Displacement of the wall in the half-length point of the structure (Displacements q_{26} and q_{36} for $N = 51$ and $N = 71$, respectively).

in [12, Figure 3.b]. Then, the main difference with respect to the results reported in [12] is the displacement at both ends of the tube. This is due to the fact that in [12] the tube is fixed at both ends, restricting the motion of the tube. In this thesis we do not implement this restriction, allowing greater displacements at the left hand side of the tube, as shown in Figure 3.6a.

Now, we consider the parameters used in. [10], also shown in Table 3.1. The parameters

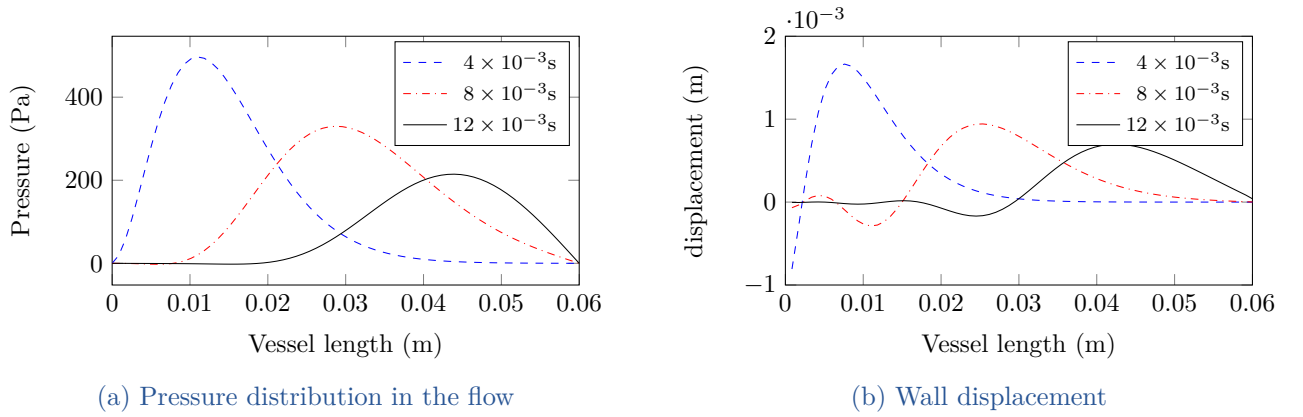


Figure 3.8 – Simulation results for flexible tube using the material parameter of [10]. (a) Static pressure distribution, \mathbf{p}_1^p , along the tube. (b) Wall displacement distribution, \mathbf{q} , along the tube.

are obtained using $N = 71$, $\beta_1 = 1.1$, $\beta_2 = 8.5 \times 10^{-5}$ and $\zeta = 0.8$ (see Table 3.3 for details). The outlet and inlet pressures are defined as $P_o = 0$ Pa and

$$P_i = \begin{cases} 666.5 \left(1 - \cos\left(\frac{6.28t}{0.003}\right)\right) \text{ Pa}, & 0 \leq t \leq 0.003\text{s} \\ 0 \text{ Pa}, & \text{otherwise} \end{cases}$$

respectively.

Figure 3.8 shows the pressure distribution and structure displacement for 3 different time instants. The pressure distributions shown in Figure 3.8.a at time instants 4×10^{-3} s, 8×10^{-3} s and 12×10^{-3} s are in correspondence with the results reported in [79, Figure 8] and [10, Figure 8] at $h = 0.01$. Similarly, the shape of the wall displacements shown in Figure 3.8.b are consistent with the results reported for the fluid-structure interface displacement in [79, Figure 9] and [10, Figure 7] at $h = 0.01$. However, a difference between our results and those shown in [79, 10] is given by the negative displacement at the left-end side of the tube in the first instants of the simulation. As explaining previously, this difference is due to the fact that at the ends of the tube a free motion of the wall is allowed.

3.5 CONCLUSION

In this chapter a scalable finite-dimensional PHS formulation for incompressible fluids has been proposed. An instrumental element, called node, is introduced to allow an appropriate coupling of incompressible fluid sections. This node is also useful to describe the pressure in the inlet and outlet boundaries of the incompressible sections. Similarly, a power-preserving interconnection that combines the properties of PHS interconnections by ports and energy, is proposed in Section 3.3. This interconnection allows us to couple the fluid and the structure models with an appropriate characterization of the fluid-structure power transfer.

In order to assess this PHS model for incompressible fluids, the pressure pulse propagation in a flexible tube is considered as a benchmark. The results obtained with this model are in correspondence with those reported in [9, 79, 10, 12] using specialized FSI algorithms.

Finally, notice that given the definition of nodes, considering a constant mass m , a pressure variations imply variations in the node volume. This volume variation implies that, when the height of two adjacent fluid sections decreases, the length $\bar{\ell}_j$ of the node between the corresponding incompressible sections tends to increase. This node formulation represents a drawback when applications with structure collisions are considered. For example, in the vocal folds vibrating cycle, when the structure collides, the assumption that node volume is small enough with respect to the volume of adjacent incompressible sections, does not hold.

In the next chapter, we consider a more realistic formulation of the fluid dynamics considering compressibility.

Finite-dimensional port-Hamiltonian FSI model for compressible fluids

The interaction between a compressible fluid and a structure is a problem studied in several research areas, such as the piston problem in mechanics [106, 107], or the bioengineering study of the human phono-respiratory system [31, 14, 15, 16].

Similarly to what has been done in Chapter 3, we propose a scalable finite-dimensional model in a longitudinal domain for a compressible fluid and its coupling with a structure with transverse motion. As case of study, we consider the fluid-structure interaction in a vocal folds system expressing the FSI between the intraglottal airflow and the vocal folds. Note that during the vibrating cycle of the vocal folds, these collide, leading to singularity in the airflow model.

Contribution

We propose a port-Hamiltonian finite-dimensional model of compressible airflow coupled with a structure using a switched power-preserving interconnection strategy. This switched interconnection method allows to represent the elastic collision and enable/disable the dynamics of the closed fluid sections during the structure collision.

4.1 FLUID DESCRIPTION

In this section we consider an isentropic and compressible fluid with an irrotational flow, described by the following equations [101]:

$$\partial_t \rho = -\operatorname{div}(\rho \mathbf{v}) \tag{4.1a}$$

$$\partial_t \mathbf{v} = -\mathbf{grad} \left(\frac{1}{2} |\mathbf{v}|^2 \right) - \frac{1}{\rho} \mathbf{grad} p - \frac{1}{\rho} \operatorname{div} \boldsymbol{\tau} \tag{4.1b}$$

where $\boldsymbol{\tau}$ denotes the Newtonian viscosity tensor, i.e.,

$$\boldsymbol{\tau} = -\mu \left(\mathbf{Grad} \mathbf{v} + [\mathbf{Grad} \mathbf{v}]^\top \right) + \left(\frac{2}{3} \mu - \kappa \right) (\operatorname{div} \mathbf{v}) \mathbf{I} \tag{4.2}$$

The static pressure of the fluid is defined from the ideal gas law, i.e.,

$$p = \frac{n \bar{R}_u T}{V} \tag{4.3}$$

where V , n and T are the volume, number of moles and temperature (in Kelvin degrees) of the gas, respectively, and \bar{R}_u is the universal gas constant.

Using the molar weight \bar{M} , the airflow pressure can be rewritten as

$$p = \frac{n\bar{M}}{V} \frac{\bar{R}_u T}{\bar{M}} = \rho (\partial_{\rho} p)_T \quad (4.4)$$

where $\rho = \bar{M}n/V$ and $(\partial_{\rho} p)_T = \bar{R}_u T / \bar{M}$ is the isothermal compressibility. Moreover, isothermal compressibility is related to the isentropic compressibility by the thermodynamic relation $(\partial_{\rho} p)_s = \gamma (\partial_{\rho} p)_T$, where γ is the specific heat ratio of the gas, $\gamma = 1.4$ for the air, and $(\partial_{\rho} p)_s = c^2$ with c the speed of sound [108, Ch. 8]. The static pressure is given by:

$$p = (\partial_{\rho} p)_s \frac{\rho}{\gamma} = \frac{c^2}{\gamma} \rho \quad (4.5)$$

From a thermodynamic point of view, the isentropic fluid can be described using the Gibbs equation:

$$du = -pd\frac{1}{\rho} \quad (4.6)$$

where u denotes the specific (per unit mass) internal energy. Using the specific enthalpy definition

$$h = u + p/\rho \quad (4.7)$$

the term $\frac{1}{\rho} \mathbf{grad} p$ in (4.1b) can be rewritten as

$$\frac{1}{\rho} \mathbf{grad} p = \mathbf{grad} h \quad (4.8)$$

4.1.1 Finite-dimensional modeling

Similarly to the finite-dimensional modeling for incompressible fluids described in Chapter 3, we divide the fluid domain in n_f sections with uniform cross-sectional area and length ℓ_f . Considering that the structure motion is only transversal to the flow, we consider a two-dimensional fluid describing the longitudinal and transverse component of the velocity field. Since we assume an irrotational flow, we can reduce the number of state variables using the following assumption.

Assumption 4.1. *Denote by ϑ and v the transverse and longitudinal components of the fluid velocity. The gradient of ϑ is given by $\partial_{\xi} \vartheta = v_c/q$ and $\partial_{\zeta} \vartheta = 0$ in each section with uniform cross-sectional area, where ζ and ξ denote the longitudinal and transverse axes, v_c and q are the velocity and height of the structure wall, respectively, and $v_c \ll v$.*

As a consequence of Assumption 4.1, in each section with uniform cross-sectional area we have $\vartheta = v_c \xi / q$. This implies an algebraic constraint between ϑ and the structure dynamics. Thus, to complete the flow description, the state variable that is chosen is the longitudinal

velocity v . Additionally, as $v_c \ll v$ we can use the following approximation $|\mathbf{v}|^2 \approx v^2$. With these considerations we reduce the velocity analysis to the longitudinal component, whose momentum equation can be described by:

$$\partial_t v = -\partial_\zeta \left(\frac{1}{2} v^2 + h \right) - \frac{\hat{\mu}}{\rho} \partial_\zeta (\partial_\zeta v) \quad (4.9)$$

where $\hat{\mu} = \frac{4}{3}\mu + \kappa$.

To describe the velocity and density of the fluid, we divide the spatial domain in n_f sections for each variable, as shown in Figures 4.1a and 4.1b. We denote by ρ_j the average density in volume \bar{V}_j between longitudinal points $\tilde{\zeta}_{j-1}$ and $\tilde{\zeta}_j$, with $\tilde{\zeta}_j = \tilde{\zeta}_0 + j\ell_f$. The average velocity in volume V_j between longitudinal points ζ_{j-1} and ζ_j , with $\zeta_j = \zeta_0 + (j + \frac{1}{2})\ell_f$ is denoted by v_j . Then, the fluid dynamics are described using a 1D staggered mesh, as shown in Figure 4.1c, where the boundary conditions are given by the momentum density in the inlet boundary, $\rho v|_{\tilde{\zeta}_0}$, and the energy plus enthalpy in the outlet boundary, $(\frac{1}{2}v^2 + h)|_{\zeta_{n_f}}$. This mesh is equivalent to the mesh proposed in [59] for one-dimensional discretization of infinite dimensional port-Hamiltonian systems.

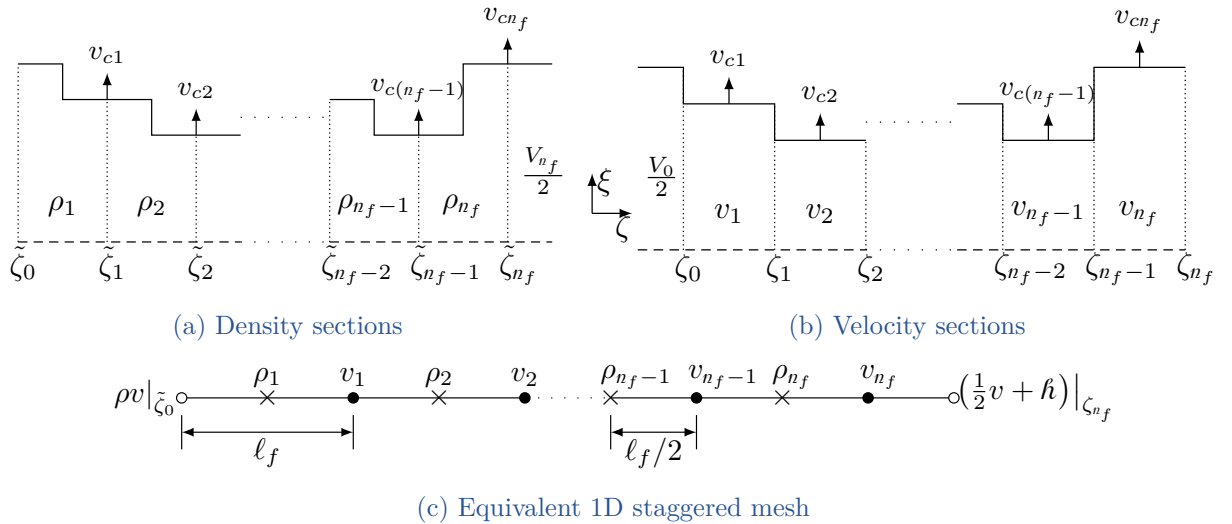


Figure 4.1 – Spatial discretization of fluid variables for the finite-dimensional model. (a) Description of the density. (b): Velocity description. (c): Equivalent one-dimensional mesh.

4.1.2 Dynamics of fluid sections

Note that for an arbitrary section j with average velocity v_j the cross-sectional area A_j is uniform and the volume is given by $V_j = A_j \ell_f$. The contact surface S_j with the mechanical structure has a velocity v_{cj} and area A_{cj} , as shown in Figure 4.2a. For a density section j , the volume is given by the combination of the half of adjacent velocity sections, $\bar{V}_j = (V_{j-1} + V_j) / 2 = \ell_f (A_j + A_{j-1}) / 2$. Similarly, the area of the contact surface is a combination of the areas of adjacent velocity sections, with the corresponding contact velocities, as shown in Figure 4.2b. Then, the dynamics of the fluid sections can be expressed as in the following proposition.

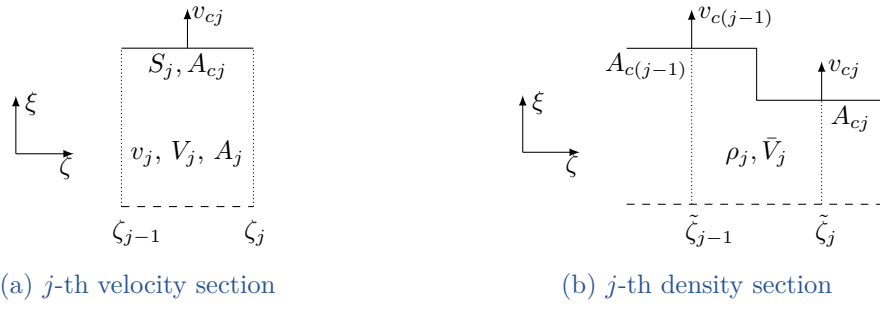


Figure 4.2 – Arbitrary j -th sections of the fluid domain. (a) Velocity section. (b) Density section. A_{cj} and v_{cj} are the area and velocity of the contact surface S_j in the velocity section with volume V_j , v_j is the corresponding average velocity and ρ_j is the average density of the section con volume \bar{V}_j .

Proposition 4.1. *Consider the division of the fluid domain described in Figure 4.1. For the j -th section of density and velocity, the fluid dynamics is described by the following ODEs:*

$$\dot{\rho}_j = \frac{1}{\bar{V}_j} \left(Q_{j-1}^m - Q_j^m - \rho_j \frac{A_{c(j-1)}}{2} v_{c(j-1)} - \rho_j \frac{A_{cj}}{2} v_{cj} \right) \quad (4.10)$$

$$\dot{v}_j = \frac{1}{\ell_f} \left(\frac{1}{2} \tilde{v}_j^2 + h_j - \left(\frac{1}{2} \tilde{v}_{j+1}^2 + h_{j+1} \right) \right) - \Phi_j \quad (4.11)$$

where ρ_j and v_j are the average density and velocity of the corresponding fluid section, $Q_j^m = A_j \rho v|_{\tilde{\zeta}_j}$ is the mass flow at $\tilde{\zeta}_j$, $\frac{1}{2} \tilde{v}_j^2 = \frac{1}{2} v^2|_{\zeta_{j-1}}$ and $h_j = h|_{\zeta_{j-1}}$ are the kinetic energy per unit mass and specific enthalpy at ζ_{j-1} and Φ_j is the average velocity drop due to energy losses in the j -th velocity section.

Proof. Consider a uniform density distribution in the volume \bar{V}_j , and integrate the continuity equation using the Leibniz integral rule and Gauss divergence theorem [101] to get the following relations:

$$\begin{aligned} \int_{\bar{V}_j} \partial_t \rho d\bar{V}_j &= - \int_{\bar{V}_j} \text{div}(\rho \mathbf{v}) d\bar{V}_j \\ \bar{V}_j \dot{\rho}_j &= Q_{j-1}^m - Q_j^m - \rho_j \frac{A_{c(j-1)}}{2} v_{c(j-1)} - \rho_j \frac{A_{cj}}{2} v_{cj} \\ \dot{\rho}_j &= \frac{1}{\bar{V}_j} \left(Q_{j-1}^m - Q_j^m - \rho_j \frac{A_{c(j-1)}}{2} v_{c(j-1)} - \rho_j \frac{A_{cj}}{2} v_{cj} \right) \end{aligned} \quad (4.12)$$

where $Q_j^m = A_j(\rho v)|_{\tilde{\zeta}_j}$ denotes the mass flow at $\zeta = \tilde{\zeta}_j$, i.e., Q_{j-1}^m and Q_j^m are the mass flow at the inlet and outlet boundaries of j -th density section, $\{A_{cj}, v_{cj}\}$ and $\{A_{c(j-1)}, v_{c(j-1)}\}$ are the area and velocity pairs of the adjacent contact surfaces, as shown in Figure 4.2, and $\rho_j = \frac{1}{\bar{V}_j} \int_{\bar{V}_j} \rho d\bar{V}_j$ is the average density in volume \bar{V}_j .

Similarly, applying the same procedure to the motion equation (4.9), we obtain:

$$\begin{aligned}
 \int_{V_j} \partial_t v dV_j &= - \int_{V_j} \partial_x \left(\frac{1}{2} v^2 + h \right) + \frac{\hat{\mu}}{\rho} \partial_x (\partial_x v) dV_j \\
 V_j \dot{v}_j &= A_j \left(\frac{1}{2} v^2 + h \right) \Big|_{x_{j-1}} - A_j \left(\frac{1}{2} v^2 + h \right) \Big|_{x_j} - \int_{V_j} \frac{\hat{\mu}}{\rho} \partial_x (\partial_x v) dV_j \\
 \dot{v}_j &= \frac{1}{\ell_f} \left(\frac{1}{2} \tilde{v}_j^2 + h_j - \left(\frac{1}{2} \tilde{v}_{j+1}^2 + h_{j+1} \right) \right) - \Phi_j
 \end{aligned} \tag{4.13}$$

where $\frac{1}{2} \tilde{v}_j^2 = \frac{1}{2} v^2|_{\zeta_{j-1}}$ and $h_j = h|_{\zeta_{j-1}}$, $\{\frac{1}{2} \tilde{v}_j^2, h_j\}$ and $\{\frac{1}{2} \tilde{v}_{j+1}^2, h_{j+1}\}$ are the kinetic energy per unit mass and specific enthalpy at the inlet and outlet boundaries of the j -th velocity section, respectively. $\Phi_j = \frac{1}{V_j} \int_{V_j} \frac{\hat{\mu}}{\rho} \partial_x (\partial_x v) dV_j$ is the average velocity drop due to energy losses in V_j , and $v_j = \frac{1}{V_j} \int_{V_j} v dV_j$ is the average longitudinal velocity in the volume V_j . \square

Note that according to the fluid domain discretization, the longitudinal velocity is defined at points $\tilde{\zeta}_j, \forall j \in \{1, \dots, n_f\}$. The kinetic energy per unit mass at point x_j is described as a weighted average of adjacent velocities, i.e., $\frac{1}{2} v^2|_{\zeta_j} = \frac{1}{2} (v|_{\tilde{\zeta}_{j-1}})^2 (1 - \alpha_j) + \frac{1}{2} (v|_{\tilde{\zeta}_j})^2 \alpha_j$, where $\alpha_j = A_j / (A_j + A_{j-1})$. Then, $\frac{1}{2} \tilde{v}_j^2$ is defined as:

$$\frac{1}{2} \tilde{v}_j^2 = \frac{1}{2} v_{j-1}^2 (1 - \alpha_j) + \frac{1}{2} v_j^2 \alpha_j \tag{4.14}$$

4.2 PORT-HAMILTONIAN FORMULATION

A scalable PHS formulation of the compressible fluid is presented in this section, starting from the definition of the total energy of the fluid.

4.2.1 Total energy of the fluid

As mentioned in the previous chapters, to obtain a port-Hamiltonian formulation, we need to describe the total energy of the system. For the discretized model described above, the kinetic energy in the j -th section with volume V_j associated with the longitudinal velocity is given by:

$$\mathcal{K}_{fj} = \int_{V_j} \frac{1}{2} \rho v^2 dV_j = V_j \left(\frac{1}{V_j} \int_{V_j} \frac{1}{2} \rho v^2 dV_j \right) \tag{4.15}$$

where the term $\frac{1}{V_j} \int_{V_j} \frac{1}{2} \rho v^2 dV_j$ is the average kinetic energy density in volume $V_j = A_j \ell_f$. Denoting by $\tilde{\rho}_j$ the average density on V_j , the average kinetic energy density can be approximated as $\frac{1}{2} \tilde{\rho}_j v_j^2$. Note that $\tilde{\rho}_j = \rho|_{\tilde{x}_j}$ is given by the average of adjacent densities, i.e., $\tilde{\rho}_j = (\rho_j + \rho_{j+1}) / 2$. Thus, \mathcal{K}_{fj} can be expressed as:

$$\mathcal{K}_{fj} = \frac{1}{4} A_j \ell_f (\rho_j + \rho_{j+1}) v_j^2 \tag{4.16}$$

In the case of the left hand side half volume $V_0/2$, shown in Figure 4.1.(b), the kinetic energy is given by:

$$\mathcal{K}_{f0} = \frac{1}{4} A_i \ell_f \rho_1 v_i^2 \quad (4.17)$$

where A_i and v_i denote the cross-sectional area and longitudinal velocity at the inlet boundary of the fluid domain. Similarly, in section n_f the average density is defined as $\tilde{\rho}_{n_f} = (\rho_{n_f} + \rho_o)/2$, where ρ_o denotes the density at the outlet boundary of the fluid domain, i.e.,

$$\mathcal{K}_{fn_f} = \frac{1}{4} A_{n_f} \ell_f (\rho_{n_f} + \rho_o) v_{n_f}^2 \quad (4.18)$$

On the other hand, to describe the stored energy in each section we define the specific internal energy of the fluid u . Considering small variations on the fluid temperature, the speed of sound c can be considered as being constant. Then, from (4.5) and (4.6) we obtain:

$$u(\rho) = \frac{c^2}{\gamma} \ln(\rho) + C_u \quad (4.19)$$

where C_u is a constant.

However, with this definition of u , the non-negativity property of the total energy depends of the appropriate choice of C_u . In this sense we consider an available internal energy $\bar{u} \geq 0$ to describe the internal energy variations. We define the relative pressure of the fluid as:

$$\hat{p} = p - p_0 = \frac{c^2}{\gamma} (\rho - \rho_0) \quad (4.20)$$

where p_0 is the pressure at reference density ρ_0 . The available internal energy \bar{u} is obtained such that it satisfies $\partial_\rho \bar{u} = \hat{p}/\rho^2$ and $\hat{h} = \bar{u} + \hat{p}/\rho$, where $\hat{h} = h - h_0$ is the relative enthalpy per unit mass and h_0 is the specific enthalpy at ρ_0 . Then, \bar{u} is defined as:

$$\bar{u} = \frac{c^2}{\gamma} \left(\ln \left(\frac{\rho}{\rho_0} \right) + \frac{\rho_0}{\rho} - 1 \right) \quad (4.21)$$

and the relative enthalpy is given by:

$$\hat{h} = \frac{c^2}{\gamma} \ln \left(\frac{\rho}{\rho_0} \right) = \partial_\rho (\rho \bar{u}) \quad (4.22)$$

The available internal energy in a density section with volume \bar{V}_j is given by

$$\bar{\mathcal{U}}_{fj} = \int_{\bar{V}_j} \rho \bar{u}(\rho) d\bar{V}_j \quad (4.23)$$

where \bar{u} is defined in (4.21). Denoting by ρ_j the average density in $\bar{V}_j = (V_{j-1} + V_j)/2$, the average density of the available internal energy in the j -th density section can be approximated by $\rho_j \bar{u}_j$ where $\bar{u}_j = \bar{u}(\rho)|_{\rho_j}$. Then, $\bar{\mathcal{U}}_{fj}$ can be expressed as:

$$\bar{\mathcal{U}}_{fj} = \frac{1}{2} (V_{j-1} + V_j) \rho_j \bar{u}_j \quad (4.24)$$

The total energy stored in the fluid is given by:

$$\mathcal{H}_f = \underbrace{\sum_{j=0}^{n_f} \mathcal{K}_{fj}}_{\mathcal{K}_f} + \underbrace{\sum_{j=1}^{n_f} \bar{\mathcal{U}}_{fj}}_{\bar{\mathcal{U}}_f} \quad (4.25)$$

4.2.2 Scalable finite-dimensional model

From the total energy (4.25), the co-energy variables associated with the j -th velocity and density are given by:

$$\partial_{v_j} \mathcal{H}_f = \frac{1}{2} A_j \ell_f (\rho_j + \rho_{j+1}) v_j = \ell_f Q_j^m \quad (4.26)$$

$$\begin{aligned} \partial_{\rho_j} \mathcal{H}_f &= \frac{1}{4} V_{j-1} v_{j-1}^2 + \frac{1}{4} V_j v_j^2 + \frac{1}{2} (V_{j-1} + V_j) \hat{h}_j = \bar{V}_j \left(\frac{1}{2} v_{j-1}^2 (1 - \alpha_j) + \frac{1}{2} v_j^2 \alpha_j + \hat{h}_j \right) \\ &= \bar{V}_j \left(\frac{1}{2} \tilde{v}_j^2 + \hat{h}_j \right) \end{aligned} \quad (4.27)$$

where $\frac{1}{2} \tilde{v}_1^2 = \frac{1}{2} v_1^2 (1 - \alpha_1) + \frac{1}{2} v_1^2 \alpha_1$ with $\alpha_1 = A_1 / (A_1 + A_i)$.

Replacing (4.26) in the density dynamics (4.10) we obtain:

$$\dot{\rho}_j = \frac{1}{\ell_f \bar{V}_j} \left(\partial_{v_{j-1}} \mathcal{H}_f - \partial_{v_j} \mathcal{H}_f \right) - \frac{\rho_j}{2} \left(A_{c(j-1)} v_{c(j-1)} + A_{cj} v_{cj} \right) \quad (4.28)$$

Similarly, considering that $h_j - h_{j+1} = \hat{h}_j - \hat{h}_{j+1}$ and using (4.27), the velocity dynamics (4.11) can be formulated as:

$$\dot{v}_j = \frac{1}{\ell_f \bar{V}_j} \partial_{\rho_j} \mathcal{H}_f - \frac{1}{\ell_f \bar{V}_{j+1}} \partial_{\rho_{j+1}} \mathcal{H}_f - \Phi_j \quad (4.29)$$

In the cases of first density and last velocity sections, the dynamics are given by:

$$\dot{\rho}_1 = \frac{1}{\bar{V}_1} Q_i^m - \frac{1}{\ell_f \bar{V}_1} \partial_{v_1} \mathcal{H}_f - \frac{\rho_1}{2} A_{c1} v_{c1} \quad (4.30)$$

$$\dot{v}_{n_f} = \frac{1}{\ell_f \bar{V}_{n_f}} \partial_{\rho_j} \mathcal{H}_f - \frac{1}{\ell_f} \left(\frac{1}{2} \tilde{v}_o^2 + \hat{h}_o \right) - \Phi_{n_f} \quad (4.31)$$

where the subscripts i and o denote the variables at inlet and outlet boundaries of the fluid domain, i.e., $Q_i^m = A_i (\rho v)|_{\bar{x}_0}$ and $\frac{1}{2} \tilde{v}_o^2 + \hat{h}_o = \left(\frac{1}{2} v^2 + \hat{h} \right)|_{x_{n_f}}$. The term $\frac{1}{2} \tilde{v}_o^2$ is evaluated by $\frac{1}{2} \tilde{v}_o^2 = \frac{1}{2} v_{n_f}^2 (1 - \alpha_o) + \frac{1}{2} (v_o^+)^2 \alpha_o$ with $\alpha_o = A_o^+ / (A_o^+ + A_{n_f})$, where v_o^+ and A_o^+ denote the average velocity and area external to the fluid domain. In case that the outlet boundary is open to the atmosphere, $\alpha_o = 1$ and $\frac{1}{2} \tilde{v}_o^2 = \frac{1}{2} (v_o^+)^2$. Similarly, $\hat{h}_o = \hat{h}(\rho)|_{\rho_o}$ where ρ_o is the fluid density at the outlet boundary.

On the other hand, the power dissipated in an arbitrary velocity section j is given by $\mathcal{E}_{\lambda_j} = \partial_{v_j} \mathcal{H}_f \Phi_j$. From (3.8) we obtain:

$$\Phi_j = d_{fj} \partial_{v_j} \mathcal{H}_f \quad (4.32)$$

where

$$d_{fj} = \frac{\lambda_j |v_j|}{(\rho_j + \rho_{j+1}) \ell_f V_j} \geq 0 \quad (4.33)$$

Then, the dynamics in the fluid domain can be written as:

$$\dot{\mathbf{v}} = -R_4 \partial_{\mathbf{v}} \mathcal{H}_f + \varphi \partial_{\boldsymbol{\rho}} \mathcal{H}_f - g_v \left(\frac{1}{2} \tilde{v}_o^2 + \hat{h}_o \right) \quad (4.34)$$

$$\dot{\boldsymbol{\rho}} = -\varphi^\top \partial_{\mathbf{v}} \mathcal{H}_f + g_\rho Q_i^m - \vartheta \mathbf{v}_c \quad (4.35)$$

where $\mathbf{v} = [v_1 \cdots v_{n_f}]^\top$ and $\boldsymbol{\rho} = [\rho_1 \cdots \rho_{n_f}]^\top$ are the sets of velocities and densities in the fluid sections, respectively. Matrices $R_4 = R_4^\top \geq 0$, φ , g_v , g_ρ and ϑ are given by:

$$R_4 = \begin{bmatrix} d_{f1} & 0 & \cdots & 0 \\ 0 & \ddots & \ddots & \vdots \\ \vdots & \ddots & \ddots & 0 \\ 0 & \cdots & 0 & d_{fn_f} \end{bmatrix}, \quad \varphi = \frac{1}{\ell_f} \begin{bmatrix} \frac{1}{V_1} & -\frac{1}{V_2} & 0 & \cdots & 0 \\ 0 & \frac{1}{V_2} & -\frac{1}{V_3} & \ddots & \vdots \\ \vdots & \ddots & \ddots & \ddots & 0 \\ \vdots & \ddots & \ddots & \frac{1}{V_{n_f-1}} & -\frac{1}{V_{n_f}} \\ 0 & \cdots & \cdots & 0 & \frac{1}{V_{n_f}} \end{bmatrix}, \quad g_v = \begin{bmatrix} 0 \\ \vdots \\ 0 \\ \frac{1}{\ell_f} \end{bmatrix}$$

$$g_\rho = \begin{bmatrix} \frac{1}{V_1} \\ 0 \\ \vdots \\ 0 \end{bmatrix} \quad \text{and} \quad \vartheta = \frac{1}{2} \begin{bmatrix} \frac{\rho_1 A_{c1}}{V_1} & 0 & \cdots & \cdots & 0 \\ \frac{\rho_2 A_{c1}}{V_2} & \frac{\rho_2 A_{c2}}{V_2} & \ddots & \ddots & \vdots \\ 0 & \ddots & \ddots & \ddots & \vdots \\ \vdots & \ddots & \frac{\rho_{n_f-1} A_{c(n_f-2)}}{V_{n_f-1}} & \frac{\rho_{n_f-1} A_{c(n_f-1)}}{V_{n_f-1}} & 0 \\ 0 & \cdots & \cdots & \frac{\rho_{n_f} A_{c(n_f-1)}}{V_{n_f}} & \frac{\rho_{n_f} A_{cn_f}}{V_{n_f}} \end{bmatrix} \quad (4.36)$$

Proposition 4.2. *Consider an isentropic and compressible fluid with an irrotational flow. Using the discretization scheme described in Section 4.1.1, the sets of velocities and densities in the fluid sections are given by $\mathbf{v} = [v_1 \cdots v_{n_f}]^\top$ and $\boldsymbol{\rho} = [\rho_1 \cdots \rho_{n_f}]^\top$, respectively. Then, the fluid dynamics can be characterized using the following port-Hamiltonian system:*

$$\dot{\mathbf{x}}_f = (J_f - R_f) \partial_{\mathbf{x}_f} \mathcal{H}_f + G_f \mathbf{u}_f \quad (4.37a)$$

$$\mathbf{y}_f = G_f^\top \partial_{\mathbf{x}_f} \mathcal{H}_f + M_f \mathbf{u}_f \quad (4.37b)$$

where $\mathbf{x}_f^\top = [\mathbf{v}^\top \boldsymbol{\rho}^\top]$ is the state vector, $\mathbf{u}_f = [Q_i^m (\frac{1}{2} \tilde{v}_o^2 + \hat{h}_o) \mathbf{v}_c^\top]^\top$ and $\mathbf{y}_f = [(\frac{1}{2} \tilde{v}_i^2 + \hat{h}_i) - Q_o^m - (\mathbf{F}_c^*)^\top]^\top$ denote the inputs and outputs, respectively, and matrices $J_f = -J_f^\top$, $R_f = R_f^\top \geq 0$ and G_f are given by:

$$J_f = \begin{bmatrix} \mathbf{0} & \varphi \\ -\varphi^\top & \mathbf{0} \end{bmatrix}, \quad R_f = \begin{bmatrix} R_4 & \mathbf{0} \\ \mathbf{0} & \mathbf{0} \end{bmatrix},$$

$$G_f = \begin{bmatrix} \mathbf{0} & -g_v & \mathbf{0} \\ g_\rho & \mathbf{0} & \vartheta \end{bmatrix}, \quad M_f = \begin{bmatrix} \mathbf{0} & \mathbf{0} & \mathbf{0} \\ \mathbf{0} & \mathbf{0} & \psi \\ \mathbf{0} & -\psi^\top & \mathbf{0} \end{bmatrix} \quad (4.38)$$

with $\psi = [0 \cdots 0 \frac{\rho_o A_{cn_f}}{2}]$.

Proof. Note that the power conjugated outputs associated with the inputs Q_i^m and $\frac{1}{2}\tilde{v}_o^2 + \hat{h}_o$ are given by $\frac{1}{2}\tilde{v}_i^2 + \hat{h}_i$ and Q_o^m , respectively. The output at the inlet boundary is approximated using the kinetic energy per unit mass plus relative specific enthalpy of the first density section. Similarly, we define the outlet output as the average mass flow in the velocity section n_f minus the mass flow displaced due to the structure motion in the right hand side half volume $V_{n_f}/2$. i.e.,

$$\frac{1}{2}\tilde{v}_i^2 + \hat{h}_i = \frac{1}{2}\tilde{v}_1^2 + \hat{h}_1 = \frac{1}{V_1}\partial_{\rho_1}\mathcal{H}_f \quad (4.39)$$

$$Q_o^m = Q_{n_f}^m - \rho_0 \frac{A_{cnf}}{2} v_{cnf} = \frac{1}{\ell_f}\partial_{v_{n_f}}\mathcal{H}_f - \rho_0 \frac{A_{cnf}}{2} v_{cnf} \quad (4.40)$$

Then, the fluid dynamics (4.34)-(4.35) can be rewritten as

$$\begin{bmatrix} \dot{\mathbf{v}} \\ \dot{\boldsymbol{\rho}} \end{bmatrix} = \begin{bmatrix} -R_4 & \boldsymbol{\varphi} \\ -\boldsymbol{\varphi}^\top & \mathbf{0} \end{bmatrix} \begin{bmatrix} \partial_v \mathcal{H}_f \\ \partial_\rho \mathcal{H}_f \end{bmatrix} + \begin{bmatrix} \mathbf{0} & g_v & \mathbf{0} \\ g_\rho & \mathbf{0} & -\vartheta \end{bmatrix} \begin{bmatrix} Q_i^m \\ \frac{1}{2}\tilde{v}_o^2 + \hat{h}_o \\ \mathbf{v}_c \end{bmatrix} \quad (4.41)$$

$$\begin{bmatrix} \frac{1}{2}\tilde{v}_i^2 + \hat{h}_i \\ -Q_o^m \\ -\mathbf{F}_c^* \end{bmatrix} = \begin{bmatrix} \mathbf{0} & g_\rho^\top \\ -g_v^\top & \mathbf{0} \\ \mathbf{0} & -\vartheta^\top \end{bmatrix} \begin{bmatrix} \partial_v \mathcal{H}_f \\ \partial_\rho \mathcal{H}_f \end{bmatrix} + \begin{bmatrix} 0 & 0 & \mathbf{0} \\ 0 & 0 & \psi \\ 0 & -\psi^\top & \mathbf{0} \end{bmatrix} \begin{bmatrix} Q_i^m \\ \frac{1}{2}\tilde{v}_o^2 + \hat{h}_o \\ \mathbf{v}_c \end{bmatrix} \quad (4.42)$$

where $\psi = [0 \ \dots \ 0 \ \frac{\rho_0 A_{cnf}}{2}]$.

Finally, defining matrices J_f , R_f , G_f and M_f as in (4.38), we obtain the port-Hamiltonian model (4.37). \square

Note that, similarly to the fluid model described in Chapter 3, the output forces $\mathbf{F}_c^* = \mathbf{F}_c + \hat{\mathbf{F}}$ are not the effective forces acting on the fluid-structure contact. The forces $\hat{\mathbf{F}}$ are associated with the volume variation in each section with uniform cross-sectional area. Note that this variation of volume is associated with the changes of height in each section, i.e., $\hat{\mathbf{F}} = \partial_{\mathbf{q}_f}\mathcal{H}_f$. Then, the set of effective forces acting on the contact surface is given by:

$$\mathbf{F}_c = \mathbf{F}_c^* - \hat{\mathbf{F}} = \vartheta^\top \partial_\rho \mathcal{H}_f + \psi^\top \left(\frac{1}{2}\tilde{v}_o^2 + \hat{h}_o \right) - \partial_{\mathbf{q}_f}\mathcal{H}_f \quad (4.43)$$

For the j -th velocity section the extra force and the output force are given by $\hat{F}_j = \partial_{q_{fj}}\mathcal{H}_f = \frac{A_{cj}}{4}(\rho_j + \rho_{j+1})v_j^2 + \frac{A_{cj}}{2}(\rho_j\bar{u}_j + \rho_{j+1}\bar{u}_{j+1})$ and $F_{cj}^* = \frac{A_{cj}}{2}(\hat{p}_j + \hat{p}_{j+1}) + \frac{A_{cj}}{4}(\rho_j\tilde{v}_j^2 + \rho_{j+1}\tilde{v}_{j+1}^2) + \frac{A_{cj}}{2}(\rho_j\bar{u}_j + \rho_{j+1}\bar{u}_{j+1})$. Then, the effective force applied on the contact surface of section j is defined as:

$$F_{cj} = \frac{A_{cj}}{4}(\rho_j\tilde{v}_j^2 + \rho_{j+1}\tilde{v}_{j+1}^2 - (\rho_j + \rho_{j+1})v_j^2) + \frac{A_{cj}}{2}(\hat{p}_j + \hat{p}_{j+1}) \quad (4.44)$$

In the next section, we will see that these extra forces are compensated through a power-preserving interconnection.

4.3 FLUID-STRUCTURE POWER-PRESERVING INTERCONNECTION

From Assumption 4.1 we obtain two conditions for the transverse velocity in each fluid section with uniform cross-sectional area, $v_j|_{\xi=q_{fj}} = v_{cj}$ and $v_j|_{\xi=0} = 0$, and as a consequence $v_{cj} \rightarrow 0$ when $q_{fj} \rightarrow 0$. This behavior is undesirable in applications such as glottis modeling, where the vocal folds collide at speed greater than 0, i.e., $v_{cj} \neq 0$ when the collision occur during the vocal folds vibrating cycle. To obtain this behavior, we consider the approach proposed in [74], using switching variables to enable or disable the power transfer between the fluid and the structure. We consider a threshold value ϵ , such that, the fluid dynamics in V_j and its effect on the mechanical structure are disabled when $q_{fj} < \epsilon$. As a consequence, we define a switching matrix $S_\epsilon = S_\epsilon^T$ as:

$$S_\epsilon = \begin{bmatrix} s_{\epsilon 1} & \cdots & 0 \\ \vdots & \ddots & \vdots \\ 0 & \cdots & s_{\epsilon n_f} \end{bmatrix} \quad (4.45)$$

where

$$s_{\epsilon j} = \begin{cases} 1, & q_{fj} > \epsilon \\ 0, & q_{fj} \leq \epsilon \end{cases} \quad (4.46)$$

The power transfer between the fluid and the structure systems is given by $\mathbf{u}_s^T \mathbf{y}_s = \mathbf{v}_c^T \mathbf{F}_c$. We define a matrix C , with elements 0 and 1, as shown in Section 3.3, that maps the output and input vectors of the mechanical model of the vocal folds to the corresponding velocities and forces of the fluid model, i.e., $S_\epsilon C \mathbf{y}_s = \mathbf{v}_c$ and $C^T S_\epsilon^T \mathbf{F}_c = \mathbf{u}_s$. The following power preserving interconnection rule to couple the fluid and structure models is used:

$$\begin{bmatrix} \mathbf{v}_c \\ \mathbf{u}_s \end{bmatrix} = \begin{bmatrix} \mathbf{0} & S_\epsilon C \\ -C^T S_\epsilon^T & \mathbf{0} \end{bmatrix} \begin{bmatrix} -\mathbf{F}_c \\ \mathbf{y}_s \end{bmatrix} \quad (4.47)$$

In this rule, matrix C defines the interconnections between the fluid and the mechanical sub-systems, and matrix S_ϵ enables or disables the fluid-structure power transfer according to the switching variables $s_{\epsilon j}, \forall j \in \{1, \dots, n_f\}$.

Consider the general mass-spring-damper model (3.43) to describe the structure motion with total stored energy \mathcal{H}_s . Including S_ϵ in the fluid equations to enable and disable the dynamics in each fluid section according to $s_{\epsilon j}$ and using the interconnection (4.47), we can write the fluid-structure dynamics as:

$$\dot{\mathbf{q}}_s = -\partial_{\pi_s} \mathcal{H}_s \quad (4.48a)$$

$$\dot{\pi}_s = -\partial_{\mathbf{q}_s} \mathcal{H}_s - R \partial_{\pi_s} \mathcal{H}_s + C^T S_\epsilon^T \mathbf{F}_c \quad (4.48b)$$

$$\dot{\mathbf{v}} = -S_\epsilon R_4 \partial_v \mathcal{H}_f + S_\epsilon \varphi \partial_\rho \mathcal{H}_f - S_\epsilon g_v \left(\frac{1}{2} \tilde{v}_o^2 + \hat{h}_o \right) \quad (4.48c)$$

$$\dot{\rho} = -\varphi^T S_\epsilon^T \partial_v \mathcal{H}_f + g_\rho Q_i^m - \vartheta S_\epsilon C \mathbf{y}_s \quad (4.48d)$$

Note that the term $g_\rho Q_i^m$ is not switched. This is given by the fact that the inlet mass flow enters through the left hand side half volume $V_0/2$ and this section have a motionless wall (see Figure 4.1).

From a computational point of view, when the dynamics of a velocity section or a density section are disabled by the switch variables, the corresponding velocity or density state variable is set to 0 or ρ_0 , respectively. This strategy is equivalent to the method proposed in [29] for a finite-element model of the glottis.

Proposition 4.3. *Consider the fluid-structure system (4.48). Denoting by $\mathcal{H}_{fs} = \mathcal{H}_f + \mathcal{H}_s$ the total stored energy, this system can be expressed as the following port-Hamiltonian system:*

$$\dot{\mathbf{x}}_{fs} = (J_{fs} - R_{fs})\partial_{\mathbf{x}_{fs}}\mathcal{H}_{fs} + G_{fs}\mathbf{u}_{fs} \quad (4.49a)$$

$$\mathbf{y}_{fs} = G_{fs}^\top \partial_{\mathbf{x}_{fs}}\mathcal{H}_{fs} \quad (4.49b)$$

where $\mathbf{x}_{fs}^\top = [\mathbf{q}_s^\top \ \boldsymbol{\pi}_s^\top \ \mathbf{v}^\top \ \boldsymbol{\rho}^\top]$ is the state vector, $\mathbf{u}_{fs} = [Q_i^m \ (\frac{1}{2}\tilde{v}_o^2 + \hat{h}_o)]^\top$ and $\mathbf{y}_{fs} = [(\frac{1}{2}\tilde{v}_i^2 + \hat{h}_i) - Q_o^m]^\top$ are the inputs and outputs, respectively, at the inlet and outlet fluid boundaries, with the matrices $J_{fs} = -J_{fs}^\top$, $R_{fs} = R_{fs}^\top \geq 0$ and G_{fs} given by:

$$J_{fs} = \begin{bmatrix} \mathbf{0} & \mathbf{I} & \mathbf{0} & \mathbf{0} \\ -\mathbf{I} & \mathbf{0} & \mathbf{0} & (\vartheta S_\epsilon C)^\top \\ \mathbf{0} & \mathbf{0} & \mathbf{0} & S_\epsilon \varphi \\ \mathbf{0} & \vartheta S_\epsilon C & \mathbf{0} & -(S_\epsilon \varphi)^\top \end{bmatrix}, \quad R_{fs} = \begin{bmatrix} \mathbf{0} & \mathbf{0} & \mathbf{0} & \mathbf{0} \\ \mathbf{0} & R & \mathbf{0} & \mathbf{0} \\ \mathbf{0} & \mathbf{0} & S_\epsilon R_4 & \mathbf{0} \\ \mathbf{0} & \mathbf{0} & \mathbf{0} & \mathbf{0} \end{bmatrix} \text{ and}$$

$$G_{fs} = \begin{bmatrix} \mathbf{0} & \mathbf{0} \\ \mathbf{0} & (\psi S_\epsilon C)^\top \\ \mathbf{0} & -S_\epsilon g_v \\ g_\rho & \mathbf{0} \end{bmatrix} \quad (4.50)$$

Proof. Considering $\mathbf{y}_s = \partial_{\boldsymbol{\pi}_s}\mathcal{H}_s$ and (4.43), the fluid-structure dynamics (4.48) can be rewritten as:

$$\begin{aligned} \dot{\mathbf{q}}_s &= \partial_{\boldsymbol{\pi}_s}\mathcal{H}_s \\ \dot{\boldsymbol{\pi}}_s &= -\partial_{\mathbf{q}_s}\mathcal{H}_s - R\partial_{\boldsymbol{\pi}_s}\mathcal{H}_s + C^\top S_\epsilon^\top \vartheta^\top \partial_{\boldsymbol{\rho}}\mathcal{H}_f + C^\top S_\epsilon^\top \psi^\top \left(\frac{1}{2}\tilde{v}_o^2 + \hat{h}_o\right) - C^\top S_\epsilon^\top \partial_{\mathbf{q}_f}\mathcal{H}_f \\ \dot{\mathbf{v}} &= -S_\epsilon R_4 \partial_{\mathbf{v}}\mathcal{H}_f + S_\epsilon \varphi \partial_{\boldsymbol{\rho}}\mathcal{H}_f - S_\epsilon g_v \left(\frac{1}{2}\tilde{v}_o^2 + \hat{h}_o\right) \\ \dot{\boldsymbol{\rho}} &= -\varphi^\top S_\epsilon^\top \partial_{\mathbf{v}}\mathcal{H}_f + g_\rho Q_i^m - \vartheta S_\epsilon C \partial_{\boldsymbol{\pi}_s}\mathcal{H}_s \end{aligned}$$

The variation of fluid section heights induced by the motion of the structure is given by the following relationship $\mathbf{q}_f = \mathbf{q}_0 + C\mathbf{q}_s$ where \mathbf{q}_0 is the set of velocity section heights at the equilibrium point at reference pressure p_0 , and C maps the displacement of the structure masses to the variation of fluid section heights. This relationship leads to:

$$\partial_{\mathbf{q}_s}\mathcal{H}_f = C^\top S_\epsilon^\top \partial_{\mathbf{q}_f}\mathcal{H}_f \quad (4.52)$$

where S_ϵ is used to enable and disable the corresponding fluid dynamics when the section heights cross the threshold value ϵ . Then, defining $\mathcal{H}_{fs} = \mathcal{H}_f + \mathcal{H}_s$ the fluid-structure dynamics can be expressed as:

$$\begin{bmatrix} \dot{\mathbf{q}}_s \\ \dot{\boldsymbol{\pi}}_s \\ \dot{\mathbf{v}} \\ \dot{\boldsymbol{\rho}} \end{bmatrix} = \begin{bmatrix} \mathbf{0} & \mathbf{I} & \mathbf{0} & \mathbf{0} \\ -\mathbf{I} & -R & \mathbf{0} & (\vartheta S_\epsilon C)^\top \\ \mathbf{0} & \mathbf{0} & -S_\epsilon R_4 & S_\epsilon \varphi \\ \mathbf{0} & -\vartheta S_\epsilon C & -(S_\epsilon \varphi)^\top & \mathbf{0} \end{bmatrix} \begin{bmatrix} \partial_{\mathbf{q}_s} \mathcal{H}_{fs} \\ \partial_{\boldsymbol{\pi}_s} \mathcal{H}_{fs} \\ \partial_{\mathbf{v}} \mathcal{H}_{fs} \\ \partial_{\boldsymbol{\rho}} \mathcal{H}_{fs} \end{bmatrix} + \begin{bmatrix} \mathbf{0} & \mathbf{0} \\ \mathbf{0} & (\psi S_\epsilon C)^\top \\ \mathbf{0} & -S_\epsilon g_v \\ g_\rho & \mathbf{0} \end{bmatrix} \begin{bmatrix} Q_i^m \\ \frac{1}{2} \tilde{v}_o^2 + \hat{h}_o \end{bmatrix}$$

$$\begin{bmatrix} \frac{1}{2} \tilde{v}_i^2 + \hat{h}_i \\ -Q_o^m \end{bmatrix} = \begin{bmatrix} \mathbf{0} & \mathbf{0} & \mathbf{0} & g_\rho^\top \\ \mathbf{0} & \psi S_\epsilon C & -(S_\epsilon g_v)^\top & \mathbf{0} \end{bmatrix} \begin{bmatrix} \partial_{\mathbf{q}_s} \mathcal{H}_{fs} \\ \partial_{\boldsymbol{\pi}_s} \mathcal{H}_{fs} \\ \partial_{\mathbf{v}} \mathcal{H}_{fs} \\ \partial_{\boldsymbol{\rho}} \mathcal{H}_{fs} \end{bmatrix}$$

Finally, defining the matrices J_{fs} , R_{fs} and G_{fs} as in (4.50), we obtain the fluid-structure port-Hamiltonian formulation (4.49). \square

4.4 EXAMPLE: AIRFLOW IN THE GLOTTIS.

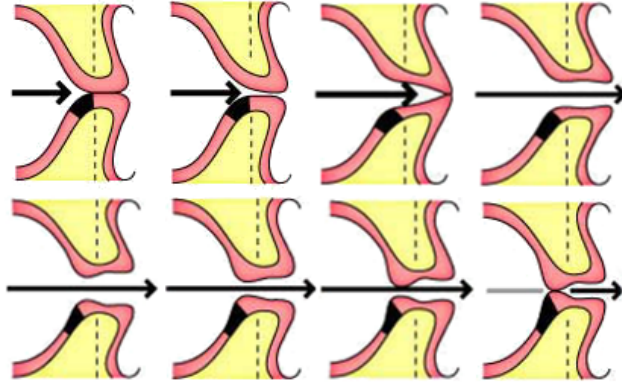


Figure 4.3 – Vibrating cycle induced by FSI between the intraglottal airflow and the vocal folds.

We consider the vibrating cycle induced by the fluid-structure interaction between the intraglottal airflow and the vocal folds [109], as shown in Figure 4.3. We use the well-know body-cover model [72] to describe the vocal folds motion. The port-Hamiltonian formulation of this system has been presented in Section 2.2. Assuming a symmetrical behavior of the vocal folds, we only consider a hemi-larynx. The state variables of the structure model are $\mathbf{q}_s = [q_1 \ q_2 \ q_3]^\top$ and $\boldsymbol{\pi}_s = [\pi_{s1} \ \pi_{s2} \ \pi_{s3}]^\top$, and the structure parameters are given in Table 4.1.

Applying the proposed discrete modeling of the fluid, we divide the fluid domain in $n_f = 38$ sections with uniform cross-sectional area and length $\ell_f = 1.5 \times 10^{-3}$ m. The glottal tract can be modeled as shown in Figure 4.4, with 14 sections in the subglottal part, 12 sections in the supraglottal part of the glottis, and 6 sections under each cover mass. The heights of each

Table 4.1 – Simulation parameters

Parameters of BCM [72]			
$m_1 = 1 \times 10^{-5} \text{Kg}$	$m_2 = 1 \times 10^{-5} \text{Kg}$	$m_3 = 5 \times 10^{-5} \text{Kg}$	$\zeta_j = 0.4, j \in \{1, 2, 3\}$
$\zeta_j^{col} = 0.4, j \in \{1, 2\}$	$\zeta_3^{col} = 0$	$k_1 = 5 \text{N/m}$	$k_2 = 3.5 \text{N/m}$
$k_3 = 100 \text{N/m}$	$k_{c1} = 15 \text{N/m}$	$k_{c2} = 10.5 \text{N/m}$	$k_{12} = 2 \text{N/m}$
$\eta_j = 10^6 \text{m}^{-2} i \in \{1, 2, 3\}$	$\eta_{cj} = 5 \times 10^6 \text{m}^{-2} i \in \{1, 2\}$	$q_{s1}^0 = 1.8 \times 10^{-4} \text{m}$	$q_{s2}^0 = 1.79 \times 10^{-4} \text{m}$
$q_{s3}^0 = 3 \times 10^{-3} \text{m}$			
Fluid parameters at 36°C			
$\rho_0 = 1.142 \text{Kg/m}$	$\gamma = 1.4$	$c = 352 \text{ m/s}$	$\epsilon = 1.8 \times 10^{-5} \text{m}$
$L = 1 \times 10^{-2} \text{m}$	$\ell = 2.5 \times 10^{-4} \text{m}$	$n = 38$	

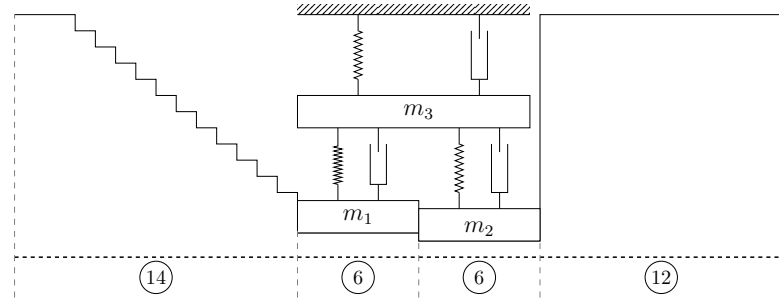


Figure 4.4 – Approximation of the glottal tract using the discretization method proposed, considering fluid sections with uniform cross-sectional areas. Dotted line represents the midsagittal plane. Circles denote the number of velocity section in each glottis part.

section are initialized as follows:

$$q_{j0} = \begin{cases} 2.5 \times 10^{-2} \text{m}, & 1 \leq j \leq 3 \\ [2.5 - 0.2(j - 3)] \times 10^{-2} \text{m}, & 4 \leq j \leq 14 \\ 1.8 \times 10^{-4} \text{m}, & 15 \leq j \leq 20 \\ 1.79 \times 10^{-4} \text{m}, & 21 \leq j \leq 26 \\ 2.5 \times 10^{-2} \text{m}, & 27 \leq j \leq 38 \end{cases} \quad (4.53)$$

To describe the viscous dissipation of the fluid we define the friction loss factor as:

$$\lambda_j^f = \frac{16}{Re} \quad (4.54)$$

where $Re = \frac{q_{fj}|v_j| \rho_j + \rho_{j+1}}{\mu}$ is the Reynolds number in each velocity section of the glottis [91]. Considering a motionless wall in the subglottal and supraglottal sections, and that only masses m_1 and m_2 are in contact with the fluid, we define the interconnection matrix C as:

$$C = \begin{bmatrix} \mathbf{0}_{14 \times 1} & \mathbf{0}_{14 \times 1} & \mathbf{0}_{14 \times 1} \\ \mathbf{1}_{6 \times 1} & \mathbf{0}_{6 \times 1} & \mathbf{0}_{6 \times 1} \\ \mathbf{0}_{6 \times 1} & \mathbf{1}_{6 \times 1} & \mathbf{0}_{6 \times 1} \\ \mathbf{0}_{12 \times 1} & \mathbf{0}_{12 \times 1} & \mathbf{0}_{12 \times 1} \end{bmatrix} \quad (4.55)$$

where $\mathbf{1}_{6 \times 1} = [1 \ 1 \ 1 \ 1 \ 1 \ 1]^\top$. Note that, given the definition of q_{j0} and C we obtain that $s_{\epsilon 1} = \dots = s_{\epsilon 14} = 1$, $s_{\epsilon 27} = \dots = s_{\epsilon 38} = 1$, $s_{\epsilon 15} = \dots = s_{\epsilon 20}$ and $s_{\epsilon 21} = \dots = s_{\epsilon 26}$ for all simulation time, i.e., from a computational point of view, only 2 switches are relevant.

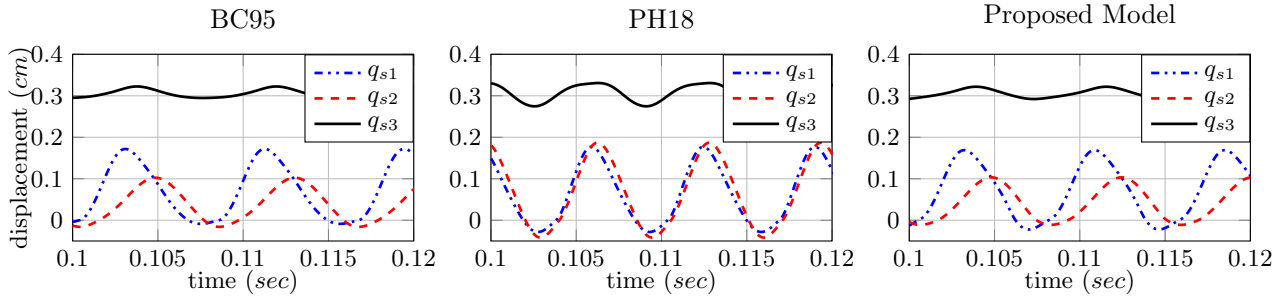


Figure 4.5 – Displacement of the masses of the vocal folds mechanical structure, $q_{sj} = q_j + q_{sj}^0$. Solid line is the body mass displacement (m_3 in Figure 4.4), dashed and dash-dotted lines are the displacements of upper and lower cover masses, respectively (m_2 and m_1 in Figure 4.4, respectively).

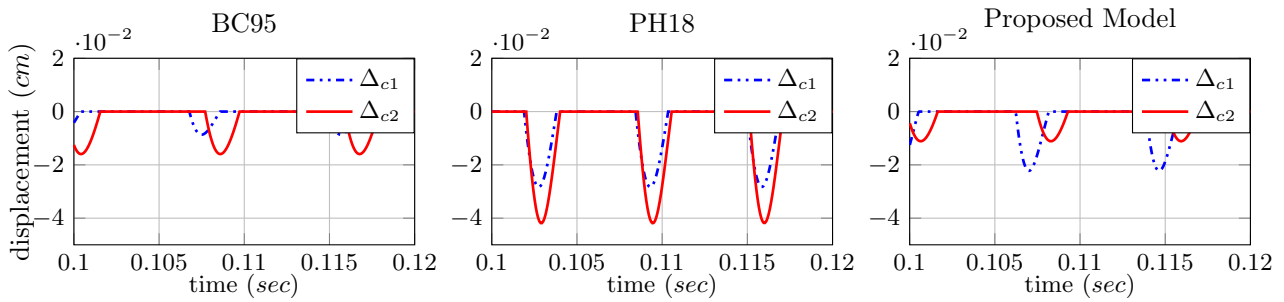


Figure 4.6 – Overlapping of cover masses during the vocal folds collisions. Solid line: deformation for the upper mass (m_2 in Figure 4.4). Dash-dot-dotted line: deformation for the lower mass (m_1 in Figure 4.4).

Simulations are performed in Matlab using the solver ODE23tb with an event location function to update the switch variables. To evaluate the results we use as reference the body-cover (BC95) model [72] and the port-Hamiltonian fluid-structure model (PH18) proposed in [74].

The movement of each mass for BC95, PH18 and the proposed model is shown in Figure 4.5. It can be noticed that in the proposed model the masses exhibit oscillations with a fundamental frequency of 129.1 Hz, in contrast with the 127.5 Hz and 139.9 Hz of the BC95 and PH18 models, respectively. The fluid-structure model PH18 presents a displacement almost parallel for the contact masses of the vocal folds, lower mass displacement q_1 (dash-dot-dotted) and upper mass displacement q_2 (dashed line), respectively), increasing the oscillation amplitude of q_2 . In contrast, for the proposed model the movement of the contact masses shows a difference in amplitude and phase between the oscillations of q_1 and q_2 , in correspondence with the wave propagation through the vocal folds structure, obtaining similar oscillations with the BC95 model.

In lumped parameter models of the vocal folds, a collision occurs when the contact masses cross the corresponding collision planes. In this thesis, given the hemi-larynx assumption, the collision plane for the contact masses is the midsagittal plane. The deformation of the vocal folds given by the elastic collision is proportional to the overlapping, Δ_{cj} , $j \in \{1, 2\}$, of the cover masses, as shown in Figure 4.6. Note that the magnitude of the tissue deformation for the PH18 model is around 2 times the one for the BC95 model. The tissue deformation in the upper section of the vocal folds (solid line) is greater than the deformation in the lower section (dash-dot-dotted line) for the PH18 model, i.e., the impact stress is minor in the lower section

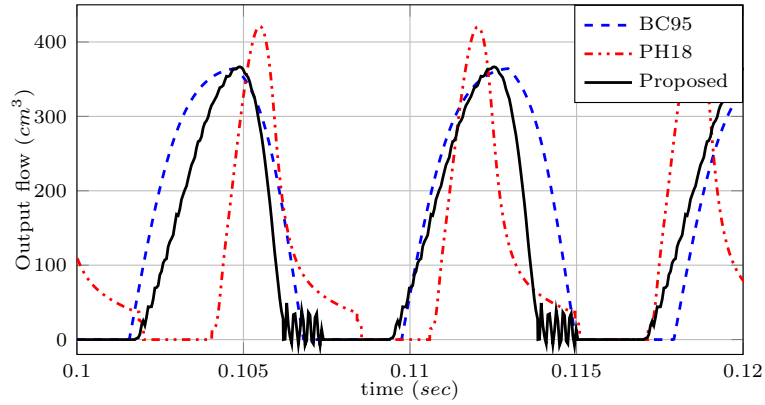


Figure 4.7 – Output Flow in one vibrating cycle.

of the vocal folds. On the contrary, in the proposed model the tissue deformation and impact stress is more important in the lower section of the vocal folds. This behavior is similar to one obtained with other lumped-parameter models [88, 95] and is consistent with the finite-element study presented in [110].

To compare the behavior of the airflow for the different models, we analyze the output flows in Figure 4.7. In general, the maximum flow in the vibration cycle occurs when the maximum opening of the glottal tract is achieved. For the PH18 model case this happens in the first quarter of the cycle, whereas for the BC95 and our model, the maximum flow occurs in the middle of the cycle. However, the output flow of the proposed model shows a soft increase in the glottis opening with a fast decline when the vocal fold is closing. This shape of the output flow is consistent with the results reported in [93, Figure 7].

Figure 4.8 shows the pressure distribution in the fluid for 3 time instants of the vibration cycle: 2 instants with a convergent shape of the vocal folds and 1 instant with a divergent shape. The pressure distributions obtained are consistent with the results of the DNN flow model proposed in [111, Figures 11-19].

Similarly, Figure 4.9 shows the behavior of kinetic and potential energies of the mechanical part of the vocal folds, \mathcal{K}_s and \mathcal{P}_s respectively, and the energies of the fluid, \mathcal{K}_f and \mathcal{U}_f , during one vibrating cycle. Note that for the PH18 model, most of the energy is stored in the mechanical system. The opposite situation occurs for the BC95 model. The proposed model presents an intermediate behavior between PH18 and BC95. Note that in the proposed model the maximum of the potential energy occurs in the maximum opening of mass m_1 and not in the maximum opening of the glottis as it is for the PH18 model. The potential energy decreases when the glottis is closing and increases slightly again when the glottis is completely closed. This latter is due to the energy stored during the elastic collision of the vocal folds. Regarding the fluid energy, it is important to note that the potential energy of the proposed model is negligible with respect to the kinetic energy. Regarding the fluid-structure energy transfer, it has been evaluated per cycle, i.e., $\int_{T_{cy}} \mathbf{u}_s^\top \mathbf{y}_s dt = \int_{T_{cy}} (\mathbf{F}^\top \mathbf{v}_c) dt$ where T_{cy} is the vibrating cycle period, obtaining a total of $20.2\mu J$ for the proposed model, in contrast with the $16.78\mu J$ and $11.28\mu J$ for the BC95 and PH18 models.

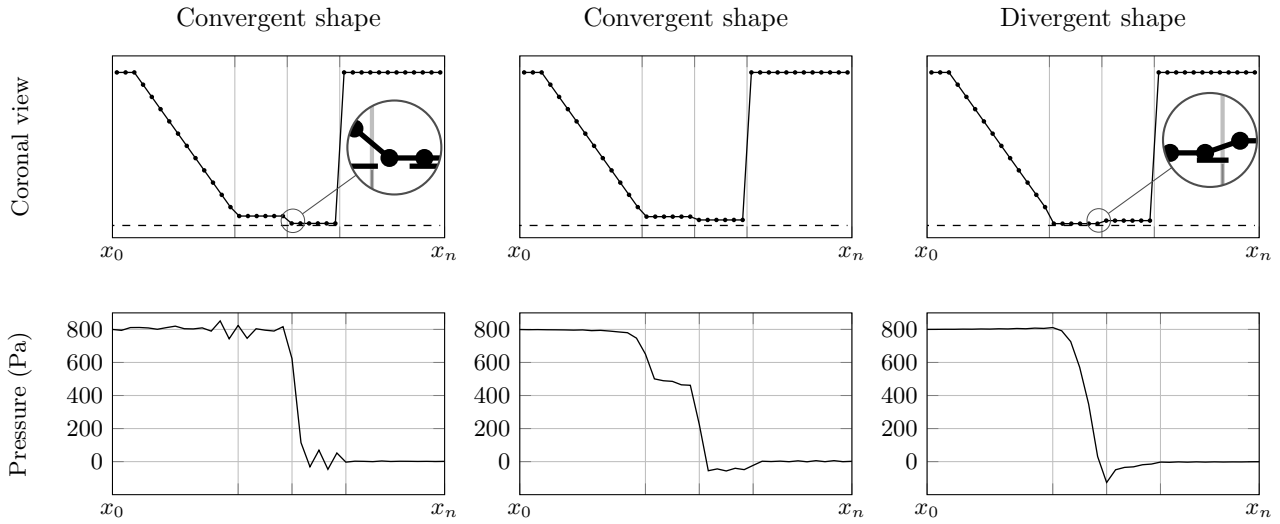


Figure 4.8 – Pressure distribution in 3 instants of the vibrating cycle. Upper row: Coronal view of the glottis, where the dots represents the heights of each velocity sections. Bottom row: Pressure distribution in the glottis.

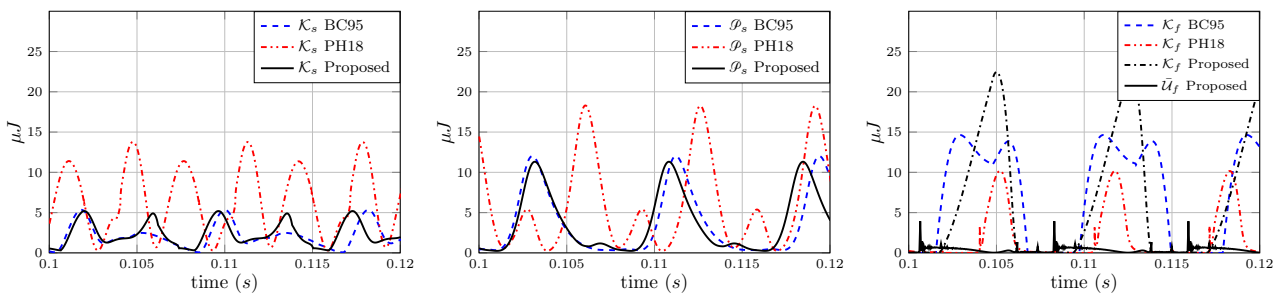


Figure 4.9 – Instantaneous energy in one vibrating cycle. Left: Kinetic energy \mathcal{K}_s of the mechanical part. Middle: Potential energy \mathcal{P}_s of the mechanical part. Right: Kinetic energy \mathcal{K}_f and available internal energy \bar{U}_f of the fluid part.

It is well known that the BC95 model describes appropriately the experimental results on the wave propagation of the real vocal folds motion and the volumetric airflow in the supraglottal section of the glottal tract. However, given the assumptions on the airflow (static and uniform flow), the energy transfers between the fluid and the mechanical parts of the model are not completely described. The effects of the closing of the vocal folds on the output airflow are neglected. The proposed model solves this drawback, keeping the advantages on the mechanical motion of the vocal folds. Additionally, the scalability of the proposed model is a clear advantage over the PH18 model.

4.5 CONCLUSION

In this chapter a scalable finite-dimensional port-Hamiltonian model for compressible fluids has been proposed. Similarly, a power-preserving interconnection based on a switching matrix S_ϵ is proposed for a fluid-structure coupling. This switched interconnection allows to obtain an appropriate description of structure collisions in systems such as the vocal folds. This switching matrix S_ϵ is also used to enable and disable the fluid dynamics in the corresponding areas of the fluid domain when the structure collides, avoiding the singularity problem in the fluid model. As simulation example we considered the FSI between the vocal folds and the intraglottal airflow. In this sense the well-known body-cover model is used to describe the structure motion. The results obtained show that the proposed scalable port-Hamiltonian model is able to replicate the oscillations and the collisions between the vocal folds. Moreover, the amplitude of masses movements and the airflow velocity are consistent with previous lumped-parameters models and real data. Similarly, the energy transfer estimated with the proposed model is greater than the predicted with other finite-dimensional models of the vocal folds.

In the previous chapters, some scalable finite-dimensional models based on the port-Hamiltonian framework have been proposed to describe the FSI in a longitudinal domain. These models in conjoint with power-preserving methods proposed, provide us of a simplified but appropriate description of a longitudinal fluid interacting with a structure with transverse motion, as shown in Sections 3.4 and 4.4. However, for a more detailed description of the fluid dynamics and the structure motion, it is necessary a more suitable modeling of the FSI system. In this sense, as a first step in this direction, an infinite-dimensional modeling of the fluid dynamics, based on the port-Hamiltonian approach, is presented in the next chapter.

Infinite-dimensional port-Hamiltonian Formulation of compressible Fluids

To obtain a more detailed description of a FSI system that the achieved with finite-dimensional models presented in the previous chapters, it is necessary an infinite-dimensional formulation. Then, as a first step, in this chapter we present infinite-dimensional models based on the port-Hamiltonian framework for Newtonian fluids. In this sense, in the following section, we consider a constant infinite dimensional domain $\Omega \subset \mathcal{X} \times \mathcal{Y} \times \mathcal{Z}$, with spatial variables $\zeta \in \mathcal{X}$, $\xi \in \mathcal{Y}$ and $\zeta \in \mathcal{Z}$ and boundary $\partial\Omega$.

There exist numerous energy-based models of compressible fluids in the literature, ranging from simple 1D formulations of isentropic fluids [112, 104] to more complex thermodynamic reactive flows [65], 3D inviscid fluids [37] and irrotational flows [62]. However, these models are constrained to one fluid class, given the assumptions used in each case.

Contribution

In this chapter general pseudo and a dissipative port-Hamiltonian formulations for 3D compressible fluids under non-isentropic and isentropic assumptions are presented. The considerations on the model structures and operators for 2D and 1D fluids are analyzed. Finally, we propose a model for 1D non-reactive fluids using the irreversible port-Hamiltonian approach.

In this chapter, we consider the state variables as functions on a spatial domain Ω , i.e., $\mathbf{x} = \mathbf{x}(\zeta, \xi, \zeta, t) \in L^2(\Omega, \mathbb{R}^n)$. For simplicity of notation, we make the time and space dependences of the variables implicit, we use a bold notation for vector and tensor functions, and capital letters for matrices. The reader is invited to refer to the Notation Section at the beginning of this thesis for details.

In the next sections, general energy-based models of 3D compressible fluids are developed using the port-Hamiltonian framework, i.e., the fluid dynamics will be described by the following PDE:

$$\partial_t \mathbf{x} = \mathcal{J} \delta_{\mathbf{x}} \mathcal{H} \tag{5.1}$$

where \mathcal{H} denotes the total energy of the fluid and \mathcal{J} is a Hamiltonian operator (see Definition 1.2). In the case that \mathcal{J} is a skew-symmetric operator that does not satisfy the Jacobi identity, the system (5.1) is called pseudo port-Hamiltonian formulation. Similarly, in a dissipative

port-Hamiltonian, the fluid dynamics are expressed as follows:

$$\partial_t \mathbf{x} = \mathcal{J} \delta_{\mathbf{x}} \mathcal{H} - \mathcal{G}^* S \mathcal{G} \delta_{\mathbf{x}} \mathcal{H} \quad (5.2)$$

where \mathcal{G}^* is the adjoint operator of \mathcal{G} , and $S > 0$ (see Section 1.2.2 for details).

5.1 NON-ISENTROPIC FLUIDS

In this section, we study the description of non-isentropic Newtonian fluids. We focus in the description of the thermal domain, specifically, in the second law of Thermodynamics. In this sense, the entropy (per unit mass) will be considered as a state variable. Entropy variations imply changes in the temperature that, at the same time, affect the fluid pressure, as shown by the ideal gas law (4.3). As a consequence, the velocity field of the fluid will be affected by the entropy. We use the port-Hamiltonian framework to describe these phenomena in the fluid dynamics. For simplicity, only nonreactive fluids are considered.

5.1.1 Governing equations

For non-isentropic fluids, the governing equations are given by the continuity, motion and change of internal energy equations [101] associated with the fluid density $\rho = \rho(\zeta, \xi, \zeta, t) \in L^2(\Omega, \mathbb{R})$, velocity field $\mathbf{v} = \mathbf{v}(\zeta, \xi, \zeta, t) \in L^2(\Omega, \mathbb{R}^3)$ and internal energy per unit mass $u = u(\zeta, \xi, \zeta, t) \in L^2(\Omega, \mathbb{R})$, respectively, given by:

$$\partial_t \rho = -\operatorname{div} \rho \mathbf{v} \quad (5.3a)$$

$$\rho \partial_t \mathbf{v} = -\rho (\mathbf{v} \cdot \mathbf{grad}) \mathbf{v} - \mathbf{grad} p - \operatorname{div} \boldsymbol{\tau} \quad (5.3b)$$

$$\partial_t u = -\mathbf{v} \cdot \mathbf{grad} u - \frac{1}{\rho} \operatorname{div} \mathbf{f}_T - \frac{p}{\rho} \operatorname{div} \mathbf{v} - \frac{1}{\rho} \boldsymbol{\tau} : \mathbf{grad} \mathbf{v} \quad (5.3c)$$

where $\boldsymbol{\tau} = \boldsymbol{\tau}(\zeta, \xi, \zeta, t) \in L^2(\Omega, \mathbb{R}^{3 \times 3})$ is the Newtonian viscosity tensor (4.2) and $\mathbf{f}_T = \mathbf{f}_T(\zeta, \xi, \zeta, t) \in L^2(\Omega, \mathbb{R}^{3 \times 3})$ is the heat flux defined as:

$$\mathbf{f}_T = -K \mathbf{grad} T \quad (5.4)$$

where $T = T(\zeta, \xi, \zeta, t) \in L^2(\Omega, \mathbb{R})$ denotes the temperature and K is the thermal conductivity matrix [69].

We denote by $\boldsymbol{\omega} = \operatorname{curl} \mathbf{v} \in L^2(\Omega, \mathbb{R}^3)$ the fluid vorticity that describes the tendency of the flow to rotate. Note that using the identity (A.1) the term $(\mathbf{v} \cdot \mathbf{grad}) \mathbf{v}$ in (5.3b), can be rewritten as $(\mathbf{v} \cdot \mathbf{grad}) \mathbf{v} = \mathbf{grad} \left(\frac{1}{2} \mathbf{v} \cdot \mathbf{v} \right) + \boldsymbol{\omega} \times \mathbf{v}$, where the term $\boldsymbol{\omega} \times \mathbf{v}$, from the point of view of energy, describes the power exchange between the velocity field components. This power exchange due to the fluid rotation can be described using a skew-symmetric matrix called Gyroscope [66, 113] defined as follows:

Definition 5.1. Let $\boldsymbol{\omega} = [\omega_1 \ \omega_2 \ \omega_3]^\top$ be the vorticity vector of the fluid. We define the fluid Gyroscope as a skew-symmetric matrix $G_{\boldsymbol{\omega}}$, such that $G_{\boldsymbol{\omega}} \mathbf{v} = \boldsymbol{\omega} \times \mathbf{v}$. For 3D fluids, the Gyroscope is given by:

$$G_{\boldsymbol{\omega}} = \begin{bmatrix} 0 & -\omega_3 & \omega_2 \\ \omega_3 & 0 & -\omega_1 \\ -\omega_2 & \omega_1 & 0 \end{bmatrix} \quad (5.5)$$

On the other hand, we use the specific form of the Gibbs equation to describe the variation of internal energy due to the variations of the fluid density and the entropy per unit mass, $s = s(\zeta, \xi, \mathfrak{z}, t) \in L^2(\Omega, \mathbb{R})$, i.e.,

$$du = -pd\left(\frac{1}{\rho}\right) + Tds \quad (5.6)$$

This implies that the thermodynamic equilibrium is given by:

$$TD_t s = D_t u - \frac{p}{\rho^2} D_t \rho \quad (5.7)$$

where the material derivative D_t is defined as $D_t = \partial_t + (\mathbf{v} \cdot \mathbf{grad})$. Considering the relationship $\mathbf{grad} \frac{p}{\rho} = \frac{1}{\rho} \mathbf{grad} p + p \mathbf{grad} \frac{1}{\rho}$ and the specific enthalpy definition (4.7), we obtain that $\frac{1}{\rho} \mathbf{grad} p = \mathbf{grad} h - T \mathbf{grad} s$, where the term $T \mathbf{grad} s$ describes the effect of the entropy variations (non-isentropic assumption) in the fluid pressure. Using the thermodynamic equilibrium (5.7) the governing equations of non-isentropic fluids can be expressed as:

$$\partial_t \rho = -\operatorname{div} \rho \mathbf{v} \quad (5.8a)$$

$$\partial_t \mathbf{v} = -\mathbf{grad} \left(\frac{1}{2} \mathbf{v} \cdot \mathbf{v} + h \right) - G_\omega \mathbf{v} + T \mathbf{grad} s - \frac{1}{\rho} \operatorname{div} \boldsymbol{\tau} \quad (5.8b)$$

$$\partial_t s = -\mathbf{v} \cdot \mathbf{grad} s - \frac{\boldsymbol{\tau}}{\rho T} : \mathbf{Grad} \mathbf{v} - \frac{\mathbf{f}_s}{\rho T} \cdot \mathbf{grad} T - \frac{1}{\rho} \operatorname{div} \mathbf{f}_s \quad (5.8c)$$

where $\mathbf{f}_s = -\frac{K}{T} \mathbf{grad} T$ is the entropy flux by heat conduction [101].

Note that the irreversible entropy production, i.e., second law of Thermodynamics, is given by the following non-negative condition [69]:

$$-\frac{1}{\rho T} \boldsymbol{\tau} : \mathbf{Grad} \mathbf{v} - \frac{\mathbf{f}_s}{\rho T} \cdot \mathbf{grad} T \geq 0 \quad (5.9)$$

where $-\frac{1}{\rho T} \boldsymbol{\tau} : \mathbf{Grad} \mathbf{v}$ is the rate of entropy production associated with the dissipation of kinetic energy into heat by viscosity friction, and $-\frac{\mathbf{f}_s}{\rho T} \cdot \mathbf{grad} T$ is the rate of entropy production due to heat flux.

5.1.2 Pseudo port-Hamiltonian formulation

We denote by $\mathbf{x} = [\rho \ \mathbf{v}^\top \ s]^\top$ the set of state variables for a non-isentropic fluid. Considering that the specific internal energy is a function of the fluid density and the specific entropy, as stated by the Gibbs equation (5.6), the total energy of the fluid described in (5.8) is given by:

$$\mathcal{H} = \int_{\Omega} \left(\frac{1}{2} \rho \mathbf{v} \cdot \mathbf{v} + \rho u(\rho, s) \right) d\Omega \quad (5.10)$$

The fluid efforts are given by the variational derivative of the energy, namely

$$\delta_{\mathbf{x}} \mathcal{H} = \begin{bmatrix} \delta_{\rho} \mathcal{H} \\ \delta_{\mathbf{v}} \mathcal{H} \\ \delta_s \mathcal{H} \end{bmatrix} = \begin{bmatrix} \frac{1}{2} \mathbf{v} \cdot \mathbf{v} + h \\ \rho \mathbf{v} \\ \rho T \end{bmatrix} \quad (5.11)$$

Using (5.11), the fluid dynamics in (5.8) can be related with the energy through the fluid efforts, i.e.,

$$\partial_t \rho = - \operatorname{div} \delta_{\mathbf{v}} \mathcal{H} \quad (5.12a)$$

$$\partial_t \mathbf{v} = - \mathbf{grad} \delta_{\rho} \mathcal{H} - \frac{1}{\rho} G_{\omega} \delta_{\mathbf{v}} \mathcal{H} + \frac{\delta_s \mathcal{H}}{\rho} \mathbf{grad} s - \frac{1}{\rho} \mathbf{div} \left[\boldsymbol{\tau} \frac{\delta_s \mathcal{H}}{\rho} \right] \quad (5.12b)$$

$$\begin{aligned} \partial_t s = & - \frac{\delta_{\mathbf{v}} \mathcal{H}}{\rho} \cdot \mathbf{grad} s - \frac{\boldsymbol{\tau}}{\rho T} : \mathbf{Grad} \frac{\delta_{\mathbf{v}} \mathcal{H}}{\rho} \\ & + \frac{1}{\rho T} \left\| \mathbf{grad} \frac{\delta_s \mathcal{H}}{\rho} \right\|_{\frac{K}{T}}^2 + \frac{1}{\rho} \operatorname{div} \left[\frac{K}{T} \mathbf{grad} \frac{\delta_s \mathcal{H}}{\rho} \right] \end{aligned} \quad (5.12c)$$

The operators and the corresponding adjoints that describe the power exchanges between the fluid component are defined in the following Lemmas.

Lemma 5.1. Denote by \mathcal{D}_p the operator defined as $\mathcal{D}_p(\cdot) = [\mathbf{grad} s] \frac{\dot{\cdot}}{\rho}$, that describes the effect of the entropy variation on the pressure gradient. The adjoint operator \mathcal{D}_p^* in the effort space of the fluid is given by $\mathcal{D}_p^*(\cdot) = [\mathbf{grad} s] \cdot \frac{\dot{\cdot}}{\rho}$.

Proof. Consider the inner product

$$\begin{aligned} \langle \delta_{\mathbf{v}} \mathcal{H}, \mathcal{D}_p \delta_s \mathcal{H} \rangle_{\Omega} &= \int_{\Omega} \delta_{\mathbf{v}} \mathcal{H} \cdot \mathcal{D}_p \delta_s \mathcal{H} d\Omega = \int_{\Omega} \delta_{\mathbf{v}} \mathcal{H} \cdot [\mathbf{grad} s] \frac{\delta_s \mathcal{H}}{\rho} d\Omega \\ &= \int_{\Omega} \frac{\delta_{\mathbf{v}} \mathcal{H}}{\rho} \cdot [\mathbf{grad} s] \delta_s \mathcal{H} d\Omega = \int_{\Omega} \left([\mathbf{grad} s] \cdot \frac{\delta_{\mathbf{v}} \mathcal{H}}{\rho} \right) \delta_s \mathcal{H} d\Omega \end{aligned}$$

Defining $\mathcal{D}_p^*(\cdot) = [\mathbf{grad} s] \cdot \frac{\dot{\cdot}}{\rho}$ we obtain that $\langle \delta_{\mathbf{v}} \mathcal{H}, \mathcal{D}_p \delta_s \mathcal{H} \rangle_{\Omega} = \langle \mathcal{D}_p^* \delta_{\mathbf{v}} \mathcal{H}, \delta_s \mathcal{H} \rangle_{\Omega}$, i.e., \mathcal{D}_p^* is the adjoint of \mathcal{D}_p . \square

Lemma 5.2. Let $\boldsymbol{\tau}$ be a symmetric second order tensor and $\mathcal{D}_{\tau}(\cdot) = -\frac{1}{\rho} \mathbf{div} \left(\frac{\boldsymbol{\tau}}{\rho T} \cdot \right)$ an operator acting on the entropy effort $\delta_s \mathcal{H}$. The formal adjoint operator \mathcal{D}_{τ}^* in the effort space of the fluid is given by $\mathcal{D}_{\tau}^*(\cdot) = \frac{\boldsymbol{\tau}}{\rho T} : \mathbf{Grad} \frac{\dot{\cdot}}{\rho}$, such that

$$\langle \delta_{\mathbf{v}} \mathcal{H}, \mathcal{D}_{\tau} \delta_s \mathcal{H} \rangle_{\Omega} - \langle \mathcal{D}_{\tau}^* \delta_{\mathbf{v}} \mathcal{H}, \delta_s \mathcal{H} \rangle_{\Omega} = - \int_{\partial\Omega} [\boldsymbol{\tau} \cdot \mathbf{n}] \cdot \frac{\delta_{\mathbf{v}} \mathcal{H}}{\rho} \partial\Omega \quad (5.13)$$

Proof. Consider the inner product

$$\begin{aligned} \langle \delta_{\mathbf{v}} \mathcal{H}, \mathcal{D}_{\tau} \delta_s \mathcal{H} \rangle_{\Omega} &= \int_{\Omega} \delta_{\mathbf{v}} \mathcal{H} \cdot [\mathcal{D}_{\tau} \delta_s \mathcal{H}] d\Omega \\ &= - \int_{\Omega} \delta_{\mathbf{v}} \mathcal{H} \cdot \left[\frac{1}{\rho} \mathbf{div} \left[\boldsymbol{\tau} \frac{\delta_s \mathcal{H}}{\rho T} \right] \right] d\Omega \end{aligned}$$

Using the property (A.10) considering $\boldsymbol{\sigma} = \boldsymbol{\tau} \frac{\delta_s \mathcal{H}}{\rho T}$ and $\mathbf{u} = \frac{\delta_v \mathcal{H}}{\rho}$, the inner product in the previous equation can be rewritten as:

$$\begin{aligned} \langle \delta_v \mathcal{H}, \mathcal{D}_\tau \delta_s \mathcal{H} \rangle_\Omega &= \int_\Omega \delta_s \mathcal{H} \frac{\boldsymbol{\tau}}{\rho T} : \mathbf{Grad} \left[\frac{\delta_v \mathcal{H}}{\rho} \right] d\Omega - \int_{\partial\Omega} \frac{\delta_v \mathcal{H}}{\rho} \cdot \left[\left[\frac{\boldsymbol{\tau} \delta_s \mathcal{H}}{\rho T} \right] \cdot \mathbf{n} \right] \partial\Omega \\ &= \int_\Omega \left(\left[\frac{\boldsymbol{\tau}}{\rho T} : \mathbf{Grad} \frac{\cdot}{\rho} \right] \delta_v \mathcal{H} \right) \delta_s \mathcal{H} d\Omega - \int_{\partial\Omega} \frac{\delta_v \mathcal{H}}{\rho} \cdot \left[\left[\frac{\boldsymbol{\tau} \delta_s \mathcal{H}}{\rho T} \right] \cdot \mathbf{n} \right] \partial\Omega \\ &= \langle \mathcal{D}_\tau^* \delta_v \mathcal{H}, \delta_s \mathcal{H} \rangle_\Omega - \int_{\partial\Omega} \frac{\delta_v \mathcal{H}}{\rho} \cdot \left[\left[\frac{\boldsymbol{\tau} \delta_s \mathcal{H}}{\rho T} \right] \cdot \mathbf{n} \right] \partial\Omega \end{aligned}$$

Considering boundary conditions equal to 0, $\langle \delta_v \mathcal{H}, \mathcal{D}_\tau \delta_s \mathcal{H} \rangle_\Omega = \langle \mathcal{D}_\tau^* \delta_v \mathcal{H}, \delta_s \mathcal{H} \rangle_\Omega$, i.e., \mathcal{D}_τ^* is the formal adjoint of \mathcal{D}_τ . Finally, from (5.11), $\frac{\delta_s \mathcal{H}}{\rho T} = 1$, i.e., operators \mathcal{D}_τ and \mathcal{D}_τ^* implicitly contain the effort associated with the fluid entropy, obtaining the relationship (5.13). \square

Lemma 5.3. *Let \mathcal{D}_T be a differential operator defined as*

$$\mathcal{D}_T = \mathcal{Q}_T - \mathcal{R}_T \quad (5.14)$$

where $\mathcal{Q}_T(\cdot) = \frac{1}{\rho T} \left\| \mathbf{grad} \frac{\cdot}{\rho} \right\|_{S_T}^2$ describes the entropy production associated with the heat flux, such that $\mathcal{Q}_T \delta_s \mathcal{H} \geq 0, \forall \delta_s \mathcal{H}$; and $\mathcal{R}_T = \mathcal{G}_T^* S_T \mathcal{G}_T$ describes the entropy diffusion, where the operator $\mathcal{G}_T^*(\cdot) = \frac{1}{\rho} \mathbf{div}(\cdot)$ is the formal adjoint of $\mathcal{G}_T(\cdot) = -\mathbf{grad} \frac{\cdot}{\rho}$ and $S_T = K/T \geq 0$. Then, the entropy rate of change due to the heat flux can be expressed as:

$$-\frac{1}{\rho T} \mathbf{div} \mathbf{f}_T = \mathcal{D}_T \delta_s \mathcal{H} \quad (5.15)$$

satisfying

$$\langle \delta_s \mathcal{H}, \mathcal{D}_T \delta_s \mathcal{H} \rangle_\Omega = - \int_{\partial\Omega} \frac{\delta_s \mathcal{H}}{\rho} (\mathbf{f}_s \cdot \mathbf{n}) \partial\Omega \quad (5.16)$$

Proof. Note that $\frac{1}{\rho T} \mathbf{div} \mathbf{f}_T = \frac{\mathbf{f}_s}{\rho T} \cdot \mathbf{grad} T + \frac{1}{\rho} \mathbf{div} \mathbf{f}_s$. Defining $S_T = K/T$ we obtain:

$$-\frac{\mathbf{f}_s}{\rho T} \mathbf{grad} T = \frac{1}{\rho T} \left\| \mathbf{grad} \frac{\delta_s \mathcal{H}}{\rho} \right\|_{S_T}^2 \quad \text{and} \quad -\frac{1}{\rho} \mathbf{div} \mathbf{f}_s = \frac{1}{\rho} \mathbf{div} \left[S_T \mathbf{grad} \frac{\delta_s \mathcal{H}}{\rho} \right]$$

Given that the divergence is the formal adjoint of minus the gradient, it is easy to verify that $\mathcal{G}_T^* = \frac{1}{\rho} \mathbf{div}$ is the formal adjoint of $\mathcal{G}_T = -\mathbf{grad} \frac{\cdot}{\rho}$. Then, the entropy rate of change due to the heat flux can be expressed as

$$-\frac{1}{\rho T} \mathbf{div} \mathbf{f}_T = (\mathcal{Q}_T - \mathcal{R}_T) \delta_s \mathcal{H} = \mathcal{D}_T \delta_s \mathcal{H}$$

The inner product on the left hand side of (5.16) can be expressed as:

$$\begin{aligned} \langle \delta_s \mathcal{H}, \mathcal{D}_T \delta_s \mathcal{H} \rangle_\Omega &= \int_\Omega \left(\frac{\delta_s \mathcal{H}}{\rho T} \left\| \mathbf{grad} \frac{\delta_s \mathcal{H}}{\rho} \right\|_{S_T}^2 + \frac{\delta_s \mathcal{H}}{\rho} \mathbf{div} \left[S_T \mathbf{grad} \frac{\delta_s \mathcal{H}}{\rho} \right] \right) d\Omega \\ &= - \int_\Omega \left(\mathbf{f}_s \cdot \mathbf{grad} \frac{\delta_s \mathcal{H}}{\rho} + \frac{\delta_s \mathcal{H}}{\rho} \mathbf{div} \mathbf{f}_s \right) d\Omega \\ &= - \int_\Omega \mathbf{div} \left[\frac{\delta_s \mathcal{H}}{\rho} \mathbf{f}_s \right] d\Omega \end{aligned}$$

Finally, using (A.8) we obtain (5.16). \square

Notice that the operator \mathcal{D}_T has been separated in 2 parts, \mathcal{Q}_T and \mathcal{R}_T , in order to describe the physical phenomena, entropy production and diffusion, associated with the entropy flux. Such that, the non-negative condition (5.9) associated with the irreversible entropy production can be expressed as:

$$-\mathcal{D}_\tau^* \delta_{\mathbf{v}} \mathcal{H} + \mathcal{Q}_T \delta_s \mathcal{H} \geq 0 \quad (5.17)$$

However, as shown in Section 5.4, the temperature in a ideal gas is a function of the specific entropy and the fluid density, $T = T(\rho, s)$. Then, defining $\alpha(\mathbf{x}) \in L^2(\Omega, \mathbb{R})$ and $F(\mathbf{x}) \in L^2(\Omega, \mathbb{R}^3)$ as $\alpha(\mathbf{x}) = \frac{1}{\rho}$ and $F(\mathbf{x}) = \frac{K}{\rho T^2(\rho, s)} \mathbf{grad} T(\rho, s)$, respectively, the operator \mathcal{D}_T can be rewritten as:

$$\mathcal{D}_T \delta_s \mathcal{H} = F^\top(\mathbf{x}) \mathbf{grad} (\alpha(\mathbf{x}) \delta_s \mathcal{H}) + \alpha(\mathbf{x}) \operatorname{div} (F(\mathbf{x}) \delta_s \mathcal{H}). \quad (5.18)$$

This implies that, according Theorem A.6, the operator \mathcal{D}_T is formally skew-adjoint. Thus, using Lemmas 5.1-5.3, the governing equations for non-isentropic fluids can be expressed as an energy-based model, as shown in the next proposition

Proposition 5.1. *Consider a non-isentropic Newtonian compressible fluid, whose total energy is described by (5.10). Then, the governing equations in (5.8) can be expressed as the pseudo infinite-dimensional port-Hamiltonian system*

$$\partial_t \mathbf{x} = \mathcal{J} \delta_{\mathbf{x}} \mathcal{H} \quad (5.19)$$

where $\mathbf{x} = [\rho \ \mathbf{v}^\top \ s]^\top$ is the state vector, $\delta_{\mathbf{x}} \mathcal{H}$ denotes the effort vector of the fluid, and \mathcal{J} is an formal skew-symmetric operator defined as:

$$\mathcal{J} = \begin{bmatrix} 0 & -\operatorname{div} & 0 \\ -\mathbf{grad} & \frac{1}{\rho} G_\omega & \mathcal{D}_p + \mathcal{D}_\tau \\ 0 & -\mathcal{D}_p^* - \mathcal{D}_\tau^* & \mathcal{D}_T \end{bmatrix} \quad (5.20)$$

satisfying

$$\dot{\mathcal{H}} = \langle \mathbf{f}_\partial, \mathbf{e}_\partial \rangle_\Omega \quad (5.21)$$

where $\langle \mathbf{f}_\partial, \mathbf{e}_\partial \rangle_\Omega$ denotes the power supplied through the boundary $\partial\Omega$, and the boundary flows \mathbf{f}_∂ and efforts \mathbf{e}_∂ are given by

$$\mathbf{f}_\partial = \begin{bmatrix} -(\rho \mathbf{v} \cdot \mathbf{n})|_{\partial\Omega} \\ -\mathbf{v}|_{\partial\Omega} \\ -(\mathbf{f}_s \cdot \mathbf{n})|_{\partial\Omega} \end{bmatrix} \quad \text{and} \quad \mathbf{e}_\partial = \begin{bmatrix} \left(\frac{1}{2} \mathbf{v} \cdot \mathbf{v} + h \right) |_{\partial\Omega} \\ (\boldsymbol{\tau} \cdot \mathbf{n})|_{\partial\Omega} \\ T|_{\partial\Omega} \end{bmatrix} \quad (5.22)$$

The time derivative of the total entropy of the fluid, $\mathcal{S} = \int_\Omega \rho s d\Omega$, is

$$\dot{\mathcal{S}} = \int_\Omega \sigma_s d\Omega \geq 0 \quad (5.23)$$

for boundary conditions equal to 0, which is in correspondence with the second law of Thermodynamics.

Proof. The governing equations (5.8) can be rewritten as function of the fluid efforts (5.11), as shown in (5.12). Using the operators defined in Lemmas 5.2 and 5.3 we obtain

$$\begin{bmatrix} \partial_t \rho \\ \partial_t \mathbf{v} \\ \partial_t s \end{bmatrix} = \begin{bmatrix} 0 & -\operatorname{div} & 0 \\ -\mathbf{grad} & \frac{1}{\rho} G_\omega & \mathcal{D}_p + \mathcal{D}_\tau \\ 0 & -\mathcal{D}_p^* - \mathcal{D}_\tau^* & \mathcal{Q}_T - \mathcal{R}_T \end{bmatrix} \begin{bmatrix} \delta_\rho \mathcal{H} \\ \delta_{\mathbf{v}} \mathcal{H} \\ \delta_s \mathcal{H} \end{bmatrix}$$

where the entropy production is given by the operators \mathcal{D}_τ^* and \mathcal{Q}_T , as shown in (5.17). From (5.14) and (5.18) we define \mathcal{J} as in (5.20) and the state $\mathbf{x} = [\rho \ \mathbf{v}^\top \ s]^\top$, obtaining the system (5.19).

The energy balance for this system is given by:

$$\begin{aligned} \dot{\mathcal{H}} &= \langle \delta_{\mathbf{x}} \mathcal{H}, \mathcal{J} \delta_{\mathbf{x}} \mathcal{H} \rangle_\Omega = \int_\Omega \delta_{\mathbf{x}} \mathcal{H} \cdot \mathcal{J} \delta_{\mathbf{x}} \mathcal{H} d\Omega \\ &= - \langle \delta_\rho \mathcal{H}, \operatorname{div} \delta_{\mathbf{v}} \mathcal{H} \rangle_\Omega - \langle \delta_{\mathbf{v}} \mathcal{H}, \mathbf{grad} \delta_\rho \mathcal{H} \rangle_\Omega + \langle \delta_{\mathbf{v}} \mathcal{H}, \mathcal{D}_\tau \delta_s \mathcal{H} \rangle_\Omega - \langle \delta_s \mathcal{H}, \mathcal{D}_\tau^* \delta_{\mathbf{v}} \mathcal{H} \rangle_\Omega \\ &\quad + \langle \delta_s \mathcal{H}, \mathcal{D}_T \delta_s \mathcal{H} \rangle_\Omega - \int_\Omega \delta_{\mathbf{v}} \mathcal{H} \cdot \frac{1}{\rho} G_\omega \delta_{\mathbf{v}} \mathcal{H} d\Omega \end{aligned}$$

Note that, given the skew-symmetric property of the Gyroscope, we have that $\delta_{\mathbf{v}} \mathcal{H} \cdot \frac{1}{\rho} G_\omega \delta_{\mathbf{v}} \mathcal{H} = 0$. Then, using Lemmas 5.2 and 5.3, and Theorem A.2, the energy balance can be expressed as

$$\dot{\mathcal{H}} = \int_{\partial\Omega} \delta_\rho \mathcal{H} (-\delta_{\mathbf{v}} \mathcal{H} \cdot \mathbf{n}) + [\boldsymbol{\tau} \cdot \mathbf{n}] \cdot \frac{\delta_{\mathbf{v}} \mathcal{H}}{\rho} + \frac{\delta_s \mathcal{H}}{\rho} (\mathbf{f}_s \cdot \mathbf{n}) \partial\Omega$$

Substituting the fluid efforts (5.11), and the boundary flows and efforts in (5.22), we obtain the energy balance (5.21).

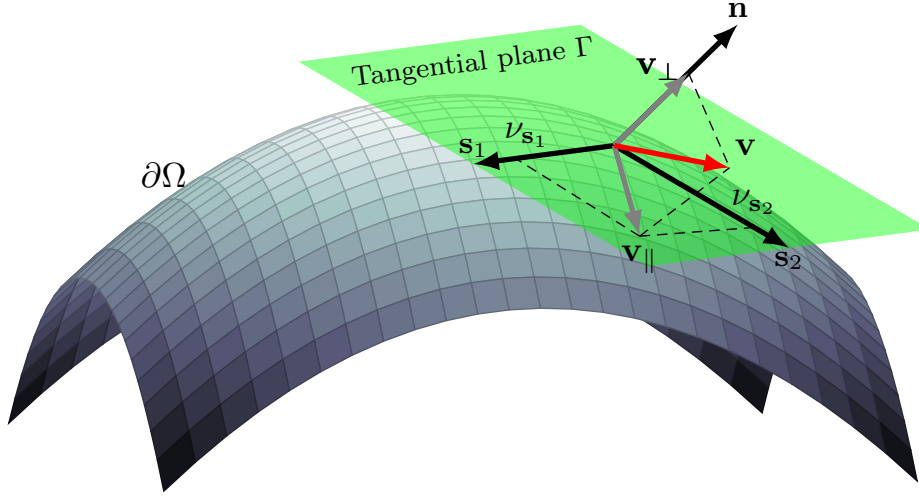
Note that the variational derivate of the total entropy \mathcal{S} is given by $\delta_{\mathbf{x}} \mathcal{S} = [s \ 0 \ \rho]^\top$, hence

$$\begin{aligned} \dot{\mathcal{S}} &= \int_\Omega \delta_{\mathbf{x}} \mathcal{S} \partial_t \mathbf{x} d\Omega = \int_\Omega \delta_{\mathbf{x}} \mathcal{S} \mathcal{J} \delta_{\mathbf{x}} \mathcal{H} d\Omega \\ &= - \int_\Omega (s \operatorname{div} \delta_{\mathbf{v}} \mathcal{H} + \rho \mathcal{D}_p^* \delta_{\mathbf{v}} \mathcal{H} + \rho \mathcal{G}_T^* S_T \mathcal{G}_T \delta_s \mathcal{H}) d\Omega + \int_\Omega \rho (\mathcal{Q}_T \delta_s \mathcal{H} - \mathcal{D}_\tau^* \delta_{\mathbf{v}} \mathcal{H}) d\Omega \\ &= \int_\Omega \sigma_s d\Omega - \int_\Omega (s (\operatorname{div} \delta_{\mathbf{v}} \mathcal{H}) + \delta_{\mathbf{v}} \mathcal{H} \cdot \mathbf{grad} s + \operatorname{div} \mathbf{f}_s) d\Omega \end{aligned}$$

where $\sigma_s = \rho (\mathcal{Q}_T \delta_s \mathcal{H} - \mathcal{D}_\tau^* \delta_{\mathbf{v}} \mathcal{H})$ denotes the density of irreversible entropy production. Using the Theorem A.2 we obtain

$$\dot{\mathcal{S}} = \int_\Omega \sigma_s d\Omega - \int_{\partial\Omega} [s \delta_{\mathbf{v}} \mathcal{H} + \mathbf{f}_s] \cdot \mathbf{n} \partial\Omega$$

Finally, assuming that the system is isolated, i.e., $\int_{\partial\Omega} [s \delta_{\mathbf{v}} \mathcal{H} + \mathbf{f}_s] \cdot \mathbf{n} \partial\Omega = 0$, and given the non-negative condition (5.17), then, the density of irreversible entropy production satisfies the inequality $\sigma_s \geq 0$, obtaining (5.23). \square


 Figure 5.1 – Normal vector and tangential plane to the boundary surface $\partial\Omega$

Remark 5.1. Note that the system (5.19) is similar to a Stokes-Dirac structure because of the skew-symmetry of the operators involved, and the associated power balance (5.20) with the appropriate boundary efforts and flows. However, since \mathcal{D}_τ , \mathcal{D}_τ^* and \mathcal{D}_T depend explicitly on the effort variable $\delta_s \mathcal{H} = \rho T$, and not only on the energy variables (ρ, \mathbf{v}, s) , then, the Jacobi identity is not satisfied and (5.19)-(5.21) do not define a Dirac structure. as a consequence, (5.19) is a pseudo port-Hamiltonian system.

An alternative formulation of non-isentropic fluids is obtained considering the flow and effort associated with the entropy diffusion by heat flux, i.e., $\mathbf{f}_d = \mathcal{G}_T \delta_s \mathcal{H}$ and $\mathbf{e}_d = S_T \mathbf{f}_d$, respectively. This leads to the following representation:

$$\begin{bmatrix} \partial_t \rho \\ \partial_t \mathbf{v} \\ \partial_t s \\ \mathbf{f}_d \end{bmatrix} = \begin{bmatrix} 0 & -\text{div} & 0 & 0 \\ -\mathbf{grad} & \frac{1}{\rho} G_\omega & \mathcal{D}_\tau & 0 \\ 0 & -\mathcal{D}_\tau^* & \mathcal{Q}_T & -\mathcal{G}_T^* \\ 0 & 0 & \mathcal{G}_T & 0 \end{bmatrix} \begin{bmatrix} \delta_\rho \mathcal{H} \\ \delta_{\mathbf{v}} \mathcal{H} \\ \delta_s \mathcal{H} \\ \mathbf{e}_d \end{bmatrix} \quad (5.24)$$

where $\mathbf{e}_d = -\mathbf{f}_s$ denotes the entropy flux.

Similarly, an alternative to define the boundary conditions is to consider the normal and tangential contributions of the viscous tensor. We denote by Γ , the tangential plane to the boundary surface $\partial\Omega$, as shown in Figure 5.1. Considering the pair of orthogonal unitary vectors $(\mathbf{s}_1, \mathbf{s}_2) \in \Gamma$, i.e.,

$$\mathbf{n} \cdot \mathbf{s}_1 = \mathbf{n} \cdot \mathbf{s}_2 = \mathbf{s}_1 \cdot \mathbf{s}_2 = 0 \quad (5.25)$$

the velocity field can be expressed as $\mathbf{v} = \mathbf{v}_\perp + \mathbf{v}_\parallel$ where $\mathbf{v}_\perp = (\mathbf{v} \cdot \mathbf{n}) \mathbf{n}$ denotes the normal projection and $\mathbf{v}_\parallel = -\mathbf{n} \times [\mathbf{n} \times \mathbf{v}] = (\mathbf{v} \cdot \mathbf{s}_1) \mathbf{s}_1 + (\mathbf{v} \cdot \mathbf{s}_2) \mathbf{s}_2$, for any $(\mathbf{s}_1, \mathbf{s}_2) \in \Gamma$ that satisfies (5.25), is the tangential projection of \mathbf{v} . Then, given that $[\boldsymbol{\tau} \cdot \mathbf{n}] \cdot \mathbf{v} = \boldsymbol{\tau} : \mathbf{v} \mathbf{n}$ and using the

normal and tangential formulation of \mathbf{v} , the boundary conditions defined on the right hand side of (5.13) can be rewritten as:

$$-\int_{\partial\Omega} [\boldsymbol{\tau} \cdot \mathbf{n}] \cdot \frac{\delta_{\mathbf{v}} \mathcal{H}}{\rho} \partial\Omega = -\int_{\partial\Omega} (\nu_{\mathbf{n}} \tau_{\mathbf{n}} + \nu_{\mathbf{s}_1} \tau_{\mathbf{s}_1} + \nu_{\mathbf{s}_2} \tau_{\mathbf{s}_2}) \partial\Omega \quad (5.26)$$

where

$$\begin{aligned} \nu_{\mathbf{n}} &= \frac{\delta_{\mathbf{v}} \mathcal{H}}{\rho} \cdot \mathbf{n} = \mathbf{v} \cdot \mathbf{n} & \tau_{\mathbf{n}} &= \boldsymbol{\tau} : \mathbf{nn} \\ \nu_{\mathbf{s}_1} &= \frac{\delta_{\mathbf{v}} \mathcal{H}}{\rho} \cdot \mathbf{s}_1 = \mathbf{v} \cdot \mathbf{s}_1 & \text{and } \tau_{\mathbf{s}_1} &= \boldsymbol{\tau} : \mathbf{s}_1 \mathbf{n} \\ \nu_{\mathbf{s}_2} &= \frac{\delta_{\mathbf{v}} \mathcal{H}}{\rho} \cdot \mathbf{s}_2 = \mathbf{v} \cdot \mathbf{s}_2 & \tau_{\mathbf{s}_2} &= \boldsymbol{\tau} : \mathbf{s}_2 \mathbf{n} \end{aligned} \quad (5.27)$$

are the normal and tangential contributions of the velocity field, and the viscous tensor, respectively. Thus, the boundary ports variables can be rewritten as:

$$\mathbf{f}_{\partial} = \begin{bmatrix} -(\rho \mathbf{v} \cdot \mathbf{n})|_{\partial\Omega} \\ -\nu_{\mathbf{n}}|_{\partial\Omega} \\ -\nu_{\mathbf{s}_1}|_{\partial\Omega} \\ -\nu_{\mathbf{s}_2}|_{\partial\Omega} \\ -(\mathbf{f}_s \cdot \mathbf{n})|_{\partial\Omega} \end{bmatrix} \quad \mathbf{e}_{\partial} = \begin{bmatrix} \left(\frac{1}{2} \mathbf{v} \cdot \mathbf{v} + h\right)|_{\partial\Omega} \\ \tau_{\mathbf{n}}|_{\partial\Omega} \\ \tau_{\mathbf{s}_1}|_{\partial\Omega} \\ \tau_{\mathbf{s}_2}|_{\partial\Omega} \\ T|_{\partial\Omega} \end{bmatrix} \quad (5.28)$$

Additionally, another point to highlight is the fact that, under an inviscid assumption, the term $\frac{1}{\rho} \mathbf{div} \left(\frac{\boldsymbol{\tau}}{\rho T} \cdot \right)$ in the operator \mathcal{D}_{τ} and the term $\frac{\boldsymbol{\tau}}{\rho T} : \mathbf{Grad} \frac{\cdot}{\rho}$ in the operator \mathcal{D}_{τ}^* are equal to 0. Then, the non-negative condition (5.17) of entropy production is only due to the heat flux of the fluid, i.e., $\sigma_s = \mathcal{Q}_T \delta_s \mathcal{H} \geq 0$.

5.2 ISENTROPIC FLUIDS

In this section we consider that the heat production given by the dissipation of kinetic energy into heat by viscous friction and the temperature diffusion generate small and smooth variations in the fluid temperature. This implies that the entropy production by these phenomena is sufficiently small such that the specific entropy s advects with the flow, i.e., $\partial_t s = -\mathbf{v} \cdot \mathbf{grad} s$. If s is initially uniform throughout the fluid, then s will remain constant and the entropy balance in (5.12) can be neglected. This justifies the use of the isentropic equations for small disturbances in the fluid variables [114]. Additionally, if the viscous effects in the velocity field are negligible, the fluid can be considered as a reversible process, as shown in [37]. However, if it is necessary to consider the viscous friction, the process is irreversible and the divergence of the viscous tensor can be considered as a dissipative term, as shown in [62] for fluids with irrotational flow. In this section, we present a general dissipative port-Hamiltonian formulation for isentropic compressible fluids.

5.2.1 Governing equations

Given the isentropic assumption, the Gibbs equation that describes the changes of the specific internal energy is reduced to

$$du = -pd\frac{1}{\rho} \quad (5.29)$$

Similarly, the entropy dynamic in (5.8) is neglected. Then, the governing equations for isentropic fluids are given by:

$$\partial_t \rho = -\operatorname{div} \rho \mathbf{v} \quad (5.30a)$$

$$\partial_t \mathbf{v} = -\operatorname{grad} \left(\frac{1}{2} \mathbf{v} \cdot \mathbf{v} + h \right) - G_\omega \mathbf{v} - \frac{1}{\rho} \operatorname{div} \boldsymbol{\tau} \quad (5.30b)$$

In this case, the model does not have the power exchange between the velocity field and the specific entropy, described in (5.19) by the adjoint operators \mathcal{D}_τ and \mathcal{D}_τ^* . The conversion of kinetic energy into heat by viscous friction is now considered as a power dissipation. In this sense the term $\frac{1}{\rho} \operatorname{div} \boldsymbol{\tau}$ can be expressed as a dissipative element [40], as shown in the following lemma.

Lemma 5.4. *Consider a viscous Newtonian fluid. Defining the operators $\mathcal{G}_r(\cdot) = \operatorname{curl} \frac{\cdot}{\rho}$ and $\mathcal{G}_c(\cdot) = \operatorname{div} \frac{\cdot}{\rho}$, and the corresponding formal adjoints $\mathcal{G}_r^*(\cdot) = \frac{1}{\rho} \operatorname{curl}(\cdot)$ and $\mathcal{G}_c^*(\cdot) = -\frac{1}{\rho} \operatorname{grad}(\cdot)$. Then, the rate of change of the velocity associated with the viscous tensor, $\frac{1}{\rho} \operatorname{div} \boldsymbol{\tau}$, can be expressed as a dissipative port-Hamiltonian term associated with the velocity effort, namely,*

$$\frac{1}{\rho} \operatorname{div} \boldsymbol{\tau} = \mathcal{G}_\tau^* S_\tau \mathcal{G}_\tau [\rho \mathbf{v}] \quad (5.31)$$

where $\mathcal{G}_\tau^* = \begin{bmatrix} \mathcal{G}_r^* & \mathcal{G}_c^* \end{bmatrix}$, $S_\tau = \begin{bmatrix} \mu \mathbf{I} & 0 \\ 0 & \hat{\mu} \end{bmatrix} \geq 0$ and $\mathcal{G}_\tau = \begin{bmatrix} \mathcal{G}_r \\ \mathcal{G}_c \end{bmatrix}$, with $\hat{\mu} = \frac{4}{3}\mu + \kappa$.

Proof. Consider the viscosity tensor (4.2). Applying the identities (A.4)-(A.6) we obtain

$$\begin{aligned} \frac{1}{\rho} \operatorname{div} \boldsymbol{\tau} &= \frac{1}{\rho} \operatorname{div} \left[-\mu \left[\operatorname{Grad} \mathbf{v} + \left[\operatorname{Grad} \mathbf{v} \right]^\top \right] \right] + \frac{1}{\rho} \operatorname{div} \left[\left(\frac{2}{3}\mu - \kappa \right) (\operatorname{div} \mathbf{v}) \mathbf{I} \right] \\ &= \frac{1}{\rho} \operatorname{curl} \left[\mu \operatorname{curl} \mathbf{v} \right] - \frac{1}{\rho} \operatorname{grad} \left[\left(\frac{4}{3}\mu + \kappa \right) \operatorname{div} \mathbf{v} \right] \end{aligned}$$

Note that $\mathcal{G}_r^* = \frac{1}{\rho} \operatorname{curl}$ is the formal adjoint of $\mathcal{G}_r = \operatorname{curl} \frac{\cdot}{\rho}$, as shown in Theorem A.4, and $\mathcal{G}_c^* = -\frac{1}{\rho} \operatorname{grad}$ is the adjoint of $\mathcal{G}_c = \operatorname{div} \frac{\cdot}{\rho}$. The divergence of the fluid viscosity tensor can be expressed as the sum of two dissipative terms, namely:

$$\frac{1}{\rho} \operatorname{div} \boldsymbol{\tau} = \mathcal{G}_r^* \mu \mathcal{G}_r [\rho \mathbf{v}] + \mathcal{G}_c^* \hat{\mu} \mathcal{G}_c [\rho \mathbf{v}] \quad (5.32)$$

where $\mathcal{G}_r^* \mu \mathcal{G}_r [\rho \mathbf{v}]$ denotes the energy dissipation by the fluid rotation and $\mathcal{G}_c^* \hat{\mu} \mathcal{G}_c [\rho \mathbf{v}]$ the describes the energy dissipation by fluid compression. Finally, rearranging terms, we obtain (5.31) \square

Applying Lemma 5.4 the governing equations (5.30) can be expressed as:

$$\partial_t \rho = -\operatorname{div} \rho \mathbf{v} \quad (5.33a)$$

$$\partial_t \mathbf{v} = -\operatorname{grad} \left(\frac{1}{2} \mathbf{v} \cdot \mathbf{v} + h \right) - G_\omega \mathbf{v} - \mathcal{G}_\tau^* S_\tau \mathcal{G}_\tau [\rho \mathbf{v}] \quad (5.33b)$$

Notice that, from the viscous tensor, the fluid energy losses are given by two different phenomena: the friction between streamlines when the flow rotates and the friction between fluid particles when the fluid expands or compresses. These losses are zero under irrotational and incompressible assumptions, respectively. In some applications such as pipelines, the fluid is modeled as a 1D incompressible flow. In this case, from Lemma 5.4, this system does not have energy dissipation. However, given the roughness of the internal surface of the pipe, the fluid has an energy dissipation due to the friction of the flow with the pipe wall. To model this dissipation source, a term of the form $\frac{\lambda}{2D}\rho|v|v$ is added *ad-hoc* to the momentum balance, where D is the pipe diameter, λ is a loss factor and v is the flow velocity [115, 116].

5.2.2 Dissipative port-Hamiltonian formulation

For isentropic fluids, the specific internal energy depends only of the fluid density, as shown in (5.29). Then, the total energy is given by:

$$\mathcal{H} = \int_{\Omega} \left(\frac{1}{2} \rho \mathbf{v} \cdot \mathbf{v} + \rho u(\rho) \right) d\Omega \quad (5.34)$$

and the fluid efforts are

$$\begin{bmatrix} \delta_{\rho} \mathcal{H} \\ \delta_{\mathbf{v}} \mathcal{H} \end{bmatrix} = \begin{bmatrix} \frac{1}{2} \mathbf{v} \cdot \mathbf{v} + h \\ \rho \mathbf{v} \end{bmatrix} \quad (5.35)$$

Proposition 5.2. *Consider an isentropic Newtonian fluid with state variables given by $\mathbf{x} = [\rho \ \mathbf{v}^{\top}]^{\top}$. The fluid dynamics can be expressed by the following dissipative port-Hamiltonian system:*

$$\partial_t \mathbf{x} = [\mathcal{J} - \mathcal{G}^* S \mathcal{G}] \delta_{\mathbf{x}} \mathcal{H} \quad (5.36)$$

where the operators \mathcal{J} , \mathcal{G}^* and \mathcal{G} , and matrix S are

$$\mathcal{J} = \begin{bmatrix} 0 & -\text{div} \\ -\mathbf{grad} & -\frac{1}{\rho} G_{\omega} \end{bmatrix}, \quad \mathcal{G}^* = \begin{bmatrix} 0 & 0 \\ 0 & \mathcal{G}_{\tau}^* \end{bmatrix}, \quad \mathcal{G} = \begin{bmatrix} 0 & 0 \\ 0 & \mathcal{G}_{\tau} \end{bmatrix} \quad \text{and} \quad S = \begin{bmatrix} 0 & 0 \\ 0 & S_{\tau} \end{bmatrix}, \quad (5.37)$$

respectively, and the following relationship holds for the rate of change of the energy:

$$\dot{\mathcal{H}} \leq \langle \mathbf{f}_{\partial}, \mathbf{e}_{\partial} \rangle_{\partial\Omega} \quad (5.38)$$

where

$$\mathbf{f}_{\partial} = \begin{bmatrix} -(\mathbf{n} \cdot \delta_{\mathbf{v}} \mathcal{H}) \\ \delta_{\mathbf{v}} \mathcal{H}|_{\partial\Omega} \end{bmatrix} \quad \text{and} \quad \mathbf{e}_{\partial} = \begin{bmatrix} \left(\delta_{\rho} \mathcal{H} + \frac{e_c}{\rho} \right) |_{\partial\Omega} \\ -\mathbf{n} \times \mathbf{e}_r |_{\partial\Omega} \end{bmatrix} \quad (5.39)$$

are the boundary flows and efforts, with \mathbf{e}_r and e_c as the efforts associated with the power dissipation by fluid rotation and compression, respectively.

Proof. Considering the fluid efforts (5.35), then (5.33) can be rewritten as:

$$\begin{bmatrix} \partial_t \rho \\ \partial_t \mathbf{v} \end{bmatrix} = \begin{bmatrix} 0 & -\text{div} \\ -\mathbf{grad} & -\frac{1}{\rho} G_\omega - \mathcal{G}_r^* S_r \mathcal{G}_r \end{bmatrix} \begin{bmatrix} \delta_\rho \mathcal{H} \\ \delta_\mathbf{v} \mathcal{H} \end{bmatrix}$$

Defining the state vector as $\mathbf{x} = [\rho \ \mathbf{v}^\top]^\top$, operators \mathcal{J} , \mathcal{G}^* and \mathcal{G} , and matrix S as shown in (5.37), the dissipative port-Hamiltonian formulation (5.36) is obtained.

We denote by $\mathbf{f}_r = \mathcal{G}_r \delta_\mathbf{v} \mathcal{H}$ and $\mathbf{e}_r = \mu \mathbf{f}_r$ the flow and effort variables associated with the dissipation of fluid rotation, respectively, and by $f_c = \mathcal{G}_c \delta_\mathbf{v} \mathcal{H}$ and $e_c = \hat{\mu} f_c$ the flow and efforts variables associated with the dissipation of fluid compression, respectively. The dissipative port-Hamiltonian system (5.36) can be expressed as the following extended skew-symmetric representation:

$$\begin{bmatrix} \partial_t \rho \\ \partial_t \mathbf{v} \\ \mathbf{f}_r \\ f_c \end{bmatrix} = \underbrace{\begin{bmatrix} 0 & -\text{div} & 0 & 0 \\ -\mathbf{grad} & \frac{1}{\rho} G_\omega & -\mathcal{G}_r^* & -\mathcal{G}_c^* \\ 0 & \mathcal{G}_r & 0 & 0 \\ 0 & \mathcal{G}_c & 0 & 0 \end{bmatrix}}_{\mathcal{J}_e} \begin{bmatrix} \delta_\rho \mathcal{H} \\ \delta_\mathbf{v} \mathcal{H} \\ \mathbf{e}_r \\ e_c \end{bmatrix} \quad (5.40)$$

The rate of change of the total energy is given by:

$$\dot{\mathcal{H}} = \int_\Omega \delta_\mathbf{x} \mathcal{H} \cdot \partial_t \mathbf{x} d\Omega = \int_\Omega \delta_\mathbf{x} \mathcal{H} \cdot \mathcal{J} \delta_\mathbf{x} \mathcal{H} d\Omega - \int_\Omega \delta_\mathbf{v} \mathcal{H} \cdot \mathcal{G}_r^* \mathbf{e}_r d\Omega - \int_\Omega \delta_\mathbf{v} \mathcal{H} \cdot \mathcal{G}_c^* e_c d\Omega$$

where

$$\begin{aligned} \int_\Omega \delta_\mathbf{x} \mathcal{H} \cdot \mathcal{J} \delta_\mathbf{x} \mathcal{H} d\Omega &= - \int_\Omega \left(\delta_\rho \mathcal{H} (\text{div} \delta_\mathbf{v} \mathcal{H}) + \delta_\mathbf{v} \mathcal{H} \cdot [\mathbf{grad} \delta_\rho \mathcal{H}] d\Omega - \int_\Omega \frac{\delta_\mathbf{v} \mathcal{H}}{\rho} \cdot G_\omega \delta_\mathbf{v} \mathcal{H} \right) d\Omega \\ \int_\Omega \delta_\mathbf{v} \mathcal{H} \cdot \mathcal{G}_r^* \mathbf{e}_r d\Omega &= \int_\Omega \frac{\delta_\mathbf{v} \mathcal{H}}{\rho} \cdot [\mathbf{curl} \ \mathbf{e}_r] d\Omega \\ \int_\Omega \delta_\mathbf{v} \mathcal{H} \cdot \mathcal{G}_c^* e_c &= - \int_\Omega \frac{\delta_\mathbf{v} \mathcal{H}}{\rho} \cdot [\mathbf{grad} \ e_c] d\Omega \end{aligned}$$

Considering the definition of \mathcal{G}_r and \mathcal{G}_c in Lemma 5.4, and applying Theorems A.2 and A.4, $\dot{\mathcal{H}}$ can be rewritten as

$$\begin{aligned} \dot{\mathcal{H}} &= - \int_{\partial\Omega} \delta_\rho \mathcal{H} (\delta_\mathbf{v} \mathcal{H} \cdot \mathbf{n}) \partial\Omega - \int_\Omega e_c (\mathcal{G}_c \delta_\mathbf{v} \mathcal{H}) d\Omega - \int_{\partial\Omega} e_c \left(\frac{\delta_\mathbf{v} \mathcal{H}}{\rho} \cdot \mathbf{n} \right) \partial\Omega \\ &\quad - \int_\Omega \mathbf{e}_r \cdot [\mathcal{G}_r \delta_\mathbf{v} \mathcal{H}] - \int_{\partial\Omega} \left[\mathbf{e}_r \times \frac{\delta_\mathbf{v} \mathcal{H}}{\rho} \right] \cdot \mathbf{n} \partial\Omega \end{aligned}$$

Using the definition of dissipation efforts and the cross product identity $\mathbf{n} \cdot [\mathbf{u}_1 \times \mathbf{u}_2] = \mathbf{u}_2 \cdot [\mathbf{n} \times \mathbf{u}_1]$, we obtain

$$\dot{\mathcal{H}} = - \int_\Omega \begin{bmatrix} \mathbf{f}_r \\ f_c \end{bmatrix} \cdot \begin{bmatrix} \mu \mathbf{I} & 0 \\ 0 & \hat{\mu} \end{bmatrix} \begin{bmatrix} \mathbf{f}_r \\ f_c \end{bmatrix} d\Omega - \int_{\partial\Omega} \left(\left(\delta_\rho \mathcal{H} + \frac{e_c}{\rho} \right) (\delta_\mathbf{v} \mathcal{H} \cdot \mathbf{n}) + \frac{\delta_\mathbf{v} \mathcal{H}}{\rho} \cdot [\mathbf{n} \times \mathbf{e}_r] \right) \partial\Omega$$

On the other hand, using

$$\begin{bmatrix} \mathbf{e}_\partial \\ \mathbf{f}_\partial \end{bmatrix} = \mathcal{R} \begin{bmatrix} \delta_\rho \mathcal{H}|_{\partial\Omega} \\ \delta_{\mathbf{v}} \mathcal{H}|_{\partial\Omega} \\ \mathbf{e}_r|_{\partial\Omega} \\ e_c|_{\partial\Omega} \end{bmatrix} \quad \text{with} \quad \mathcal{R} = \begin{bmatrix} 1 & 0 & 0 & \frac{1}{\rho} \\ 0 & 0 & -\mathbf{n} \times & 0 \\ 0 & -\mathbf{n} \cdot & 0 & 0 \\ 0 & \frac{1}{\rho} & 0 & 0 \end{bmatrix} \quad (5.41)$$

we obtain the boundary flows and efforts in (5.39). Then, the rate of change of the fluid total energy can be expressed as:

$$\dot{\mathcal{H}} = - \left\langle \begin{bmatrix} \mathbf{f}_r \\ f_c \end{bmatrix}, S_\tau \begin{bmatrix} \mathbf{f}_r \\ f_c \end{bmatrix} \right\rangle_\Omega + \langle \mathbf{f}_\partial, \mathbf{e}_\partial \rangle_{\partial\Omega}$$

Finally, given that $\left\langle \begin{bmatrix} \mathbf{f}_r \\ f_c \end{bmatrix}, S_\tau \begin{bmatrix} \mathbf{f}_r \\ f_c \end{bmatrix} \right\rangle_\Omega \geq 0$, the relationship (5.38) is obtained. \square

Notice that the boundary effort $-\mathbf{n} \times \mathbf{e}_r|_{\partial\Omega} = \mu \boldsymbol{\omega} \times \mathbf{n}|_{\partial\Omega}$ is equivalent to the vorticity boundary condition $\boldsymbol{\omega} \times \mathbf{n}|_{\partial\Omega}$ [117, 118], using only the tangential part of the classical kinematic condition $\boldsymbol{\omega}|_{\partial\Omega}$ [119].

Similarly, equation (5.41) denotes the boundary port variables for the extended skew-symmetric operator \mathcal{J}_e in (5.40), and it is equivalent to the boundary port variables definition proposed in [40] for 1D dissipative systems.

Additionally, under different assumptions, the fluid model proposed in (5.36), corresponds to port-Hamiltonian models of isentropic fluids described in the literature, as shown in the following remarks.

Remark 5.2. Consider that the isentropic fluid has an irrotational flow. This implies that operators \mathcal{G}_r and \mathcal{G}_r^* , and Gyroscope matrix G_ω vanish. Then, the port-Hamiltonian formulation in Proposition 5.2, can be expressed as:

$$\begin{bmatrix} \partial_t \rho \\ \partial_t \mathbf{v} \\ f_c \end{bmatrix} = \underbrace{\begin{bmatrix} 0 & -\text{div} & 0 \\ -\mathbf{grad} & 0 & -\mathcal{G}_c^* \\ 0 & \mathcal{G}_c & 0 \end{bmatrix}}_{\mathcal{J}_e} \begin{bmatrix} \delta_\rho \mathcal{H} \\ \delta_{\mathbf{v}} \mathcal{H} \\ e_c \end{bmatrix} \quad (5.42)$$

satisfying the balance $\dot{\mathcal{H}} \leq \langle \mathbf{f}_\partial, \mathbf{e}_\partial \rangle_{\partial\Omega}$, with boundary ports $\mathbf{f}_\partial, \mathbf{e}_\partial$ given by $\mathbf{f}_\partial = -(\mathbf{n} \cdot \delta_{\mathbf{v}} \mathcal{H})|_{\partial\Omega}$ and $\mathbf{e}_\partial = (\delta_\rho \mathcal{H} + \frac{e_c}{\rho})|_{\partial\Omega}$, obtaining the fluid model in [62].

Remark 5.3. Consider the fluid as isentropic and inviscid. This implies that the operators associated with the viscous tensor vanish. Then, the port-Hamiltonian formulation in Proposition 5.2, can be expressed as:

$$\begin{bmatrix} \partial_t \rho \\ \partial_t \mathbf{v} \end{bmatrix} = \underbrace{\begin{bmatrix} 0 & -\text{div} \\ -\mathbf{grad} & -\frac{G_\omega}{\rho} \end{bmatrix}}_{\mathcal{J}_e} \begin{bmatrix} \delta_\rho \mathcal{H} \\ \delta_{\mathbf{v}} \mathcal{H} \end{bmatrix} \quad (5.43)$$

satisfying the balance $\dot{\mathcal{H}} = \langle \mathbf{f}_\partial, \mathbf{e}_\partial \rangle_{\partial\Omega}$, with boundary ports $(\mathbf{f}_\partial, \mathbf{e}_\partial)$ given by $\mathbf{f}_\partial = -(\mathbf{n} \cdot \delta_{\mathbf{v}} \mathcal{H})|_{\partial\Omega}$ and $\mathbf{e}_\partial = \delta_\rho \mathcal{H}|_{\partial\Omega}$. This formulation is equivalent to the fluid model in [37].

5.3 CONSIDERATIONS FOR 2D AND 1D FLOWS

Cross product and the Curl are 3D mathematical operators, hence their definitions have to be carefully adapted for 2D fluids.

Let us denote by $\{\zeta, \xi\}$ the variables associated with the axes of a 2D velocity field $\mathbf{v} = [v \ v]^\top$. The vorticity is a scalar defined as $\omega = -\partial_\xi v + \partial_\zeta v$. For convenience we rewrite ω as:

$$\omega = -\text{div} [W\mathbf{v}] \quad (5.44)$$

where $W = \begin{bmatrix} 0 & -1 \\ 1 & 0 \end{bmatrix}$ is a rotation matrix.

Then, the Gyroscope G_ω is a 2D velocity field given by:

$$G_\omega = \omega W = \begin{bmatrix} 0 & -\omega \\ \omega & 0 \end{bmatrix} \quad (5.45)$$

On the other hand, with respect to the dissipative terms of the viscosity tensor, the operators \mathcal{G}_r and \mathcal{G}_r^* for 2D fluids are defined as:

$$\mathcal{G}_r(\cdot) = -\text{div} \left[W \frac{\cdot}{\rho} \right] = [-\partial_\xi \ \partial_\zeta] \frac{\cdot}{\rho} \quad (5.46)$$

$$\mathcal{G}_r^*(\cdot) = \frac{1}{\rho} W^\top \mathbf{grad} (\cdot) = \frac{1}{\rho} \begin{bmatrix} \partial_\xi \\ -\partial_\zeta \end{bmatrix} (\cdot) \quad (5.47)$$

Given the operator definitions (5.45)-(5.47), the port-Hamiltonian formulations (5.19) and (5.36) can be used to describe non-isentropic and isentropic 2D fluids, respectively.

Regarding the boundary conditions for non-isentropic fluids, notice that the tangential contributions in 2D problems are given by the vector \mathbf{s} orthogonal to \mathbf{n} . This implies that the boundary conditions (5.26) associated with the heat generation by viscous friction in $\partial\Omega$, can be expressed as:

$$-\int_{\partial\Omega} \mathbf{v} \cdot [\boldsymbol{\tau} \cdot \mathbf{n}] \partial\Omega = -\int_{\partial\Omega} \nu_{\mathbf{n}} \tau_{\mathbf{n}} + \nu_{\mathbf{s}} \tau_{\mathbf{s}} \partial\Omega \quad (5.48)$$

where $\nu_{\mathbf{n}} = \mathbf{v} \cdot \mathbf{n}$, $\nu_{\mathbf{s}} = \mathbf{v} \cdot \mathbf{s}$, $\tau_{\mathbf{n}} = \boldsymbol{\tau} : \mathbf{nn}$ and $\tau_{\mathbf{s}} = \boldsymbol{\tau} : \mathbf{sn}$ describe the normal and tangential velocity and viscous tensor contributions. The boundary port variables of the pseudo port-Hamiltonian formulation in Proposition 5.1 for a 2D fluid are given by:

$$\mathbf{f}_\partial = \begin{bmatrix} -(\rho \mathbf{v} \cdot \mathbf{n})|_{\partial\Omega} \\ -\nu_{\mathbf{n}}|_{\partial\Omega} \\ -\nu_{\mathbf{s}}|_{\partial\Omega} \\ -(\mathbf{f}_s \cdot \mathbf{n})|_{\partial\Omega} \end{bmatrix} \quad \mathbf{e}_\partial = \begin{bmatrix} \left(\frac{1}{2} \mathbf{v} \cdot \mathbf{v} + h\right)|_{\partial\Omega} \\ \tau_{\mathbf{n}}|_{\partial\Omega} \\ \tau_{\mathbf{s}}|_{\partial\Omega} \\ T|_{\partial\Omega} \end{bmatrix} \quad (5.49)$$

In the case of 1D fluids, all terms associated the vorticity vanish, and $\text{div} = \mathbf{grad} = \partial_\zeta$. Thus, in a 1D fluid domain $\Omega = \{\zeta \in [a, b] \subset \mathbb{R}\}$, the velocity field, viscous tensor and entropy flux are given by the scalar functions $v = v(\zeta)$, $\tau = -\hat{\mu} \partial_\zeta v(\zeta)$ and $\mathbf{f}_s = -\frac{k}{T(\zeta)} \partial_\zeta T(\zeta)$, respectively, where k is the scalar thermal conduction. Similarly, the outward unitary vector to the

boundaries is given by $\mathbf{n}|_a = -1$ and $\mathbf{n}|_b = 1$. With these considerations, the fluid formulations in Propositions 5.1 and 5.2 can be reduced to 1D models equivalent to port-Hamiltonian-based fluid formulations found in the literature, as shown in the following Remarks.

Remark 5.4. *Using the considerations for differential operator and fluid variables described above, the pseudo port-Hamiltonian formulation in Proposition 5.1 can be expressed as:*

$$\begin{bmatrix} \partial_t \rho \\ \partial_t v \\ \partial_t s \end{bmatrix} = \begin{bmatrix} 0 & -\partial_\zeta & 0 \\ -\partial_\zeta & 0 & \frac{1}{\rho} \partial_\zeta s - \frac{1}{\rho} \partial_\zeta \left(\frac{\tau}{\rho T} \cdot \right) \\ 0 & -\frac{1}{\rho} \partial_\zeta s - \frac{\tau}{\rho T} \partial_\zeta \left(\frac{1}{\rho} \cdot \right) & \frac{1}{\rho T} \|\partial_\zeta \dot{\cdot}\|_{k/T}^2 + \frac{1}{\rho} \partial_\zeta \left(\frac{k}{T} \partial_\zeta \left(\frac{\dot{\cdot}}{\rho} \right) \right) \end{bmatrix} \begin{bmatrix} \delta_\rho \mathcal{H} \\ \delta_v \mathcal{H} \\ \delta_s \mathcal{H} \end{bmatrix} \quad (5.50)$$

where $\mathcal{H} = \int_a^b \left(\frac{1}{2} \rho v^2 + \rho u(\rho, s) \right) d\zeta$ and the boundary port variables are given by the boundary flows and efforts, \mathbf{f}_∂ and \mathbf{e}_∂ respectively, defined as $\mathbf{f}_\partial = \left[-\rho v|_b \quad \rho v|_a \quad -v|_b \quad v|_a \quad -f_s|_b \quad f_s|_a \right]^\top$ and $\mathbf{e}_\partial = \left[\left(\frac{1}{2} v^2 + h \right)|_b \quad \left(\frac{1}{2} v^2 + h \right)|_a \quad \tau|_b \quad \tau|_a \quad T|_b \quad T|_a \right]^\top$, satisfying the balance $\dot{\mathcal{H}} = \mathbf{f}_\partial^\top \mathbf{e}_\partial$. This fluid model is equivalent to the formulation proposed in [65] for reactive fluids, neglecting the chemical reaction part.

Remark 5.5. *Using the 1D considerations previously described, the dissipative port-Hamiltonian formulation in Proposition 5.2 can be reduced to*

$$\begin{bmatrix} \partial_t \rho \\ \partial_t v \\ f_c \end{bmatrix} = \begin{bmatrix} 0 & -\partial_\zeta & 0 \\ -\partial_\zeta & 0 & -\frac{1}{\rho} \partial_\zeta \\ 0 & -\partial_\zeta \dot{\cdot} & 0 \end{bmatrix} \begin{bmatrix} \delta_\rho \mathcal{H} \\ \delta_v \mathcal{H} \\ e_c \end{bmatrix} \quad (5.51)$$

where $e_c = \hat{\mu} f_c$, the total energy is defined as $\mathcal{H} = \int_a^b \left(\frac{1}{2} \rho v^2 + \rho u(\rho) \right) d\zeta$ and the boundary port variables are given by the boundary flows $\mathbf{f}_\partial = \left[-\rho v|_b \quad \rho v|_a \right]^\top$ and the boundary efforts $\mathbf{e}_\partial = \left[\left(\frac{1}{2} v^2 + h + \frac{e_c}{\rho} \right)|_b \quad \left(\frac{1}{2} v^2 + h + \frac{e_c}{\rho} \right)|_a \right]^\top$, satisfying the balance $\dot{\mathcal{H}} = \mathbf{f}_\partial^\top \mathbf{e}_\partial$. This dissipative formulation is equivalent to the model used in [104] to describe compressible fluids in pipelines, without the gravitational effects. In this sense, notice that the dissipative term $-\frac{1}{\rho} \partial_\zeta e_c$ is equivalent to the term $-\frac{\lambda}{2D} |v|v$ used in [104], where λ is the friction coefficient, as shown in Section 3.1.2. Moreover, considering an inviscid fluid (i.e., $e_c = 0$) the model (5.51) corresponds to the fluid model used in [112] for control proposes.

5.4 ON THERMODYNAMICS AND AVAILABLE INTERNAL ENERGY OF COMPRESSIBLE FLUIDS

In previous sections the specific internal energy for non-isentropic and isentropic fluids is defined implicitly. In this section the thermodynamical properties of non-reactive compressible fluids are analyzed. We provide an explicit definition for the specific internal energy and we describe the utility of using available functions to characterize the variations of the total energy of the fluid.

5.4.1 Non-isentropic fluid

We consider the ideal gas law (4.3). Defining the constant $r = \bar{R}_u/\bar{M}$ where \bar{R}_u is the universal gas constant and \bar{M} the molar weight of the gas, the fluid pressure can then be described as:

$$p = rT\rho \quad (5.52)$$

where $r = c_p - c_v$, with c_p and c_v the specific heat capacity at constant pressure and constant volume, respectively. According to [120, 121] a good approximation of the specific internal energy is given by

$$u = c_v T = \frac{p}{(\gamma - 1)\rho} \quad (5.53)$$

where $\gamma = c_p/c_v$ is the specific heat ratio.

On the other hand, according to [114, p.295] for gases where the internal energy is proportional to the temperature, such as (5.53), the specific entropy is given by:

$$s = c_v \ln \left(\frac{p}{\rho^\gamma} \right) + \text{constant} \quad (5.54)$$

Then, the pressure can be expressed as:

$$p = A e^{s/c_v} \rho^\gamma \quad (5.55)$$

where A is a constant. Using this pressure relation, we obtain the following explicit definition for the temperature and the specific internal energy:

$$T(s, \rho) = \frac{A}{r} e^{s/c_v} \rho^{\gamma-1} \quad (5.56)$$

$$u(s, \rho) = \frac{A}{\gamma - 1} e^{s/c_v} \rho^{\gamma-1} = \frac{A}{\gamma - 1} e^{s/c_v} \left(\frac{1}{\rho} \right)^{-\gamma+1} \quad (5.57)$$

These definitions of pressure, temperature and specific internal energy, (5.55)-(5.57), satisfy the Gibbs equation (5.6), i.e.,:

$$\begin{aligned} du &= \left(\partial_{\frac{1}{\rho}} u \right) d\frac{1}{\rho} + (\partial_s u) ds = \left(-A e^{s/c_v} \rho^\gamma \right) d\frac{1}{\rho} + \left(\frac{A}{c_v (\gamma - 1)} \rho^{\gamma-1} \right) ds \\ &= -p d\frac{1}{\rho} + T ds \end{aligned}$$

Similarly, the following thermodynamic relationships are satisfied:

$$\partial_\rho u = A e^{s/c_v} \rho^{\gamma-2} = \frac{p}{\rho^2} \quad (5.58)$$

$$\partial_\rho(\rho u) = \frac{\gamma}{\gamma - 1} A e^{s/c_v} \rho^{\gamma-1} = c_p T = h \quad (5.59)$$

$$\partial_s(\rho u) = \frac{A}{c_v(\gamma - 1)} e^{s/c_v} \rho^\gamma = \rho T \quad (5.60)$$

Hence, (5.57) is an adequate formulation for the specific internal energy used in (5.19) for non-isentropic compressible fluids.

5.4.2 Isentropic fluid

Now we consider a fluid under a isentropic assumption, i.e., $s = s_0$ is constant. In this case, the fluid pressure is defined as[114]:

$$p = \bar{A}\rho^\gamma \quad (5.61)$$

where $\bar{A} = Ae^{s_0/c_v}$ is a constant. Then, the temperature and the specific internal energy depend only on the fluid density, i.e.,

$$T(\rho) = \frac{\bar{A}}{r}\rho^{\gamma-1} \quad (5.62)$$

$$u(\rho) = \frac{\bar{A}}{\gamma-1}\rho^{\gamma-1} = \frac{\bar{A}}{\gamma-1}\left(\frac{1}{\rho}\right)^{-\gamma+1} \quad (5.63)$$

Note that (5.63) satisfies the Gibbs equation (5.29), i.e.,

$$\begin{aligned} du &= \left(\partial_{\frac{1}{\rho}}u\right) d\frac{1}{\rho} = \left(-\bar{A}\rho^\gamma\right) d\frac{1}{\rho} \\ &= -pd\frac{1}{\rho} \end{aligned}$$

Another important thermodynamic relationship is given in terms of the speed of sound c and the isentropic compressibility $(\partial_\rho p)_s$, i.e.,

$$c^2 = (\partial_\rho p)_s = \gamma\bar{A}\rho^{\gamma-1} = (\gamma-1)c_p T = \gamma\frac{p}{\rho} \quad (5.64)$$

Then, the pressure, temperature and internal energy can be expressed as follows:

$$p = \frac{c^2}{\gamma}\rho, \quad T = \frac{c^2}{c_p(\gamma-1)} \quad \text{and} \quad u = \frac{c^2}{\gamma(\gamma-1)}, \quad (5.65)$$

where u satisfies the relationships $\partial_\rho(\rho u) = h = \frac{\gamma}{\gamma-1}\bar{A}\rho^{\gamma-1} = \frac{c^2}{\gamma-1}$ and $\partial_\rho u = \bar{A}\rho^{\gamma-2} = \frac{c^2}{\gamma\rho} = \frac{p}{\rho^2}$. Thus, the definition (5.63) for the specific internal energy can be used in the dissipative port-Hamiltonian model for isentropic fluids (5.36).

5.4.3 Considerations for small temperature variations.

In this section we consider small variations of the temperature in an isentropic fluid domain. The pressure can be approximated using the speed of sound at a reference temperature, as shown next.

Proposition 5.3. *Consider that the fluid temperature is bounded, i.e., $T \in [T_1, T_2]$, and define $\xi = \overline{\Delta T}/T_1$ as the maximum relative variation of temperature in the fluid domain, where $\overline{\Delta T} = T_2 - T_1$. Denoting by c_*^2 the square of the speed of sound at reference temperature $T^* \in [T_1, T_2]$, the pressure of the fluid can be approximated by:*

$$p^* = \frac{c_*^2}{\gamma}\rho \quad (5.66)$$

with relative error $\varepsilon_p \leq \xi$.

Proof. Define the temperature $T = T^* + \Delta T$ where T^* is the reference temperature and the speed of sound $c_* = \sqrt{(\gamma - 1)c_p T^*}$ at the reference temperature T^* . Then, from (5.64) we obtain:

$$c^2 = (\gamma - 1)c_p (T^* + \Delta T) = c_*^2 + (\gamma - 1)c_p \Delta T$$

The relative error of the pressure is given by:

$$\varepsilon_p = \frac{|p - p^*|}{p} = \frac{|c^2 - c_*^2|}{c^2} = \frac{\Delta T}{T}$$

Considering that $\Delta T \leq \overline{\Delta T}$ and $T \geq T_1$ we obtain that $\varepsilon_p \leq \frac{\overline{\Delta T}}{T_1} = \xi$. \square

The pressure approximation described in the previous proposition is suitable for applications with small variations of the temperature, such as for example, the air exhalation in the human phono-respiratory system, where the temperature varies from $310.15^\circ K (37^\circ C)$ in the lungs to $305.15^\circ K (32^\circ C)$ in the vocal tract, leading to a maximum relative variation of $\xi = 0.016$.

To use the pressure definition (5.66) in the fluid model (5.36), it is necessary to redefine the specific internal energy and enthalpy formulas. Using the Gibbs equation (5.29), we obtain:

$$u^* = \frac{c_*^2}{\gamma} \ln(\rho) + C_u \quad (5.67)$$

$$h^* = \frac{c_*^2}{\gamma} (\ln(\rho) + 1) + C_u \quad (5.68)$$

where C_u is a constant, and the following relationships are satisfied $\partial_\rho u^* = \frac{p^*}{\rho^2}$ and $\partial_\rho(\rho u^*) = h^*$.

According to (5.30), the fluid dynamics is affected by the use of **grad** h^* in the momentum balance (see Chapter 4). The error in the fluid dynamics is given by

$$\varepsilon_h = \left| \frac{\mathbf{grad} h - \mathbf{grad} h^*}{\mathbf{grad} h} \right| \quad (5.69)$$

where $\left| \frac{\mathbf{grad} h - \mathbf{grad} h^*}{\mathbf{grad} h} \right| := \begin{bmatrix} \left| \frac{\partial_\zeta h - \partial_\zeta h^*}{\partial_\zeta h} \right| \\ \left| \frac{\partial_\xi h - \partial_\xi h^*}{\partial_\xi h} \right| \\ \left| \frac{\partial_\delta h - \partial_\delta h^*}{\partial_\delta h} \right| \end{bmatrix}$.

Then, using the specific enthalpy defined in Section 5.4.2 and (5.68), and considering that $\gamma \geq 1$, the error ε_h can be expressed as:

$$\varepsilon_h = \left| \frac{\frac{c^2}{\rho} \mathbf{grad} \rho - \frac{c_*^2}{\gamma \rho} \mathbf{grad} \rho}{\frac{c^2}{\rho} \mathbf{grad} \rho} \right| = \left| \frac{c_*^2}{\gamma} - c^2 \right| \mathbf{I} \leq \left| \frac{c_*^2 - c^2}{c^2} \right| \mathbf{I} \leq \xi \mathbf{I} \quad (5.70)$$

This implies that the approximation error in the dynamics is bounded by ξ .

5.4.4 Available specific internal energy

An advantage of the port-Hamiltonian framework is the use of the total energy as a Lyapunov function to evaluate the system's stability [42, 44]. A desirable feature of the total energy is that $\mathcal{H}(\mathbf{x}_0) = 0$ and $\mathcal{H}(\mathbf{x}) > 0, \forall \mathbf{x} \neq \mathbf{x}_0$ where \mathbf{x}_0 is a dynamic equilibrium point of the system.

As shown in previous sections the total energy of compressible fluids is given by:

$$\mathcal{H} = \int_{\Omega} \frac{1}{2} \rho \mathbf{v} \cdot \mathbf{v} + \rho u(\mathbf{x}) d\Omega \quad (5.71)$$

where $u(\mathbf{x})$ describes the specific internal energy of the fluid. In the non-isentropic compressible fluid model (5.19) with state variables ρ , \mathbf{v} and s , given the specific internal energy (5.57) the total energy $\mathcal{H}(\rho, \mathbf{v}, s)$ is non-negative and it has a minimum $\mathcal{H}(0, \mathbf{v}, s) = 0$ for any $\{\mathbf{v}, s\}$ and $\mathcal{H}(\rho, \mathbf{0}, -\infty) = 0$ for any ρ . This implies that $\mathcal{H}(\rho, \mathbf{v}, s)$ has an infinite number of minimum points, making it difficult to analyze the stability of the system using this function. Another problem is given by the fact that the pair $\rho = 0$ and $s = -\infty$ does not define a practical dynamic equilibrium point for the fluid. Similarly, for isentropic compressible fluids with specific internal energy (5.63), the total energy $\mathcal{H}(\rho, \mathbf{v})$ is non-negative and has a minimum $\mathcal{H}(0, \mathbf{v}) = 0$ for any \mathbf{v} , i.e., as in the non-isentropic case, the total energy $\mathcal{H}(\rho, \mathbf{v})$ has an infinite number of unpractical minima.

To address these problems, as shown in Chapter 4, it is convenient to define the total energy using an availability function, $\bar{u}(\mathbf{x})$, that describes the changes of specific internal energy with respect to a reference point \mathbf{x}_0 . The framework of the thermodynamic availability function, formalized for the control of thermodynamic systems in [122] and with roots in [123] and [124], has been used to derive Lyapunov conditions for the stability analysis of irreversible thermodynamic systems by many authors [125, 126, 127, 128, 129] just to cite a few. This available specific internal energy can be defined as:

$$\bar{u}(\mathbf{x}) = u(\mathbf{x}) - u(\mathbf{x}_0) + f_u(\mathbf{x}) \quad (5.72)$$

where $f_u(\mathbf{x})$ is a function used to guarantee the non-negativity of \bar{u} such that $f_u(\mathbf{x}_0) = 0$. Then, the fluid total energy can be described as:

$$\bar{\mathcal{H}}(\mathbf{x}) = \int_{\Omega} \frac{1}{2} \rho \mathbf{v} \cdot \mathbf{v} + \rho \bar{u}(\mathbf{x}) d\Omega \quad (5.73)$$

One can notice that this total energy definition is a non-negative function, $\bar{\mathcal{H}}(\mathbf{x}) \geq 0$ with minimum $\bar{\mathcal{H}}(\mathbf{x}_0) = 0$.

Now denote by p_0 and h_0 the pressure and the specific enthalpy at $\mathbf{x} = \mathbf{x}_0$, respectively, such that $\mathbf{grad} p_0 = 0$ and $\mathbf{grad} h_0 = 0$. Then, the terms $\mathbf{grad} p$ and $\mathbf{grad} h$ in (5.30) and (5.33) of isentropic compressible fluids, can be rewritten as $\mathbf{grad} p = \mathbf{grad} \hat{p}$ and $\mathbf{grad} h = \mathbf{grad} \hat{h}$, respectively, where $\hat{p} = p - p_0$ and $\hat{h} = h - h_0$. This implies that to use the total energy (5.73) in a port-Hamiltonian formulation of isentropic compressible fluids, the available specific internal energy (5.72) must satisfy the following relationship:

$$d\bar{u} = -\hat{p} d\frac{1}{\rho} \quad (5.74)$$

Solving (5.74) we obtain that

$$f_u(\mathbf{x}) = p_0 \left(\frac{1}{\rho} - \frac{1}{\rho_0} \right) \quad (5.75)$$

and the available specific internal energy for isentropic compressible fluids is given by:

$$\bar{u}(\rho) = \frac{\bar{A}}{\gamma - 1} \rho^{\gamma-1} - \frac{\bar{A}}{\gamma - 1} \rho_0^{\gamma-1} + p_0 \left(\frac{1}{\rho} - \frac{1}{\rho_0} \right) \quad (5.76)$$

In this case, the total energy $\bar{\mathcal{H}}(\rho, \mathbf{v})$ has a minimum $\bar{\mathcal{H}}(\rho_0, \mathbf{0}) = 0$ where ρ_0 is the reference density and the efforts associated with the total energy (5.73) are given by:

$$\begin{bmatrix} \delta_\rho \bar{\mathcal{H}} \\ \delta_{\mathbf{v}} \bar{\mathcal{H}} \end{bmatrix} = \begin{bmatrix} \frac{1}{2} \mathbf{v} \cdot \mathbf{v} + \partial_\rho (\rho \bar{u}) \\ \rho \mathbf{v} \end{bmatrix} \quad (5.77)$$

Notice that $\mathbf{grad} \hat{h} = \mathbf{grad} \hat{h} = \mathbf{grad} \partial_\rho (\rho \bar{u})$. Then, (5.30) can be expressed as the dissipative port-Hamiltonian system proposed in (5.36) where the total energy, internal energy and fluid efforts are given by (5.73), (5.76) and (5.77), establishing stability and passivity properties of the system with respect to the dynamic equilibrium point.

This procedure can also be applied in the case of small temperature variations (see Section (5.4.3)), where the available internal energy and fluid efforts can be expressed as:

$$\bar{u}^*(\rho) = \frac{c_*^2}{\gamma} \ln \left(\frac{\rho}{\rho_0} \right) + p_0 \left(\frac{1}{\rho} - \frac{1}{\rho_0} \right), \text{ and } \begin{bmatrix} \delta_\rho \bar{\mathcal{H}} \\ \delta_{\mathbf{v}} \bar{\mathcal{H}} \end{bmatrix} = \begin{bmatrix} \frac{1}{2} \mathbf{v} \cdot \mathbf{v} + \partial_\rho (\rho \bar{u}^*) \\ \rho \mathbf{v} \end{bmatrix} \quad (5.78)$$

respectively, satisfying the relationship $\mathbf{grad} \hat{h}^* = \mathbf{grad} \hat{h}^* = \mathbf{grad} \partial_\rho (\rho \bar{u}^*)$, as shown in Chapter 4.

On the other hand, for non-isentropic fluids, such as those studied in Section 5.1, the available specific internal energy must satisfy the relationship

$$d\bar{u} = -\hat{p} d\frac{1}{\rho} + \hat{T} ds \quad (5.79)$$

where $\hat{T} = T - T_0$ and T_0 is the temperature at the reference density ρ_0 and reference entropy s_0 . From the solution of (5.79), functions f_u and \bar{u} are defined as

$$f_u = p_0 \left(\frac{1}{\rho} - \frac{1}{\rho_0} \right) - T_0 (s - s_0) \quad (5.80)$$

$$\bar{u}(\rho, s) = \frac{A}{\gamma - 1} e^{s/c_v} \rho^{\gamma-1} - \frac{A}{\gamma - 1} e^{s_0/c_v} \rho_0^{\gamma-1} + p_0 \left(\frac{1}{\rho} - \frac{1}{\rho_0} \right) - T_0 (s - s_0) \quad (5.81)$$

satisfying $\frac{1}{\rho} \mathbf{grad} p = \frac{1}{\rho} \mathbf{grad} \hat{p} = \mathbf{grad} \partial_\rho (\rho \bar{u}) - \hat{T} \mathbf{grad} s$. Then, using (5.81), the total energy $\bar{\mathcal{H}}(\rho, \mathbf{v}, s)$ for non-isentropic fluids, has a minimum $\bar{\mathcal{H}}(\rho_0, \mathbf{0}, s_0) = 0$ and the efforts are given by:

$$\begin{bmatrix} \delta_\rho \bar{\mathcal{H}} \\ \delta_{\mathbf{v}} \bar{\mathcal{H}} \\ \delta_s \bar{\mathcal{H}} \end{bmatrix} = \begin{bmatrix} \frac{1}{2} \mathbf{v} \cdot \mathbf{v} + \partial_\rho (\rho \bar{u}) \\ \rho \mathbf{v} \\ \rho \hat{T} \end{bmatrix} \quad (5.82)$$

However, given that the operator \mathcal{D}_τ , of Lemma 5.2, is a function of the effort ρT , we obtain that $\mathcal{D}_\tau \delta_s \mathcal{H} \neq \mathcal{D}_\tau \delta_s \bar{\mathcal{H}}$. This makes it difficult to use the energy (5.73) and efforts (5.82) in the energy-based model described in Proposition 5.1. An alternative model formulation is hence necessary to use the available specific internal energy to describe the dynamics of non-isentropic compressible fluids.

An alternative approach to describe irreversible process, such as the non-isentropic fluids, is given by the irreversible port-Hamiltonian framework.

5.5 IRREVERSIBLE PORT-HAMILTONIAN FORMULATION OF 1D COMPRESSIBLE FLUIDS

As already discussed in Section 1.2.3, the irreversible port-Hamiltonian framework is an approach focused on the description of the thermal domain, where the first and second laws of Thermodynamic are included. This approach was initially proposed in [67, 68] for finite-dimensional systems and extended to infinite-dimensional domains in [70, 71]. The dynamics of an irreversible system on a 1D domain, $\Omega := \{\zeta \in [a, b] \subset \mathbb{R}\}$, are given by:

$$\partial_t \mathbf{x} = \sum_{j=1}^n R_{1j} \mathcal{J}_{1j} \delta_{\mathbf{x}} \mathcal{H} + R_{0j} \mathcal{J}_{0j} \delta_{\mathbf{x}} \mathcal{H} + \partial_\zeta [\mathbf{R}_1 \delta_s \mathcal{H}], \zeta \in [a, b]$$

where $\mathcal{J}_{ij}, i \in \{1, 2\}$ is an operator of the form $\mathcal{J}_{ij} = P_{ij} \partial_\zeta^i$ with $P_{ij} = (-1)^{i+1} P_{ij}^\top$. The terms $R_{ij}, i \in \{1, 2\}$ are defined as $\gamma_{ij} \{\mathcal{S}, \mathcal{H}\}_{\mathcal{J}_{ij}}^*$ where $\gamma_{ij} > 0$ and $\{\mathcal{S}, \mathcal{H}\}_{\mathcal{J}_{ij}}^*$ denotes a locally defined operators, defined in (1.31), between the total entropy \mathcal{S} and the total energy \mathcal{H} of the system. The vector $\mathbf{R}_1 = [R_{11}, \dots, R_{1n}]^\top$ satisfies the relationship $\sum_{j=1}^n R_{1j} \mathcal{J}_{1j} \delta_{\mathbf{x}} \mathcal{H} = [\mathbf{0} \quad \mathbf{R}_1^\top \partial_\zeta \delta_{\mathbf{x}} \mathcal{H}]^\top$ (see Section 1.2.3 for details).

In the following, we use this approach to develop an irreversible port-Hamiltonian formulation for non-reactive compressible fluids in a 1D domain.

5.5.1 Governing equations of non-reactive thermodynamic compressible fluid

We consider a 1D non-isentropic compressible fluid given by

$$\partial_t \rho = -\partial_\zeta \rho v \tag{5.83a}$$

$$\partial_t v = -\partial_\zeta \left(\frac{1}{2} v^2 \right) - \frac{1}{\rho} \partial_\zeta p - \frac{1}{\rho} \partial_\zeta \tau \tag{5.83b}$$

$$\partial_t u = -v \partial_\zeta u - \frac{1}{\rho} \partial_\zeta f_T - \frac{p}{\rho} \partial_\zeta v - \frac{\tau}{\rho} \partial_\zeta v \tag{5.83c}$$

where ρ denotes the density per unit length, $\tau = -\mu \partial_\zeta v$ is the shear stress of the fluid and $f_T = -k \partial_\zeta T$ is the heat flux, with μ and k the fluid viscosity and thermal conductivity, respectively.

In a 1D domain the material derivative is defined as $D_t = \partial_t + v\partial_\zeta$. Then, using the local equilibrium (5.7) and the Gibbs equation (5.6), as shown in Section 5.1.1, the governing equations can be expressed as:

$$\partial_t \rho = -\partial_\zeta \rho v \quad (5.84a)$$

$$\partial_t v = -\partial_\zeta \left(\frac{1}{2} v^2 \right) - \partial_\zeta \left(u + \frac{p}{\rho} \right) + T \partial_\zeta s - \frac{1}{\rho} \partial_\zeta \tau \quad (5.84b)$$

$$\partial_t s = -v \partial_\zeta s - \frac{1}{\rho T} \partial_\zeta f_T - \frac{\tau}{\rho T} \partial_\zeta v \quad (5.84c)$$

where u and p are given by (5.57) and (5.55), respectively.

Then, defining the total energy of the fluid as:

$$\mathcal{H} = \int_a^b \frac{1}{2} \rho v^2 + \rho u(\rho, s) d\zeta \quad (5.85)$$

where $\begin{bmatrix} \delta_\rho \mathcal{H} \\ \delta_v \mathcal{H} \\ \delta_s \mathcal{H} \end{bmatrix} = \begin{bmatrix} \frac{1}{2} v^2 + u + p/\rho \\ \rho v \\ \rho T \end{bmatrix}$, the fluid dynamics are given by:

$$\begin{bmatrix} \partial_t \rho \\ \partial_t v \\ \partial_t s \end{bmatrix} = \begin{bmatrix} 0 & -\partial_\zeta & 0 \\ -\partial_\zeta & 0 & \frac{1}{\rho} \partial_\zeta s - \frac{1}{\rho} \partial_\zeta \left(\frac{\tau}{\rho T} \cdot \right) \\ 0 & -\frac{1}{\rho} \partial_\zeta s - \frac{\tau}{\rho T} \partial_\zeta \left(\frac{1}{\rho} \cdot \right) & \frac{1}{\rho T} \partial_\zeta \left(\kappa \partial_\zeta \left(\frac{1}{\rho} \cdot \right) \right) \end{bmatrix} \begin{bmatrix} \delta_\rho \mathcal{H} \\ \delta_v \mathcal{H} \\ \delta_s \mathcal{H} \end{bmatrix} \quad (5.86)$$

5.5.2 Irreversible port-Hamiltonian formulation

To obtain the irreversible port-Hamiltonian formulation of the system (5.86), it is necessary to identify the reversible and irreversible parts, \mathcal{W}_r and \mathcal{W}_i , respectively, of the system dynamics, such that $\partial_t \mathbf{x} = \mathcal{W}_r + \mathcal{W}_i$. In this particular case, the fluid governing equations (5.86) can be expressed as:

$$\begin{bmatrix} \partial_t \rho \\ \partial_t v \\ \partial_t s \end{bmatrix} = \underbrace{\begin{bmatrix} 0 & -\partial_\zeta & 0 \\ -\partial_\zeta & 0 & \frac{1}{\rho} \partial_\zeta s \\ 0 & -\frac{1}{\rho} \partial_\zeta s & 0 \end{bmatrix}}_{\text{reversible part } \mathcal{W}_r} \begin{bmatrix} \delta_\rho \mathcal{H} \\ \delta_v \mathcal{H} \\ \delta_s \mathcal{H} \end{bmatrix} + \underbrace{\begin{bmatrix} 0 & 0 & 0 \\ 0 & 0 & -\frac{1}{\rho} \partial_\zeta \left(\frac{\tau}{\rho T} \cdot \right) \\ 0 & -\frac{\tau}{\rho T} \partial_\zeta \left(\frac{1}{\rho} \cdot \right) & \frac{1}{\rho T} \partial_\zeta \left(\kappa \partial_\zeta \left(\frac{1}{\rho} \cdot \right) \right) \end{bmatrix}}_{\text{irreversible part } \mathcal{W}_i} \begin{bmatrix} \delta_\rho \mathcal{H} \\ \delta_v \mathcal{H} \\ \delta_s \mathcal{H} \end{bmatrix}$$

Notice that the reversible part can be described by an operator having the form (1.15), i.e.,

$$\mathcal{W}_r = \mathcal{J}(\mathbf{x}) \delta_{\mathbf{x}} \mathcal{H} \quad (5.87)$$

where $\mathbf{x} = [\rho \ v \ s]^\top$ is the state vector of the fluid dynamics and the operator $\mathcal{J}(\mathbf{x})$ is given by

$$\mathcal{J}(\mathbf{x}) = P_1 \partial_\zeta + P_0(\mathbf{x}) \quad (5.88)$$

with

$$P_1 = \begin{bmatrix} 0 & -1 & 0 \\ -1 & 0 & 0 \\ 0 & 0 & 0 \end{bmatrix} \quad \text{and} \quad P_0(\mathbf{x}) = \begin{bmatrix} 0 & 0 & 0 \\ 0 & 0 & \frac{1}{\rho} \partial_\zeta s \\ 0 & -\frac{1}{\rho} \partial_\zeta s & 0 \end{bmatrix}$$

Regarding the irreversible part \mathcal{W}_i , it is necessary to introduce the definition of modulated skew-symmetric operator, as follows.

Definition 5.2. Let \mathcal{J} be a skew-symmetric operator that satisfies the Jacobi identity. Then, a modulated operator $\tilde{\mathcal{J}}$ is defined as the formal skew-symmetric operator of the form:

$$\tilde{\mathcal{J}}\mathbf{e} = M^\top(\mathbf{x})\mathcal{J}[M(\mathbf{x})\mathbf{e}] \quad (5.89)$$

where $M(\mathbf{x})$ depends on the state variables.

Notice that \mathcal{W}_i can be expressed as:

$$\mathcal{W}_i = \begin{bmatrix} 0 \\ -\frac{1}{\rho}\partial_\zeta\tau \\ \sigma_T + \sigma_\tau - \frac{1}{\rho}\partial_\zeta f_s \end{bmatrix} \quad (5.90)$$

where $\sigma_\tau = -\frac{\tau}{\rho T}\partial_\zeta\left(\frac{1}{\rho}\delta_v\mathcal{H}\right) = \frac{\mu}{\rho T}(\partial_\zeta v)^2$ and $\sigma_T = -\frac{t_s}{\rho T}\partial_\zeta\left(\frac{1}{\rho}\delta_s\mathcal{H}\right) = \frac{k}{\rho T^2}(\partial_\zeta T)^2$ are the entropy creation due to viscous friction and heat conduction, respectively. Similarly, $-\frac{1}{\rho}\partial_\zeta\tau$ and $-\frac{1}{\rho}\partial_\zeta f_s$ describe diffusion phenomena in the velocity and entropy variables, and $f_s = -\frac{k}{T}\partial_\zeta T$ denotes the specific entropy flux. Defining the entropy creation terms as $\sigma_\tau = \frac{1}{\rho}R_{1\tau}\partial_\zeta v$ and $\sigma_T = \frac{1}{\rho}R_{1T}\partial_\zeta T$, the following relationships are obtained:

$$R_{1\tau} = \frac{\mu}{T}\partial_\zeta v = -\frac{\tau}{T} \quad \text{and} \quad R_{1T} = \frac{k}{T^2}\partial_\zeta T = -\frac{f_s}{T} \quad (5.91)$$

Then, using (5.91), the irreversible part of the governing equations can be rewritten as:

$$\begin{aligned} \mathcal{W}_i = & R_{1\tau} \underbrace{\begin{bmatrix} 0 & 0 & 0 \\ 0 & \frac{1}{\rho} & 0 \\ 0 & 0 & \frac{1}{\rho} \end{bmatrix} \begin{bmatrix} 0 & 0 & 0 \\ 0 & 0 & 1 \\ 0 & 1 & 0 \end{bmatrix} \partial_\zeta \left(\begin{bmatrix} 0 & 0 & 0 \\ 0 & \frac{1}{\rho} & 0 \\ 0 & 0 & \frac{1}{\rho} \end{bmatrix} \begin{bmatrix} \delta_\rho \mathcal{H} \\ \delta_v \mathcal{H} \\ \delta_s \mathcal{H} \end{bmatrix} \right)}_{\tilde{\mathcal{J}}_{1\tau}\delta_{\mathbf{x}}\mathcal{H}} \\ & + R_{1T} \underbrace{\begin{bmatrix} 0 & 0 & 0 \\ 0 & \frac{1}{\rho} & 0 \\ 0 & 0 & \frac{1}{\rho} \end{bmatrix} \begin{bmatrix} 0 & 0 & 0 \\ 0 & -\frac{\mu T}{k} & 0 \\ 0 & 0 & 1 \end{bmatrix} \partial_\zeta \left(\begin{bmatrix} 0 & 0 & 0 \\ 0 & \frac{1}{\rho} & 0 \\ 0 & 0 & \frac{1}{\rho} \end{bmatrix} \begin{bmatrix} \delta_\rho \mathcal{H} \\ \delta_v \mathcal{H} \\ \delta_s \mathcal{H} \end{bmatrix} \right)}_{\tilde{\mathcal{J}}_{1T}\delta_{\mathbf{x}}\mathcal{H}} - \frac{1}{\rho}\partial_\zeta \begin{bmatrix} 0 \\ \tau \\ f_s \end{bmatrix} \end{aligned} \quad (5.92)$$

with modulated operators

$$\tilde{\mathcal{J}}_{1\tau}\mathbf{e} = M^\top(\mathbf{x})P_{1\tau}\partial_\zeta[M(\mathbf{x})\mathbf{e}] \quad (5.93)$$

$$\tilde{\mathcal{J}}_{1T}\mathbf{e} = M^\top(\mathbf{x})P_{1T}\partial_\zeta[M(\mathbf{x})\mathbf{e}] \quad (5.94)$$

with

$$M(\mathbf{x}) = \begin{bmatrix} 0 & 0 & 0 \\ 0 & \frac{1}{\rho} & 0 \\ 0 & 0 & \frac{1}{\rho} \end{bmatrix}, \quad P_{1\tau} = \begin{bmatrix} 0 & 0 & 0 \\ 0 & 0 & 1 \\ 0 & 1 & 0 \end{bmatrix}, \quad \text{and} \quad P_{1T} = \begin{bmatrix} 0 & 0 & 0 \\ 0 & -\frac{\mu T}{k} & 0 \\ 0 & 0 & 1 \end{bmatrix}$$

Reformulating $R_{1\tau}$ and R_{1T} according to Definition 1.6, i.e., $R_{1\tau} = \gamma_{1\tau}\{\mathcal{S}, \mathcal{H}\}_{\tilde{\mathcal{J}}_{1\tau}}^*$ and $R_{1T} = \gamma_{1T}\{\mathcal{S}, \mathcal{H}\}_{\tilde{\mathcal{J}}_{1T}}^*$, where $\{\mathcal{S}, \mathcal{H}\}_{\tilde{\mathcal{J}}_{1\tau}}^*$ and $\{\mathcal{S}, \mathcal{H}\}_{\tilde{\mathcal{J}}_{1T}}^*$ are locally defined operators of the form (1.31), and the total entropy \mathcal{S} is defined as:

$$\mathcal{S} = \int_a^b \rho s d\zeta \quad (5.95)$$

we obtain that $\{\mathcal{S}, \mathcal{H}\}_{\tilde{\mathcal{J}}_{1\tau}}^* = \partial_\zeta v$, $\{\mathcal{S}, \mathcal{H}\}_{\tilde{\mathcal{J}}_{1T}}^* = \partial_\zeta T$, $\gamma_{1\tau} = \frac{\mu}{T} > 0$ and $\gamma_{1T} = \frac{\hbar}{T^2} > 0$. Then, the irreversible part of the fluid dynamics can be expressed as:

$$\mathcal{W}_i = R_{1\tau} \tilde{\mathcal{J}}_{1\tau} \delta_{\mathbf{x}} \mathcal{H} + R_{1T} \tilde{\mathcal{J}}_{1T} \delta_{\mathbf{x}} \mathcal{H} + M^\top(\mathbf{x}) \partial_\zeta \left(M(\mathbf{x}) \begin{bmatrix} 0 \\ \mathbf{R}_1 \end{bmatrix} \delta_s \mathcal{H} \right) \quad (5.96)$$

where $\mathbf{R}_1 = [R_{1\tau} \ R_{1T}]^\top$ and satisfies

$$R_{1\tau} \tilde{\mathcal{J}}_{1\tau} \delta_{\mathbf{x}} \mathcal{H} + R_{1T} \tilde{\mathcal{J}}_{1T} \delta_{\mathbf{x}} \mathcal{H} = \begin{bmatrix} 0_{2 \times 1} \\ [0 \ \mathbf{R}_1^\top] M^\top(\mathbf{x}) \partial_\zeta (M(\mathbf{x}) \delta_{\mathbf{x}} \mathcal{H}) \end{bmatrix}$$

Proposition 5.4. *Let \mathcal{H} be the total energy defined in (5.85). Using the skew-symmetric operators \mathcal{J} , $\tilde{\mathcal{J}}_{1\tau}$ and $\tilde{\mathcal{J}}_{1T}$, defined in (5.88), (5.93) and (5.94) respectively, the governing equations (5.84) of a non-reactive compressible fluid can be expressed as the following irreversible port-Hamiltonian system*

$$\partial_t \mathbf{x} = \mathcal{J} \delta_{\mathbf{x}} \mathcal{H} + R_{1\tau} \tilde{\mathcal{J}}_{1\tau} \delta_{\mathbf{x}} \mathcal{H} + R_{1T} \tilde{\mathcal{J}}_{1T} \delta_{\mathbf{x}} \mathcal{H} + M^\top(\mathbf{x}) \partial_\zeta \left(M(\mathbf{x}) \begin{bmatrix} 0 \\ \mathbf{R}_1 \end{bmatrix} \delta_s \mathcal{H} \right) \quad (5.97)$$

with boundary inputs and outputs given by

$$\mathbf{u}(t) = \begin{bmatrix} \left(\frac{1}{2} v^2 + \hbar \right) (b) \\ -\tau(b) \\ -f_s(b) \\ \left(\frac{1}{2} v^2 + \hbar \right) (a) \\ -\tau(a) \\ -f_s(a) \end{bmatrix} \quad \text{and} \quad \mathbf{y}(t) = \begin{bmatrix} -(\rho v) (b) \\ v(b) \\ T(b) \\ (\rho v) (a) \\ -v(a) \\ -T(a) \end{bmatrix} \quad (5.98)$$

where $\mathbf{x} = [\rho \ v \ s]^\top$, $\mathcal{J} \delta_{\mathbf{x}} \mathcal{H}$ describes the reversible part of the fluid dynamics and $R_{1\tau} \tilde{\mathcal{J}}_{1\tau} \delta_{\mathbf{x}} \mathcal{H} + R_{1T} \tilde{\mathcal{J}}_{1T} \delta_{\mathbf{x}} \mathcal{H} + M^\top(\mathbf{x}) \partial_\zeta \left(M(\mathbf{x}) \begin{bmatrix} 0 \\ \mathbf{R}_1 \end{bmatrix} \delta_s \mathcal{H} \right)$ describes irreversible part, satisfying the balances

$$\dot{\mathcal{H}} = \mathbf{u}^\top \mathbf{y} \quad (5.99)$$

$$\dot{\mathcal{S}} = \int_a^b \sigma_s d\zeta - (s\rho v + f_s)|_a^b \quad (5.100)$$

where $\sigma_s = \gamma_{1\tau} \left(\{\mathcal{S}, \mathcal{H}\}_{\tilde{\mathcal{J}}_{1\tau}}^* \right)^2 + \gamma_{1T} \left(\{\mathcal{S}, \mathcal{H}\}_{\tilde{\mathcal{J}}_{1T}}^* \right)^2 \geq 0$.

Proof. Using (5.87) and (5.96) the PDE (5.97) is obtained. On the other hand, the energy balance is given by $\dot{\mathcal{H}} = \int_a^b \delta_{\mathbf{x}} \mathcal{H}^\top \partial_t \mathbf{x} d\zeta$. Then, using (5.97) the energy balance can be expressed as:

$$\begin{aligned} \dot{\mathcal{H}} &= \int_a^b (\delta_{\mathbf{x}} \mathcal{H})^\top \mathcal{J} \delta_{\mathbf{x}} \mathcal{H} d\zeta + \int_a^b (\delta_{\mathbf{x}} \mathcal{H})^\top \left[R_{1\tau} \tilde{\mathcal{J}}_{1\tau} \delta_{\mathbf{x}} \mathcal{H} + R_{1T} \tilde{\mathcal{J}}_{1T} \delta_{\mathbf{x}} \mathcal{H} \right] d\zeta \\ &\quad + \int_a^b (\delta_{\mathbf{x}} \mathcal{H})^\top \left[M^\top(\mathbf{x}) \partial_\zeta \left(M(\mathbf{x}) \begin{bmatrix} 0 \\ \mathbf{R}_1 \end{bmatrix} \delta_s \mathcal{H} \right) \right] d\zeta \end{aligned}$$

From the definition of \mathcal{J} in (5.88), $\int_a^b (\delta_{\mathbf{x}}\mathcal{H})^\top \mathcal{J} \delta_{\mathbf{x}}\mathcal{H} d\zeta = \int_a^b (\delta_{\mathbf{x}}\mathcal{H})^\top P_1 \partial_\zeta \delta_{\mathbf{x}}\mathcal{H} d\zeta$ where $P_1 = \begin{bmatrix} 0 & -1 & 0 \\ -1 & 0 & 0 \\ 0 & 0 & 0 \end{bmatrix}$. Similarly, the irreversible part of the fluid dynamic satisfies the relationship:

$$R_{1\tau} \tilde{\mathcal{J}}_{1\tau} \delta_{\mathbf{x}}\mathcal{H} + R_{1T} \tilde{\mathcal{J}}_{1T} \delta_{\mathbf{x}}\mathcal{H} = \begin{bmatrix} 0 \\ 0 \\ [0 \ \mathbf{R}_1^\top] M^\top(\mathbf{x}) \partial_\zeta [M(\mathbf{x}) \delta_{\mathbf{x}}\mathcal{H}] \end{bmatrix}$$

Then, the energy balance can be rewritten as:

$$\begin{aligned} \dot{\mathcal{H}} &= \int_a^b (\delta_{\mathbf{x}}\mathcal{H})^\top P_1 \partial_\zeta \delta_{\mathbf{x}}\mathcal{H} d\zeta + \int_a^b (\delta_{\mathbf{x}}\mathcal{H})^\top \begin{bmatrix} 0 \\ 0 \\ [0 \ \mathbf{R}_1^\top] M^\top(\mathbf{x}) \partial_\zeta [M(\mathbf{x}) \delta_{\mathbf{x}}\mathcal{H}] \end{bmatrix} d\zeta \\ &\quad + \int_a^b (\delta_{\mathbf{x}}\mathcal{H})^\top \left[M^\top(\mathbf{x}) \partial_\zeta \left(M(\mathbf{x}) \begin{bmatrix} 0 \\ \mathbf{R}_1 \end{bmatrix} \delta_s \mathcal{H} \right) \right] d\zeta \\ &= - \int_a^b \partial_\zeta (\delta_\rho \mathcal{H} \delta_v \mathcal{H}) d\zeta + \int_a^b \partial_\zeta \left([M(\mathbf{x}) \delta_{\mathbf{x}}\mathcal{H}]^\top M(\mathbf{x}) \begin{bmatrix} 0 \\ \mathbf{R}_1 \end{bmatrix} \delta_s \mathcal{H} \right) d\zeta \\ &= - (\delta_\rho \mathcal{H} \delta_v \mathcal{H}) \Big|_a^b + \left(\frac{1}{\rho} \delta_v \mathcal{H} R_{1\tau} \frac{1}{\rho} \delta_s \mathcal{H} \right) \Big|_a^b + \left(\frac{1}{\rho} \delta_s \mathcal{H} R_{1T} \frac{1}{\rho} \delta_s \mathcal{H} \right) \Big|_a^b \\ &= - \left(\left(\frac{1}{2} v^2 + h \right) \rho v \right) \Big|_a^b - (v\tau) \Big|_a^b - (Tf_s) \Big|_a^b \end{aligned}$$

Defining the boundary inputs and outputs as shown in (5.98), the relationship (5.99) is obtained.

Regarding the entropy balance, we have that

$$\begin{aligned} \dot{\mathcal{S}} &= \int_a^b [\delta_{\mathbf{x}}\mathcal{S}]^\top \partial_t \mathbf{x} d\zeta \\ &= \int_a^b \left([\delta_{\mathbf{x}}\mathcal{S}]^\top \mathcal{J} \delta_{\mathbf{x}}\mathcal{H} + [\delta_{\mathbf{x}}\mathcal{S}]^\top M^\top(\mathbf{x}) \partial_\zeta \left(M(\mathbf{x}) \begin{bmatrix} 0 \\ \mathbf{R}_1 \end{bmatrix} \delta_s \mathcal{H} \right) \right) d\zeta \\ &\quad + \int_a^b \left(\underbrace{R_{1\tau} [\delta_{\mathbf{x}}\mathcal{S}]^\top \tilde{\mathcal{J}}_{1\tau} \delta_{\mathbf{x}}\mathcal{H}}_{\{\mathcal{S}, \mathcal{H}\}_{\tilde{\mathcal{J}}_{1\tau}}^*} + \underbrace{R_{1T} [\delta_{\mathbf{x}}\mathcal{S}]^\top \tilde{\mathcal{J}}_{1T} \delta_{\mathbf{x}}\mathcal{H}}_{\{\mathcal{S}, \mathcal{H}\}_{\tilde{\mathcal{J}}_{1T}}^*} \right) d\zeta \end{aligned}$$

where $[\delta_{\mathbf{x}}\mathcal{S}]^\top = [s \ 0 \ \rho]$. Notice that $[\delta_{\mathbf{x}}\mathcal{S}]^\top \mathcal{J} \delta_{\mathbf{x}}\mathcal{H} = -s \partial_\zeta \delta_v \mathcal{H} - \delta_v \mathcal{H} \partial_\zeta s = -\partial_\zeta (s \delta_v \mathcal{H})$ and $[\delta_{\mathbf{x}}\mathcal{S}]^\top M^\top(\mathbf{x}) = [0 \ 0 \ 1]$. Then, the entropy balance $\dot{\mathcal{S}}$ is given by

$$\begin{aligned} \dot{\mathcal{S}} &= \int_a^b \sigma_s d\zeta - \int_a^b \partial_\zeta (s \delta_v \mathcal{H} + f_s) d\zeta \\ &= \int_a^b \sigma_s d\zeta - (s \rho v + f_s) \Big|_a^b \end{aligned}$$

where $\sigma_s = \gamma_{1\tau} \left(\{\mathcal{S}, \mathcal{H}\}_{\tilde{\mathcal{J}}_{1\tau}}^* \right)^2 + \gamma_{1T} \left(\{\mathcal{S}, \mathcal{H}\}_{\tilde{\mathcal{J}}_{1T}}^* \right)^2 \geq 0$. □

Notice that if the system is isolated, the energy balance (5.99) is reduced to $\dot{\mathcal{H}} = 0$ and the entropy balance (5.100) is reduced to the inequality $\dot{\mathcal{S}} \geq 0$, i.e., the fluid description in Proposition 5.4 satisfies the first and second laws of Thermodynamics.

Remark 5.6. Notice that the structure of the irreversible part of system (5.97) is modulated, in contrast to the irreversible port-Hamiltonian formulation on infinite dimensional spaces given in Definition 1.6 (see Chapter 1 Section 1.2.3 for details). The presence of matrix $M(\mathbf{x})$ in the last term of the right hand side of (5.97), and in operators $\tilde{\mathcal{J}}_{1T}$ and $\tilde{\mathcal{J}}_{1\tau}$, is due to the state variables of the compressible fluids. In the case of incompressible fluids, this matrix vanishes, obtaining a standard irreversible port-Hamiltonian formulation.

To illustrate the previous Remark (5.6), as an example we consider a simple 1D shallow-water system described by:

$$\partial_t h = -\partial_\zeta (hv) \quad (5.101a)$$

$$\partial_t (\rho_0 v) = -\partial_\zeta \left(\frac{1}{2} \rho_0 v^2 + \rho_0 g h \right) - \frac{1}{2} \lambda_f \rho_0 |v|v \quad (5.101b)$$

$$\partial_t u = \frac{1}{2} \lambda_f \rho_0 h |v|v^2 - \partial_\zeta f_T \quad (5.101c)$$

where $h = h(\zeta, t)$ is the water height, $v = v(\zeta, t)$ is the average velocity of the fluids, $u = u(\zeta, t)$ denotes the internal energy per unit length, f_T is the heat flux, g is the constant of gravity and ρ_0 is the mass per unit area. The last term on the right hand side of (5.101b) describes the dissipation of kinetic energy by viscous friction, where λ_f is a dimensionless factor [104]. The term $\frac{1}{2} \lambda_f \rho_0 h |v|v^2$ in (5.101c) denotes the heat production by viscous friction. The term $\frac{1}{2} \lambda_f \rho_0 |v|$ is equivalent to the friction coefficients used in [130] and [131]. The thermodynamic properties of u are given by the Gibbs equation, $du = Tds$, where $s = s(\zeta, t)$ is the entropy per unit length. The total energy of this system is given by:

$$\mathcal{H} = \int_a^b \frac{1}{2} \rho_0 h v^2 + \frac{1}{2} \rho_0 g h^2 + u(s) d\zeta$$

Using the thermodynamic equilibrium $\partial_t u = T \partial_t s$, the dynamics of s can be expressed as:

$$\partial_t s = \frac{1}{2} \frac{\lambda_f}{T} \rho_0 h |v|v^2 - \frac{1}{T} \partial_\zeta (\kappa \partial_\zeta T)$$

Defining the state vector as $\mathbf{x} = [h, \rho_0 v, s]^\top$, the fluid efforts are given by $\delta_{\mathbf{x}} \mathcal{H} = [\frac{1}{2} \rho_0 v^2 + \rho_0 g h, hv, T]^\top$ and the shallow-water equations can be expressed as:

$$\partial_t \mathbf{x} = \mathcal{J} \delta_{\mathbf{x}} \mathcal{H} + R_1 \mathcal{J}_1 \delta_{\mathbf{x}} \mathcal{H} + R_0 \mathcal{J}_0 \delta_{\mathbf{x}} \mathcal{H} + \partial_\zeta \left(\begin{bmatrix} 0 \\ 0 \\ R_1 \end{bmatrix} \delta_s \mathcal{H} \right) \quad (5.102)$$

where $\mathcal{J} = P \partial_\zeta$, $\mathcal{J}_0 = P_0$ and $\mathcal{J}_1 = P_1 \partial_\zeta$ are skew-symmetric operators with

$$P = \begin{bmatrix} 0 & -1 & 0 \\ -1 & 0 & 0 \\ 0 & 0 & 0 \end{bmatrix}, \quad P_0 = \begin{bmatrix} 0 & 0 & 0 \\ 0 & 0 & -1 \\ 0 & 1 & 0 \end{bmatrix} \quad \text{and} \quad P_1 = \begin{bmatrix} 0 & 0 & 0 \\ 0 & 0 & 0 \\ 0 & 0 & 1 \end{bmatrix}$$

and $R_0 = \gamma_0 \{\mathcal{S}, \mathcal{H}\}_{\mathcal{J}_0}^*$ and $R_1 = \gamma_1 \{\mathcal{S}, \mathcal{H}\}_{\mathcal{J}_1}^*$, where $\{\mathcal{S}, \mathcal{H}\}_{\mathcal{J}_0}^* = hv$, $\{\mathcal{S}, \mathcal{H}\}_{\mathcal{J}_1}^* = \partial_\zeta T$, $\gamma_0 = \frac{1}{2} \frac{\lambda_f \rho_0 |v|}{Th} > 0$ and $\gamma_1 = \frac{\kappa}{T^2} > 0$.

Notice that, for the incompressible fluid described by the shallow-water equations, the irreversible part of the system (5.102) is in correspondence with the standard irreversible port-Hamiltonian formulation described in Definition 1.6. That is, the matrix $M(\mathbf{x})$ that appear in the irreversible port-Hamiltonian formulation of compressible fluids, is a consequence of the compressibility assumption.

5.6 CONCLUSION

In this chapter, general port-Hamiltonian formulations for 3D compressible fluids have been presented. For non-isentropic fluids a pseudo port-Hamiltonian model was proposed in Proposition 5.1. This model presents an appropriate description of the thermal domain, satisfying the second law of Thermodynamic, as shown in (5.23). However, operators \mathcal{D}_τ and \mathcal{D}_τ^* depend explicitly on the entropy effort $\delta_s \mathcal{H} = \rho T$ and, as a consequence, the system (5.19) does not define a Dirac structure. In the case of isentropic fluids, the dissipation of kinetic energy by viscous friction is considered as a dissipative term [40], obtaining the dissipative port-Hamiltonian model in Proposition 5.2. As shown in Section 5.3, these port-Hamiltonian formulations can also be used for 1D and 2D compressible fluids, making the appropriate considerations in the corresponding operators. Moreover, considering the suitable assumptions, proposed formulations are equivalent to other fluid models in the literature.

Finally, we presented an alternative formulation based on the irreversible port-Hamiltonian framework to describe non-isentropic compressible fluids in 1D. Unlike the pseudo port-Hamiltonian formulation described in Proposition 5.1, this approach allows us to avoid the presence of fluid efforts in the differential operators that describe the dynamics. Additionally, we obtain an appropriate description of the first and second law of Thermodynamic, as shown in Proposition 5.4. However, given the compressibility assumption, a matrix $M(\mathbf{x})$ appears in the irreversible part of the model, obtaining a formulation that differs from the standard form of irreversible port-Hamiltonian systems on infinite dimensional domains, described in Definition (1.6).

Chapter 6

Conclusion

In this thesis a finite-dimensional approach based on the port-Hamiltonian framework to describe the FSI between a longitudinal fluid and a structure with transverse motion has been presented. A finite-dimensional formulation based on a mass-spring-damper description has been proposed in Chapter 2 to characterize the transverse motion of the structure in the longitudinal domain. To describe incompressible fluids, the fluid domain is divided into n_f sections of length ℓ_f with uniform cross-sectional areas, where the fluid dynamics are characterized through the average longitudinal momentum. Additionally, a novel instrumental element, called node, has been proposed in Chapter 3. This node allows us to define the static pressure in an infinitesimal zone between two incompressible sections of the fluid domain, providing an appropriate way, from the port-Hamiltonian point of view, to couple finite-dimensional port-Hamiltonian models of adjacent incompressible sections. In the case of compressible fluids, a description based on a 1D staggered grid has been proposed in Chapter 4. The flow behavior is characterized by the average longitudinal velocity of n_f sections with uniform cross-sectional areas and the corresponding n_f average densities.

To connect the fluid and the structure subsystems, a power-preserving interconnection that combines the features of the interconnection by ports and the interconnection by energy of PHS, has been presented in Chapter 3. This interconnection provides a suitable description of the power-transfer between both subsystems. In cases where the structure collides closing a section of the fluid domain, a switching interconnection approach has been proposed in Chapter 4. To this end, we use a switching matrix S_ϵ to enable and disable the fluid-structure interconnection in the corresponding sections, according to a threshold value. Similarly, this matrix S_ϵ is used to enable and disable the corresponding fluid dynamics during the collision, allowing us to avoid the singularities of the fluid model when the fluid domain is closed.

The finite-dimensional approach used in this thesis, allows to reduce the complexity of the FSI model with respect to the classical computational formulations that requires several algorithms to guarantee the stability of the numerical results. Moreover, the proposed finite-dimensional models show an appropriated description of the FSI behavior, as it can be seen in the numerical simulations. These simulations show results in correspondence with other model in the literature. Additionally, the scalability of the proposed models allows to set the spatial resolution, along the longitudinal domain, of the variables of interest. This setting can be made varying the number of fluid sections n_f and structure sections n_s . Moreover, as shown in Section 4.4, the number of fluid sections and the number of structure sections may be different, allowing greater freedom in the description of the fluid and the structure domains.

The analysis of the FSI behavior using the models proposed is constrained by the symmetry hypotheses considered in this thesis, such as an axisymmetric behavior of flexible tubes and an symmetric movement of the vocal folds in the glottis. Similarly, the structure dynamics are reduced to the transverse motion only. Similarly, the fluid dynamics analysis is limited to the longitudinal velocity of the flow. To study phenomena, such as vena contracta and coandrea effects in the glottis during the vibrating cycle of the vocal folds, a more complex model is required.

In Chapter 5, we presented general formulations based on the port-Hamiltonian framework for 3D isentropic and non-isentropic compressible fluids. These formulations can also be used in 1D and 2D fluid problems modifying the differential operators. Similarly, under appropriate assumptions, the proposed models are equivalent to other formulations in the literature. In the case of non-isentropic fluids, we have obtained a pseudo port-Hamiltonian formulation. That is given by the dependency of the differential operators on the fluid efforts associated with the entropy state variable. This implies that the system described in Proposition 5.1 does not define a Dirac structure. Additionally, an alternative formulation based on the irreversible port-Hamiltonian framework is proposed for 1D non-isentropic fluids. The advantage of this formulation is that it encompasses the first and second principles of thermodynamics as a structural property of the system, which is particularly convenient for stability analysis and passivity based control design.

FUTURE WORK

For a practical use of the finite-dimensional models proposed in this thesis, as for example in the study of pathogenesis of phonotraumatic diseases of the vocal folds, the next step is the parameter identification from real data. However, the application of system identification methods, such as maximum likelihood and Bayesian inference, to the models proposed has the own challenges that need be considered in future projects. Similarly, one advantage of the finite-dimensional models presented in this thesis, is the simplicity of the PHS framework to define new inputs for the model, as for example external forces acting on the masses of the structure model. This is useful for control applications in future works. Other possible research areas where the proposed model can be useful is in system identification and filtering. Consider for example the voice production process. During phonation we use myoelectric signals that change the strain of the Thyroarytenoid muscle in the vocal folds (see Figure 2.4). These changes can be interpreted in two ways: the first one is to consider that the structure model has time varying parameters; the second one is to consider these changes as an external force acting on the masses of the structure model. In the first case we can use system identification methods to estimate the parameters of the system from real data. In the second case where we consider external forces acting on the structure model. Recent advances in filtering for systems subject to unknown inputs, will be used to estimate these forces. This information can be useful for the design of biomedical implants.

As future work with the infinite-dimensional models proposed in Chapter 5, we consider the study of techniques such as Arbitrary Lagrangian-Eulerian methods [19, 26] and meshless methods [132], and their compatibility with the port-Hamiltonian framework, to describe systems with time varying domains. Another research line to be considered in future works

is the extension of the infinite-dimensional port-Hamiltonian formulations to non-Newtonian fluids. Regarding the irreversible port-Hamiltonian approach, we consider the extension of the formulation described in Proposition 5.4 to 3D compressible fluids and the development of passivity-based control methods suitable for the structure of irreversible port-Hamiltonian systems on infinite dimensional domains.

Appendix A

Useful Identities and Theorems

The set of mathematical identities [101, Appendix A] used in this work are described below:

$$(\mathbf{u} \cdot \mathbf{grad}) \mathbf{u} = \mathbf{grad} \left(\frac{1}{2} \mathbf{u} \cdot \mathbf{u} \right) + [\mathbf{curl} \mathbf{u}] \times \mathbf{u} \quad (\text{A.1})$$

$$\boldsymbol{\sigma} : [\mathbf{Grad} \mathbf{u}] = \text{div} [\boldsymbol{\sigma} \cdot \mathbf{u}] - \mathbf{u} \cdot \text{div} \boldsymbol{\sigma} \quad (\text{A.2})$$

$$\text{div} [f\mathbf{u}] = [\mathbf{grad} f] \cdot \mathbf{u} + f \text{div} \mathbf{u} \quad (\text{A.3})$$

$$\text{div} (\mathbf{Grad} \mathbf{u}) = \mathbf{grad} (\text{div} \mathbf{u}) - \mathbf{curl} [\mathbf{curl} \mathbf{u}] \quad (\text{A.4})$$

$$\text{div} ([\mathbf{Grad} \mathbf{u}]^\top) = \mathbf{grad} (\text{div} \mathbf{u}) \quad (\text{A.5})$$

$$\text{div} [(\text{div} \mathbf{u}) I] = \mathbf{grad} (\text{div} \mathbf{u}) \quad (\text{A.6})$$

$$\text{div} [\mathbf{u} \times \mathbf{v}] = \mathbf{v} \cdot [\mathbf{curl} \mathbf{u}] - \mathbf{u} \cdot [\mathbf{curl} \mathbf{v}] \quad (\text{A.7})$$

where f is a scalar, \mathbf{u} is a vector and $\boldsymbol{\sigma}$ is a symmetric second order tensor.

Theorem A.1 (Gauss Divergence Theorem). *Let be a domain Ω , enclosed by the boundary surface $\partial\Omega$, then*

$$\int_{\Omega} (\text{div} \mathbf{u}) d\Omega = \int_{\partial\Omega} (\mathbf{u} \cdot \mathbf{n}) \partial\Omega \quad (\text{A.8})$$

where \mathbf{n} denotes the outward unitary vector to the boundary $\partial\Omega$

Proof. See [101, p. 704] □

Theorem A.2 (Adjoint of div). *Let be the Hilbert space of the square integrable scalar functions, denoted by $\mathcal{H}_0 = L^2(\Omega, \mathbb{R})$, and the Hilbert space of the square integrable vector functions, denoted by $\mathcal{H}_1 = L^2(\Omega, \mathbb{R}^n)$. Given the operators $\text{div} : \mathcal{H}_1 \rightarrow \mathcal{H}_0$ and $\mathbf{grad} : \mathcal{H}_0 \rightarrow \mathcal{H}_1$, where $-\mathbf{grad}$ is the formal adjoint of div , then,*

$$\int_{\Omega} f (\text{div} \mathbf{u}) d\Omega + \int_{\Omega} [\mathbf{grad} f] \cdot \mathbf{u} d\Omega = \int_{\partial\Omega} f (\mathbf{u} \cdot \mathbf{n}) \partial\Omega \quad (\text{A.9})$$

Proof. Denote by $\langle f_1, f_2 \rangle_{\mathcal{H}_0} = \int_{\Omega} f_1 f_2 d\Omega$ and $\langle \mathbf{u}_1, \mathbf{u}_2 \rangle_{\mathcal{H}_1} = \int_{\Omega} \mathbf{u}_1 \cdot \mathbf{u}_2 d\Omega$ the inner products in \mathcal{H}_0 and \mathcal{H}_1 , respectively. Then,

$$\begin{aligned} \langle f, \operatorname{div} \mathbf{u} \rangle_{\mathcal{H}_0} + \langle \mathbf{grad} f, \mathbf{u} \rangle_{\mathcal{H}_1} &= \int_{\Omega} f (\operatorname{div} \mathbf{u}) d\Omega + \int_{\Omega} [\mathbf{grad} f] \cdot \mathbf{u} d\Omega \\ &= \int_{\Omega} f (\operatorname{div} \mathbf{u}) + [\mathbf{grad} f] \cdot \mathbf{u} d\Omega \\ &\stackrel{(A.3)}{=} \int_{\Omega} \operatorname{div} [f \mathbf{u}] d\Omega \\ &\stackrel{(A.8)}{=} \int_{\partial\Omega} f (\mathbf{u} \cdot \mathbf{n}) \partial\Omega \end{aligned}$$

where for BC equal to 0, the relationship $\langle f, \operatorname{div} \mathbf{u} \rangle_{\mathcal{H}_2} = \langle -\mathbf{grad} f, \mathbf{u} \rangle_{\mathcal{H}_1}$ is obtained. \square

Theorem A.3. [60] Consider the Hilbert space of the square integrable vector functions \mathcal{H}_1 , and the Hilbert space of square integrable second order tensors $\mathcal{H}_2 := L^2(\Omega, \mathbb{R}^{n \times n})$. Given the operators $\mathbf{div} : \mathcal{H}_2 \rightarrow \mathcal{H}_1$ and $\mathbf{Grad} : \mathcal{H}_1 \rightarrow \mathcal{H}_2$. Then, the formal adjoint of \mathbf{div} is $-\mathbf{Grad}$ and for any symmetric tensor $\boldsymbol{\sigma} \in \mathcal{H}_2$ and vector $\mathbf{u} \in \mathcal{H}_1$, the following relationship is satisfied

$$\int_{\Omega} [\mathbf{div} \boldsymbol{\sigma}] \cdot \mathbf{u} d\Omega + \int_{\Omega} \boldsymbol{\sigma} : [\mathbf{Grad} \mathbf{u}] d\Omega = \int_{\partial\Omega} \mathbf{u} \cdot [\boldsymbol{\sigma} \cdot \mathbf{n}] \partial\Omega \quad (\text{A.10})$$

Proof. Denote by $\langle \boldsymbol{\sigma}_1, \boldsymbol{\sigma}_2 \rangle_{\mathcal{H}_2} = \int_{\Omega} \boldsymbol{\sigma}_1 : \boldsymbol{\sigma}_2 d\Omega$ inner product in \mathcal{H}_2 , where $\boldsymbol{\sigma}_1 : \boldsymbol{\sigma}_2 = \operatorname{Tr}(\boldsymbol{\sigma}_1^{\top} \boldsymbol{\sigma}_2)$. Considering $\mathbf{div} \boldsymbol{\sigma} = [\operatorname{div} \sigma_1 \cdots \operatorname{div} \sigma_n]^{\top}$ where $\sigma_j = [\sigma_{1j} \cdots \sigma_{nj}]^{\top}$ is the j -th column of tensor $\boldsymbol{\sigma}$. Then, we obtain:

$$\begin{aligned} \langle \mathbf{div} \boldsymbol{\sigma}, \mathbf{u} \rangle_{\mathcal{H}_1} &= \int_{\Omega} [\mathbf{div} \boldsymbol{\sigma}] \cdot \mathbf{u} d\Omega = \int_{\Omega} \sum_j v_j \operatorname{div} \sigma_j d\Omega \\ &\stackrel{(A.3)}{=} \sum_j \int_{\Omega} -\sigma_j \cdot \mathbf{grad} u_j + \operatorname{div} [\sigma_j u_j] d\Omega \\ &= - \int_{\Omega} \operatorname{Tr} (\boldsymbol{\sigma}^{\top} \mathbf{Grad} \mathbf{u}) d\Omega + \sum_j \int_{\partial\Omega} u_j (\sigma_j \cdot \mathbf{n}) \partial\Omega \\ &= - \langle \boldsymbol{\sigma}, \mathbf{Grad} \mathbf{u} \rangle_{\mathcal{H}_2} + \int_{\partial\Omega} \mathbf{u} \cdot [\boldsymbol{\sigma}^{\top} \cdot \mathbf{n}] \partial\Omega \end{aligned}$$

Thus, for BC equal to 0 we obtain $\langle \mathbf{div} \boldsymbol{\sigma}, \mathbf{u} \rangle_{\mathcal{H}_1} = \langle \boldsymbol{\sigma}, -\mathbf{Grad} \mathbf{u} \rangle_{\mathcal{H}_2}$, i.e., $-\mathbf{Grad}$ is the formal adjoint of \mathbf{div} .

Now, considering that $\boldsymbol{\sigma}$ is a symmetric tensor in \mathcal{H}_2 , $\mathbf{u} \cdot [\boldsymbol{\sigma}^{\top} \cdot \mathbf{n}] = \mathbf{u} \cdot [\boldsymbol{\sigma} \cdot \mathbf{n}]$, obtaining the relationship (A.10). \square

Theorem A.4. Let $\operatorname{curl} \doteq$ be the adjoint operator of $\frac{1}{\rho} \operatorname{curl}$. Then,

$$\int_{\Omega} \mathbf{u}_1 \cdot \left[\operatorname{curl} \frac{\mathbf{u}_2}{\rho} \right] d\Omega - \int_{\Omega} \left[\frac{1}{\rho} \operatorname{curl} \mathbf{u}_1 \right] \cdot \mathbf{u}_2 d\Omega = \int_{\partial\Omega} \frac{1}{\rho} [\mathbf{u}_2 \times \mathbf{u}_1] \cdot \mathbf{n} \partial\Omega \quad (\text{A.11})$$

Proof. Considering the inner product $\langle \mathbf{u}_1, \mathbf{curl} \frac{\mathbf{u}_2}{\rho} \rangle_{\mathcal{H}_1}$ we obtain

$$\begin{aligned} \left\langle \mathbf{u}_1, \mathbf{curl} \frac{\mathbf{u}_2}{\rho} \right\rangle_{\mathcal{H}_1} &= \int_{\Omega} \mathbf{u}_1 \cdot \left[\mathbf{curl} \frac{\mathbf{u}_2}{\rho} \right] d\Omega \\ &\stackrel{(A.7)}{=} \int_{\Omega} \left(\operatorname{div} \left[\frac{\mathbf{u}_2}{\rho} \times \mathbf{u}_1 \right] + \frac{\mathbf{u}_2}{\rho} \cdot [\mathbf{curl} \mathbf{u}_1] \right) d\Omega \\ &\stackrel{(A.8)}{=} \int_{\Omega} \left[\frac{1}{\rho} \mathbf{curl} \mathbf{u}_1 \right] \cdot \mathbf{u}_2 d\Omega + \int_{\partial\Omega} \left[\frac{\mathbf{u}_2}{\rho} \times \mathbf{u}_1 \right] \cdot \mathbf{n} d\Omega \end{aligned}$$

Rewritten previous equation we obtain the relationship (A.11). Similarly, considering boundary conditions equal to 0, $\langle \mathbf{u}_1, \mathbf{curl} \frac{\mathbf{u}_2}{\rho} \rangle_{\mathcal{H}_1} = \langle \frac{1}{\rho} \mathbf{curl} \mathbf{u}_1, \mathbf{u}_2 \rangle_{\mathcal{H}_1}$, i.e., $\mathbf{curl} \frac{\cdot}{\rho}$ is the formal adjoint of $\frac{1}{\rho} \mathbf{curl} \cdot$. \square

Theorem A.5. Let $\mathbf{x} \in \mathcal{H}_1$ be the state vector of a dynamic system, $F(\mathbf{x}) \in \mathcal{H}_1$ and $\alpha(\mathbf{x}) \in \mathcal{H}_0$ be square integrable vector and scalar functions, respectively, such that, for any $f \in \mathcal{H}_0$ we obtain that $F(\mathbf{x})f \in \mathcal{H}_1$ and $\alpha(\mathbf{x})f \in \mathcal{H}_0$. Define the operator $\mathcal{D} : \mathcal{H}_0 \rightarrow \mathcal{H}_0$ as $\mathcal{D}f = \alpha(\mathbf{x})\operatorname{div} (F(\mathbf{x})f)$. Then, the formal adjoint $\mathcal{D}^* : \mathcal{H}_0 \rightarrow \mathcal{H}_0$ of \mathcal{D} is given by $\mathcal{D}^*f = -F^\top(\mathbf{x})\mathbf{grad} (\alpha(\mathbf{x})f) : \mathcal{H}_0 \rightarrow \mathcal{H}_0$.

Proof. Let $f_j, j \in \{1, 2\}$ be a square integrable scalar function. Consider $f_j^\alpha \in \mathcal{H}_0$ and $\mathbf{f}_j^F \in \mathcal{H}_1$ as the scalar and vector functions defined as $f_j^\alpha = \alpha(\mathbf{x})f_j$ and $\mathbf{f}_j^F = F(\mathbf{x})f_j$, respectively. Using the inner product $\langle f_1, \mathcal{D}f_2 \rangle_{\mathcal{H}_0}$, we obtain that:

$$\begin{aligned} \langle f_1, \mathcal{D}f_2 \rangle_{\mathcal{H}_0} &= \int_{\Omega} f_1 \alpha(\mathbf{x}) \operatorname{div} (F(\mathbf{x})f_2) d\Omega = \int_{\Omega} f_1^\alpha \operatorname{div} \mathbf{f}_2^F d\Omega \\ &\stackrel{(A.9)}{=} - \int_{\Omega} [\mathbf{grad} f_1^\alpha] \cdot \mathbf{f}_2^F d\Omega + \int_{\partial\Omega} f_1^\alpha (\mathbf{f}_2^F \cdot \mathbf{n}) \partial\Omega \\ &= - \int_{\Omega} [\mathbf{grad} (\alpha(\mathbf{x})f_1)] \cdot F(\mathbf{x})f_2 d\Omega + \int_{\partial\Omega} f_1^\alpha (\mathbf{f}_2^F \cdot \mathbf{n}) \partial\Omega \\ &= - \int_{\Omega} [F^\top(\mathbf{x})\mathbf{grad} (\alpha(\mathbf{x})f_1)] f_2 d\Omega + \int_{\partial\Omega} f_1^\alpha (\mathbf{f}_2^F \cdot \mathbf{n}) \partial\Omega \end{aligned} \quad (A.12)$$

Then, considering boundary conditions equal to 0, we obtain the relationship $\langle f_1, \mathcal{D}f_2 \rangle_{\mathcal{H}_0} = \langle -F^\top(\mathbf{x})\mathbf{grad} (\alpha(\mathbf{x})f_1), f_2 \rangle_{\mathcal{H}_0}$, i.e., $\mathcal{D}^*(\cdot) = -F^\top(\mathbf{x})\mathbf{grad} (\alpha(\mathbf{x})\cdot)$ is the formal adjoint of \mathcal{D} . \square

Theorem A.6. Let $\bar{\mathcal{D}} : \mathcal{H}_0 \rightarrow \mathcal{H}_0$ be an operator defined as $\bar{\mathcal{D}}f = F^\top(\mathbf{x})\mathbf{grad} (\alpha(\mathbf{x})f) + \alpha(\mathbf{x})\operatorname{div} (F(\mathbf{x})f)$, such that, for any $f \in \mathcal{H}_0$ we obtain that $F(\mathbf{x})f \in \mathcal{H}_1$ and $\alpha(\mathbf{x})f \in \mathcal{H}_0$. Then, the $\bar{\mathcal{D}}$ is a formal skew-adjoint operator.

Proof. Let $f_j, j \in \{1, 2\}$ be a square integrable scalar function. Consider $f_j^\alpha \in \mathcal{H}_0$ and $\mathbf{f}_j^F \in \mathcal{H}_1$ as the scalar and vector functions defined as $f_j^\alpha = \alpha(\mathbf{x})f_j$ and $\mathbf{f}_j^F = F(\mathbf{x})f_j$, respectively. Then, inner product $\langle f_1, \bar{\mathcal{D}}f_2 \rangle_{\mathcal{H}_0}$ is given by:

$$\langle f_1, \bar{\mathcal{D}}f_2 \rangle_{\mathcal{H}_0} = \int_{\Omega} \left(f_1 F^\top(\mathbf{x})\mathbf{grad} (\alpha(\mathbf{x})f_2) + f_1 \alpha(\mathbf{x}) \operatorname{div} (F(\mathbf{x})f_2) \right) d\Omega \quad (A.13)$$

Using (A.12) the expression (A.13) is rewritten as:

$$\begin{aligned}
 \langle f_1, \bar{\mathcal{D}}f_2 \rangle_{\mathcal{H}_0} &= - \int_{\Omega} \left(f_1 F^\top(\mathbf{x}) \mathbf{grad} (\alpha(\mathbf{x})f_1) + f_2 \alpha(\mathbf{x}) \operatorname{div} (F(\mathbf{x})f_1) \right) d\Omega \\
 &\quad + \int_{\partial\Omega} \left(f_1^\alpha (\mathbf{f}_2^F \cdot \mathbf{n}) + f_2^\alpha (\mathbf{f}_1^F \cdot \mathbf{n}) \right) \partial\Omega \\
 &= - \langle \bar{\mathcal{D}}f_1, f_2 \rangle_{\mathcal{H}_0} + \int_{\partial\Omega} \left(f_1^\alpha (\mathbf{f}_2^F \cdot \mathbf{n}) + f_2^\alpha (\mathbf{f}_1^F \cdot \mathbf{n}) \right) \partial\Omega \tag{A.14}
 \end{aligned}$$

Finally, considering boundary conditions equal to 0, from (A.14) we have that $\langle f_1, \bar{\mathcal{D}}f_2 \rangle_{\mathcal{H}_0} = \langle -\bar{\mathcal{D}}f_1, f_2 \rangle_{\mathcal{H}_0}$. This implies that the formal adjoint of $\bar{\mathcal{D}}$ is given by $\bar{\mathcal{D}}^* = -\bar{\mathcal{D}}$, i.e., $\bar{\mathcal{D}}$ is a formal skew-adjoint operator. \square

Bibliography

- [1] Y. Bazilevs, K. Takizawa, and T. E. Tezduyar, *Computational Fluid-Structure Interaction*, ser. Wiley Series in Computational Mechanics. Chichester, UK: John Wiley & Sons, Ltd, jan 2013.
- [2] H.-J. Bungartz and M. Schäfer, Eds., *Fluid-Structure Interaction*, ser. Lecture Notes in Computational Science and Engineering. Berlin, Heidelberg: Springer Berlin Heidelberg, 2006, vol. 53.
- [3] B. Dose, H. Rahimi, B. Stoevesandt, and J. Peinke, “Fluid-structure coupled investigations of the NREL 5 MW wind turbine for two downwind configurations,” *Renewable Energy*, vol. 146, pp. 1113–1123, feb 2020.
- [4] G. Santo, M. Peeters, W. Van Paeppegem, and J. Degroote, “Effect of rotor–tower interaction, tilt angle, and yaw misalignment on the aeroelasticity of a large horizontal axis wind turbine with composite blades,” *Wind Energy*, vol. 23, no. 7, pp. 1578–1595, jul 2020.
- [5] J. Piquee, M. Saeedi, C. Breitsamter, R. Wüchner, and K.-U. Bletzinger, “Numerical Investigations of an Elasto-Flexible Membrane Airfoil Compared to Experiments,” in *New Results in Numerical and Experimental Fluid Mechanics XI: Contributions to the 20th STAB/DGLR Symposium Braunschweig, Germany, 2016*, ser. Notes on Numerical Fluid Mechanics and Multidisciplinary Design. Springer International Publishing, 2018, vol. 136, pp. 421–431.
- [6] H. Truong, T. Engels, D. Kolomenskiy, and K. Schneider, “A mass-spring fluid-structure interaction solver: Application to flexible revolving wings,” *Computers & Fluids*, vol. 200, p. 104426, mar 2020.
- [7] T. Nakata and H. Liu, “A fluid–structure interaction model of insect flight with flexible wings,” *Journal of Computational Physics*, vol. 231, no. 4, pp. 1822–1847, feb 2012.
- [8] G. Vergara-Hermosilla, D. Matignon, and M. Tucsnak, “Well-Posedness and input-output stability for a system modelling rigid structures floating in a viscous fluid,” in *21st IFAC World Congress*, Berlin, 2020, pp. 7581–7586.
- [9] J. Degroote, R. Haelterman, S. Annerel, P. Bruggeman, and J. Vierendeels, “Performance of partitioned procedures in fluid-structure interaction,” *Computers & Structures*, vol. 88, no. 7-8, pp. 446–457, 2010.
- [10] M. Bukač, S. Čanić, and B. Muha, “A partitioned scheme for fluid–composite structure interaction problems,” *Journal of Computational Physics*, vol. 281, pp. 493–517, jan 2015.

- [11] F. He, L. Hua, and L.-j. Gao, “A hemodynamic model with a seepage condition and fluid–structure interactions for blood flow in arteries with symmetric stenosis,” *Journal of Biological Physics*, vol. 45, no. 2, pp. 183–192, jun 2019.
- [12] A. Lozovskiy, M. A. Olshanskii, and Y. V. Vassilevski, “Analysis and assessment of a monolithic FSI finite element method,” *Computers & Fluids*, vol. 179, pp. 277–288, 2019.
- [13] S. L. Thomson, L. Mongeau, and S. H. Frankel, “Aerodynamic transfer of energy to the vocal folds,” *The Journal of the Acoustical Society of America*, vol. 118, no. 3, pp. 1689–1700, sep 2005.
- [14] H. Sadeghi, S. Kniesburges, S. Falk, M. Kaltenbacher, A. Schützenberger, and M. Döllinger, “Towards a Clinically Applicable Computational Larynx Model,” *Applied Sciences*, vol. 9, no. 11, p. 2288, jun 2019.
- [15] L. Schickhofer, J. Malinen, and M. Mihaescu, “Compressible flow simulations of voiced speech using rigid vocal tract geometries acquired by MRI,” *The Journal of the Acoustical Society of America*, vol. 145, no. 4, pp. 2049–2061, 2019.
- [16] L. Schickhofer and M. Mihaescu, “Analysis of the aerodynamic sound of speech through static vocal tract models of various glottal shapes,” *Journal of Biomechanics*, vol. 99, p. 109484, 2020.
- [17] A. R. da Silva, G. P. Scavone, and M. van Walstijn, “Numerical simulations of fluid-structure interactions in single-reed mouthpieces,” *The Journal of the Acoustical Society of America*, vol. 122, no. 3, pp. 1798–1809, sep 2007.
- [18] A. Eken and M. Sahin, “A parallel monolithic approach for fluid-structure interaction in a cerebral aneurysm,” *Computers & Fluids*, vol. 153, pp. 61–75, aug 2017.
- [19] T. Richter, *Fluid-structure Interactions: Models, Analysis and Finite Elements*, ser. Lecture Notes in Computational Science and Engineering. Cham: Springer International Publishing, 2017, vol. 118.
- [20] K. K. L. Wong, P. Thavornpattanapong, S. C. P. Cheung, and J. Tu, “Numerical Stability of Partitioned Approach in Fluid-Structure Interaction for a Deformable Thin-Walled Vessel,” *Computational and Mathematical Methods in Medicine*, vol. 2013, pp. 1–10, 2013.
- [21] P. Causin, J. F. Gerbeau, and F. Nobile, “Added-mass effect in the design of partitioned algorithms for fluid-structure problems,” *Computer Methods in Applied Mechanics and Engineering*, vol. 194, no. 42-44, pp. 4506–4527, 2005.
- [22] A. R. Ghigo, J. M. Fullana, and P. Y. Lagrée, “A 2D nonlinear multiring model for blood flow in large elastic arteries,” *Journal of Computational Physics*, vol. 350, pp. 136–165, 2017.

-
- [23] V. John, *Finite Element Methods for Incompressible Flow Problems*, ser. Springer Series in Computational Mathematics, R. Bank, R. Graham, W. Hackbusch, J. Stoer, R. Varga, and H. Yserentant, Eds. Cham: Springer International Publishing, 2016, vol. 51.
- [24] T. E. Tezduyar and S. Sathe, “Modelling of fluid–structure interactions with the space–time finite elements: Solution techniques,” *International Journal for Numerical Methods in Fluids*, vol. 54, no. 6-8, pp. 855–900, jun 2007.
- [25] J. Donea, A. Huerta, J.-P. Ponthot, and A. Rodríguez-Ferran, “Arbitrary Lagrangian-Eulerian Methods,” in *Encyclopedia of Computational Mechanics*, E. Stein, R. de Borst, and T. J. R. Hughes, Eds. Chichester, UK: John Wiley & Sons, Ltd, nov 2004, vol. 1, ch. 14.
- [26] M. Souli and D. J. Benson, *Arbitrary Lagrangian- Eulerian and Fluid – Structure Interaction*. Jhon Wiley & Sons, 2010.
- [27] Y. Bazilevs, K. Takizawa, and T. E. Tezduyar, “Challenges and Directions in Computational Fluid-Structure Interaction,” *Mathematical Models and Methods in Applied Sciences*, vol. 23, no. 02, pp. 215–221, feb 2013.
- [28] W. R. Holmes and L. Edelstein-Keshet, “A Comparison of Computational Models for Eukaryotic Cell Shape and Motility,” *PLoS Computational Biology*, vol. 8, no. 12, p. e1002793, dec 2012.
- [29] P. Švancara, J. Horáček, and V. Hruža, “FE Modelling of the Fluid-Structure-Acoustic Interaction for the Vocal Folds Self-Oscillation,” in *Vibration Problems ICOVP 2011*, ser. Springer Proceedings in Physics, J. Náprstek, J. Horáček, M. Okrouhlík, B. Marvalová, F. Verhulst, and J. T. Sawicki, Eds. Dordrecht: Springer Netherlands, 2011, vol. 139, pp. 801–807.
- [30] P. Bhattacharya and T. Siegmund, “Validation of a flow–structure-interaction computation model of phonation,” *Journal of Fluids and Structures*, vol. 48, pp. 169–187, jul 2014.
- [31] W. Jiang, X. Zheng, and Q. Xue, “Computational Modeling of Fluid–Structure–Acoustics Interaction during Voice Production,” *Frontiers in Bioengineering and Biotechnology*, vol. 5, feb 2017.
- [32] H. H. Yeh, S. W. Rabkin, and D. Grecov, “Hemodynamic assessments of the ascending thoracic aortic aneurysm using fluid-structure interaction approach,” *Medical & Biological Engineering & Computing*, vol. 56, no. 3, pp. 435–451, mar 2018.
- [33] P. Sváček and J. Horáček, “Finite element approximation of flow induced vibrations of human vocal folds model: Effects of inflow boundary conditions and the length of subglottal and supraglottal channel on phonation onset,” *Applied Mathematics and Computation*, vol. 319, pp. 178–194, 2018.
-

- [34] B. Maschke and A. van der Schaft, “Port-Controlled Hamiltonian Systems: Modelling Origins and Systemtheoretic Properties,” *IFAC Proceedings Volumes*, vol. 25, no. 13, pp. 359–365, jun 1992.
- [35] —, “A Hamiltonian approach to stabilization of nonholonomic mechanical systems,” in *IEEE Conference on Decision and Control*, vol. 3. Lake Buena Vista, FL, USA: IEEE, 1994, pp. 2950–2954.
- [36] A. van der Schaft and B. Maschke, “On the Hamiltonian formulation of nonholonomic mechanical systems,” *Reports on Mathematical Physics*, vol. 34, no. 2, pp. 225–233, aug 1994.
- [37] —, “Hamiltonian formulation of distributed-parameter systems with boundary energy flow,” *Journal of Geometry and Physics*, vol. 42, no. 1-2, pp. 166–194, may 2002.
- [38] A. Macchelli, “Port Hamiltonian Systems. A unified approach for modeling and control finite and infinite dimensional physical systems,” Ph.D. dissertation, University of Bologna, 2002.
- [39] Y. Le Gorrec, H. Zwart, and B. Maschke, “Dirac structures and Boundary Control Systems associated with Skew-Symmetric Differential Operators,” *SIAM Journal on Control and Optimization*, vol. 44, no. 5, pp. 1864–1892, jan 2005.
- [40] J. A. Villegas, Y. Le Gorrec, H. Zwart, and B. Maschke, “Boundary control for a class of dissipative differential operators including diffusion systems,” *Proceedings of the 17th International Symposium on Mathematical Theory of Networks and Systems*, pp. 297–304, 2006.
- [41] A. van der Schaft, *L2-Gain and Passivity Techniques in Nonlinear Control*, 3rd ed., ser. Communications and Control Engineering. Cham: Springer International Publishing, 2017.
- [42] V. Duindam, A. Macchelli, S. Stramigioli, and H. Bruyninckx, *Modeling and Control of Complex Physical Systems*. Berlin, Heidelberg: Springer Berlin Heidelberg, 2009.
- [43] B. Jacob and H. J. Zwart, *Linear Port-Hamiltonian Systems on Infinite-dimensional Spaces*, ser. Operator Theory: Advances and Applications. Basel: Springer Basel, 2012, vol. 223.
- [44] A. van der Schaft and D. Jeltsema, *Port-Hamiltonian Systems Theory: An Introductory Overview*. Boston, MA, USA: now Publishers Inc, 2014.
- [45] A. Falaize and T. Hélie, “Passive simulation of the nonlinear port-Hamiltonian modeling of a Rhodes Piano,” *Journal of Sound and Vibration*, vol. 390, pp. 289–309, mar 2017.
- [46] N. Lopes and T. Hélie, “A power-balanced model of a valve exciter including shocks and based on a conservative jet for brass instruments : Simulations and comparison with standard models,” in *International Symposium on Musical Acoustics*, Le Mans, France, 2014, pp. 1–5.

-
- [47] —, “Energy Balanced Model of a Jet Interacting With a Brass Player’s Lip,” *Acta Acustica united with Acustica*, vol. 102, no. 1, pp. 141–154, jan 2016.
- [48] T. Hélie and F. Silva, “Self-oscillations of a Vocal Apparatus: A Port-Hamiltonian Formulation,” in *International Conference on Geometric Science of Information*, ser. Lecture Notes in Computer Science, F. Nielsen and F. Barbaresco, Eds., 2017, vol. 10589, pp. 375–383.
- [49] V. Wetzel, T. Hélie, and F. Silva, “Power balanced time-varying lumped parameter model of a vocal tract: Modelling and simulation,” in *Proceedings of the 26th International Congress on Sound and Vibration, ICSV 2019*, Montréal, 2019, pp. 1–7.
- [50] N. M. Trang Vu, L. Lefevre, and B. Maschke, “Port-Hamiltonian formulation for systems of conservation laws: application to plasma dynamics in Tokamak reactors,” *IFAC Proceedings Volumes*, vol. 45, no. 19, pp. 108–113, 2012.
- [51] S. Aoues, F. L. Cardoso-Ribeiro, D. Matignon, and D. Alazard, “Modeling and control of a rotating flexible spacecraft: A port-hamiltonian approach,” *IEEE Transactions on Control Systems Technology*, vol. 27, no. 1, pp. 355–362, 2019.
- [52] M. Angerer, S. Music, and S. Hirche, “Port-Hamiltonian based control for human-robot team interaction,” in *2017 IEEE International Conference on Robotics and Automation (ICRA)*. IEEE, may 2017, pp. 2292–2299.
- [53] J. Lequeur and M. Tucsnak, “The piston problem in a port-Hamiltonian formalism,” *IFAC-PapersOnLine*, vol. 48, no. 13, pp. 212–216, 2015.
- [54] F. L. Cardoso-Ribeiro, D. Matignon, and V. Pommier-Budinger, “Modeling of a Fluid-structure coupled system using port-Hamiltonian formulation,” *IFAC-PapersOnLine*, vol. 48, no. 13, pp. 217–222, 2015.
- [55] —, “A port-Hamiltonian model of liquid sloshing in moving containers and application to a fluid-structure system,” *Journal of Fluids and Structures*, vol. 69, no. December 2016, pp. 402–427, feb 2017.
- [56] —, “Port-Hamiltonian model of two-dimensional shallow water equations in moving containers,” *IMA Journal of Mathematical Control and Information*, vol. 37, no. 4, pp. 1348–1366, dec 2020.
- [57] H. Bansal, H. Zwart, L. Iapichino, W. Schilders, and N. van der Wouw, “Port-Hamiltonian modelling of fluid dynamics models with variable cross-section,” 2020, preprint accepted for 24th International Symposium on Mathematical Theory of Networks and Systems (MTNS 2020). [Online]. Available: <https://www.win.tue.nl/~hbansal>
- [58] P. J. Olver, *Applications of Lie Groups to Differential Equations*, ser. Graduate Texts in Mathematics, F. W. Gehring, P. R. Halmos, and C. C. Moore, Eds. New York, NY: Springer US, 1986, vol. 107.
-

- [59] V. Trenchant, H. Ramirez, Y. Le Gorrec, and P. Kotyczka, “Finite differences on staggered grids preserving the port-Hamiltonian structure with application to an acoustic duct,” *Journal of Computational Physics*, vol. 373, pp. 673–697, nov 2018.
- [60] A. Brugnoli, D. Alazard, V. Pommier-Budinger, and D. Matignon, “Port-Hamiltonian formulation and symplectic discretization of plate models Part I: Mindlin model for thick plates,” *Applied Mathematical Modelling*, vol. 75, pp. 940–960, 2019.
- [61] —, “Port-Hamiltonian formulation and symplectic discretization of plate models Part II: Kirchhoff model for thin plates,” *Applied Mathematical Modelling*, vol. 75, pp. 961–981, 2019.
- [62] D. Matignon and T. Hélie, “A class of damping models preserving eigenspaces for linear conservative port-Hamiltonian systems,” *European Journal of Control*, vol. 19, no. 6, pp. 486–494, 2013.
- [63] H. Bansal, P. Schulze, M. Abbasi, H. Zwart, L. Iapichino, W. Schilders, and N. van de Wouw, “Port-Hamiltonian Formulation of Two-phase Flow Models,” Eindhoven University of Technology, Tech. Rep., 2020.
- [64] M. Grmela and H. C. Öttinger, “Dynamics and thermodynamics of complex fluids. I. Development of a general formalism,” *Physical Review E - Statistical Physics, Plasmas, Fluids, and Related Interdisciplinary Topics*, vol. 56, no. 6, pp. 6620–6632, 1997.
- [65] R. Altmann and P. Schulze, “A port-Hamiltonian formulation of the Navier–Stokes equations for reactive flows,” *Systems & Control Letters*, vol. 100, pp. 51–55, feb 2017.
- [66] L. A. Mora, Y. Le Gorrec, D. Matignon, H. Ramírez, and J. Yuz, “About dissipative and pseudo Port-Hamiltonian Formulations of irreversible Newtonian Compressible Flows,” in *21st IFAC World Congress in Berlin, Germany*, 2020, pp. 11 692–11 697.
- [67] H. Ramírez, “Control of irreversible thermodynamic processes using port-Hamiltonian systems defined on pseudo-Poisson and contact structures,” Ph.D., Universidad de Concepción, Chile - Université Claude Bernard Lyon 1, France, 2012.
- [68] H. Ramirez, B. Maschke, and D. Sbarbaro, “Irreversible port-Hamiltonian systems: A general formulation of irreversible processes with application to the CSTR,” *Chemical Engineering Science*, vol. 89, pp. 223–234, feb 2013.
- [69] H. C. Öttinger, *Beyond Equilibrium Thermodynamics*. Hoboken, NJ, USA: John Wiley & Sons, Inc., mar 2005.
- [70] H. Ramirez and Y. Le Gorrec, “An irreversible port-Hamiltonian formulation of distributed diffusion processes,” *IFAC-PapersOnLine*, vol. 49, no. 24, pp. 46–51, 2016.
- [71] H. Ramirez, Y. Le Gorrec, and B. Maschke, “Irreversible port-Hamiltonian systems on infinite dimensional spaces,” AS2M ENSMM/FEMTO-ST, Tech. Rep., 2020.

-
- [72] B. H. Story and I. R. Titze, “Voice simulation with a body-cover model of the vocal folds,” *The Journal of the Acoustical Society of America*, vol. 97, no. 2, pp. 1249–1260, feb 1995.
- [73] M. Encina, J. Yuz, M. Zanartu, and G. Galindo, “Vocal fold modeling through the port-Hamiltonian systems approach,” in *2015 IEEE Conference on Control Applications (CCA)*. IEEE, sep 2015, pp. 1558–1563.
- [74] L. A. Mora, J. I. Yuz, H. Ramírez, and Y. Le Gorrec, “A port-Hamiltonian Fluid-Structure Interaction Model for the Vocal folds,” *IFAC-PapersOnLine*, vol. 51, no. 3, pp. 62–67, 2018.
- [75] R. Ogden, *Non-Linear Elastic Deformations*. New York: Dover Publications, INC, 1984.
- [76] T. Bodnár, G. P. Galdi, and Š. Nečasová, Eds., *Fluid-Structure Interaction and Biomedical Applications*, ser. Advances in Mathematical Fluid Mechanics. Basel: Springer Basel, 2014.
- [77] R. S. Lakes, *Viscoelastic Solids*, ser. CRC Mechanical Engineering Series. CRC Press, nov 1999.
- [78] L. Rakotomanana, *Eléments de dynamique des solides et structures déformables*, ser. Mécanique. Presses polytechniques et universitaires romandes, 2009.
- [79] M. Bukač, S. Čanić, R. Glowinski, B. Muha, and A. Quaini, “A modular, operator-splitting scheme for fluid-structure interaction problems with thick structures,” *International Journal for Numerical Methods in Fluids*, vol. 74, no. 8, pp. 577–604, mar 2014.
- [80] F. Chouly, A. Van Hirtum, P. Y. Lagrée, X. Pelorson, and Y. Payan, “Numerical and experimental study of expiratory flow in the case of major upper airway obstructions with fluid-structure interaction,” *Journal of Fluids and Structures*, vol. 24, no. 2, pp. 250–269, 2008.
- [81] Y. Wang, A. Quaini, and S. Čanić, “A Higher-Order Discontinuous Galerkin/Arbitrary Lagrangian Eulerian Partitioned Approach to Solving Fluid–Structure Interaction Problems with Incompressible, Viscous Fluids and Elastic Structures,” *Journal of Scientific Computing*, vol. 76, no. 1, pp. 481–520, jul 2018.
- [82] T. Spenke, N. Hosters, and M. Behr, “A multi-vector interface quasi-Newton method with linear complexity for partitioned fluid–structure interaction,” *Computer Methods in Applied Mechanics and Engineering*, vol. 361, p. 112810, apr 2020.
- [83] S. T. Ha and H. G. Choi, “Investigation on the effect of density ratio on the convergence behavior of partitioned method for fluid–structure interaction simulation,” *Journal of Fluids and Structures*, vol. 96, p. 103050, 2020.
- [84] S. T. Ha, L. C. Ngo, M. Saeed, B. J. Jeon, and H. Choi, “A comparative study between partitioned and monolithic methods for the problems with 3D fluid-structure interaction of blood vessels,” *Journal of Mechanical Science and Technology*, vol. 31, no. 1, pp. 281–287, jan 2017.
-

- [85] J. Kuhnert, I. Michel, and R. Mack, “Fluid structure interaction (FSI) in the meshfree finite pointset method (FPM): Theory and applications,” *Lecture Notes in Computational Science and Engineering*, vol. 129, pp. 73–92, 2019.
- [86] L. A. Mora, Y. Le Gorrec, H. Ramírez, and J. Yuz, “Fluid-Structure Port-Hamiltonian Model for Incompressible Flows in Tubes with Time Varying Geometries,” *Mathematical and Computer Modelling of Dynamical Systems*, vol. 26, no. 5, pp. 409–433, sep 2020.
- [87] J. Lemaitre, “Introduction to Elasticity and Viscoelasticity,” in *Handbook of Materials Behavior Models*. Elsevier, 2001, pp. 71–74.
- [88] K. Ishizaka and J. L. Flanagan, “Synthesis of Voiced Sounds From a Two-Mass Model of the Vocal Cords,” *Bell System Technical Journal*, vol. 51, no. 6, pp. 1233–1268, jul 1972.
- [89] J. Seikel, D. King, and D. Drumright, *Anatomy and physiology for speech, language, and hearing*, 4th ed. Cengage Learning, 2009.
- [90] A. K. Miri, “Mechanical characterization of vocal fold tissue: A review study,” *Journal of Voice*, vol. 28, no. 6, pp. 657–667, 2014.
- [91] F. Alipour, D. A. Berry, and I. R. Titze, “A finite-element model of vocal-fold vibration,” *The Journal of the Acoustical Society of America*, vol. 108, no. 6, pp. 3003–3012, dec 2000.
- [92] J. E. Kelleher, T. Siegmund, M. Du, E. Naseri, and R. W. Chan, “The anisotropic hyperelastic biomechanical response of the vocal ligament and implications for frequency regulation: A case study,” *The Journal of the Acoustical Society of America*, vol. 133, no. 3, pp. 1625–1636, 2013.
- [93] T. E. Shurtz and S. L. Thomson, “Influence of numerical model decisions on the flow-induced vibration of a computational vocal fold model,” *Computers & Structures*, vol. 122, pp. 44–54, jun 2013.
- [94] X. Zheng, R. Mittal, Q. Xue, and S. Bielamowicz, “Direct-numerical simulation of the glottal jet and vocal-fold dynamics in a three-dimensional laryngeal model,” *The Journal of the Acoustical Society of America*, vol. 130, no. 1, pp. 404–415, jul 2011.
- [95] I. Steinecke and H. Herzel, “Bifurcations in an asymmetric vocal-fold model,” *The Journal of the Acoustical Society of America*, vol. 97, no. 3, pp. 1874–1884, mar 1995.
- [96] J. C. Lucero and J. Schoentgen, “Smoothness of an equation for the glottal flow rate versus the glottal area,” *The Journal of the Acoustical Society of America*, vol. 137, no. 5, pp. 2970–2973, may 2015.
- [97] B. D. Erath, M. Zañartu, K. C. Stewart, M. W. Plesniak, D. E. Sommer, and S. D. Peterson, “A review of lumped-element models of voiced speech,” *Speech Communication*, vol. 55, no. 5, pp. 667–690, jun 2013.
- [98] N. J. Lous, G. C. Hofmans, R. N. Veldhuis, and A. Hirschberg, “A Symmetrical Two-Mass Vocal-Fold Model Coupled to Vocal Tract and Trachea, with Application to Prosthesis Design,” *Acta Acustica united with Acustica*, vol. 84, no. 6, pp. 1135–1150, 1998.

- [99] P. Gresho and R. Sani, *Incompressible Flow and the Finite Element Method. Advection-Diffusion and Isothermal Laminar Flow*. New York, USA: John Wiley & Sons, Inc., 1998.
- [100] G. Papadakis, “Coupling 3D and 1D fluid-structure-interaction models for wave propagation in flexible vessels using a finite volume pressure-correction scheme,” *Communications in Numerical Methods in Engineering*, vol. 25, no. 5, pp. 533–551, may 2009.
- [101] R. B. Bird, W. E. Stewart, E. N. Lightfoot, and D. J. Klingenberg, *Introductory transport phenomena*. USA: John Wiley & Sons, Inc., 2015.
- [102] L. A. Mora, H. Ramírez, J. I. Yuz, and Y. Le Gorrec, “A Scalable port-Hamiltonian Model for Incompressible Fluids in Irregular Geometries,” *IFAC-PapersOnLine*, vol. 52, no. 2, pp. 102–107, 2019.
- [103] R. L. Panton, *Incompressible Flow*, 4th ed. New Jersey, USA: John Wiley & Sons, Inc., 2013.
- [104] P. Kotyczka, “Discretized models for networks of distributed parameter port-Hamiltonian systems,” in *Proceedings of the 8th International Workshop on Multidimensional Systems (nDS13)*, no. 2. Erlangen, Germany: VDE, 2013, pp. 63–67.
- [105] J. W. Murdock, *Fundamental Fluid Mechanics for the Practicing Engineer*, ser. Mechanical Engineering, F. L. L., Ed. USA: CRC Press, 1993, vol. 82.
- [106] R. P. Sinha, “Solution of Unsteady Fluid Dynamic and Energy Equations for High-Speed Oscillating Compressible Flows and Blast Wave Propagations,” *Journal of Thermal Science and Engineering Applications*, vol. 13, no. 1, feb 2021.
- [107] A.-S. Treton, G. Haine, and D. Matignon, “Modelling the 1D piston problem as interconnected port-Hamiltonian systems,” in *21st IFAC World Congress*, Berlin, 2020.
- [108] L. Landau and E. Lifshitz, *Fluid Mechanics*, 2nd ed., ser. Course of Theoretical Physics. Pergamon Press, 1987, vol. 6.
- [109] L. A. Mora, H. Ramírez, J. I. Yuz, Y. Le Gorrec, and M. Zañartu, “Energy-based fluid–structure model of the vocal folds,” *IMA Journal of Mathematical Control and Information*, dec 2020. [Online]. Available: <https://academic.oup.com/imamci/advance-article/doi/10.1093/imamci/dnaa031/6025508>
- [110] C. Tao, J. J. Jiang, and Y. Zhang, “Simulation of vocal fold impact pressures with a self-oscillating finite-element model,” *The Journal of the Acoustical Society of America*, vol. 119, no. 6, pp. 3987–3994, jun 2006.
- [111] Y. Zhang, X. Zheng, and Q. Xue, “A Deep Neural Network Based Glottal Flow Model for Predicting Fluid-Structure Interactions during Voice Production,” *Applied Sciences*, vol. 10, no. 2, p. 705, jan 2020.

- [112] A. Macchelli, Y. Le Gorrec, and H. Ramírez, “Boundary Energy-Shaping Control of an Ideal Compressible Isentropic Fluid in 1-D,” *IFAC-PapersOnLine*, vol. 50, no. 1, pp. 5598–5603, jul 2017.
- [113] F. L. Cardoso-Ribeiro, “Port-Hamiltonian modeling and control of a fluid-structure system : Application to sloshing phenomena in a moving container coupled to a flexible structure,” Doctoral Thesis, Université Fédérale Toulouse Midi-Pyrénées/ISAE Supaéro, 2016.
- [114] R. J. LeVeque, *Finite Volume Methods for Hyperbolic Problems*, ser. Cambridge Texts in Applied Mathematics. Cambridge, U.K.: Cambridge University Press, aug 2002.
- [115] Z. Kowalczyk and M. S. Tatara, “Improved model of isothermal and incompressible fluid flow in pipelines versus the Darcy-Weisbach equation and the issue of friction factor,” *Journal of Fluid Mechanics*, 2020.
- [116] E. Hauge, O. M. Aamo, and J.-M. Godhavn, “Model Based Pipeline Monitoring with Leak Detection,” *IFAC Proceedings Volumes*, vol. 40, no. 12, pp. 318–323, 2007.
- [117] V. Ruas, “A New Formulation of the Three-dimensional Velocity-Vorticity System in Viscous Incompressible Flow,” *ZAMM*, vol. 79, no. 1, pp. 29–36, jan 1999.
- [118] X. Wu, J. Wu, and J. Wu, “Effective Vorticity-Velocity Formulations for Three-Dimensional Incompressible Viscous Flows,” *Journal of Computational Physics*, vol. 122, no. 1, pp. 68–82, nov 1995.
- [119] M. A. Olshanskii, T. Heister, L. G. Rebholz, and K. J. Galvin, “Natural vorticity boundary conditions on solid walls,” *Computer Methods in Applied Mechanics and Engineering*, vol. 297, pp. 18–37, 2015.
- [120] M. Massoud, *Engineering Thermofluids*. Berlin/Heidelberg: Springer-Verlag, 2005.
- [121] R. J. LeVeque, *Numerical Methods for Conservation Laws*, 2nd ed., ser. Lectures in Mathematics ETH Zürich. Basel, Switzerland: Birkhäuser Basel, 1992.
- [122] A. A. Alonso and B. Erik Ydstie, “Process systems, passivity and the second law of thermodynamics,” *Computers & Chemical Engineering*, vol. 20, pp. S1119–S1124, jan 1996.
- [123] J. H. Keenan, “Availability and irreversibility in thermodynamics,” *British Journal of Applied Physics*, vol. 2, no. 7, pp. 183–192, jul 1951.
- [124] J. C. Willems, “Dissipative dynamical systems part I: General theory,” *Archive for Rational Mechanics and Analysis*, vol. 45, no. 5, pp. 321–351, 1972.
- [125] A. A. Alonso and B. Ydstie, “Stabilization of distributed systems using irreversible thermodynamics,” *Automatica*, vol. 37, no. 11, pp. 1739–1755, nov 2001.

- [126] H. Hoang, F. Couenne, C. Jallut, and Y. Le Gorrec, “The port Hamiltonian approach to modeling and control of Continuous Stirred Tank Reactors,” *Journal of Process Control*, vol. 21, no. 10, pp. 1449–1458, dec 2011.
- [127] —, “Lyapunov-based control of non isothermal continuous stirred tank reactors using irreversible thermodynamics,” *Journal of Process Control*, vol. 22, no. 2, pp. 412–422, feb 2012.
- [128] B. Ydstie, “Passivity based control via the second law,” *Computers & Chemical Engineering*, vol. 26, no. 7-8, pp. 1037–1048, aug 2002.
- [129] H. Ramírez, Y. Le Gorrec, B. Maschke, and F. Couenne, “On the passivity based control of irreversible processes: A port-Hamiltonian approach,” *Automatica*, vol. 64, pp. 105–111, feb 2016.
- [130] J. H. Atkinson, J. J. Westerink, and J. M. Hervouet, “Similarities between the quasi-bubble and the generalized wave continuity equation solutions to the shallow water equations,” *International Journal for Numerical Methods in Fluids*, vol. 45, no. 7, pp. 689–714, 2004.
- [131] J. P. Vila, F. Chazel, and P. Noble, “2D Versus 1D Models for Shallow Water Equations,” *Procedia IUTAM*, vol. 20, pp. 167–174, 2017.
- [132] A. J. Katz, “Meshless methods for computational fluid dynamics,” Ph.D. Dissertation, Stanford University, 2009.

List of Figures

1.1	Examples of FSI systems in engineering, biology and biomedical sciences.	2
1.2	Adaptive mesh and remeshing of the fluid domain in interface-tracking techniques [28].	3
1.3	Longitudinal fluid flow interacting with a mechanical structure with transverse motion.	4
1.4	Illustrative examples of power-preserving interconnections. a) Mass-spring system uses interconnection by ports b) levitated ball uses interconnection by energy.	7
2.1	Mechanical description of the structure motion	17
2.2	Cylindrical flexible tube description.	18
2.3	Cross-sectional view of the flexible tube and the forces acting at a point by an axisymmetric circumferential strain. The expansion velocity v is axisymmetric.	19
2.4	Tissue layers of the structure of vocal folds. Dotted line: Midasagittal plane of the glottis.	22
2.5	Simplification of the vocal folds mechanics using the body-cover model. Δ_j 's represents the tissue deformations during the vocal folds vibration cycle.	23
2.6	Vocal folds collision description using the body-cover model. Left: tissue compression during the collision. Right: overlap of the cover mass to describe the collision.	24
2.7	Body-cover model of vocal folds showing a Hemi-larynx representation for symmetrical vocal folds oscillations. Left: 3-dimensional view, displaying the mass positions. Right: bottom view, displaying the contact surfaces.	25
2.8	Stored potential energy of collision spring (left) and the corresponding applied force over mass m_j . Normalized behavior, $k_{cj} = 1$ and $\eta_{cj} = 1$, for $j \in \{1, 2\}$	26
3.1	Spatial discretization of the fluid domain. a) Division of the fluid domain in n_f sections with uniform cross-sectional area. b) Definition of nodes between adjacent incompressible fluid sections.	30
3.2	Coupling incompressible fluid sections using nodes with compressible behavior.	32
3.3	Inputs/outputs diagram of the node j and the adjacent incompressible sections.	38
3.4	Finite-dimensional formulation of the fluid-structure system. MSD-based description of the structure motion. Fluid dynamics description based on nodes (red) and incompressible fluid sections.	42

3.5	Finite-dimensional formulation of the fluid-structure system with $n_f \neq n_s$	43
3.6	Static pressure (Pa) distribution, \mathbf{p}_1^p , along the tube and scaled structure displacements for different time instants and two different numbers of sections. Dashed boxes: static pressure undershoot and negative displacement of the walls.	46
3.7	Displacement of the wall in the half-length point of the structure (Displacements q_{26} and q_{36} for $N = 51$ and $N = 71$, respectively).....	46
3.8	Simulation results for flexible tube using the material parameter of [10]. (a) Static pressure distribution, \mathbf{p}_1^p , along the tube. (b) Wall displacement distribution, \mathbf{q} , along the tube.....	47
4.1	Spatial discretization of fluid variables for the finite-dimensional model. (a) Description of the density. (b): Velocity description. (c): Equivalent one-dimensional mesh.....	51
4.2	Arbitrary j -th sections of the fluid domain. (a) Velocity section. (b) Density section. A_{c_j} and v_{c_j} are the area and velocity of the contact surface S_j in the velocity section with volume V_j , v_j is the corresponding average velocity and ρ_j is the average density of the section con volume \bar{V}_j	52
4.3	Vibrating cycle induced by FSI between the intraglottal airflow and the vocal folds.....	60
4.4	Approximation of the glottal tract using the discretization method proposed, considering fluid sections with uniform cross-sectional areas. Dotted line represents the midsagittal plane. Circles denote the number of velocity section in each glottis part.....	61
4.5	Displacement of the masses of the vocal folds mechanical structure, $q_{sj} = q_j + q_{sj}^0$. Solid line is the body mass displacement (m_3 in Figure 4.4), dashed and dash-dotted lines are the displacements of upper and lower cover masses, respectively (m_2 and m_1 in Figure 4.4, respectively).	62
4.6	Overlapping of cover masses during the vocal folds collisions. Solid line: deformation for the upper mass (m_2 in Figure 4.4). Dash-dot-dotted line: deformation for the lower mass (m_1 in Figure 4.4).	62
4.7	Output Flow in one vibrating cycle.....	63
4.8	Pressure distribution in 3 instants of the vibrating cycle. Upper row: Coronal view of the glottis, where the dots represents the heights of each velocity sections. Bottom row: Pressure distribution in the glottis.	64
4.9	Instantaneous energy in one vibrating cycle. Left: Kinetic energy \mathcal{K}_s of the mechanical part. Middle: Potential energy \mathcal{P}_s of the mechanical part. Right: Kinetic energy \mathcal{K}_f and available internal energy $\bar{\mathcal{U}}_f$ of the fluid part.....	64
5.1	Normal vector and tangential plane to the boundary surface $\partial\Omega$	74

List of Tables

3.1	Material parameters of the structure and the fluid.....	45
3.2	Parameters of the fluid-structure model [12].	45
3.3	Parameters of the fluid-structure model using the material specifications of [10]. .	46
4.1	Simulation parameters	61

Título : Modelado puerto-Hamiltoniano de Interacciones Fluido-Estructura en un Dominio Longitudinal

Palabras clave : Interacción fluido-estructura, sistemas puerto-Hamiltonianos, modelado en dimensión finita, fluidos Newtonianos

Resumen : Esta Tesis presenta un modelado basado en sistemas puerto-Hamiltonianos de las interacciones fluido-estructura en un dominio longitudinal. Primeramente, se presenta un modelado de dimensión finita basado en una formulación masa-resorte-amortiguador para describir el movimiento de la estructura. Segundamente, la dinámica de los fluidos Newtonianos se describe dividiendo el dominio de los fluidos en n_f secciones con área transversal uniforme. Para fluidos incompresibles, se utiliza un elemento instrumental, llamado nodo, para permitir un acoplamiento apropiado, desde un punto de vista puerto-Hamiltoniano, de las secciones del fluido. Para fluidos compresibles, se utiliza una malla escalonada para describir la velocidad longitudinal y la densidad en el dominio del fluido. Para acoplar los modelos de dimensión finita del fluido y la estructura, se usa una interconexión que preserva la energía y se presenta un enfoque de conmutación para los problemas con colisión de la estructura. Las simulaciones muestran que los resultados obtenidos con los modelos propuestos se corresponden con formulaciones más complejas encontradas en la literatura. Terceramente, la descripción de sistemas con dominios variables utilizando el enfoque puerto-Hamiltoniano de dimensión infinita es estudiada. Como paso inicial, se presentan varias formulaciones de dimensión infinita para fluidos Newtonianos compresibles isentrópicos y no isentrópicos en un dominio 3D constante. Finalmente, se propone una formulación basada en el enfoque puerto-Hamiltoniano irreversible de dimensión infinita para fluidos Newtonianos compresibles no isentrópicos unidimensionales.

Titre : Modélisation Port-Hamiltonienne De L'interaction Fluide-Structure Dans Un Domaine Longitudinal

Mots clefs: Interactions fluide-structure, systèmes port-Hamiltoniens, modélisation à dimension finie, fluides Newtoniens

Résumé : Dans cette thèse on s'intéresse à la modélisation Hamiltonienne à ports (PHS) des interactions fluide-structure dans le domaine longitudinal. Dans un premier temps, le mouvement de la structure mécanique est modélisé en dimension finie à l'aide d'éléments masse-ressort-amortisseur. Dans un second temps, la dynamique des fluides newtoniens est décrite en divisant le domaine spatial en sous sections uniformes. Dans le cas des fluides incompressibles, un élément instrumental, appelé nœud, est utilisé pour permettre le couplage approprié entre sections de fluides. Dans le cas des fluides compressibles un maillage en quinconces est utilisé afin de caractériser la vitesse longitudinale et la densité aux différents points du domaine fluide. Les modèles discrétisés du fluide et de la structure mécanique sont ensuite interconnectés de manière conservative de puis-

sance. Une variable de commutation est utilisée lorsque la structure entre en collision, obturant de ce fait une section du domaine fluide. Les simulations montrent que les résultats obtenus à partir des modèles proposés sont en correspondance avec des formulations plus complexes trouvées dans la littérature. Finalement la description de la classe de systèmes considérée avec domaine variant dans le temps est explicitée à l'aide du formalisme Hamiltonien à ports. Dans un troisième temps, une formulation Hamiltonienne à ports de dimension infinie est proposée pour la dynamique des fluides newtoniens compressibles isentropiques et non isentropiques en dimension 3. Une première formulation thermodynamique basée sur la formulation Hamiltonienne à ports irréversible est finalement proposée pour les fluides newtoniens compressibles unidimensionnels.

Title : Port-Hamiltonian Modeling of Fluid-Structure Interactions in a Longitudinal Domain

Keywords : Fluid-structure interactions, port-Hamiltonian systems, finite-dimensional modeling, Newtonian fluids

Abstract : This Thesis presents modeling based on port-Hamiltonian systems (PHS) of the fluid-structure interaction in a longitudinal domain. Firstly, finite-dimensional modeling based on a mass-spring-damper formulation is presented to describe the transverse motion of the structure. Secondly, the dynamics of Newtonian fluids are described by dividing the fluid domain into n_f sections with uniform cross-sectional area. For incompressible fluids, an instrumental element, called node, is used to allow appropriate coupling, from a PHS point of view, of the fluid sections. For compressible fluids, a staggered mesh is used to characterize the longitudinal velocity and the density in n_f points of the fluid domain for each variable. To be able to couple the finite-dimensional models of the fluid and the structure, a power-preserving intercon-

nection is used, and a switching approach is presented to model the cases where the structure collides closing a section of the fluid domain, such as in the case of the vocal folds. The obtained simulation results show that the proposed models are in correspondence with more complex formulations found in the literature. Finally, the description of the considered class of systems with time-varying domains using the infinite-dimensional PHS framework is studied. The thesis also presents some first approaches of general infinite-dimensional formulations for isentropic and non-isentropic compressible Newtonian fluids in a constant 3D domain, and a formulation based on the infinite-dimensional irreversible PHS approach is proposed for 1D non-isentropic compressible Newtonian fluids.